INVESTIGATION OF URANIUM AND VARIOUS LIGAND COMPLEXES IN THE GAS PHASE USING ELECTROSPRAY IONIZATION ION TRAP MASS SPECTROMETRY

A Thesis by

Wen-Fang Winnie Chien

B.S., Wichita State University, Wichita, KS, 2004

Submitted to the College of Liberal Arts and Sciences
and the faculty of the Graduate School of
Wichita State University
in partial fulfillment of
the requirements for the degree of
Master of Science

December 2007

© Copyright 2007 by Wen-Fang Winnie Chien

All Rights Reserved

INVESTIGATION OF URANIUM AND VARIOUS LIGAND COMPLEXES IN THE GAS PHASE USING ELECTROSPRAY IONIZATION ION TRAP MASS SPECTROMETRY

The following faculty members have examined the final copy of this thesis for form and content and recommend that it be accepted in partial fulfillment of the requirements for the degree of Master of Science, with a major in Chemistry

_____

Michael Van Stipdonk, Committee Chair

We have read this thesis
and recommend its acceptance

_____

David M. Eichhron, Committee Member

_____

Francis D'Souza, Committee Member

_____

William C. Groutas, Committee Member

_____

T. S. Ravigururajan, Committee Member

ACKNOWLEDGEMENTS

I would like to express my deepest appreciation to my advisor Dr. Michael Van Stipdonk for the time and patience that he has put out through my research and my undergraduate and graduate years at Wichita State University. He has always encourages us to achieve bigger and greater things in science and in life. I am extremely honored to work with a great scientist like him.

I would also like to thank my thesis committee members, Dr. Eichhorn, Dr. D'Souza, Dr. Groutas, and Dr. T. S. Ravigururajan for taking time to guide me through classes and also for the great advises and supports that they gave throughout my studies. Thank you for being my committee members.

In addition I would like to thank my group members for their endless aid and encouragement toward my research, studies, and my growth as a person.

Finally I want to dedicate all the work to my mother for all of her support through the numerous international phone calls, and without inheriting her strong mind I could never achieve what I am today. Mom, even though you could not be present to see my achievement in education in the United States, I want you to know that I am proud to be your daughter.

For the funding sources, I would like to acknowledge, the National Science Foundation (CAREER-0239800), Kansas NSF EPSCoR Program and Kansas

Technology Enterprise Corporation, NIH K-BRIN Program and Teaching Assistantship form Wichita State University.

ABSTRACT

The speciation and reactivity of uranium is a topic of sustained interest because species dependent chemistry controls processes ranging from nuclear fuel processing to mobility and fate in the geological surface. Past condensed phase studies have shown uranium a wide range of oxidation states and coordinate ion numbers in the environment. These studies have also suggested the strong interactions such as charge transfer between the uranium cations and solvent molecules cause the latter to behave like equatorial ligands. Studying and understanding intrinsic uranium chemistry is challenging because it is difficult to gain explicit control over the interactions of solvent and non-solvent ligands with uranyl ions in the condensed phase. An attractive alternative, therefore, is to monitor reaction in the gas phase (i.e. a solution free environment) in order to gain control over the chemical species chosen for study and the specific neutral reagents.

Recent studies shown that ion-trap mass spectrometry can be applied to the study of intrinsic metal and metal-complex chemistry by generating the metal complexes as ions through electrospray ionization ESI and allowing species to interact with neutral reagents present in the collision gas. Throughout these series of uranyl studies, ESI is used to produce gas-phase ions from solutions containing uranyl nitrate complexes in deionized water. Several studies were conducted to

monitor uranium and ligands behavior under different systems by controlling factors such as the numbers of ligands attached to the uranium dioxo cation center, ligand degrees of freedom, and ligand basicities. These studies were designed to gain clear insight to the intrinsic behavior of uranium complexes.

TABLE OF CONTENTS

CHAPTER **PAGE**

1. INTRODUCTION……1

2. EPERIMENTAL METHODS……..…4

Mass spectrometry (MS) and Tandem Mass Spectrometry (MS/MS)……...4

Electrospray Ionization (ESI)……5

Quadrupole Ion Trap Mass Analyzer……..……7

Reagents and Experimental Procedure……11

3. ELUCIDATION OF THE COLLISION INDUCED DISSOCIATION PATHWAYS OF WATER AND ALCOHOL COORDINATED COMPLEXES CONTAINNING THE URANYL CATION……16

4. INTRINSIC HYDRATION OF MONOPOSITIVE URANYL HYDROXIDE, NITRATE, AND ACETATE CATIONS……..……32

5. COLLISION INDUCED DISSOCIATION (CID) TANDEM MASS SPECTROMETRY (MS^n) OF DESFERRIOXAMINE SIDEROPHORE COMPLEXES FROM ELECTROSPRATY IONIZATIONOF UO_2^{2+}, Fe^{3+}, AND Ca^{2+} SOLUTION……49

6. OXIDATIONOF 2-PROPANOL LIGANDS DURING COLLISION INDUCED DISSOCIATIONOF A GAS-PHASE URANYL COMPLEX……74

TABLE OF CONTENTS (Cont.)

CHAPTER **PAGE**

7. PRODUCTION AND COLLISION-INDUCED DISSOCIATION OF GAS PHASE WATER-ALCOHOL-COORDINATED URANYL COMPLEXES CONTAINING HALIDE OR PERCHLORATE ANIONS……...……..97

8. GAS-PHASE COMPLEXES CONTAINING THE URANYL ION AND ACETONE……120

9. GAS-PHASE URANYL-NITRILE COMPLEX ION……155

10. BINDING OF MOLECULAR O_2 TO DI-AND TRI- LIGATED $[UO_2]^+$.....189

11. CONCULSIONS AND FUTURE WORK…….224

REFERENCES……..228

CHAPTER 1
INTRODUCTION

Uranium was first discovered in a mineral called pitchblend and was named after the planet Uranus by a German chemist called Martin Klaproth in 1789. Fission of uranium was discovered in 1938, which lead to intense study of the element for applications in energy production and atomic weapons. Uranium has sixteen isotopes, three of which exist naturally. ^{234}U, ^{235}U, and ^{238}U have abundances of approximately 0.0055%, 0.72%, and 99.27%, respectively [1].

Uranium can exist in solution in a range of oxidation states, and solution-phase chemistry of the element has been studied extensively. In solution, the chemistry of uranium is dominated by the uranyl ion; UO_2^{2+}, for which recent theoretical studies have suggested that strong interactions between the cation and solvent molecules, with significant charge transfer, cause the solvating species to behave like equatorial ligands. Therefore, specific interactions with solvent are likely to influence the physico-chemical behavior of the uranyl ion and its complexes in the environment. This prospect has motivated investigation of a range of uranyl complexes using spectroscopic techniques such as ultraviolet-visible, infrared and Raman spectroscopy and x-ray absorption fine structure to look into the complex composition and stability [2-8]. One major problem in assessing species-dependent behavior of

uranium in the solution-phase studies is difficulty in gaining explicit control over solvation and complexation steps and thus rigorous speciation.

One effective approach to circumvent this problem is to move the investigations into the gas-phase, where better control of complex composition can be gained. Several recent studies have shown that the combination of electrospray ionization (ESI) and ion-trap mass spectrometry (ITMS) can be used to explore the intrinsic chemistry of metal ion complexes [9-11].

There are several advantages to the use of ion-trap mass spectrometry, which include the ability to (1) isolate and store ionized species with explicitly defined compositions, (2) use a single or multiple collision-induced dissociation (CID) stages to determine chemical composition and structure, (3) conduct energy-resolved CID experiments to assess relative ion stability and (4) conduct time-resolved ion isolation experiments to probe gas-phase association reactions [12].

The overall aim of the experiments reported in this thesis was to determine the utiltity of electrospray ionization (ESI) and multiple-stage ion trap tandem mass spectrometry (MS) to generate and characterize gas-phase complexes featuring series of the uranyl ion coordinated by a range of anionic and neutral ligands. The specific objectives of these research are the following: (1) generate water and alcohol coordinated complexes containing the uranyl cation and elucidate their general CID

pathways, (2) determine whether time-resolved isolation experiments in the ITMS could be used to study the intrinsic hydration rates of uranyl hydroxide, nitrate, and acetate cations, (3) make and study gas-phase complexes that contain uranyl ion with a ligand (desferrioxamine, DEF) that resembles those used by bacteria to scavenge Fe from the environment, (4) determine the fragmentation pathways and investigate the intrinsic behavior of doubly-charged uranyl-acetone complexes, (5) develop a general approach to make gas-phase, solvated uranyl-anion complexes, including halide or perchlorate anions, (6) determine whether gas-phase studies of uranyl ion chemistry could provide information that is complementary to and consistent with prior condensed phase studies. To accomplish this goal, the conversion of 2-propanol ligands to acetone, which has been observed in the solid-phase experiments that involve uranyl ion exchanged into zeolite cavites, was examined; (7) investigate and analyze the general pathways and intrinsic behavior for uranyl-nitrile complexes and (8) explore intrinsic reactions between the U(V) dioxo cations $[UO_2]^+$ ligated acetone ligands and molecular oxygen.

CHAPTER 2
EXPERIMENTAL METHODS

2.1 Mass Spectrometry (MS) and Tandem Mass Spectrometry (MS/MS)

Mass spectrometry (MS) is an important analytical tool used in various areas, including medicinal, forensic, and pharmaceutical chemistry because of its high sensitivity, selectivity and low detection limits. Every mass spectrometer, in general, is composed of three parts: an ion source, the mass analyzer, and an ion detector [13].

Tandem mass spectrometry is an approach used to provide enhanced composition or structure information, and is commonly abbreviated either as MS/MS or MS^n. The tandem mass spectrometry approach involved expansion of the experiment to include multiple mass analysis stages. One approach is to perform a "tandem in space" experiment, in which two or more mass analyzers are coupled. Another is the "tandem in time" approach, in which one mass analyzer is used multiple times. With the quadrupole ion-trap mass mass spectrometer used in these studies, up to 10 mass analysis steps can be used to scrutinize the fragmentation of a selected ion of interest and it can be expanded up to ten mass analyzers shown in figure (2.1). From the fragmentation patterns for a given precursor ion one is able to determine or confirm the composition and structure of particular complexes and

further investigate its kinetic behaviors in the gas phase.

In tandem mass spectrometry, ions of a particular m/z ratio are selected in the first stage of mass analysis. The kinetic energy of the precursor ions is then increased using applied electric fields. Energetic collisions between the accelerated ions and a collision gas, such as helium, raise the internal energies of the former and induce unimolecular dissociation reactions. The m/z values of the product ions are subsequently determined using a second stage of mass analysis.

2.2 Electrospray Ionization

Electrospray ionization (ESI) is a soft method for generating ions out of solution phase species. In electrospray, ionization is carried out by pushing solution through the tip of a small-bore needle to which is applied an electric potential, typically 4-6 kilovolts. The electric potential causes the solution to break down into small, highly charged droplets. These droplets are desolvated using a stream of N_2 until the droplets reach a critical point known as the Rayleigh limit, where the surface tension of the droplet is exceeded by electrostatic repulsion of the multiple charges. The droplets then undergo a Coulombic explosion, which yields even smaller and less highly-charged droplets. These smaller droplets are fully desolvated using a heated metal capillary to ultimately produce bare, gas-phase ions [14]. The electrospray

ionization process is shown in figure 2.1. Unlike other conventional ionization methods such as electron impact or chemical ionization, ESI is a “gentle” method in which gaseous phase ions with low internal energy are produced: this leads to high abundances of intact molecule ions that can be transferred to high vaccum and the mass analyzer.

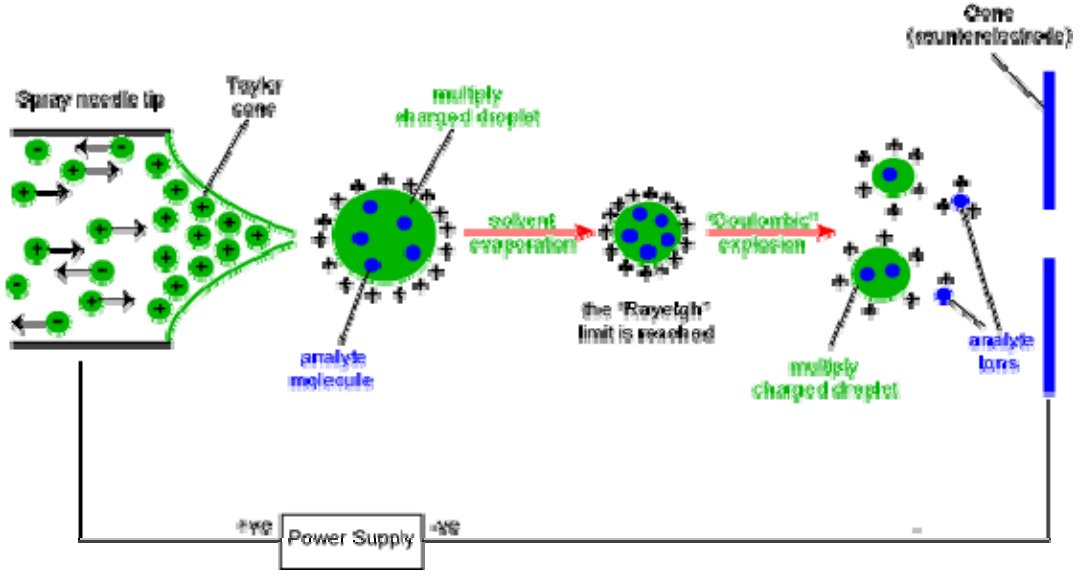

Figure 2.1

(figure taken from www.bris.ac.uk)

ESI can be applied to ionize a wide range of species ranging in size from several tens to several tens of thousands of mass units. While most commonly used to generate ions from large biopolymers such as peptides and proteins, ESI can also be employed to make ionic clusters and metal complexes, including those held together

by hydrogen bonding and other non-covalent interactions. For example, in the intrinsic hydration of monopositive uranyl hydroxide, nitrate, and acetate cations studies, uranyl nitrate solid dissolved in deionized H_2O will produce, by ESI, ions with the general formula $(UO_2A(S)_n)^+$ where A is an anion such as nitrate or hydroxide, and S are solvent molecules like H_2O.

2.3 Quadrupole Ion Trap Analyzer (QIT)

There are many advantages associated with the quadrupole ion trap mass analyzer. These include high sensitivity and mass resolution accompany, and the potential for multiple stage “tandem in time” mass spectrometry experiments. The quadruple mass filter and quadruple ion trap were invented by Wolfgang Paul and co-workers in the early 1950, to determine the mass to charge ratio of ions [15]. Initial development of the quadrupole ion trap analyzer was of interest primarily to the physics community [15]. However, with the development of “mass-selective stability” mode of operation by Hans Dehmelt, more practical uses of the ion trap analyzer, particularly for chemical analysis were invented. Two of the most important advancements that led to the modern use of the ion trap, use of mass selective instability and Helium gas within the trapping volume, were made by George Stafford and co-workers at Finnigan MAT [15]. These two developments simplified operation

of the instrument and significantly improved the mass resolution. The operation of the ion trap mass analyzer is based on ion motion due to the application of quadropolar radio-frequency (rf) electric fields. A classic quadrupole ion trap mass analyzer typically consists of three electrodes with hyperbolic surfaces, a central ring electrode, and two adjacent end cap electrodes shown in figure 2.2-1 and 2.2-2 [15].

The quadrupole ion trap mass analyzer acts as an “electric field test-tube” which confines the gaseous ions in either a positive or negative mode. The confining capacity begins from the forces exerted by application of rf and dc voltages to the central ring and end-cap electrodes.

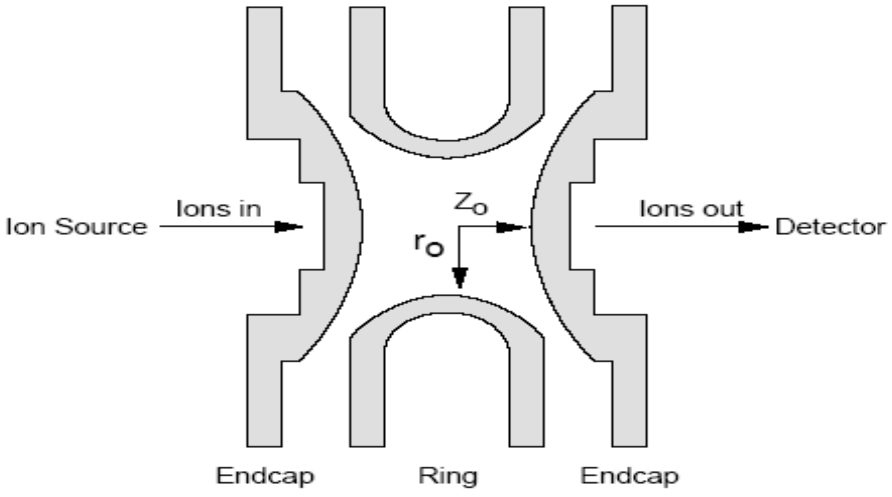

Figure 2.2 Quadrupole mass analyzer

http://www.abrf.org/ABRFNews/1996/September1996/sep96iontrap.html

In the ion trap, ionized molecules collide with a damping gas, usually helium or

argon deliberately introduced into the trap. The collisions with the damping gas are important because they thermalize the ions, and thus decrease their internal energy on average. In addition, the collisions direct ion trajectories toward the center of the ion trap. Thermalization is important, as collisional activation to induce dissociation involves “pumping” ions with a well defined average internal energy that is relatively low. The collection of ions in the center of the ion trap is important to the resolving power of the ion trap in the mass-selected instability mode, as mass measaurement is based on mass-selective ejection of ions from the center of the trap to a detector.

In the trap, and confined to the center by the damping gas, ions oscillate within the x and y plane at frequencies which depend on their m/z values. The theory behind the ion motion is described by mathematical equation known as the Mathieu equation. Mathieu’s studies of the region of stability and instability in a dynamic quadrupolar electric field can be applied to describe the ion’s trajectories in the trap during ion confinement. In the figure 2.3, the Mathieu stability diagram shows the shaded region between radial and axial stability. An ion of certain m/z will have a_z and q_z Mathieu parameter values according to the amplitude of the voltage applied to the ring electrode of the ion trap.

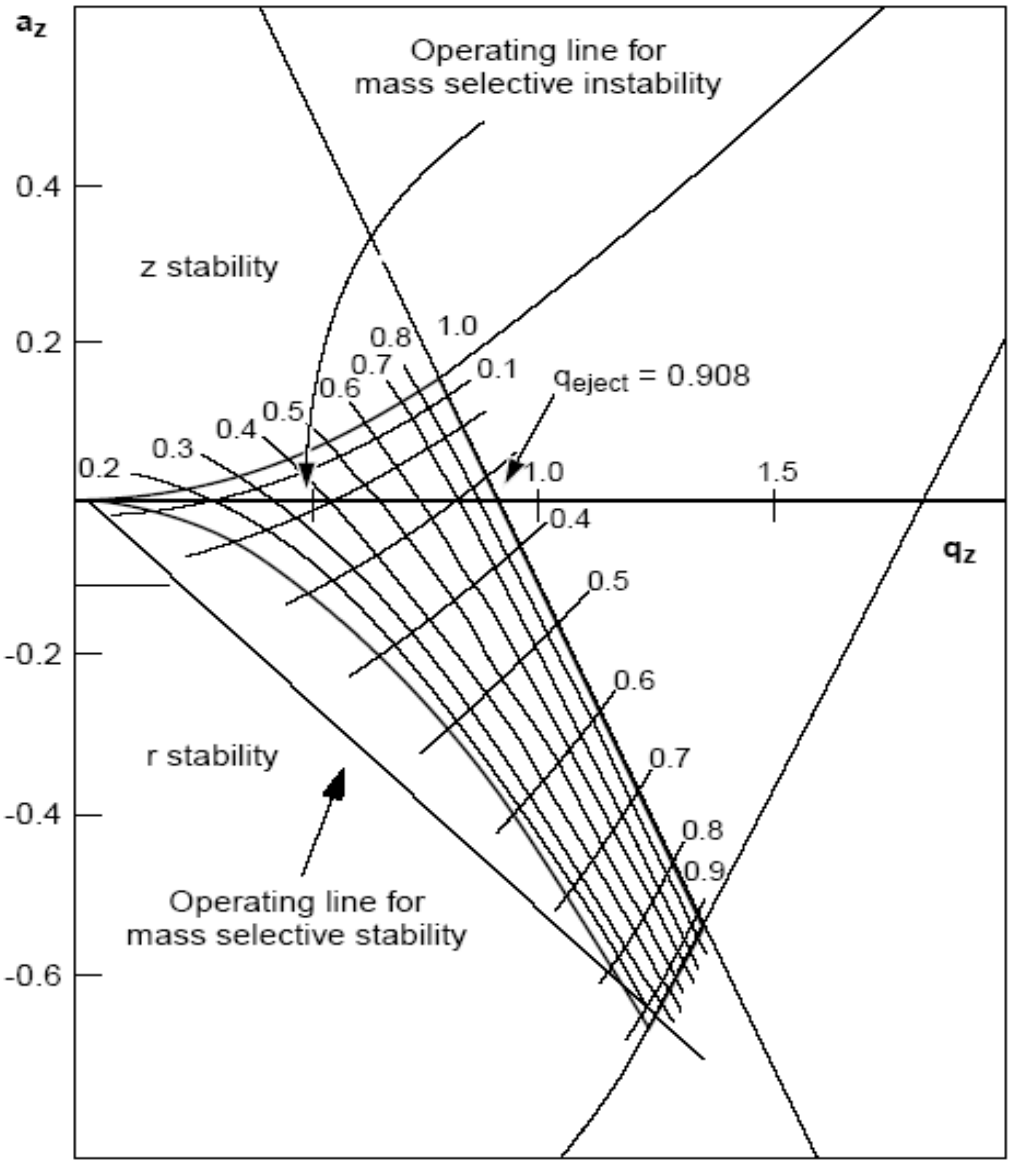

Figure 2.3 The Mathieu stability diagram for the quadrupole ion trap

Figure taken from

http://www.abrf.org/ABRFNews/1996/September1996/sep96iontrap.html

These values can either fall within or out of the boundaries of the stability diagram. Ions are stable in both the r and the z-direction when the parameter a_z, and q_z fall within the shaded area, and in this case the ion will be trapped within the

volume of space defined by the quadrupolar field. When the parameters lie outside the boundaries of the stability region the ion will be ejected. Use of the ion trap for mass analysis involves altering the potential applied to the electrodes such that ions of specific m/z values are given Matthieu a and q values such that they fall outside the stability region. When this happens, the ions are ejected from the ion trap, strike a detector sensitive to charged particles, and are counted [16].

2.4 Reagents and Experimental Procedure

The experiments described in this thesis cover a wide range of topics. For each study, mass spectra, collision-induced dissociation and ion-molecule reactions were investigated using a Finnigan LCQ-Deca quadrupole ion-trap mass spectrometer (ThermoFinnigan Corporation, San Jose, CA). Reagent information for the experiments described in each chaper are provided here. Specific experimental details relevant to each experimental trial are provided in the individual chapters. The uranyl nitrate stock solution and respective water:alcohol solutions were infused into the instrument using the syringe pump at a flow rate of 5 μL/min. The atmospheric pressure ionization stack settings (transfer lens voltages, quadrupole and octapole voltage offsets and tube lens voltage) were optimized for maximum ion transmission to the ion trap mass analyzer by using the auto-tune

routine within the LCQ Tune program. Following the instrument tune, the spray needle voltage was maintained at +5 kV and the N_2 sheath gas flow at 25 units (arbitrary to the LCQ instrument, corresponding to approximately .375 liters/min). To ensure maximum yield of solvated uranyl cation complexes, the capillary (desolvation) temperature was maintained between 110 °C and 130 °C. The ion trap analyzer was operated at a pressure of ~1.5 X 10^{-5} torr. Helium gas was used as the bath/buffer gas to improve trapping efficiency and as the collision gas for CID experiments.

(1). $UO_2(NO_3)_2 \cdot 6H_2O$ was purchased from Fluka/Sigma-Aldrich (St. Louis, MO) and was used as received. Methanol (MeOH), ethanol (EtOH),1,1-d_2 ethyl alcohol (d_2EtOH), 2,2,2-d_3 ethyl alcohol (d_3EtOH), ethyl-d5 alcohol (d_5EtOH) and *n*-propanol (*n*-PrOH) were purchased from Aldrich Chemical (St. Louis, MO) and used as received. A stock solution (1X10^{-3} M) of $UO_2(NO_3)_2 \cdot 6H_2O$ was prepared by dissolving the appropriate amount of solid material in deionized H_2O.

(2). Intrinsic Hydration of Monopositive Uranyl Hydroxide, Nitrate, and Acetate cations, in this studies uranyl nitrate hexahydrate, $UO_2(NO_3)_2 \cdot 6H_2O$, and acetate were purchased from Fluka/Sigma-Aldrich, and it was used as received. Prepared uranyl nitrate and acetate solution in mixture of deionized water were introduced into the mass spectrometer by electrospary ionization wih constant flow rate of 3-5 μl/min.

(3). In the third studies of collision induced dissociation of desferrioxamine siderophore, desferrioxamine (DEF), uranyl nitrate hexahydrate, Methanol, Methanol-*d1* (CH_3OD), D_2O and acetic anhydride were purchased from Aldrich Chemical (St. Louis, MO, USA) and were used as received. Stock solution of $1x10^{-3}$ concentration of uranyl nitrate and the same concentration of Fe(III) nitrate, Ca nitrate, and DEF were generated by mixing appropriate amount of solids and dissolving in deionized water. DEF was mixed with uranyl nitrate, Fe(III) nitrate, and Ca nitrate separately for collision induced dissociation analysis.

(4). Uranyl nitrate hexahydrate, $UO_2(NO_3)_2•6H_2O$ was purchased from Fluka/Sigma-Aldrich (St. Louis, MO) and used as received. 2-propanol (2-PrOH), d_6 2-propanol (d_6 2-PrOH, $[(CD_3)_2CHOH]$), and d_7 2-propanol (d_7 2-PrOH, $[(CD_3)_2CDOH]$) were purchased from Aldrich Chemical (St. Louis, MO) and used as received. A stock solution ($1x10^{-3}$ M) of $UO_2(NO_3)_2•6H_2O$ was prepared by dissolving the appropriate amount of solid material in deionized H_2O.

(5). The uranyl oxide (UO_3) used to prepare the various uranyl-anion solids examined in this study was a gift from J. David Van Horn at the University of Missouri-Kansas City. Solids assumed to be uranyl chloride, $UO_2(Cl)_2•(H_2O)_x$; bromide, $UO_2(Br)_2•(H_2O)_x$; iodide, $UO_2(I)_2•(H_2O)_x$ and perchlorate; $UO_2(ClO_4)_2•(H_2O)_x$ were prepared by first dissolving solid UO_3 in the respective mineral acids, followed

by evaporation over gentle heat to dryness. Our goal was not the rigorous synthesis of uranyl-halide compounds, but precursor materials for production of gas-phase uranyl-halide complexes by ESI. Preparation of a fluoride version was not attempted. For ESI, stock solutions (ca. 10^{-3} M based on measured amount of solid and assumed composition) of each uranyl solid were prepared by dissolving the appropriate amount of material in deionized H_2O.

(6). Uranyl nitrate hexahydrate, $UO_2(NO_3)_2 \bullet 6H_2O$ was purchased from Fluka/Sigma-Aldrich (St. Louis, MO) and used as received. A stock solution of uranyl nitrate solutions (1 mM concentration) was prepared by dissolving the appropriate amount of solid in deionized H_2O. Spray solutions for the ESI experiment were prepared by combining portions of the $UO_2(NO_3)_2 \bullet 6H_2O$ stock solution with acetone such that the composition ranged from 2-75% acetone by volume.

(7). Uranyl nitrate hexahydrate, $UO_2(NO_3)_2 \bullet 6H_2O$ was purchased from Fluka/Sigma-Aldrich (St. Louis, MO). Acetonitrile (acn), propionitrile (pn), and benzonitrile (bzn) (>99% purity) were purchased from Aldrich Chemical (St. Louis, MO) and used as received. A stock solution of uranyl nitrate (1 mM concentration) was prepared by dissolving the appropriate amount of solid in deionized H_2O. Spray solutions for the ESI experiment were prepared by combining portions of the $UO_2(NO_3)_2 \bullet 6H_2O$ stock solution and nitrile in a 1:100 relative molar ratio. For 1 mL

total solution volume, the amount of nitrile added ranged from 5μ-L for acn to 9.8μ-L for bzn.

(8) The spray solutions used in the binding of molecular O_2 to di- and tri-ligated $[UO_2]^+$consisted of the uranyl nitrate dissolved in a concentration of 1mM in 10% volume and volume of acetone and water.

CHAPTER 3

ELUCIDATION OF THE COLLISION INDUCED DISSOCIATION PATHWAYS OF WATER AND ALCOHOL COORDINATED COMPLEXES CONTAINNG THE URANYL CATION

INTRODUCTION

In previous decades, reaction between small molecules of O_2, CO, CO_2, COS, or D_2O and U^+ were extensively studied by Armentrout and Beauchamp [103]. Later studies by Gibson, and by Schwartz and coworkers involved reactions of U^+ and UO^+ with organic compounds such as alkanes and alcohols [17-20]. Studies by Duckworth and coworkers [21], Schwarz and coworkers [22], and Gibson [23] later demonstrated the tendency for U^+ to be oxidized other small molecules. All of these studies involved lower oxidation states of uranium; however, the typical complexes in the solution phase and the environment feature uranium in higher oxidation states such as IV and VI.

In these experiments, the use of ESI and ion-trap mass spectrometry to study intrinsic chemistry of species that contain uranyl ion (uranium in the +6 oxidation state) was investigated. Of particular interest was the types of species that could be generated using ESI, and the fragmentation pathways for these ions when subjected to CID and multiple-stage tandem MS.

EXPERIMENTAL

ESI mass spectra were collected using the Finnigan LCQ-Deca ion-trap mass spectrometer. For detail experimental parameters please refer to section 2.4. CID experiments were performed by setting the isolation width between 5 and 12 u (depending on the species), the activation Q, which is used to adjust the *q* value for the resonant excitation of the precursor ion during the CID portion of the experiment, was set at .3 and the (mass) normalized collision energy at 10–20% (of 5 V). In all cases, activation times for CID were 30 ms.

RESULTS AND DISCUSSION

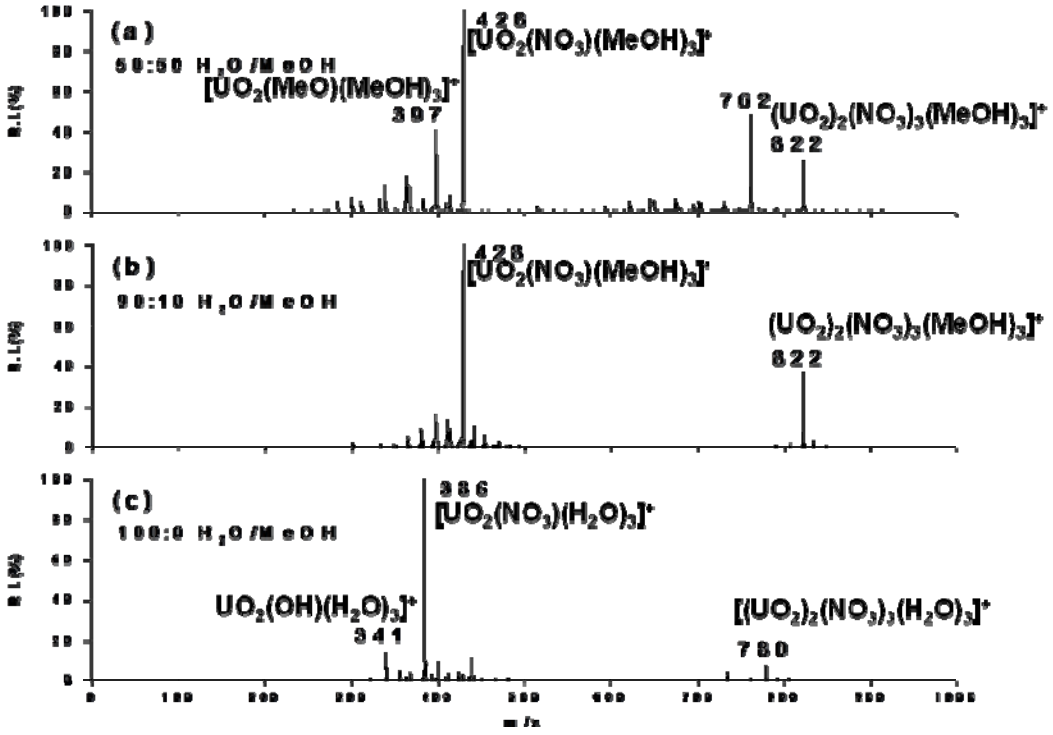

Figure 3.1 (a), 3.1 (b), and 3.1 (c)

Figure 3.1 shows mass spectra that were generated from experiments in which $UO_2(NO_3)_2$ was dissolved in three different solvent systems. Figure 3.1 (a) shows the peaks generated by ESI when $UO_2(NO_3)_2$ was dissolved in a 50:50 mixture of H_2O and MeOH. The spectrum shown in Figure 3.1 (b) was collected from a sample composed of $UO_2(NO_3)_2$ dissolved in 90:10 H_2O/MeOH, while the spectrum in Figure 3.1 (c) was generated using a solution of $UO_2(NO_3)_2$ dissolved in deionized H_2O, without MeOH. In figures 3.1 (a) and 3.1 (b), the m/z value for the dominant ion is consistent with a composition that includes a single UO_2^{2+} cation, one nitrate anion and three coordinating MeOH molecules, and is expressed as $[UO_2(NO_3)(MeOH)_3]^+$. An analogous species, with MeOH replaced by H_2O, was observed at m/z 386 in the spectrum of uranyl nitrate dissolved in deionized H_2O, $[UO_2(NO_3)(H_2O)_3]^+$. The less abundant ion at m/z 341 is assigned the composition $[UO_2(OH)(H_2O)_3]^+$, i.e. the nitrate anion was replaced by hydroxide. A prominent peak was found at m/z 397 when the solvent system contained a large fraction of MeOH, the m/z value for this ion is consistent with formation of a complex that includes UO_2^{2+}, MeO^-, and three coordinating MeOH molecules, $[UO_2(MeO)(MeOH)_3]^+$. In addition, in the lower mass region of the spectrum there were complex ions containing UO_2^{2+} with either nitrate or MeO^- as anion and 1 or 2 H_2O or MeOH molecules as coordinating ligands.

The ions that appear in the upper mass range, at m/z 822 and m/z 780, in figures

3.1 (a) and 3.1 (c), respectively can be assigned compositions that suggest the addition of a single, stoichiometric $UO_2(NO_3)_2$ unit to the species at 428 and 386, respectively. A third prominent peak with a m/z value of approximately 762 was also observed. Attempts to isolate the m/z 762 peak for a high resolution scan to measure an accurate m/z value failed, which suggests that the ion is unstable and decomposes during the slow scan out rates associated with the high-resolution scans. There are several possible composition assignments for this mass; however, identification of the particular mass remains uncertain.

Alcohol	m/z	Composition
Methanol	333	$[UO_2(MeO)(MeOH)]^+$
	365	$[UO_2(MeO)(MeOH)_2]^+$
	397	$[UO_2(MeO)(MeOH)_3]^+$
	364	$[UO_2(NO_3)(MeOH)]^+$
	396	$[UO_2(NO_3)(MeOH)_2]^+$
	428	$[UO_2(NO_3)(MeOH)_3]^+$
	762	Unidentified
	822	$[UO_2(NO_3)_3(MeOH)_3]^+$
Ethanol	361	$[UO_2(EtOH)(EtOH)]^+$
	407	$[UO_2(EtO)(EtOH)_2]^+$
	452	$[UO_2(MeO)(EtOH)_3]^+$
	378	$[UO_2(NO_3)(EtOH)]^+$
	424	$[UO_2(NO_3)(EtOH)_2]^+$
	470	$[UO_2(NO_3)(EtOH)_3]^+$
	864	$[UO_2(NO_3)_3(EtOH)_3]^+$
n-Propanol	369	$[UO_2(nPrO)(nPrOH)]^+$
	449	$[UO_2(nPrO)(nPrOH)_2]^+$
	509	$[UO_2(nPrO)(nPrOH)_3]^+$
	393	$[UO_2(nPrO)(nPrOH)]^+$
	452	$[UO_2(nPrO)(nPrO)_2]^+$
	512	$[UO_2(NO_3)(nPrO)_3]^+$
	906	$[UO_2(NO_3)_3(nPrO)_3]^+$
No alcohol	305	$[UO_2(OH)(H_2O)]^+$
	323	$[UO_2(OH)(H_2O)_2]^+$
	341	$[UO_2(OH)(H_2O)_3]^+$
	350	$[UO_2(NO_3)(H_2O)]^+$
	368	$[UO_2(NO_3)(H_2O)_2]^+$
	386	$[UO_2(NO_3)(H_2O)_3]^+$
	780	$[UO_2(NO_3)_3(H_2O)_3]^+$

Table 3.1. The table show compositions of prominent ions observed in the ESI mass spectra of uranyl nitrate sprayed from alcohol/water solutions.

In the 50:50 H_2O/MeOH solution of $UO_2(NO_3)_2$, the dominant ions generated by ESI contain MeOH ligands around uranyl-anion cores. When the solvent system was switched to 90:10 H_2O/MeOH, the MeOH-coordinated uranyl-anion species were still present if not dominant in the ESI mass spectrum. The persistence of the MeOH-solvated complex ions suggests that UO_2^{2+} has a higher affinity for alcohol molecules than for H_2O, which is consistent with the tendency for alcohols to be stronger donors to metal ions in the gas phase [24].

Table 3.1 shows the composition assignments for the major species generated by ESI, using spray solutions of $UO_2(NO_3)_2$ dissolved in 50:50 ROH/H_2O where ROH was methanol, ethanol, or n-propanol. These peak composition assignments were further verified by multiple-stage CID, except for those unstable species that did not survive the ion isolation step required for the dissociation experiment. An investigation of n-butanol in the spray solvent system was made. However, precipitation of solid, presumably uranyl-butoxide, within the fused silica transport capillary used in the ESI instrument, resulted, and mass spectra were not collected.

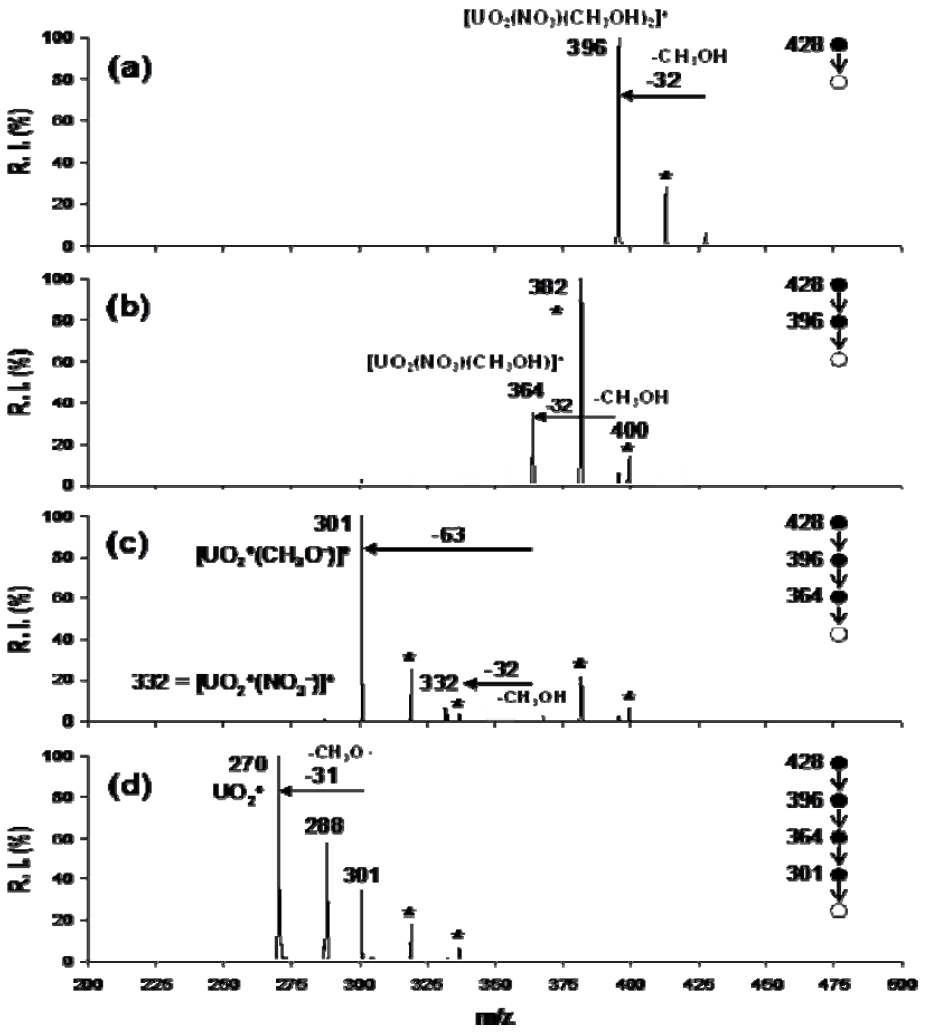

Figure 3.2 (a), (b), (c), (d) Multiple stage CID spectra of $[UO_2(NO_3)(MeOH)_3]^+$

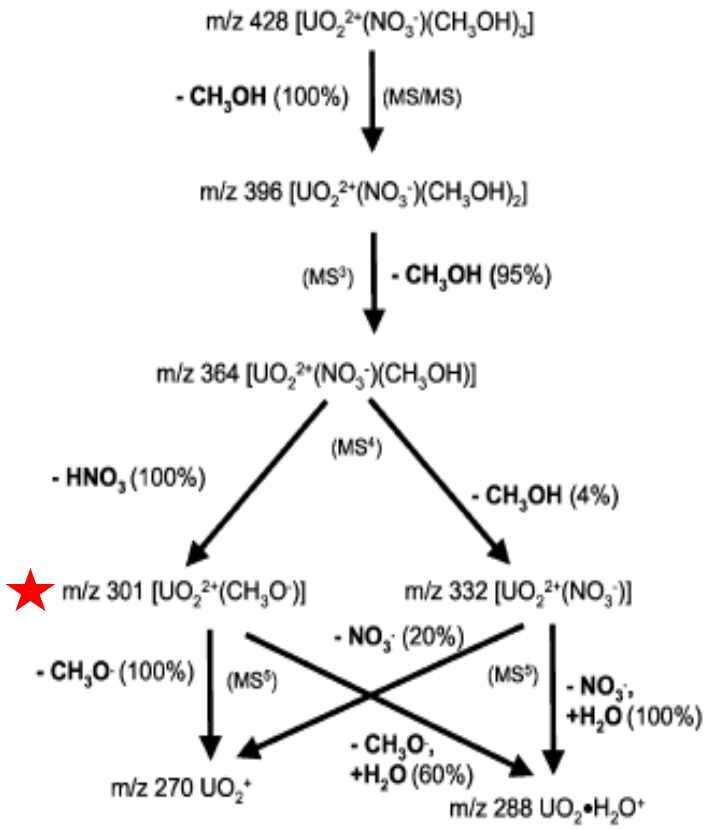

Scheme 3.1 MS^n pathways for the dissociation of $[UO_2(NO_3)(MeOH)_3]^+$

The multiple-stage CID of $[UO_2(NO_3)(MeOH)_3]^+$ at m/z 428 provides a representative illustration of the fragmentation behavior for the alcohol-containing complexes. Figure 3.2 shows the product ions produced by $[UO_2(NO_3)(MeOH)_3]^+$. The product ion spectra produced at each CID stage were complex, containing both product ions from fragmentation reactions, and H_2O adducts to those product ions formed by association reactions with adventitious H_2O present as a contaminant in the He buffer/bath gas (H_2O adducts are identified with * in figures). Peaks that are H_2O adducts of products generated by CID can be identified by very characteristic

peak tails and chemical mass shifts (shifts of ~.2-.3 mass units lower than expected mass) [26]. In addition, the adducts can be identified in our experiments by isolating expected product ions in the ion trap for periods of 100-300 msec, without an imposed collisional activation. During the isolation step, all ionized species except the one chosen for storage are resonantly ejected from the ion trap. The appearance of peaks 18 mass units higher than the isolated ion is indicative of the formation of H_2O adducts; [9-11] the abundance of the adducts generally increases as the isolation and storage time are extended. The formation of abundant H_2O adducts indicates that several of the uranyl complex ions show a significant tendency to accept ligands via gas-phase association reactions in the ion trap. The reaction kinetics for the addition of one or more H_2O ligands to UO_2^{2+} and related species generated by ion-induced sputtering of solid UO_3 has been investigated [25]. The kinetics for the addition of H_2O to uranyl-nitrate, -hydroxide and –acetate will be described in a later chapter

The fragmentation pathways for the multiple-stage CID of the m/z 428 ion, $[UO_2(NO_3)(MeOH)_3]^+$, are shown in scheme 3.1. The principal fragmentation pathway for $[UO_2(NO_3)(MeOH)_3]^+$ involved a loss of 32 mass units (u), which is attributed to the elimination of a single MeOH ligand. In the next CID stage (MS^3), a second MeOH molecule was eliminated to generate $[UO_2(NO_3^-)(MeOH)]^+$ at m/z 364.

A second, minor, pathway involved the loss of 95 u, consistent with the elimination of MeOH and HNO_3, to produce an ion at m/z 301. CID of $[UO_2(NO_3)(MeOH)]^+$ (m/z 364) leads primarily to loss of HNO_3 to generate $[UO_2(MeO)]^+$ at m/z 301 (shown next to a red star). Formation of the uranyl methoxide species is consistent with the general tendency of lanthanide and actinide species to form alkoxides complexes [44-46].

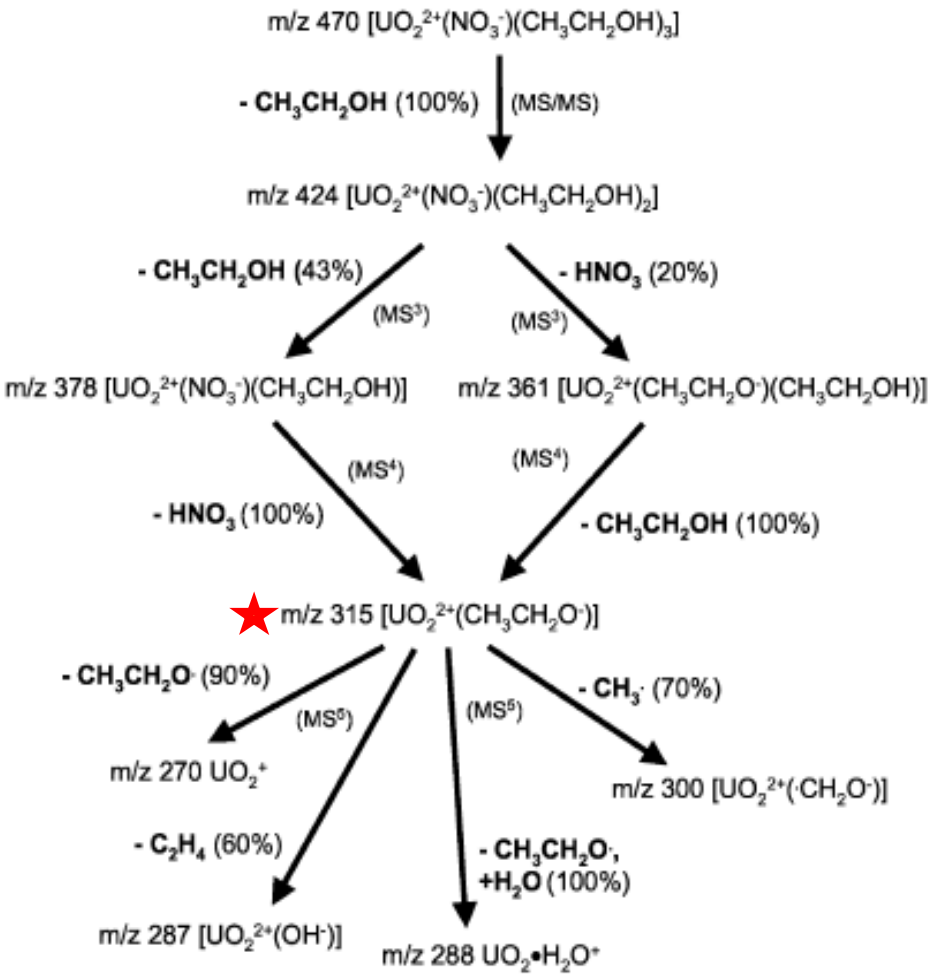

Scheme 3.2. MS^n pathways for the dissocitation of $[UO_2(NO_3)(EtOH)_3]^+$.

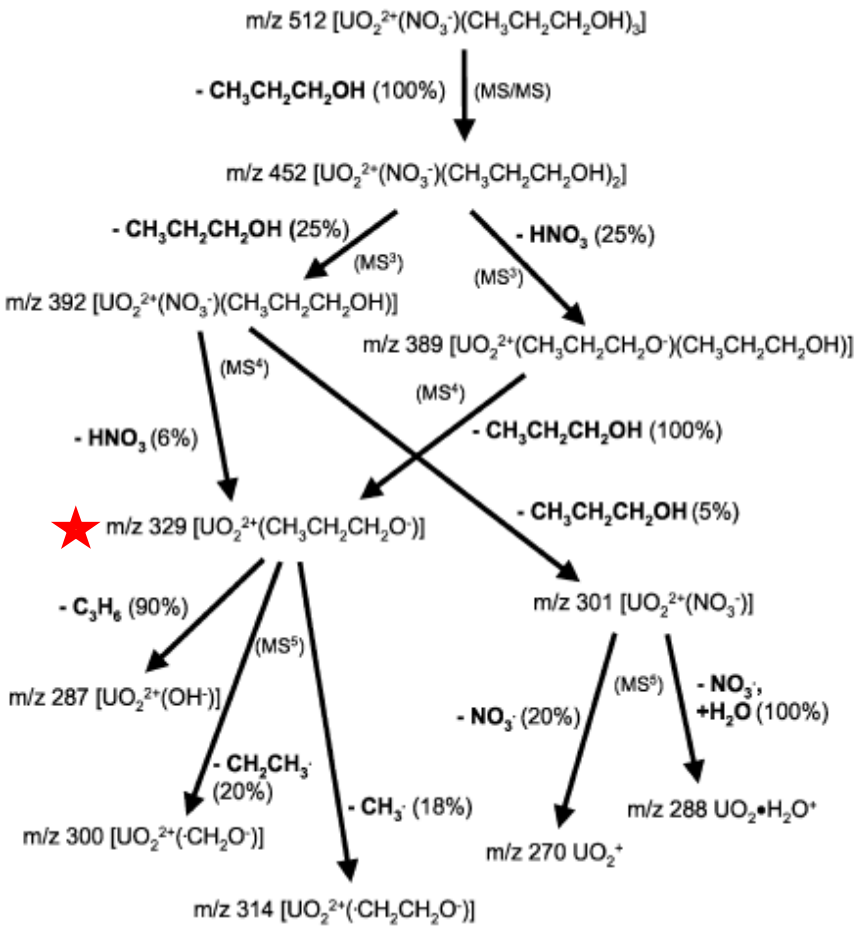

Scheme 3.3. MS^n pathways for the dissociation of $[UO_2(NO_3)(nPrOH)_3]^+$.

The multiple-stage CID pathways for $[UO_2(NO_3)(EtOH)_3]^+$ and $[UO_2(NO_3)(nPrOH)_3]^+$, shown in schemes 3.2 and 3.3 were largely the same as the pathway measured for $[UO_2(NO_3)(MeOH)_3]^+$, including the formation at the end of the fragmentation cascade of $[UO_2(EtO)]^+$ and $[UO_2(n\text{-}PrO)]^+$ at m/z 315 and 329, respectively. However, several major differences were oberseved. An increasing tendency for the larger, ligated alkoxide complexes to eliminate HNO_3 was one of the major differences. The tendency to lose HNO_3 in earlier stages of the multiple-stage

CID experiment followed the trend n-PrOH > EtOH > MeOH. Loss of HNO_3 from the gas-phase complexes must involve transfer of a proton from a bound alcohol ligand to the nitrate ligand and the trend observed is consistent with the known acidities of the alcohols in the gas phase [27,28], which increases with the size of the alkyl group. The second difference between the ethanol and n-propanol from methanol as ligands was the activation of fragmentation pathways that involved cleavage of C-C bonds within the alcohol ligand. The third observed difference was the formation of uranyl hydroxide $[UO_2(OH)]^+$ at the MS^5 stage of a product ion. CID of $[UO_2(OH)]^+$ produced m/z 270 (UO_2^+) by the elimination of 17u. In the case of $[UO_2(EtO)]^+$, formation of $[UO_2(OH)]^+$ involves transfer of an H atom from the alkyl group to the oxygen atom, with the elimination of a neutral alkene as shown in scheme 3.4. Therefore the tendency to form uranium complexes with alkoxides being the anion and alcohol as the coordination ligands increases as the size of alcohol increase.

The MS^n pathways of $[UO_2^{2+}(NO_3^-)(H_2O)_3]^+$ m/z 386 were also obtained and evaluated under CID in the ion trap from the aqueous solution of $UO_2(NO_3)_2$ shown in figure 3.3. Elimination of H_2O molecules occurred when $[UO_2(NO_3)(H_2O)_3]^+$ was subjected to multiple stage CID, ultimately furnishing the uranyl-nitrate ion, $[UO_2(NO_3)]^+$, at m/z 332. Subsequent CID of the $[UO_2(NO_3)]^+$ resulted in the formation of product ions at m/z 270 and 288. The ion at m/z 288 is the reduced

form of uranyl ion [UO_2^+] coordinated by water. Further CID on ion at m/z 288

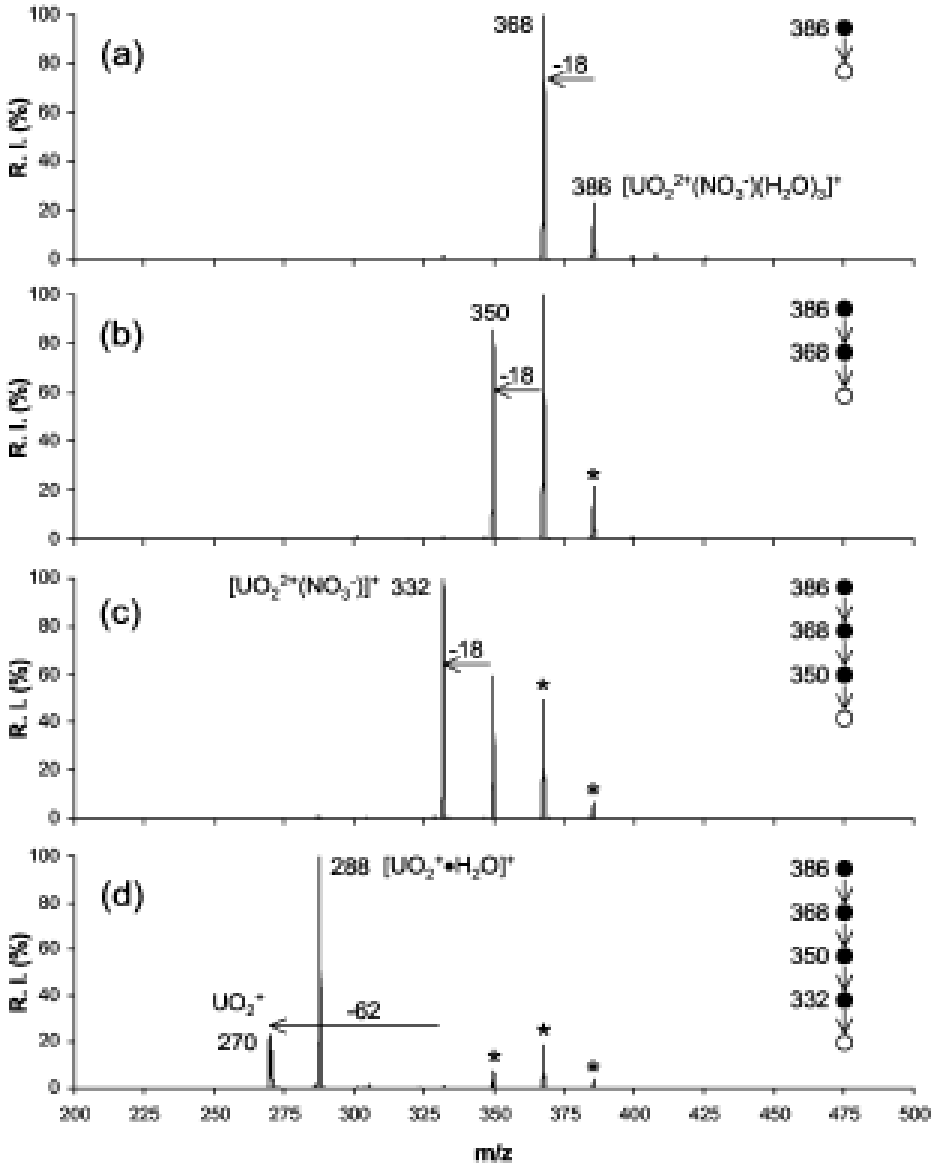

Figure 3.3 MS^n stage CID spectra of the $[UO_2(NO_3)(H_2O)_3]^+$

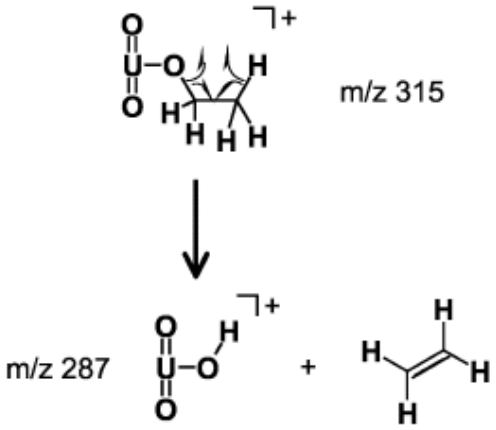

Scheme 3.4. Proposed reaction to generate m/z 287 from $[UO_2(EtO)]^+$

caused loss of 18 u, which is consistent with the loss of H_2O to form UO_2^+ at m/z 270. The m/z 288 ion is most likely generated through collisions in the ion trap that involve H_2O in the He bath gas, as in the reaction:

$[UO_2(NO_3)]^+ + H_2O \rightarrow [UO_2(NO_3)\ (H_2O)]^+ \rightarrow [UO_2(H_2O)]^+ + NO_3$

where formation of an activated intermediate with a composition of $[UO_2(NO_3)(H_2O)]^+$ is followed by loss of nitrate radical with the electron transfer to the uranyl ion to UO_2^+. The tendency to form an H_2O adduct to the uranyl center were observed in a similar fashion in the CID of $[UO_2(MeO)]^+$, and of $[UO_2(EtO)]^+$ species.

The multiple-stage CID of $[UO_2(OH)(H_2O)_3]^+$ at m/z 341 is shown in figure 3.5. The water ligands are eliminated in the MS/MS, MS^3, and MS^4 stages to ultimately furnish $[UO_2(OH)]^+$ at m/z 287. The reduced form of UO_2^{2+} at m/z 270 was generated when when $[UO_2(OH)]^+$ was subjected to an additional CID step.

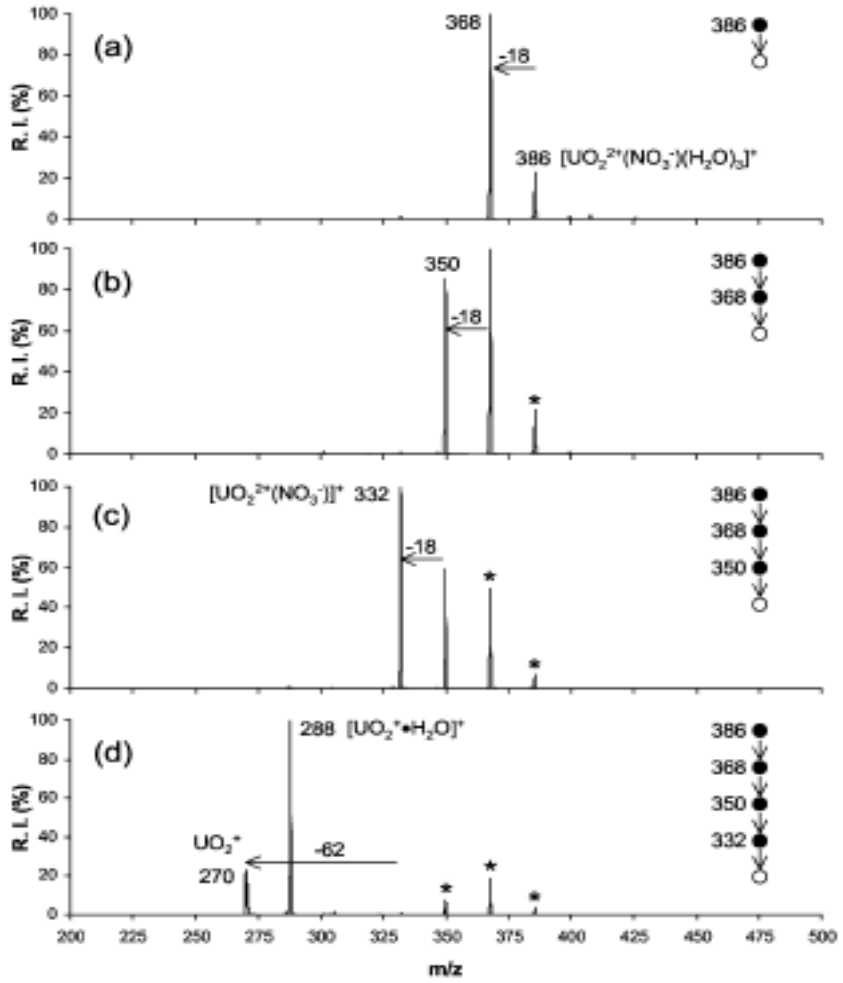

Figure 3.5 (a), (b), (c), (d). Multiple stage CID spectra of $[UO_2(OH)(H_2O)_3]^+$ which is a complex ion generated by ESI form $UO_2(NO_3)_2$ dissolved in the deionized water.

SUMMARY

ESI can be used effectively to generate gas-phase ions that contain uranium in a high oxidation state, U(VI) and coordinated by simple solvent molecules. Complex ions that contained UO_2^{2+} with counter anions such as hydroxide, nitrate or alkoxides and coordinating H_2O and alcohol ligands were produced easily using spray solutions

of $UO_2(NO_3)_2$ dissolved in deionized H_2O or H_2O/alcohol mixtures. The CID pathways for the complex ions can be divided into two general catergory: (a) those that involve the elimination of intact solvent ligands and (b) the elimination, in the case of nitrate complexes, of HNO_3 through a reaction that involves transfer of H from an alcohol ligand to nitrate.

CHATPER 4

INTRINSIC HYDRATION OF MONOPOSITIVE URANYL HYDROXIDE, NITRATE, AND ACETATE CATIONS

INTRODUCTION

As demonstrated in the experiments described in the previous chapter, the combination of electrospray ionization and ion-trap mass spectrometry can be used effectively to generate and study the intrinsic chemistry behavior of uranyl species. As was apparent in the CID studies of "solvated", gas-phase complexes featuring the uranyl ion coordinated by hydroxide, nitrate or a series of alkoxides [33], ions having the general formula $[(UO_2A)(S)_n]^+$, where A represents hydroxide, nitrate or alkoxide and S represented water or alcohol and $1 \leq n \leq 3$. While CID generally caused loss of one or more coordinating solvent ligands from the complex ion, myriad peaks representing formation of H_2O adducts to product ions were also observed. In the experiments described in this chapter, the goal was to determine whether "time-resolved" mass spectrometry could be used to study the temporal evolution of the H_2O adducts, using as precursors for the hydration reactions bare uranyl-hydroxide, uranyl-nitrate and uranyl-acetate cations. Significantly, these three types of anions represent those most likely to be found in and around regions of interred uranium waste. For these experiments, multiple CID stages were used to

eliminate coordinating water and/or acetic acid ligands from the “solvated” forms of the gas-phase cations to leave the monopositive cationic species $(UO_2A)^+$. These ions were then isolated and stored, without imposed collisional activation, to react with adventitious H_2O present in the ITMS for time periods ranging from 1 ms to 10 sec. From these experiments we have been able to determine relative intrinsic hydration tendencies for the complexes, which is an important step towards understanding the interactions between ligated uranium and solvent molecules.

EXPERIMENTAL

ESI-MS, multiple-stage CID and ion-molecule reactions were carried out using established procedures developed previously in the Van Stipdonk laboratory and described in detail in section 2.4 [30, 31, 33]. Briefly, all experiments were conducted using the Thermo-Finnigan LCQ-Deca ITMS. Stock uranyl nitrate or acetate solutions were prepared by dissolving the appropriate amount of the respective salts in deionized H_2O to produce a final UO_2^{2+} concentration of 1 mM. The stock solutions were infused into the ESI-MS instrument using the incorporated syringe pump at a flow rate of 5 µl/min.

CID was performed using isolation widths of 3 mass units, an activation Q (used to adjust the q_z value for the resonant excitation of the precursor ion during the CID

experiment) value of .3, activation amplitudes of 10-20% (of 5V) and activation times of 30 ms. Because the q_z value influences the kinetic energies of the trapped ions, a constant value was used when studying the reactions of precursor ions having different masses. The kinetic energy of the reactant ions is known to be inversely proportional to the rate of reaction, [34] principally because the reverse reaction of the activated complex is speeded up, and we found this to be explicitly true in our previous study of dioxo uranium cations [35]. Even though the studies reported in this chapter were conducted at pressures where the reverse reactions were probably negligible, utilization of a constant q_z value improves reaction comparability. For intrinsic hydration investigations, all charged species other than the uranyl complex of interest were resonantly ejected from the ion trap. For quantitative comparisons, the complex ions were isolated and stored within the ion trap for times ranging from 1 to 1000 ms, to react with H_2O present within the He bath gas. Following the isolation period, the precursor and product ions were scanned out of the trap and detected as part of the automated mass analysis operation.

Kinetic modeling of the addition of H_2O to the uranyl-anion complexes was performed as follows. Fractional abundances of reactant and product ions were calculated by dividing the relative intensities of the precursor (complex) ion and adduct ions by the total ion abundance. The changes in fractional abundances with

time were used to obtain relative values of the rate constants for the addition reactions using the Chemical Kinetic Simulator^{TM} software package (CKS), available through a no cost license on the IBM website, which employs a stochastic algorithm to model the reacting system [36-39]. The reactions involved were assumed to be kinetically simple, having rate equations based upon reaction stoichiometry. In reality, the water addition reactions are most likely ternary, that is, the He bath gas serves to collisionally stabilize activated intermediates and eliminate back reactions. Thus, the temporal evolution of the reactant ion and adduct intensities indicated that our experiments were conducted under pseudo-first order reaction conditions. [40] Previous studies have confirmed that the concentration of water present in the ion trap is large compared to the concentrations of solvent and reactant ion species that enter during the ESI process [31]. The rate constants for the addition reactions were changed incrementally until the concentration curves generated by the model fit the observed fractional abundances. The concentration of H_2O is a required input parameter for CKS and which kept constant during all experiments. Although concentration of water molecules in our ion trap cannot be quantitatively determined, [H_2O] was estimated at ~8 x 10^{10} molecules cm^{-3} (or half of the total pressure) based upon ambient conditions existing in the ion trap (298K and 5x10^{-6} torr). Uncertainty in [H_2O] in these experiments probably contributes most to the absolute uncertainty of

the rate constant measurements, and therefore the rate constant measurements are used in relative comparisons. The value measured for the reaction of $(UO_2OH)^+$ + H_2O was within 30% of the value independently measured using a different ion trap technique [35] which provides some confidence in the accuracy of the absolute *k* values [31]. Also, rate constants for the reaction that involves formation of the respective monohydrate species calculated using CKS were consistent with the order of magnitude of maximum rate constants predicted using the average dipole orientation (ADO) theory, [23,41,42] which has been successfully employed to interpret kinetic data for other chemical systems investigated using ion trap mass spectrometers. [43, 44] Rate constants calculated for the formation of the second and third hydrates were fairly insensitive to minor adjustments in the rate constants (5%-20%) but larger changes created significant deviation of the modeled concentration curves from the observed fractional abundances.

Precision in the rate constant measurements was dependent on the experimentally derived kinetic profiles; for trials conducted on the same day, the precision of individual ion abundances were on the order of 5-10% (relative standard deviation), and all trends were fully reproducible in 5 separate trials. Rate constant precision was bounded by calculating maximum and minimum values for the initial hydration reactions from 'bootstrapped' data sets generated by incorporating

abundance values from individual data sets that showed the largest variations. These analyses showed a maximum deviation of ~9% compared with the average values reported herein.

Preliminary ab-initio calculations were performed using the Gaussian 98 group of programs. [45] Our principal interest was in the lowest energy conformation of the uranyl-anion trihydrate complexes rather than absolute energy, enthalpy and free energy values. The complexes were optimized using density functional theory calculations and the B3LYP-SDD basis set. To test the general accuracy of the calculations for the determination of most-probable complex *geometry*, conformations of tetra-, $[UO_2(H_2O)_4]^{2+}$, and pentahydrated, $[UO_2(H_2O)_5]^{2+}$, uranyl ion were modeled. The lowest energy conformations for both species, as generated using the B3LYP-SDD basis set, matched those reported in previous studies of similar systems using other basis sets. [46, 47]

Results and Discussion:

Figure 4.1 shows the kinetic profiles for the intrinsic hydration of (a) $(UO_2OH)^+$, (b) $(UO_2NO_3)^+$ and (c) $(UO_2CH_3CO_2)^+$: in all three examples, decreasing precursor ion abundance was accompanied by increases in the abundance of species representing the addition of a first, second and third H_2O ligand. The addition of a fourth H_2O ligand was not observed, even when the isolation time was extended to 10 seconds.

The reaction schemes used for kinetic modeling and associated pseudo-first order rate constants are shown below.

$$(UO_2A)^+ + H_2O \rightarrow [(UO_2A)(H_2O)]^+ \qquad k_1$$

$$[(UO_2A)(H_2O)]^+ + H_2O \rightarrow [(UO_2A)(H_2O)_2]^+ \qquad k_2$$

$$[(UO_2A)(H_2O)_2]^+ + H_2O \rightarrow [(UO_2A)(H_2O)_3]^+ \qquad k_3$$

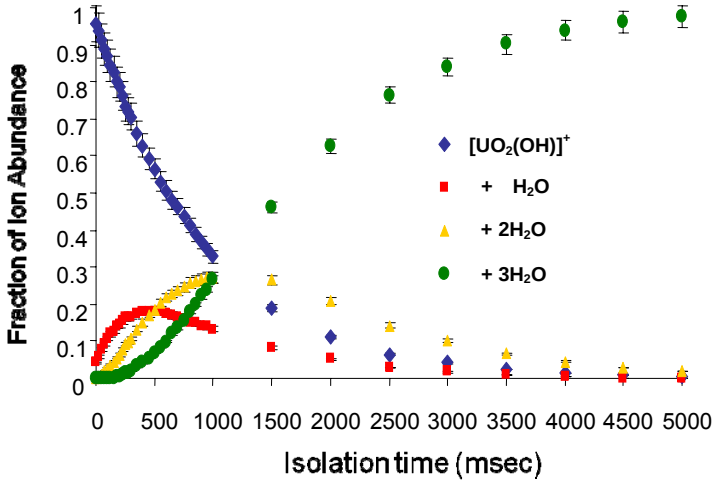

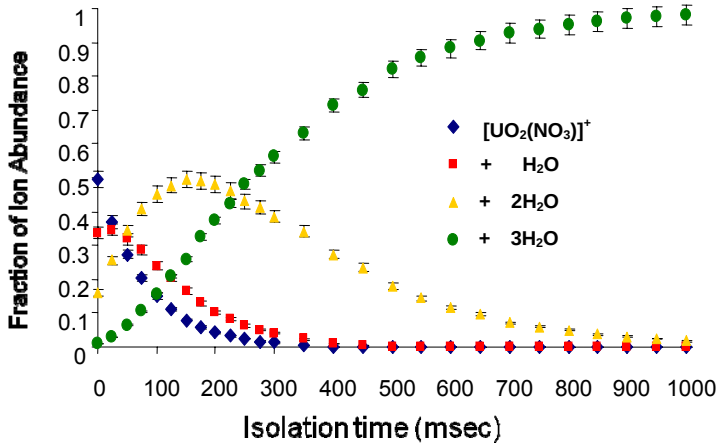

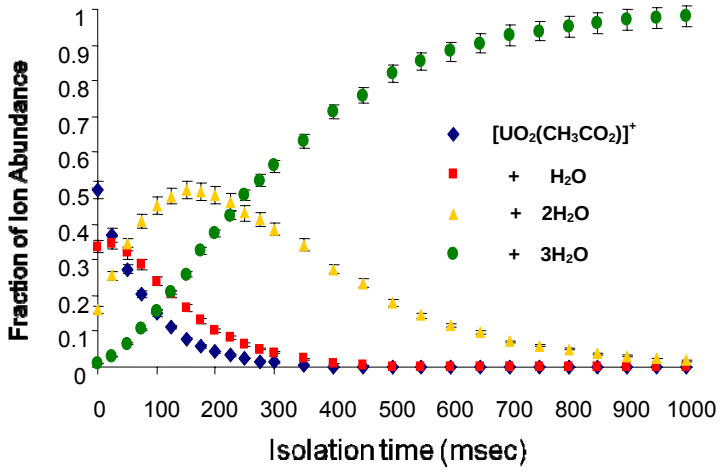

Figure 4.1. Kinetic profiles for the intrinsic gas phase hydration of $[UO_2OH]^+$ (b) $[UO_2NO_3]^+$ (c) $[UO_2CH_3CO_2]^+$. Note the differences in the isolation time scales due to $[UO_2OH]^+$ specie is reactive in longer time period. The standard deviation is represented

For reaction 1, which involves the uranyl-hydroxide cation, $(UO_2OH)^+$, no reverse reactions were needed to accurately model the hydration kinetics. This is contratry to an earlier study of the hydration of $(UO_2OH)^+$ [35] using an ion trap-secondary ion mass spectrometer (IT-SIMS). In the earlier study it was stated that addition of back reactions was necessary to computationally replicate the observed kinetic profiles. The different observations between the earlier SIMS measurement and the ESI-ITMS result from this set of experiments probably reflect the fact that the uranyl species in the secondary ion mass spectrometry experiments were allowed to react at partial pressures of H_2O that were at least an order of magnitude lower than in the ESI-ITMS experiments, and thus may not have been completely thermalized. In fact, recent

studies [21, 48] suggest that the buffer gas in the ion trap can assist in the dissipation of excess reaction energy, which supports this hypothesis.

The treatment of reaction rates for the IT-SIMS experiments resulted in explicit rate constants for both the forward and reverse reactions, which allows for a comparison of the k_1 values measured in the two experiments. The value of 3×10^{-11} $cm^3s^{-1}molecule^{-1}$ measured using the ESI-MS is in good agreement with the value of 4×10^{-11} $cm^3s^{-1}molecule^{-1}$ measured previously using the IT-SIMS. [40]

Computed rate constants for the addition of the first H_2O ligand in table 4.1 were found to decrease in the order $(UO_2CH_3COO)^+ \geq (UO_2NO_3)^+ >> (UO_2OH)^+$, and were greater by a factor of ~10 for the acetate and nitrate containing complexes when compared to the hydroxide version. Within experimental error, rate constants for addition of a second H_2O ligand did not change significantly for $(UO_2NO_3)^+$ and $(UO_2CH_3COO)^+$. In contrast to the behavior observed for nitrate and acetate, addition of the second H_2O ligand to $(UO_2OH)^+$ was > 3 times faster than addition of the first H_2O (again in close agreement with the results of the recent IT-SIMS study. [35]). Rate constants for the addition of the third H_2O ligand were lower (relative to the constants for the addition of the second H_2O) by factors of ~ 2, 3 and 6 for $(UO_2OH)^+$, $(UO_2NO_3)^+$ and $(UO_2CH_3COO)^+$, respectively.

Ion-molecule complex formation rates in the gas phase depend upon intrinsic

factors such as the masses of the species involved, ionic charge, molecular polarizability and molecular dipole moment, and the dependence upon these factors has been quantified using reparameterized average-dipole-orientation (ADO) theory [50-51]. ADO theory has been used to predict capture rate constants, which provide the maximum value for the reaction rate constants of ion/molecule reactions occurring in the gas phase. Calculated capture rate constants for the sequential hydration of the uranyl complexes are shown in Table 4.1.

	Modeled			ADO			% Efficiency		
Anion	k_1	k_2	k_3	k_1	k_2	k_3	k_1	k_2	k_3
CH_3COO^-	4.0×10^{-10}	3.8×10^{-10}	6.0×10^{-11}	2.13×10^{-9}	2.13×10^{-9}	2.13×10^{-9}	19	18	2.8
NO_3^-	3.5×10^{-10}	3.8×10^{-10}	1.3×10^{-10}	2.13×10^{-9}	2.13×10^{-9}	2.12×10^{-9}	16	18	6.1
OH^-	2.9×10^{-11}	9.9×10^{-11}	4.6×10^{-11}	2.14×10^{-9}	2.14×10^{-9}	2.13×10^{-9}	1.4	4.6	2.2

Table 4.1. The rate constants of uranyl hydroxide, nitrate, and acetate complexes moldeled to experiment maximum as calculated by ADO theory. Estimated precision on rate constants is 5-10%.

The change in percent efficiency, calculated by modeled/ADO, of the hydration reactions may be qualitatively interpreted as a measure of the combined contribution of several factors to the hydration behavior of the complexes. These factors include the ability of the complex to distribute excess energy from reactive collisions, the electronic influence of existing ligands on the ion's ability to attract and bond additional ligands, and the influence of geometry and intramolecular interactions on

complex stability.

The basicities of the anionic ligands increase in the order NO_3^- < CH_3COO^- < OH^-. Total electron density around the metal center of the uranyl complex is expected to increase with increasing basic strength of the anionic ligand. The magnitudes of the stability constants for the uranyl-anion complexes [7] are consistent with this expectation. Also, the O=U=O symmetrical Raman stretching frequencies decrease with increasing basicity of the anion, indicating a weakening of the U=O bonds as the basic strength of the anion increases, [7, 47, 52] and consistent with increased electron density being present at the metal center. For the formation of the $[(UO_2A)H_2O]^+$ complexes, our results demonstrate that the hydration tendency is lowest for the most basic ligand i.e. $(UO_2OH)^+$. However, only a weak correlation between anion basicity and hydration rate was observed for $(UO_2NO_3)^+$ vs. $(UO_2CH_3CO_2)^+$, and their monohydrates, suggesting that other factors may significantly influence the initial intrinsic hydration tendencies of these complexes. Additional degrees of freedom (df) within nitrate and acetate could distribute excess energy from reactive collisions within the molecule and stabilize the uranyl-anion-water complex, and this stabilization would lead to greater hydration reactivity of complexes containing these anions relative to the OH^- complex. The earlier study of gas-phase uranyl complexes showed that multiple-stage CID of

alcohol-coordinated uranyl nitrate will generate monopositive uranyl alkoxides [32] via the elimination of HNO_3. Preliminary studies of intrinsic hydration indicate that, relative to uranyl hydroxide, the rate constants for the formation of the monohydrate to the methoxide, ethoxide, *n*-propoxide and *n*-butoxide increase by factors of ~5, 14, 30 and 34, respectively [48]. The rate constants for the formation of the di and trihydrates also increase with the size and complexity of the alkyl group of the alkoxide. Similar results have been observed in preliminary investigation of the intrinsic hydration of uranyl acetate, propanoate and butanoate (i.e. the rates, in general, increase with the size and complexity of the carboxy anion). Taken together, the results suggest a positive influence on hydration rate by increased df. Attempts to generate monopositive cations containing chloride, bromide and iodide failed as the precursor complex ions eliminate HCl, HBr and HI to generate $(UO_2OH)^+$.

In general, hydration rates would be expected to decrease as the number of water molecules coordinated to the uranyl-anion complex increases, due to increased electron density transferred to the U(VI) ion; therefore, the increase in k_2 relative to k_1 observed for $(UO_2OH)^+$ is of particular interest. The larger value for k_2, which describes addition of H_2O to $[(UO_2OH)(H_2O)]^+$, supports the hypothesis that additional df may be important to the stabilization of adducts, because the monohydrate has additional df compared with $(UO_2OH)^+$. On the other hand, intramolecular hydrogen

bonding might increase stabilization of the nascent $[(UO_2OH)(H_2O)]^+$ complex, and previous modeling studies have shown that these intramolecular interactions influence the preferred geometries of gas phase complexes [53]. The relative ordering of the rate constants is similar to that reported for earlier studies of hydrate thermodynamics for first row transition metal monocations M^+, which showed that the bond energy for the second water molecule was greater than or equal to that of the first [54-59]. Because this trend was not observed for alkali metals, it was rationalized in terms of orbital rehybridization. Because orbital rehybridization should also be significant in the uranyl system, [52] measurement of bond energies for the three H_2O molecules attached to $(UO_2OH)^+$ is needed, but cannot be accomplished using the present experimental setup.

Regardless of the coordinating anion, the uranyl complexes investigated here accepted a maximum of $3H_2O$ ligands. Work by Vachet and Callahan suggested that the nitrate and acetate anions, within gas-phase transition metal complexes, are primarily bidentate ligands [60]. The acceptance of 3 H_2O ligands by $(UO_2NO_3)^+$ and $(UO_2CH_3CO_2)^+$ is consistent with the formation of gas-phase complexes with pentagonal bipyramidal conformation, with two equatorial coordination sites occupied by O atoms of the anions, reminiscent of the structures of uranyl complexes in solution [61-63] and generated computationally [46]. To evaluate this possibility,

density functional theory (DFT) calculations using the B3LYP functional and SDD basis set were conducted. Using the SDD command, a Stuttgart-Dresden effective core potential and associated basis set is placed on U, and the D95V basis set applied to all other atoms. The octahedral structure of $[(UO_2OH)(H_2O)_3]^+$ had been recently calculated by Oda and Aoshima [47], and was repeated here to evaluate the B3LYP-SDD approach. The minimized structure had an axial U=O bond distance of 1.799 Å, which was in excellent agreement with the previously reported values for hydroxy-uranyl complexes [47, 64, 65]. The equatorial U-OH bond (2.04 Å) was 0.05 Å shorter than the value calculated by Oda and Aoshima, and the equatorial U-OH_2 bond lengths (2.44-2.47 Å) were ~ 0.1 Å shorter. These variations are not particularly surprising since a different basis set was used, and Oda noted minor variations depending on the basis set employed. This comparison provided some validation for the computational approach [7, 47, 52].

Calculations generated two energetically competitive conformations for each of the trihydrate complexes containing uranyl nitrate and acetate (Figure 4.2). The axial U=O bond length was 1.780 Å for these complexes; this value was shorter than that for the hydroxy complex, consistent with earlier studies. [7, 47, 52] The lowest energy conformation for hydrated $(UO_2NO_3)]^+$ included the nitrate ligand as bidentate with respect to U. The H_2O ligands are oriented vertically (parallel to the axis of the

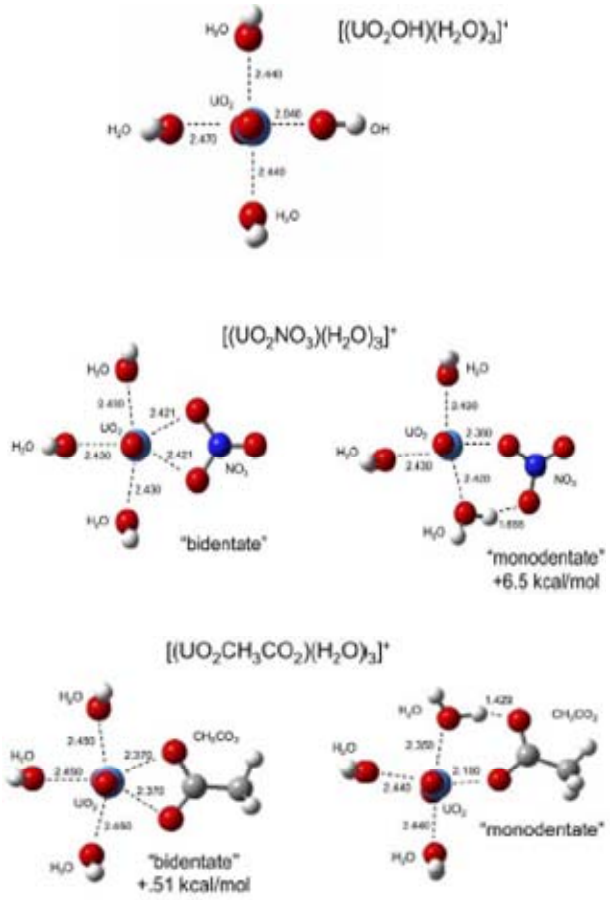

Figure 4.2

uranyl ion), in accord with structures for hydrated UO_2^{2+} reported earlier [46, 47]. A second stable conformation was identified in which the nitrate ion is monodentate with respect to U; this was ca. 6.5 kcal/mol higher in energy, and involved a hydrogen bond between nitrate and one H_2O ligand. The calculations suggested that the monodentate conformation for hydrated $(UO_2CH_3CO_2)^+$ is lowest energy, but that the mono- and bidentate conformations differed by only ~.5 kcal/mol. The fact that the

monodentate structure is more stable in the case of $(UO_2CH_3CO_2)^+$ may be attributed to the hydrogen bond between acetate and a rotated *cis*-H_2O ligand, in which a H atom is within 1.429 Å of the carbonyl oxygen atom. The uranyl acetate complex is assumed to be capable of converting to a conformation that includes coordination at only 4 equatorial sites, which together with the fact that the hydrated uranyl hydroxide complex contains fewer than 5 equatorial ligands, shows that the acceptance of an additional H_2O ligand to complete the coordination sphere does not occur readily under the gas-phase.

SUMMARY

In summary, the results of the set of experiments reported in this chapter indicate that the intrinsic hydration of monopositive uranyl-ligand complexes is markedly influenced by the nature of the coordinating ligand. The experimental approach thus provides an avenue for understanding ligation of UO_2^{2+} complexed with other anions such as phosphates, polycarboxylates, and silicates that are important in industrial and environmental processes. Future experimental and theoretical studies of these systems will further clarify the preferred geometries of the complexes and the extent to which degrees of freedom in the anion and intramolecular hydrogen bonding contribute to stabilization of the collision complexes.

Systematic variation of the Lewis and Bronsted acid/base properties of the ligands are underway, which should enable discernment of the relative roles of ligand basicity, degrees of freedom, and intramolecular hydrogen bonding in fostering solvent interactions. We are also currently pursuing the production of analogous doubly and singly charged uranyl complexes (i.e, similar composition and coordination number/structure) to facilitate an investigation of the influence of overall complex charge state on hydration tendency

CHAPTER 5

COLLISION-INDUCED DISSOCIATION TANDEM MASS SPECTROMETRY OF DESFERRIOXAMINE SIDEROPHORE COMPLEXES FROM ELECTROSPRAY IONIZATION OF UO_2^{2+}, Fe^{3+} AND Ca^{2+} SOLUTIONS

INTRODUCTION

In the past two chapters it was shown that ESI and tandem (ion-trap) spectrometry can be used to investigate uranium-ligand complexes. In this chapter are described experiments that demonstrate the ability of ESI-tandem mass spectrometry to investigate deferrioxamine complexes with UO_2^{2+}, Fe^{3+}, and Ca^{2+}. Desferrioxamine B (DEF) is a trihydroxamate siderophore typical of those produced by fungi and bacteria in low-Fe environments for the purpose of metal sequestration [66-68]. Deprotonated DEF exhibits a high affinity for iron because the three bidentate hydroxamates (see structure, Scheme 5.1) can occupy all six coordination sites around Fe, but the ligand will also form complexes with other metals, including actinide species [69-74] such as the uranyl dication UO_2^{2+}. In fact, hydroxamate siderophores have been considered for actinide decorporation from humans [75, 76] and for industrial separations [77]. In actinide complexation, DEF is capable of occupying all available coordination sites, [72,78] which has the effect of blocking adsorption to anionic sites common to mineral oxides typical of the geologic subsurface [79–81]. This phenomenon may enhance actinide mobility which could

augment the geographic extent of contamination [82–86]. hence finding approaches for sensitive, explicit detection of U complexes (such as those formed with DEF) in groundwater is a focus for our group and others [87–89].

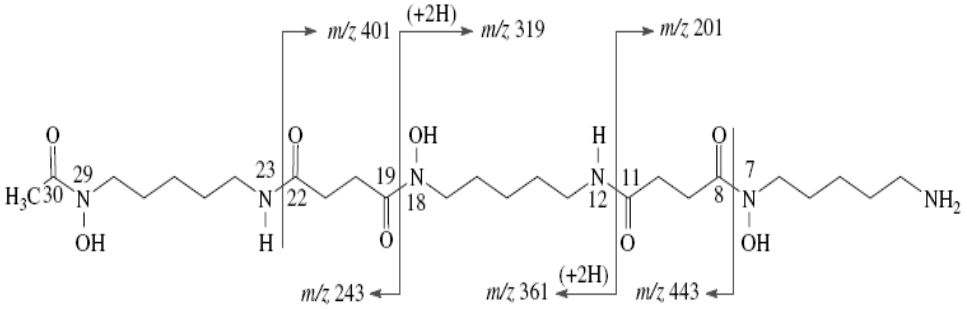

Scheme 5.1. Structure of fully protonated DEF. Hydroxamate functional groups are located at positions 7–8, 18–19 and 29–30. Cleavages account for fragment ions observed in the CID spectra of $[DEF + H]^+$ (*m*/*z* 561) and/or $[DEF + 2H]^{2+}$ (*m*/*z* 281) (see Fig. 5.2). Here, and in subsequent schemes, the arrows point toward the portion of the molecule that retains the charge. The parenthetical additions/subtractions are calculated from the mass and composition of the fully protonated, neutral DEF, and are required to account for ionization of the metal complexes and to account for H rearrangements.

In natural environments, identification and study of specific U complexes is challenging because the concentrations of the metal species are low, and a large number of chemical species is likely to be encountered at any given time. As noted in earlier chapters, ESI-MS is a versatile method for study of metal organic complexes from solution, [90-93] and the technique has been applied to the analysis of

siderophores and metal–siderophore complexes. Gledhill and co-workers investigated Fe(III)–hydroxamate siderophores using ESI-MS, and showed that intact complexes could be readily analyzed and quantified [87,88]. Crumbliss and co-workers have extensively studied dihydroxamate siderophores using ESI-MS, and showed that 1 : 1 complexes and multimetal complexes could be formed not only with Fe [94,95] but also with Al and Ga [96]. In addition, ESI-MS has been used to characterize L-hydroxycarboxylate [97] and pyoverdin [89] siderophores. As a whole, the prior studies have shown that intact protonated siderophore molecules and their Fe complexes were readily detectable. However, ESI-MS analyses of transition metal species can be complicated by multiple ionization, complexation and fragmentation processes, which can obfuscate identification of solution-phase species. Significantly less is known about the ESI-MS behavior of actinide species in solutions where a siderophore is present. These considerations motivated the MS/MS study of the CID fragmentation reactions of DEF complexes produced using ESI-MS described in this chapter. The fragmentation behavior provides a basis for manipulation of the gas-phase ion chemistry that can be used for efficient design of selective analytical strategies that are critical for identifying siderophore complexes in natural matrices. In addition to UO_2^{2+} complexes, the fragmentation behavior of analogous Fe^{3+} and Ca^{2+} complexes was also examined, because complexes of

these cations would also be expected in natural soil water systems typical of calcareous regions of the western USA, where actinides have been buried. Fe^{3+} was of particular interest because it is prevalent in radioactive landfills where rusting steel drums are interred together with radionuclides. In addition, evaluation of Ca^{2+} complexes allowed the assessment of the influence of another divalent cation in mediating CID pathways.

EXPERIMENTAL

Desferrioxamine (DEF) was purchased from Sigma Chemical (St. Louis, MO, USA). A stock solution containing 1 x 10^{-3} M $UO_2(NO_3)_2 \cdot 6H_2O$ and 1 x 10^{-3} M DEF was prepared by dissolving the appropriate amount of solid material in deionized H_2O. A 1 x 10^{-3} M Fe(III) nitrate solution was mixed with a 1 x 10^{-3} M DEF solution and then analyzed. Similarly, a 1 x 10^{-3} M Ca nitrate solution was mixed with a 1 x 10^{-3} M DEF solution and then analyzed. In the experiments where the effect of pH on UO_2^{2+} complex formation was evaluated, pH was adjusted using 1 M HNO_3 and 1 M NaOH to achieve the desired value, and was monitored using hydrion paper. Acetylation specific to the amino group was performed by incubating DEF in acetic anhydride overnight at 60°C. Following the incubation stage, the excess acetic anhydride and acetic acid byproduct were removed in vacuum desiccators to leave solid

N-acetylated DEF. The product was then used without further purification. Hydrogen–deuterium exchange reactions of amine, amide and hydroxamate positions were carried out by incubating an appropriate amount of DEF in a mixture of D_2O and MeOD for ~2 h. Following the exchange period, the deuterated DEF solution was diluted using the deuterated solvents and combined with an appropriate volume of uranyl nitrate hexahydrate or iron(III) nitrate solution also prepared with deuterated solvent for ESI analysis.

ESI mass spectra were collected using the Finnigan LCQDeca ion-trap mass spectrometer. The metal nitrate stock solution and water–methanol–DEF solutions were infused into the ESI-MS instrument using the syringe pump at a flow-rate of 3–5 μl min^{-1}. The atmospheric pressure ionization stack settings for the LCQ were optimized for maximum ion transmission to the ion-trap mass analyzer by using the autotune routine within the LCQ Tune program. Following the instrument tune, the spray needle voltage was maintained at +5 kV and the N_2 sheath gas flow at 25 units (arbitrary to the LCQ instrument, corresponding to ~375 l min^{-1}). To ensure maximum yield of solvated metal cation complexes, the capillary (desolvation) temperature was maintained between 110 and 130°C. The ion-trap analyzer was operated at a pressure of ~1.5 x 10^{-5} Torr (1 Torr =133.3 Pa). Helium gas, admitted directly into the ion trap, was used as the bath/buffer gas to improve trapping efficiency and as the

collision gas for CID experiments. CID experiments were performed by setting the isolation width between 5 and 12 mass units (depending on the species), the activation *Q* at 0.3 and the activation amplitude at 10–20% (of 5 V). In all cases, activation times for CID were 30 ms.

RESULTS AND DISCUSSION

ESI-MS analyses of UO_2^{2+} + DEF solutions

The positive ion mass spectrum derived from the DEF–$UO_2(NO_3)_2$ solution (1 mM in both components, pH 3.5) contained ions specific to the uranyl–DEF complexes in addition to ions from the components that were not associated with each other (Fig.5.1 (a)). Uncomplexed DEF was observed as both the protonated and doubly protonated molecules, $[DEF + H]^+$ and $[DEF + 2H]^{2+}$ at *m*/*z* 561 and 281, respectively. No uncomplexed uranyl was observed in this experiment; however, at higher $[UO_2]^{2+}$: [DEF] ratios, *m*/*z* 428 and 397 became abundant; these ions corresponded to $[UO_2(NO_3)(MeOH)]^+$ and $[UO_2(MeO)(MeOH)_3]^+$ [26]. Abundant uranyl–DEF complexes were also formed: $[UO_2(DEF)]^{2+}$ and $[UO_2(DEF\text{-}H)]^{2+}$ were observed at *m*/*z* 415 and 829, respectively. Low abundance ions at *m*/*z* 319, 243 and 201 are salient fragment ions arising from protonated DEF. The presence of DEF species in different states of protonation/deprotonation suggested that pH might exert

a strong influence over the complexes formed. When the solution pH was increased to 8 (Fig. 5.1(b)), $[UO_2(DEF\text{-}H)]^+$ accounted for nearly all of the signal in the spectrum, which is consistent with the fact that DEF is deprotonated in this complex. There was no evidence for the attachment of solvent molecules to either the $[UO_2(DEF)]^{2+}$ or $[UO_2(DEF–H)]^+$ complexes. The lack of solvent clustering contrasted with the behavior observed for $[UO_2(anion)]^+$ complexes studied previously and discussed in chapter 3 and 4: when the anion was nitrate,methoxy or hydroxy, three additional solvent molecules were observed (where the solvent was either methanol or water) [26, 98]. In the present case, both DEF and $[DEF\text{-}H]^-$ appear to occupy all of the equatorial coordination sites, which prohibits attachment of any solvent molecules. The exhaustive coordination by DEF observed here is reminiscent of the behavior of other hydroxamate siderophores, in which 9-coordinate with Pu species has been reported [78].

CID of uncomplexed DEF specie

The CID fragmentation of the uncomplexed DEF ions was reported earlier by DeHoffmann and Stroobant [100], and was reexamined here to provide a consistent basis for comparison with the metal complexes. Fragmentation at the amide and hydroxamate linkages accounted for all six of the fragment ions observed (Fig. 5.2, Scheme 5.1). The most abundant ions arose from fragmentation of the hydroxamate

bonds at positions 7–8 and 18–19, forming *m*/*z*

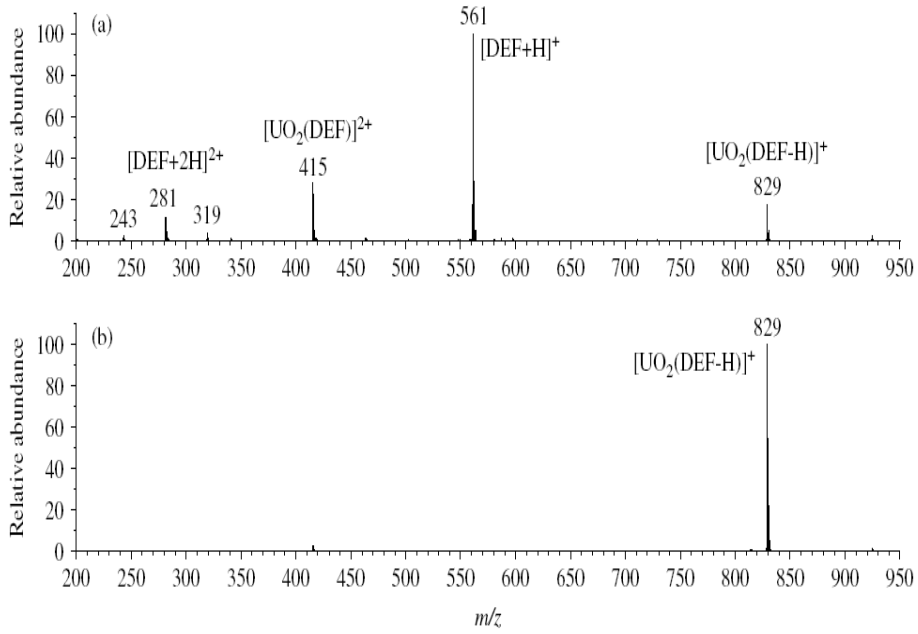

Figure 5.1. Cation ESI mass spectrum of an equimolar solution of DEF and UO_2^{2+} Analyte solution at (a) pH 3.5 and (b) pH 8.

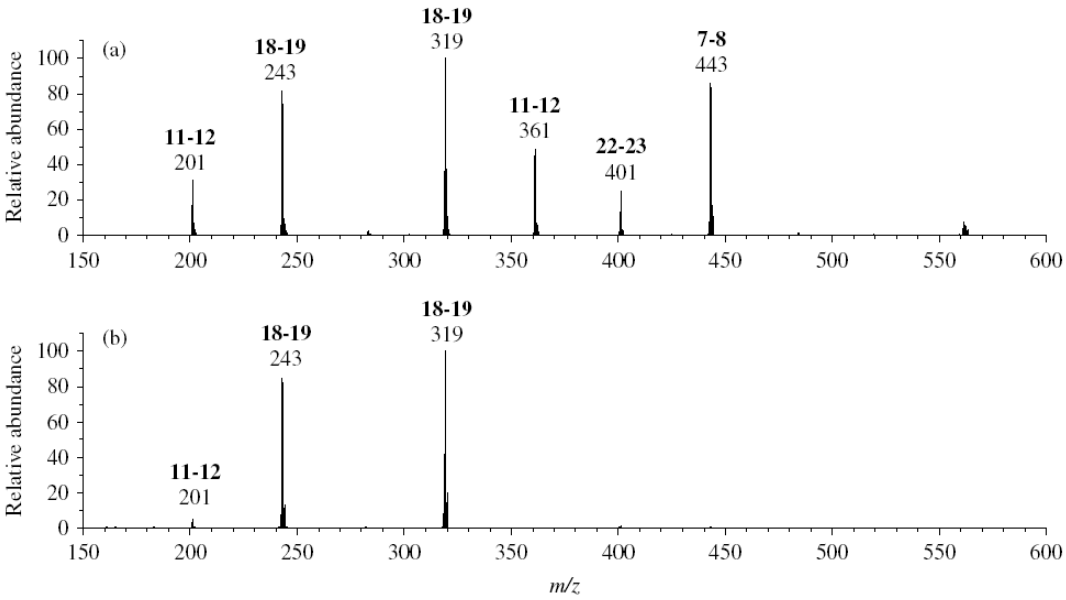

Figure 5.2. CID spectra of (a) $[DEF + H]^+$, *m*/*z* 561, and (b) $[DEF + 2H]^{2+}$, *m*/*z* 281. Bond cleavages and *m*/*z* values are annotated (see Scheme 5.1).

443, 319 and 243, respectively. Ions of *m*/*z* 443 and 243 were formed by acyl charge retention, with elimination of a neutral species containing a terminal hydroxylamine; *m*/*z* 319 resulted from H transfer that produced a protonated hydroxylamine by elimination of a deprotonated, acyl-bearing neutral species. Fragmentations involving the 11–12 and 22–23 amide bonds was also observed, but at lower abundance than hydroxamate cleavages. Charge retention by the acyl fragment accounted for *m*/*z* 201 and 401, and H transfer from the acyl to the amine formed *m*/*z* 361. The fragmentation pathways were substantiated by the CID spectrum of protonated, *N*-acetylated DEF, in which the amine terminus was derivatized. CID of protonated, *N*-acetylated DEF generated product ions at *m*/*z* 443 and 361 (the same as in the underivatized molecule), consistent with the addition of the acetyl group to the amine terminus of the eliminated neutral. Product ions expected to contain the amino group (those at *m*/*z* 401, 319 and 201 in the unacetylated compound) were shifted in mass by 42 u, consistent with the expected retention of the acetyl derivative by the ion. CID of DEF with all exchangeable sites occupied with deuterium was consistent with the cleavage sites and mechanisms suggested. The CID spectrum of the doubly charged $[DEF + 2H]^{2+}$ resulted in fragmentation that was nearly exclusively localized at the 18–19 hydroxamate. Charge separation produced the acyl fragment at *m*/*z* 243 and the protonated

hydroxylamine at *m*/*z* 319, which suggested that the protons tend to be localized in positions 1–18, the amine terminus. In this case, simple cleavage of 18–19 would produce the observed ions without necessitating proton transfer.

CID of UO_2^{2+}–DEF complexes

The purpose of this study was to identify the probable cleavage sites within the uranyl–DEF complex to assist the development of protocol to interpret the CID spectra of unknown complexes in the future, rather than to provide detailed mechanistic information about the fragmentation reactions. The latter pursuit would involve significant isotope labeling and/or computational studies and was beyond the scope of the work presented in this chapter. The CID behavior of $[UO_2(DEF + H)]^+$ complex (*m*/*z* 829) was similar to that of protonated DEF in that abundant cleavages were observed at the 7–8 and 18–19 hydroxamate moieties (Fig. 5.3, Scheme 5.2). Loss of the neutral hydroxylamine fragment from 1–7 produced the base peak at *m*/*z* 711 (loss of 118 u), in a process directly analogous to that observed in protonated DEF. This loss is increased by 42 u (to 160 u) in the CID spectrum of the amine-acetylated derivative of DEF, and increased to 122 u for the deuterium-exchanged form of DEF. The former point shows that the acetylated amine-bearing 1–7 fragment is eliminated in the CID reaction, while the latter point is

consistent with the elimination of three exchangeable sites (amine NH_2 and N–OH at position 7) along with one additional exchangeable proton. The transferred proton must originate from one of the other exchangeable sites: the other two hydroxamate moieties at positions 18 and 29 are probable candidates because they are likely the most acidic sites on DEF, although participation by the amide protons is also possible. Note that in the intact $[UO_2(DEF + H)]^+$ complex one of the hydroxamates is deprotonated; therefore, transfer of the remaining hydroxylamine proton to the departing 1–7 neutral would leave the complex with two coordinating, deprotonated hydroxamate groups to balance the charge of the uranyl ion. The net charge on the complex remains +1 as a result of the remaining cationic acyl site (position 8). In addition, the oxophilic nature of the U metal center altered the fragmentation behavior at the 7–8 hydroxylamine. Cleavage of the 7–8 bond occurred with retention of the hydroxamate O, which presumably remained coordinated to the uranyl ion. The fragmentation reaction was a net elimination of $N(CH_2)_5NH_2$(100 u), which accounted for the abundant ion at *m*/*z* 729. The neutral loss shifted by 42 to 142 u for the NH_2 acetylated version of DEF, and to 102 and 103 u for the deuterium-exchanged form of DEF. The shift for the acetylated form of DEF was consistent with the elimination of the amine portion of the molecule, and the loss of 102 u was consistent with the elimination of the deuterium exchanged amino group. A more complicated pathway

must be invoked for the loss of 103 u, which suggested that an aliphatic proton was transferred to the product ion and that an additional exchangeable deuterium was eliminated with the neutral.

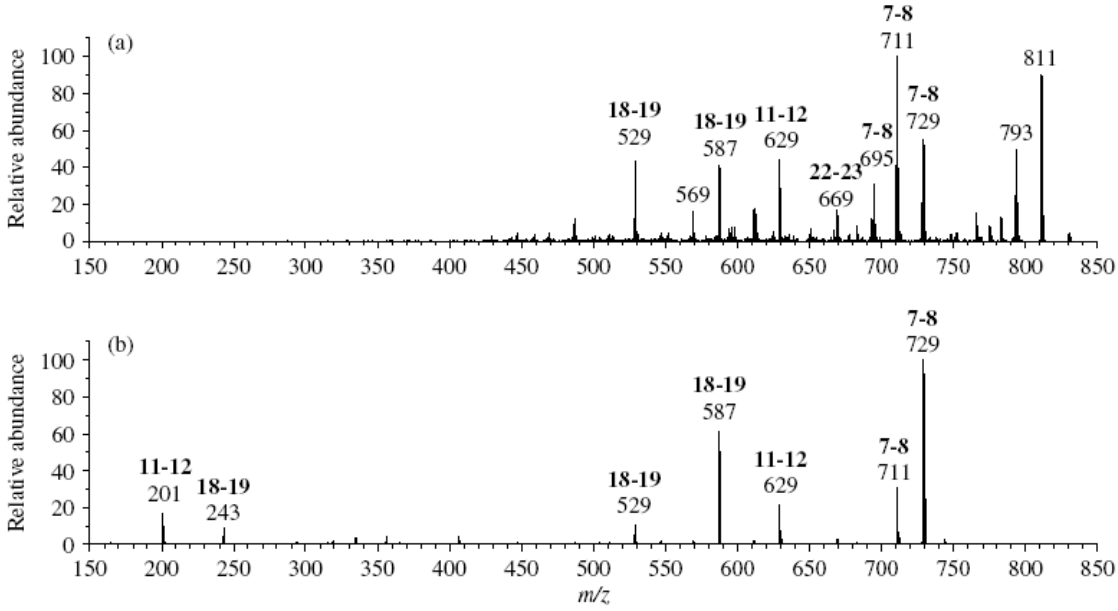

Figure 5.3. CID spectra of (a) $[UO_2(DEF + H)]^+$, *m*/*z* 829, and (b) $[UO_2(DEF)]^{2+}$, *m*/*z* 415. Bond cleavages and *m*/*z* values are annotated (see Scheme 2).

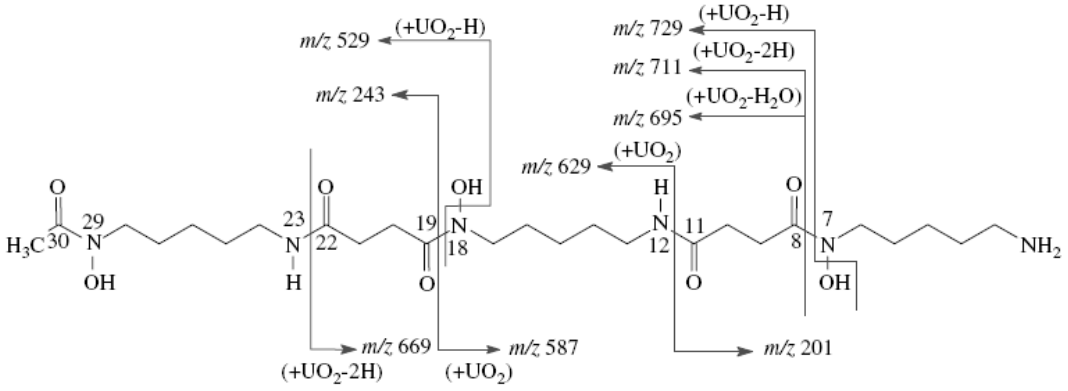

Scheme 5.2. Cleavages accounting for fragment ions observed in the CID spectra of $[UO_2(DEF + H)]^+$ (*m*/*z* 829) and/or $[UO_2(DEF)]^{2+}$ (*m*/*z* 415) (see Fig. 5.3).

The possibility that *m*/*z* 729 arose via the rapid hydration of the *m*/*z* 711 fragment ion was also considered, either concurrent with cleavage at the 7–8 position, or subsequent to it. Evidence for collision-induced ligand substitution by water occurring in uranyl cation complexes was observed for uranyl complexes, as noted in earlier chapters [26]. Hydration of the *m*/*z* 711 fragment would be significant because it would suggest that the remaining coordination sites around the uranyl axis are not completely occupied. However, although CID (MS^3) of *m*/*z* 729 resulted primarily in the elimination of water, isolation of the product ion at *m*/*z* 711 failed to produce a hydrated product ion, thus arguing against a hydration mechanism for the formation of *m*/*z* 729.

Product ions at *m*/*z* 629 and 529 were also observed in the CID spectrum of *m*/*z* 729, and also in the spectrum of the intact complex $[UO_2(DEF + H)]^+$. The ion at *m*/*z* 529 arose from cleavage of the 18–19 hydroxamate, with retention of the hydroxamate O atom (as in the case of the 7–8 hydroxamate cleavage). Cleavage of 18–19 hydroxamate also accounted for *m*/*z* 587: in this case, hydrogen is transferred from the departing 19–31 neutral to the hydroxylamine-terminated ion. The 7–8 hydroxamate cleavage is also thought to be responsible for the lower abundance ion at *m*/*z* 695, which cannot be explained simply starting from $[UO_2(DEF + H)]^+$. This ion was also seen at *m*/*z* 695 in the acetylated complex, which indicated elimination by

the amine terminus. Loss of the $HN(OH)(CH_2)_5NH_2$ plus one additional O atom would account arithmetically for the fragmentation and would be consistent with the oxophilicity of uranium, but how this occurs is unclear.

MS^3 CID of the product ion at *m*/*z* 711 generated fragment ions at *m*/*z* 683 (loss of 28 u), 612 (loss of 99 u) and 529 (loss of 182 u). The neutral loss of 28 observed in the formation of the product at *m*/*z* 683 did not shift for the deuterium-exchanged form of DEF, indicating the elimination of CO, presumably the carbonyl group at position 8. The neutral loss of 99 u is consistent with cleavage of the bond between positions 12 and 13, without proton transfer. The neutral loss was 100 u for the deuterium exchanged form of DEF is consistent with the elimination of the amide N at position 12 in the fragmentation reaction. The neutral loss of 182 and formation of the product at *m*/*z* 182 is consistent with cleavage of the 18–19 hydroxamate, with retention of the hydroxamate oxygen by product ion (see above).

Fragmentation of the amide bonds was observed, but the pathways produced ions at significantly lower abundances compared with the hydroxamate-driven cleavages. Rupture of the 11–12 and 22–23 amide bonds accounted for *m*/*z* 629 and 669. In the former reaction, the 1–11 acyl neutral was eliminated; in the latter, the 23–31 amine was lost. Water elimination was also prominent in the CID spectrum of $[UO_2(DEF + H)]^+$ (*m*/*z* 829): abundant ions corresponding to the elimination of one,

two and three H_2O molecules occurred at *m*/*z* 811, 793 and 775 (Fig. 5.3 (a)). Similar product ions were not observed following CID of $[DEF + H]^+$, which was surprising because the presence of protonated hydroxamate groups in the uncomplexed molecule would be expected to facilitate the elimination of H_2O. The peaks at *m*/*z* 811 and 793 were shifted by 42 u in the CID spectrum of the NH_2 acetylated version of DEF. However, the abundances of both products were significantly lower compared with the unacetylated form of DEF, which indicated that amine protons participate in the elimination of H_2O. The deuterium-exchanged form of DEF initially eliminated 20 u, consistent with the elimination of the first water by a mechanism that involved two protons from exchangeable sites. MS^3 investigation of the second water elimination showed losses of 18, 19 and 20 u, with the loss of 19 u being the most prominent. The multiple isotopic peaks suggested that protons at sites other than amine, amide or hydroxamate participate in the elimination of the second water molecule.

The CID spectrum of the doubly charged complex $[UO_2(DEF)]^{2+}$ at *m*/*z* 415 was considerably simplified compared with the singly charged $[UO_2(DEF + H)]^+$, and was dominated by fragmentations involving the hydroxamate moieties. In all cases, charge separation drove the fragmentation reactions, disfavoring neutral eliminations. As discussed above, fragmentation of the 7–8 hydroxamate accounted for *m*/*z* 711 and 729. Ions in which the hydroxamate oxygen was retained were more abundant

compared with the singly charged complex: this is consistent with the idea that the 7–8 hydroxamate is largely deprotonated, and hence strongly bound to uranyl. Cleavage of the 18–19 hydroxamate accounted for the formation of *m*/*z* 587, 529 and 243. The fragmentation forming *m*/*z* 529 must occur with retention of the hydroxamate oxygen at position 18.

As noted for the singly charged uranyl–DEF complex and for the uncomplexed DEF cations, amide fragmentation occurred, but was a less important process. Charge separation arising from rupture of the 11–12 amide produced the protonated amine fragment at *m*/*z* 629 and the corresponding acyl cation at *m*/*z* 201.

CID of Fe^{3+}–DEF complexes

The ESI-MS analysis of an equimolar solution of iron(III) nitrate and DEF produced simple spectra in which the most abundant ion was $[Fe(DEF + 2H)]^{+}$ at *m*/*z* 614. This result agreed with previous measurements reported by Spasojevic *et al*. [96] and Gledhill, [87] and was directly analogous to ions observed in the liquid secondary ion mass spectrum of the complexed hydroxamate siderophore ferrichrome [100]. Lower abundance $[DEF + H]^{+,}$ $[DEF +2H]^{2+}$ and $[Fe(DEF +H)]^{2+}$ were also observed. When the pH of the spray solution was increased, the relative abundance of $[Fe(DEF + 2H)]^{+}$ was modestly enhanced, consistent with the fact that

complex formation requires deprotonation of DEF.

Fragmentation of the 7–8 hydroxamate was the most important cleavage observed in the CID spectrum of $[Fe(DEF + 2H)]^+$ (Fig. 5.4 (a), Scheme 5.3). Elimination of $HONH(CH_2)_5NH_2$ was the preferred process (generating *m*/*z* 496), although retention of the hydroxamate oxygen was also observed, producing *m*/*z* 514. Cleavage of the 18–19 hydroxamate was only a minor process in the singly charged Fe^{3+} complex. Instead, rupture of the 11–12 amide accounted for the second most abundant collision-induced fragment, in which loss of the neutral from positions 1–11 formed *m*/*z* 414. The abundance of this fragment ion suggested that coordination of the 11–12 amide with Fe^{3+} was significant. A lower abundance ion at *m*/*z* 454 was also interpreted in terms of amide cleavage, involving the 22–23 bond.

Ions observed at *m*/*z* 597, 454 and 397 corresponded to processes that were not seen in CID spectra of either the protonated or the uranylated DEF cations. An abundant loss of NH_3 (rupture of 1–2) accounted for *m*/*z* 597, and fragmentation of the 12–13 and 8–9 bonds most likely produced *m*/*z* 397 and 454, respectively. These bonds were not expected to be particularly labile and may indicate insertion of Fe^{3+} into the ligand at these locations. Significantly, these bonds are proximate to complexing functional groups, which indicate that if Fe^{3+} insertion is occurring, it is not a random process but requires co-location of the metal with the target bond.

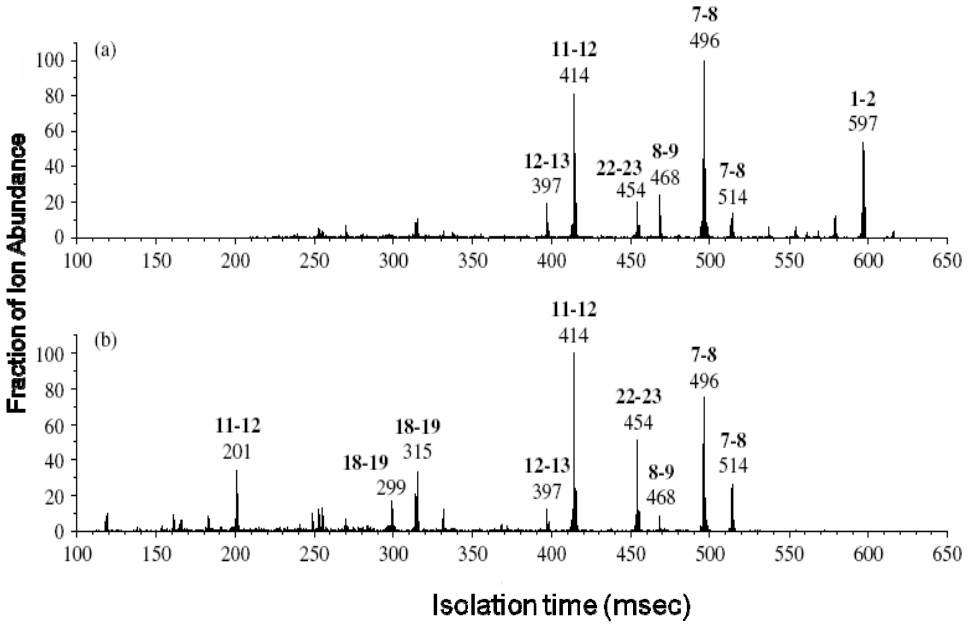

Figure 5.4. CID spectra of (a) $[Fe(DEF + 2H)]^{+}$, *m*/*z* 614, and (b) $[Fe(DEF + H)]^{2+}$, *m*/*z* 307.5. Bond cleavages and *m*/*z* values are annotated (see Scheme 3).

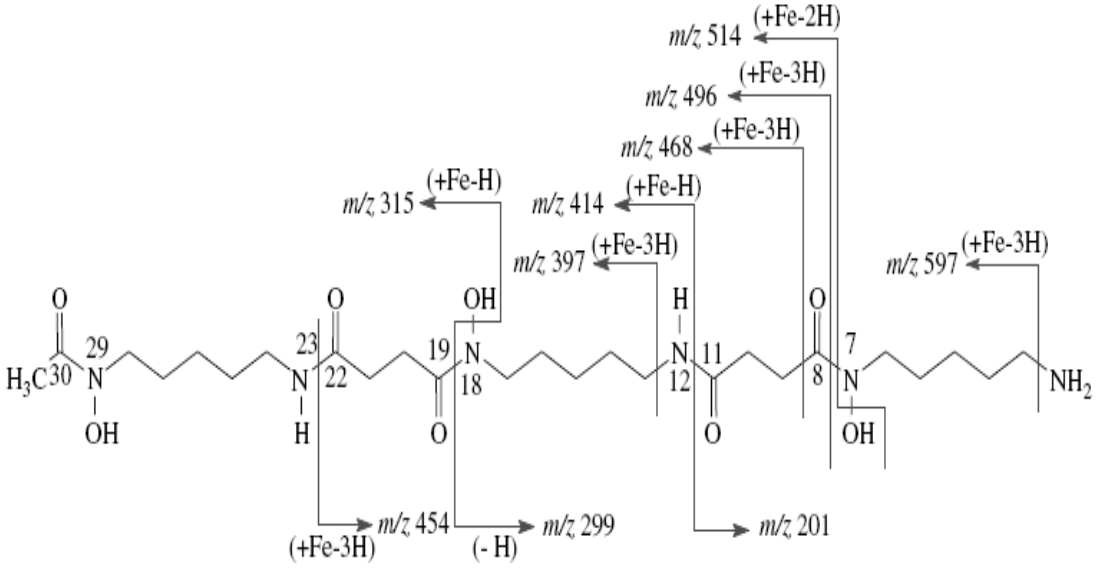

Scheme 5.3. Cleavages accounting for fragment ions observed in the CID spectra of $[Fe(DEF + 2H)]^{+}$ (*m*/*z* 614) and/or $[Fe(DEF + H)]^{2+}$ (*m*/*z* 307.5) (see Fig. 5.4).

The CID spectrum of the doubly charged $[Fe(DEF +H)]^{2+}$ complex (*m*/*z* 307.5) produced pairs of ions formed by charge separation fragmentations occurring at positions previously observed for the singly charged Fe complex. Fragmentation at 7–8 hydroxamate produced the Fe-bearing ion at *m*/*z* 496 and presumably the protonated amine terminus at *m*/*z* 119 (below the low-mass cutoff and not observed). The elimination also occurred with oxygen atom retention by the metal, producing *m*/*z* 514. Fragmentation of the 18–19 hydroxamate also occurred with retention of the hydroxylamine oxygen by the metal, and produced *m*/*z* 315 and hydroxylamine oxygen by the metal, and produced *m*/*z* 315 and 299. Cleavage of both amide bonds (11–12 and 22–23) produced ions at *m*/*z* 414 and 454 that were about as abundant as those derived from the hydroxamate bond scissions. This again suggested that the charged Fe center is interacting more significantly with the amides than was the uranyl. The ionic charge separation complements to the *m*/*z* 414 and 454 fragments were clearly observed at *m*/*z* 201 and 161, respectively.

CID of Ca^{2+} –DEF complexes

Ca^{2+} is the dominant groundwater cation in the calcareous regions typical of the western USA, and hence would be present in solution with siderophore molecules; thus recognition of complexes with group II cations would depend on understanding

fragmentation behavior. Ca^{2+}–siderophore complexes are observable using mass spectrometric approaches: Ca-substituted ferrichrome complexes have been observed previously using liquid SIMS [100]. When a solution containing 1 mM DEF and Ca^{2+} was analyzed in the present study, $[Ca(DEF + H)]^+$ was observed at *m*/*z* 599 and a lower abundance $[Ca(DEF)]^{2+}$ at *m*/*z* 300.

The CID spectrum of the singly charged complex contained a very abundant ion at *m*/*z* 499, which was produced by cleavage of the 7–8 hydroxamate with retention of the hydroxylamine oxygen atom by Ca^{2+} (Fig. 5.5(a), Scheme 5.4). The behavior indicates strong binding of the 7–8 hydroxamate with Ca^{2+}. The low-abundance ion at *m*/*z* 250 may also be related to scission of the 7–8 bond: elimination of 1–7, 19–31 and an H_2O molecule would produce the correct mass. A more straightforward explanation for the formation of *m*/*z* 250 has not been identified. Fragmentation involving the 18–19 hydroxamate was not observed in the spectrum of the singly charged Ca^{2+} complex.

As noted for the uranyl and Fe^{3+} complexes, cleavage of the amide bonds can be observed, but is less important than cleavages of the hydroxamates. Rupture of 11–12 and 22–23 bonds can account for *m*/*z* 239 and 439, respectively. There is no direct explanation for the formation of *m*/*z* 257, and we hypothesize that this may be formed from concomitant fragmentation/H_2O addition, similar to that observed in CID

of other gas-phase uranyl complexes [26].

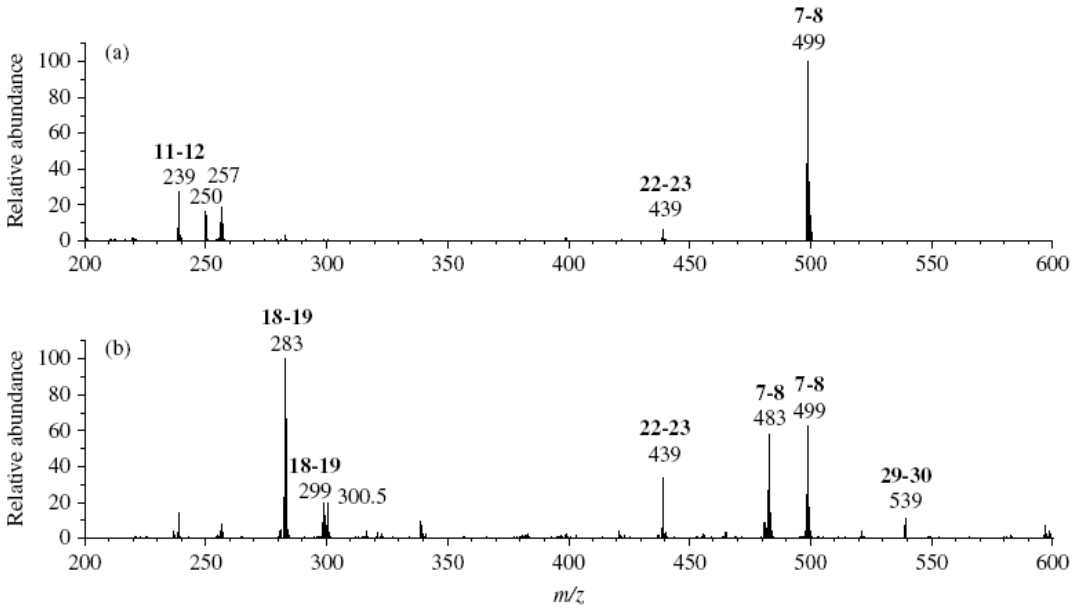

Figure 5.5. CID spectra of (a) $[Ca(DEF + H)]^+$, *m*/*z* 599, and (b) $[Ca(DEF)]^{2+}$, *m*/*z* 300. Bond cleavages and *m*/*z* values are annotated (see Scheme 5.4).

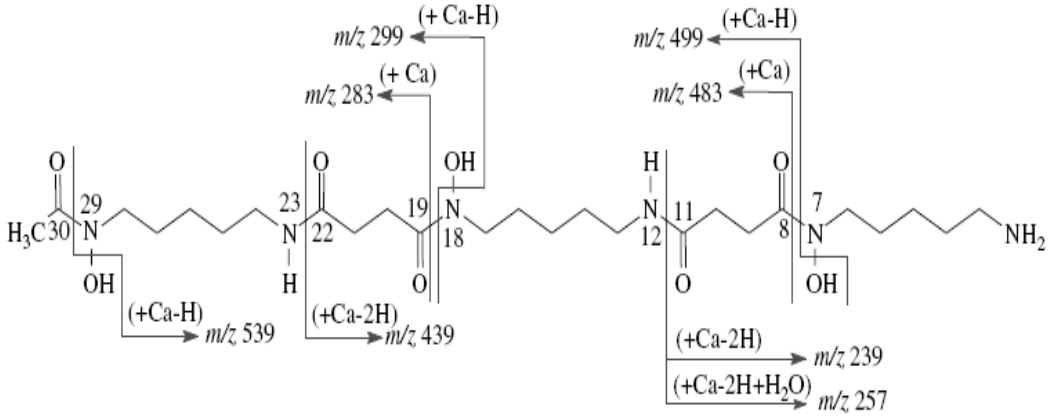

Scheme 5.4. Cleavages accounting for fragment ions observed in the CID spectra of $[Ca(DEF + H)]^+$ (*m*/*z* 599) and/or $[Ca(DEF)]^{2+}$ (*m*/*z* 300) (see Fig. 5.5).

The fragmentation of the doubly charged Ca^{2+} complex $[Ca(DEF)]^{2+}$ also contains fragment ions derived from 7–8 hydroxamate cleavage at *m*/*z* 499 and 483 (with and without oxygen atom retention by Ca^{2+}, respectively). Here, bond scission of the 18–19 hydroxamate was competitive and produced *m*/*z* 283 and 299 (with and without oxygen atom retention by Ca^{2+}, respectively). The origin of the low abundance ion at *m*/*z* 539 is less obvious, however. The most consistent explanation involves the 29–30 hydroxylamine, which has not been implicated in any DEF fragmentation thus far. Elimination of the 30–31 acetyl cation with H_2O would account for the observed mass. These cleavage reactions indicate that all three hydroxamate functional groups are actively binding to Ca^{2+} in the doubly charged complex.

Scission of the 22–23 amide linkage produced the prominent ion at *m*/*z* 439, which was significantly more abundant than the singly charged ion. In contrast, the 11–12 amide cleavage is comparatively decreased in abundance; this suggests that in the doubly charged complex, additional or alternative coordination may occur, involving other functional groups, and resulting in additional competitive fragmentation channels in the CID spectrum. The ion at *m*/*z* 300.5 is clearly doubly charged, but its origin has not been identified. Abstraction of an H radical from another neutral by an activated $[Ca(DEF)]^{2+}$ complex would explain the ion, but we

are unaware of a precedent for such a reaction.

SUMMARY

Solutions of $UO_2^{2+,}$ Fe^{3+} and Ca^{2+} with the siderophore desferrioxamine (DEF) were analyzed using ESI-MS employing a quadrupole ion trap, which permitted a detailed MS/MS examination of the CID fragmentations of singly and doubly charged DEF complexes. DEF contains three hydroxamate functional groups, which are principally responsible for binding with metal species and as a result participate in the most prevalent fragmentation reactions. Elimination reactions that cleaved the hydroxamate bonds occurred both with and without transfer of the hydroxamate oxygen atom to the metal center. The CID spectrum of $[DEF + H]^+$ contained ions from a variety of hydroxamate and amide bond cleavages, which suggested that the charge-bearing proton could be localized in several positions on the molecule. In contrast, the spectrum of the doubly charged $[DEF + 2H]^{2+}$ contained practically only ions derived from scission of the 18–19 hydroxamate, suggesting protonation at that site, and somewhere else within positions 1–18. Fragmentations of the hydroxamate functional groups were the most important processes in the CID spectrum of both the singly and doubly charged uranyl complexes. Cleavage of the amide bonds, although observable, was less significant. Losses of H_2O from the intact, singly charged

complex were unique among themolecules studied. In the Fe^{3+} complexes, elimination reactions involving the 11–12 amide were competitive with those of the 7–8 hydroxamate, which indicated that Fe^{3+} was complexed with a more extensive suite of functional groups than was the uranyl. The Fe^{3+} complexes also underwent several cleavages not related to either a hydroxamate or an amide (viz. loss of NH_3), which suggested that the metal may be participating in insertion reactions in addition to complexation. The singly charged Ca^{2+} complex fragmented predominantly at the 7–8 hydroxamate, but not at all at the 18–19 or 29–30 hydroxamate bonds; was some amide cleavage observed at the 11–12 position, which suggests that the 7–12 hydroxamate-amide combination is principally responsible for binding with Ca^{2+}. In the doubly charged Ca^{2+} complex, cleavage of the 18–19 hydroxamate complexes was equally competitive with that of the 7–8 hydroxamate, which indicated that both functional groups were deprotonated and were actively participating in complexation. Amide cleavages were observed, but were less prevalent.

In total, the CID spectra indicated that, despite the variety of possible fragmentation reactions in DEF complexes, there are prevailing generalities that allow rationalization of the observed spectra, and provide initial input for guiding the interpretation of the spectra of unknown complexes. Hydroxamate functional groups serve to focus fragmentation, which in singly charged species tends to be localized at

one group, but is partitioned between two hydroxamates for doubly charged species. Fragmentation involving amide bonds is modestly competitive, but has not been seen to be greater than fragmentation of the hydroxamate groups. A firmer understanding of these reactions will require complexation studies involving model compounds such as *N*-methylacetamide and its hydroxyl derivative.

CHAPTER 6

OXIDATION OF 2-PROPANOL LIGANDS DURING COLLISION-INDUCED DISSOCIATION OF A GAS-PHASE URANYL COMPLEX

INTRODUCTION

As noted in earlier chapters, the desire to gain an understanding of intrinsic uranium cation reactivity has motivated a wide range of mass spectrometric studies of U^+ and UO^+, which emphasized reactivity with organic compounds [17, 18, 101]. In general, U^+ has been found to form divalent complexes with the dehydrogenation of the ligated organic and production of π-complexes, and similar patterns of alkane dehydrogenation were observed for UO^+. [19] U^+ and UO^+ insertion into RO-H and R-OH bonds has been reported [20], and in the presence of organic radicals U^+ was shown to have a high affinity for σ-bound dicarbide and acetylide anions. [102]

Oxidation reactions make up a second category of gas-phase reactions involving U^+ that has been studied. For example, it has been shown that U^+ can be oxidized using O_2, CO, CO_2, COS, and D_2O, [103] and that UO^+ would undergo oxidation with O_2, and D_2O to form UO_2^+ [103].

It is clear that ESI is an effective tool for generating ions containing U in the higher states for study by mass spectrometry and ion mobility-mass spectrometry [41, 42, 104, 105], including species in higher oxidation states [26,106]. Several recent reports have demonstrated that intrinsic addition chemistry of ionic metals and metal

complexes can be investigated by the (controlled) addition of reagent gas [43,44,60,107-111] or by utilizing indigenous gaseous contaminants like H_2O or O_2 that are present within the He bath gas that is required in an ion trap to collisionally cool ions and improve trapping efficiency [9-11,32,106].

The experiments described in this chapter involved the generation by ESI of monopositive complex cations containing uranyl nitrate, hydroxide or 2-propoxide ions and coordinated by 2-propanol followed by an investigation of their multiple-stage CID. The interest in this particular system arose from previous reports of the photocatalytic conversion of 2-propanol to acetone by uranyl ion exchanged into the cavities of zeolite materials [115,116]. One of the long term goals of the Van Stipdonk research group is to use ESI to generate gas-phase ions of relevance to catalytic metal centers in condensed phases and to investigate their intrinsic chemistry by ion trap mass spectrometry. Investigations of this nature also contribute to the general understanding of intrinsic uranium chemistry. One fragmentation pathway observed during multiple stage CID of complex ions containing the uranyl ion and 2-propanol involved elimination of coordinating 2-propanol ligands and generation of a monopositive uranyl-2-propoxide cation, which was ultimately converted to the monopositive uranyl-hydroxide cation via a reactive collision with water in the ion trap. For a species including uranyl-2-propoxide

cation coordinated by a single 2-propanol molecule, a second pathway was observed in which CID caused 2-propanol to be converted to acetone, and 2-propoxide ligand to acetaldehyde: both “reaction products” were eliminated in successive CID stages to leave the U(V) species UO_2^+. The conversion reactions are supported by studies of the CID of a series of analogous complexes involvary 2-propanol labeled with deuterium in specific positions.

EXPERIMENTAL METHODS

2-propanol (2-PrOH), d_6 2-propanol (d_6 2-PrOH, $[(CD_3)_2CHOH]$), and d_7 2-propanol (d_7 2-PrOH, $[(CD_3)_2CDOH]$) were purchased from Aldrich Chemical (St. Louis, MO) and used as received. A stock solution (1×10^{-3} M) of $UO_2(NO_3)_2 \cdot 6H_2O$ was prepared by dissolving the appropriate amount of solid material in deionized H_2O.

ESI mass spectra were collected using the Finnigan LCQ-Deca ion-trap mass spectrometer. The spray solutions used in these experiments consisted of the uranyl nitrate stock solution to which was added 5% (v:v) of the various labeled and unlabeled versions of 2-PrOH. The solutions were infused into the ESI-MS instrument using the syringe pump at a flow rate of 5 µl/min. The addition of 5% by volume was chosen because optimization studies indicate that abundant alcohol coordinated uranyl complexes are produced at this level without concomitant production of

gas-phase alcohol adducts to CID product ions due to the accumulation of neutral alcohol in the ion trap.

The multiple stage CID experiments were carried out using a protocol described elsewhere [26]. Briefly, the dissociation parameters were the following. CID was performed by setting the isolation width between 5 and 12 mass units (depending on the species), the activation Q (as labeled by instrument manufacturer, used to adjust the q_z value for the resonant excitation of the precursor ion during the CID portion of the experiment) at .3 and the activation amplitude at 10-20% (of 5V). In all cases, activation times for CID were 30 msec.

RESULTS AND DISCUSSION

Figure 6.1 shows the ESI spectrum generated from a solution of uranyl nitrate dissolved in H_2O with 5% by volume of 2-propanol. The compositions of the relevant species generated by ESI using the experimental conditions employed in this study and their nominal mass to charge ratios (m/z) are listed in Table 6.1. The dominant complex ion generated by ESI was one at m/z 509 with assigned composition $[UO_2OPr(2\text{-}PrOH)_3]^+$, a monopositive uranyl 2-propoxide cation coordinated by three 2-PrOH ligands. Also observed were complex ions with composition $[UO_2NO_3(2\text{-}PrOH)_3]^+$ (m/z 512) and $[UO_2OH(2\text{-}PrOH)_3]^+$ (m/z 467). The compositions of the complex ions were confirmed using multiple-stage CID, and are consistent with

previous work that established that a maximum of three coordinating solvent molecules were accepted by monopositive uranyl-anion complexes [26, 35, 106].

The multiple-stage CID schemes for the dissociation of $[UO_2OPr(2\text{-}PrOH)_3]^+$, $[UO_2NO_3(2\text{-}PrOH)_3]^+$ and $[UO_2OH(2\text{-}PrOH)_3]^+$ are provided in figure 6.2. For $[UO_2OH(2\text{-}PrOH)_3]^+$, the first CID stage (MS/MS, figure 6.2, scheme 6.1(b)) caused the elimination of H_2O to generate $[UO_2OPr(2\text{-}PrOH)_2]^+$. For $[UO_2NO_3(2\text{-}PrOH)_3]^+$, the first CID stage instead caused the elimination of a single 2-PrOH ligand from(figure 6.2, scheme 6.1.(a)) to generate $[UO_2NO_3(2\text{-}PrOH)_2]^+$. Subsequent CID of $[UO_2NO_3(2\text{-}PrOH)_2]^+$ (MS^3 stage) caused the elimination of HNO_3 to generate

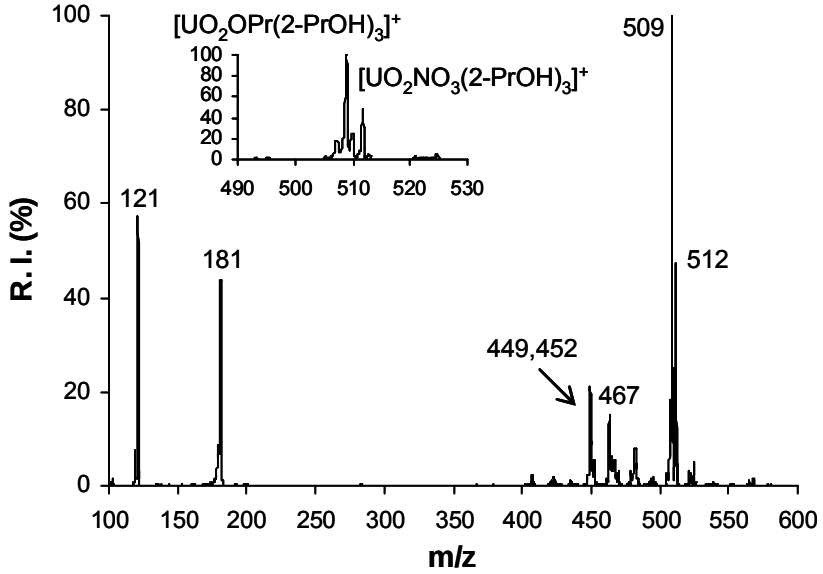

Figure 6.1. ESI mass spectrum derived from a 1 mM solution of $UO_2(NO_3)_2 \bullet (H_2O)_6$ in H_2O with 5% (by volume) 2-propanol. Inset shows expanded m/z axis to highlight the complex cations containing uranyl 2-propoxide and uranyl nitrate monocations coordinated by 2-propanol. The m/z ratios of relevant peaks are shown. The compositions assignments are listed in table 6.1

Nominal m/z value	Ion Composition
50	(2-PrOH)+H^+
121	$(2\text{-PrOH})_2+H^+$
181	$(2\text{-PrOH})_3+H^+$
407	$[UO_2OH(2\text{-PrOH})_2]^+$
467	$[UO_2OH(2\text{-PrOH})_3]^+$
389	$[UO_2OPr(2\text{-PrOH})]^+$
449	$[UO_2OPr(2\text{-PrOH})_2]^+$
509	$[UO_2OPr(2\text{-PrOH})_3]^+$
392	$[UO_2NO_3(2\text{-PrOH})]$
454	$[UO_2NO_3(2\text{-PrOH})_2]^+$
512	$[UO_2NO_3(2\text{-PrOH})_3]^+$

Table 6.1. Major relevant species generated from ESI of a 1 mM solution of $UO_2(NO_3)_2\bullet(H_2O)_6$ in H_2O with 5% (by volume) 2-propanol and their nominal m/z values

$[UO_2OPr(2\text{-PrOH})]^+$. The tendency to eliminate either H_2O or HNO_3 from complexes initially containing uranyl-hydroxide or nitrate, and apparent retention of 2-propoxide, is consistent with previously reported tendencies for lanthanide and actinide species to form alkoxide complexes [39-41], with our earlier investigation of the CID of similar complexes containing methanol, ethanol or 1-propanol [19] and with the fact that the dominant species generated directly by ESI was an alcohol-coordinated uranyl-2-propoxide cation. To probe the alcohol –OH group as the possible origin of the proton transferred to either hydroxide or nitrate, the complex ions $[UO_2NO_3(2\text{-PrOD})_3]^+$ and $[UO_2OD(2\text{-PrOD})_3]^+$ were generated by ESI by using a spray system composed of uranyl nitrate and 2-propanol dissolved in D_2O. The large

excess of deuterated solvent caused the exchange of alcohol proton for deuteron.

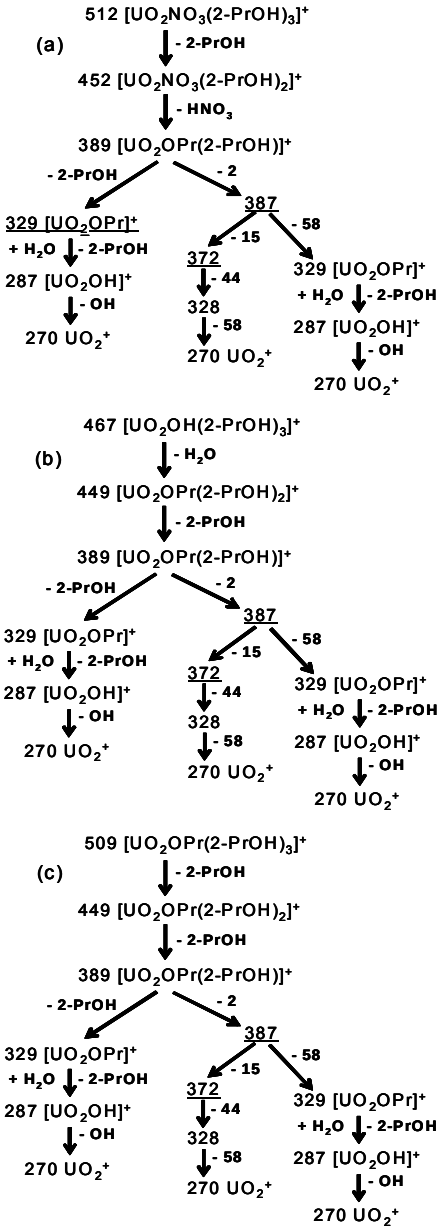

Figure 6.2 (a), (b), (c) Schemes for the multiple-stage CID of the species: (1) $[UO_2NO_3(2\text{-}PrOH)_3]^+$, (2) $[UO_2OH(2\text{-}PrOH)_3]^+$ and (3) $[UO_2OPr(2\text{-}PrOH)_3]^+$. Each precursor ion was derived from a spray solution of 1 mM solution of $UO_2(NO_3)_2 \bullet (H_2O)_6$ in water with 5% (by volume) 2-propanol. The most prominent product ion at any given CID stage is underlined. In many cases, H_2O adducts formed by gas-phase ion-molecule reactions were the most abundant ion in a CID spectrum.

For the deuterium labeled precursor complexes CID caused the elimination of DNO_3 and D_2O from $[UO_2NO_3(2\text{-}PrOD)_3]^+$ and $[UO_2OD(2\text{-}PrOD)_3]^+$, respectively, demonstrating that the reactions that liberate the small neutral species involve *intra*-complex transfer of a proton/deuteron from alcohol to NO_3 or OH. CID of $[UO_2NO_3(2\text{-}PrOH)_3]^+$, present in a minor amount in the same experiment because of incomplete hydrogen/deuterium exchange, caused the elimination of HNO_3, which suggests that loss of DNO_3 from the deuterium labeled complex did not occur via a mechanism that involved collisions with D_2O that entered the ion trap because of its use as the major spray solvent component.

Multiple dissociation steps initiated with the $[UO_2OPr(2\text{-}PrOH)_3]^+$ complex (figure 6.2 (c)) caused the successive elimination of all three 2-PrOH ligands to generate $[UO_2OPr]^+$. The uranyl-2-propoxide species was also a major product ion resulting from the multiple stage CID of the complexes initially containing uranyl nitrate and uranyl hydroxide. Subsequent CID of this species led to the formation of $[UO_2OH]^+$ at m/z 287. CID of the analogous complex ion derived from a solution containing the d_7 2-PrOH also led ultimately to the formation of $[UO_2OH]^+$ (spectrum not shown), which suggested that the uranyl hydroxide was not formed by some sort of rearrangement reaction that involved the transfer of hydrogen from an alkyl group to the oxygen atom of the coordinating 2-propoxide group.

The formation of $[UO_2OH]^+$ was also observed during the multiple-stage CID of uranyl ethoxide and uranyl 1-propoxide in the earlier investigation of complexes composed of uranyl ion, anion and solvent molecules (chapter 1 and [26]). In that study, the use of deuterium labeled alcohols produced somewhat ambiguous results regarding the formation of the species at m/z 287. In the present study, however, the formation of $[UO_2OH]^+$ from a complex containing d_7 2-propanol is difficult to reconcile with a rearrangement process that involves the transfer of hydrogen from an alkyl-group to an oxygen atom of either the uranyl ion or the alcohol: such a rearrangement/transfer reaction would presumably lead instead to the formation of $[UO_2OD]^+$ at m/z 288. The resolving power and mass accuracy of the ion trap instrument are sufficiently high to distinguish peaks at m/z 287 and 288: the latter was not observed following the CID of $[UO_2OCD(CD_3)_2]^+$. Instead, it is likely that the hydroxide is generated by reactive collisions with H_2O molecules, present as a contaminant within the ion trap, via the reaction (for non-deuterium labeled complex):

$[UO_2OCH(CH_3)_2]^+ + H_2O \rightarrow [UO_2OCH(CH_3)_2(H_2O)]^{+*} \rightarrow [UO_2OH]^+ + (CH_3)_2CHOH°$.

Such a reaction pathway is plausible based on a recent work demonstrating that CID within ion trap instruments involves a significant number of activating collisions between precursor ions and small molecules such as N_2 and H_2O present as contaminants within the He bath gas [120,121].

Regardless of which 2-PrOH coordinated uranyl-anion complex (i.e. with nitrate, hydroxide or 2-propoxide) was selected for study, the multiple stage CID experiment eventually generated a product ion with formula $[UO_2OPr(2\text{-}PrOH)]^+$ at m/z 389. Serial CID experiments corresponding to MS^3 through MS^7 are shown in Figures 6.3 (a) through 6.3 (e), respectively, and were initiated by isolation and CID of $[UO_2OPr(2\text{-}PrOH)_3]^+$ (m/z 509). This reaction eliminated 2-PrOH and formed $[UO_2OPr(2\text{-}PrOH)_2]^+$, which is the parent ion in the spectrum in figure 3a. CID of $[UO_2OPr(2\text{-}PrOH)_2]^+$ (MS^3, figure 3a) caused the elimination of 2-PrOH to generate $[UO_2OPr(2\text{-}PrOH)]^+$ at m/z 389. A prominent peak 18 mass units (u) higher corresponded to the formation of a water adduct to $[UO_2OPr(2\text{-}PrOH)]^+$. In general, the water adducts can be identified by characteristic peak tails and chemical mass shifts [24,123,124] (shifts of ~.2-.3 u lower than expected mass). In addition, the adducts were identified in our experiments by the isolation and storage of expected product ions in the ion trap for periods of 100-300 msec with minimal collisional excitation. During this isolation step all ionized species except the one chosen for storage were resonantly ejected from the ion trap. The appearance of peaks 18 units higher than the isolated ion was indicative of the formation of water adducts; [9-11] the abundance of the adducts increased as the isolation and storage time was extended.

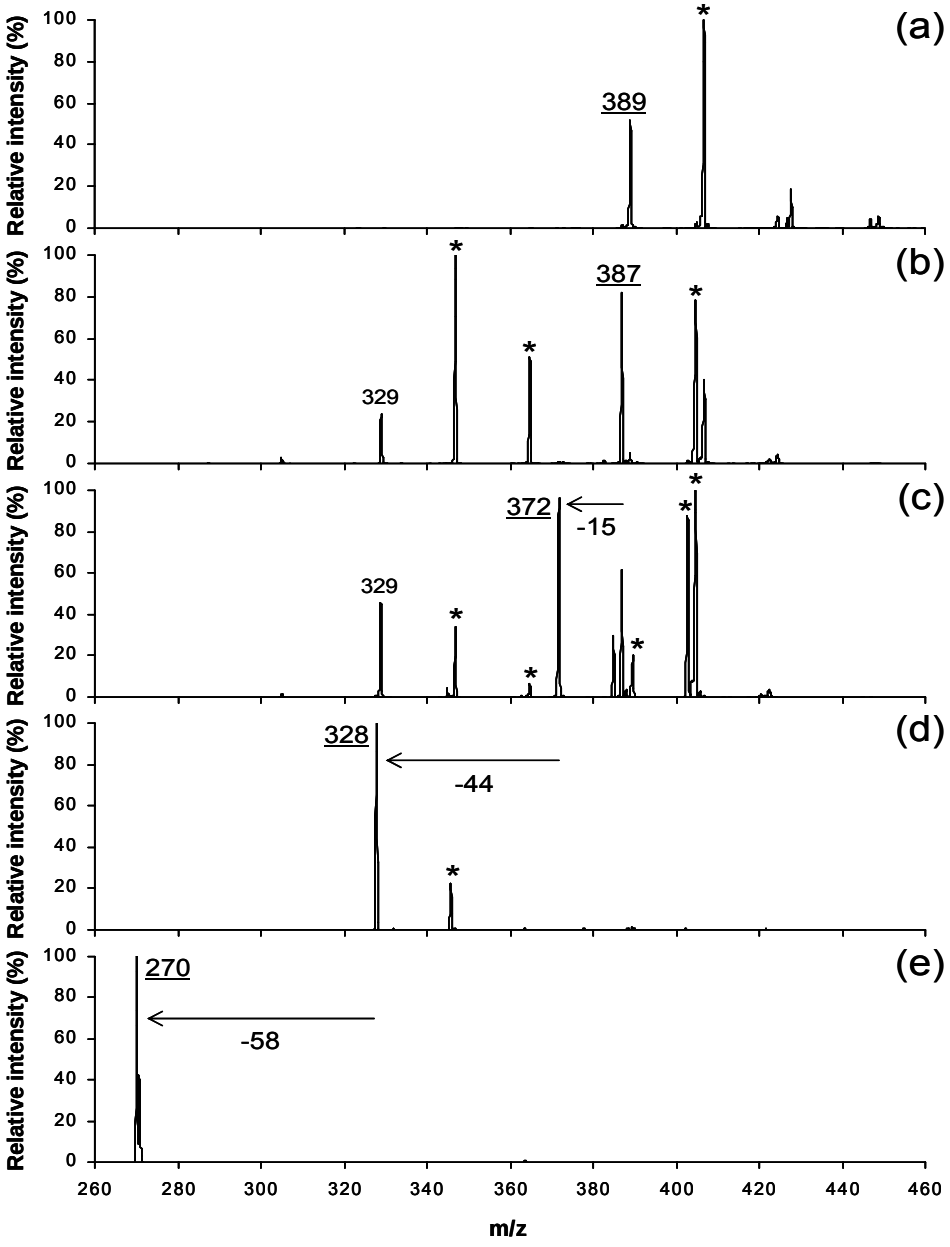

Figure 6.3 (a), (b), (c), (d), (e). Representative product ion spectra for the multiple-stage CID of the $[UO_2OPr(2\text{-}PrOH)_3]^+$ precursor ion. The spectra show the MS^3 through MS^7 CID stages. Product ions are underlined, and compositions for the peaks labeled with m/z values are provided in the text. Peaks labeled with asterisks are H_2O adducts to product ions generated by ion-molecule reactions in the ion trap.

Subsequent CID of $[UO_2OPr(2\text{-}PrOH)]^+$ (MS^4 of m/z 389, figure 6.3(b)) activated two fragmentation pathways: (1) formation of a prominent product ion at m/z 387, corresponding to the loss of 2 u, and (2) the elimination of 2-PrOH (60 u) to generate $[UO_2OPr]^+$ at m/z 329 with associated water adducts). When the species at m/z 387 was subjected to another stage of CID (MS^5, figure 6.3(c)), two fragmentation pathways were observed: (1) the elimination of 15 u to generate a product ion at m/z 372, and (2) the elimination of 58 u to furnish the ion at m/z 329. The loss of 58 u at this stage suggested the elimination of acetone as a neutral species and retention of 2-propoxide in the product ion.

CID of the species at m/z 372 (MS^6, figure 6.3(d)) caused the elimination of 44 u to generate an ion at m/z 328, and subsequent CID of this product ion (MS^7, figure 6.3(e)) caused the loss of 58 u to form UO_2^+ at m/z 270. The loss of 44 u at the MS^6 stage suggested the elimination of acetaldehyde while the elimination of 58 u at the MS^7 stage was again consistent with the hypothesized loss of acetone from the complex ion. Formation of the reduced uranyl ion at m/z 270 was confirmed by comparing the intrinsic hydration kinetics to previous measured rates for the species [35].

To investigate the fragmentation reactions/pathways observed during the multiple-stage CID experiment in greater detail, isotopically labeled precursor ions

were generated by adding the deuterated versions of 2-PrOH to the ESI spray solution. The results from the multiple stage CID experiments were condensed to fragmentation schemes for $[UO_2OPr(2\text{-PrOH})]^+$ complexes containing no deuterium (control), 2-PrOD, d_6 2-PrOH and d_7 2-PrOH which are provided in figure 6.4. For the complex ion featuring 2-PrOD, the neutral loss in the MS^4 stage shifted from 2 to 3 u, indicating participation of the proton of the –OH group in the fragmentation reaction, and no further shifts to the neutral losses at the MS^5, MS^6 and MS^7 stages were observed.

When the $[UO_2OPr(2\text{-PrOH})]^+$ complex was assembled starting from d_6 2-PrOH, the neutral loss of 2 u was also observed at the MS^4 stage. Since the d_6 2-PrOH, contains D only on the methyl groups, and hydrogen at the carbinol position and–OH positions, participation of both the carbinol and hydroxyl H atoms is clearly indicated. Indeed, the neutral loss at the MS^4 stage shifted to 3 u in the d_7 2-PrOH version of the complex (methyl *and* carbinol positions labeled with deuterium), which features complete deuterium labeling of the alkyl group.

The neutral loss of 15 u observed at the MS^5 stage for the precursor complex without deuterium label did not shift for CID of the complex containing 2-PrOD. However, the neutral loss at the same CID stage did shift by 3 (indicating the loss of 3 deuterium atoms) to 18 u for the precursor complexes containing either the d_6 and d_7

2-PrOH. The mass shift to the neutral therefore implicates the methyl groups of the intact 2-PrOH ligand or of the 2-propoxide group in the fragmentation reaction at the MS^5 stage. The elimination of 15 u was also a prominent reaction pathway observed for the CID of uranyl ethoxide and *n*-propoxide cations, i.e. $[UO_2OCH_2CH_3]^+$ and $[UO_2OCH_2CH_2CH_3]^+$, in an earlier study [26].

The neutral loss of 44 u at the MS^6 stage for the unlabeled version of the complex ion shifted to 47 and 48 u for the precursor complexes containing the d_6 2-PrOH or d_7 2-PrOH, respectively. The shifts of the neutral losses to 47 and 48 u indicate the elimination, in part, of 3 and 4 hydrogen/deuterium atoms, respectively, in the fragmentation reaction that occurs at the MS^6 CID stage. It was originally hypothesized that the loss of 44 u represented the elimination of acetaldehyde, which contains a total of 4 hydrogen atoms. For the complex generated from the d_6 2-PrOH, the 2-propoxide group contains 6 deuterium atoms on the 2 methyl groups. If one of the methyl groups is eliminated from the 2-propoxide group at the MS^5 stage, the remaining portion would bear 1 hydrogen (carbinol position) and 3 deuterium atoms (methyl group). The elimination of the hydrogen and 3 deuterium atoms along with the remaining carbon and oxygen atom totals 47 u. The elimination of 48 u instead from the complex derived from the d_7 2-PrOH is consistent with the substitution of another deuterium atom at the carbinol position.

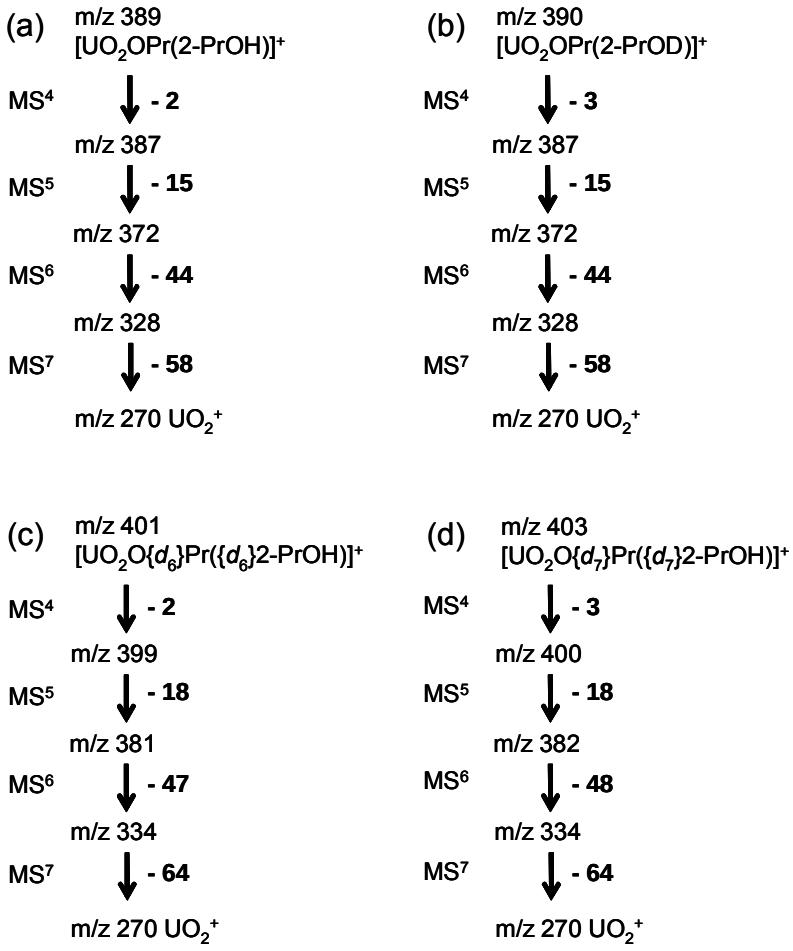

Figure 6.4. Schemes for the multiple-stage CID of the general species $[UO_2OPr(2\text{-}PrOH)]^+$, derived from a spray solutions containing $UO_2(NO_3)_2\bullet(H_2O)_6$ and: (a) non-deuterium labeled 2-propanol in H_2O, (b) non-deuterium labeled 2-propanol in D_2O (thus generating 2-PrOD), (c) d_6 2-PrOH in H_2O and (d) d_7 2-PrOH in H_2O. The schemes summarize the fragmentation pathways observed at the MS^4 through MS^7 stages initiated by CID (MS/MS) of the fully coordinated uranyl 2-propoxide monopositive cation.

The neutral loss of 58 u at the MS^7 stage did not shift for CID of the complex containing 2-PrOD. The neutral loss did shift by 6 (indicating the loss of 6

hydrogen/deuterium atoms) to 64 u for the precursor complexes containing either the d_6 and d_7 2-PrOH. The fact that the neutral eliminated was the same mass for complexes containing either the d_6 or d_7 2-PrOH, which differ in the lack of the deuterium label at the carbinol position for the former, suggests that the species eliminated as 58 u from the control complex does not bear a hydrogen or deuterium atom at that site. The formation of the 58 u species that is eventually eliminated at the MS^7 stage therefore likely requires the initial elimination of 2 u observed at the MS^4 stage. The elimination of 2 hydrogen atoms from intact 2-PrOH, one from the –OH group and the other from the secondary carbon position, would result in the generation of a species with the same composition as acetone. The acetone molecule contains 6 hydrogen atoms, and the shift in the neutral loss at the MS^7 stage when comparing the complexes derived from d_6 and d_7 2-PrOH to the complex without deuterium label indicates the elimination of a species with 6 hydrogen atoms.

The isotope labeling study suggests that two H atoms are eliminated from the intact 2-PrOH ligand, resulting in the formation of acetone that remains bound to the uranyl ion. Subsequent CID causes the elimination of a methyl radical and charge transfer to the metal center to furnish a gas-phase, monopositive cation containing UO_2 coordinated by acetaldehyde and acetone; if this is correct, then the UO_2^{2+} can be viewed as formally reduced at this stage. The acetaldehyde and acetone are then

eliminated in successive CID stages to leave the reduced uranyl cation, UO_2^+. The elimination of acetaldehyde prior to acetone is consistent with preliminary investigations in our laboratory of the relative strengths of the interactions between the two ligands and gas-phase uranyl cations.

As noted earlier, Suib and coworkers reported the photoassisted catalytic oxidation of 2-propanol to acetone by uranyl ion exchanged into the cavities of zeolite materials [115,116], and the chemistry observed with the condensed uranyl-2-propanol system was a motivation for the present gas-phase study. In the previous solid-phase experiments, the number and nature (splitting) of peaks in luminescence spectra were cited as evidence that 2-propanol was bound to an equatorial site on the uranyl ion within the zeolite matrix [117]. Other oxygen atoms within the equatorial positions were likely zeolite framework atoms, either bound to silicon or aluminum. In the present experiments, the 2-propanol molecule is certainly bound to an equatorial site of the uranyl ion, and the oxygen atom of the 2-propoxide ligand could be (crudely) analogous to the framework oxygen atom in the condensed phase system. Coordination by both 2-propanol and 2-propoxide at equatorial sites is supported by density function theory calculations currently underway in our laboratory. In the solid-phase experiments, it was suggested that the mechanism for 2-propanol conversion to acetone involved the reduction of the uranyl ion to a U(V) species within

the zeolite framework and associated oxidation of the alcohol [117]. In the solution phase, the first step in a similar transformation is reported to be the reduction of the uranyl ion [124]. In our gas-phase experiments, the initial reaction in the CID pathway that results in the conversion of 2-propanol to acetone involves the apparent elimination of two H atoms from $[UO_2OPr(2\text{-}PrOH)]^+$: such a step is possible without concomitant reduction of the uranyl ion. As demonstrated by the multiple-stage CID experiments, the successive elimination of methyl radical, acetone and acetaldehyde ultimately leads to the generation of UO_2^+, which is a reduced, U(V) dioxo cation. The abstraction of hydrogen/deuterium from the carbinol position observed in the gas phase during our experiments in particular is consistent with the observation in the solution phase of the removal of hydrogen from primary and secondary alcohols by photoexcited uranyl ion [124-126]. In the solution-phase experiments, oxidation of primary and secondary alcohols to generate aldehydes and ketones occurs in the presence of molecular oxygen.

The CID pathways involving the elimination of H atoms and CH_3 radical were not observed when complexes including either 1-propanol or *tert*-butanol were investigated. CID of the 1-propanol complex was investigated in our earlier study of uranyl complexes [26]. The fragmentation pathway observed for the complex with formula $[UO_2OPr(1\text{-}PrOH)]^+$ involved only the elimination of intact 1-propanol, while

subsequent CID of $[UO_2OPr]^+$ with 1-propoxide resulted in C-C bond scission and the elimination of CH_2CH_3 and CH_3 as radical species as well as the apparent formation of $[UO_2OH]^+$. CID of the *tert*-butanol versions of the complexes (spectra not shown) demonstrate significant dehydration reactions and the ultimate production of $[UO_2OH]^+$.

A textbook example of the oxidation of 2-propanol to acetone involves the formation of a chromate ester [127]. In this case, the alcohol is initially deprotonated in the solution phase to make an oxygen-chromium bond. A base then removes a proton from the carbinol position to generate acetone. In our experiments involving the uranyl ion, the sequence of reaction steps apparent in the multiple-stage CID experiment, including the neutral losses observed, suggests the initial reaction is the elimination of two H atoms. Whether the loss of the two atoms is the result of β type elimination, or a rapid, stepwise elimination of single atoms is not clear. In the latter case, the conversion of 2-propanol to acetone might then occur via a mechanism (similar to that proposed for chromate) involving deprotonation of the 2-propanol and ubiquitous gas-phase H_2O serving as the base to remove the second H atom. A clear role for reaction collisions with H_2O is evident with the conversion of $[UO_2OPr]^+$ to $[UO_2OH]^+$ as noted above. However, we found no evidence for any mechanism in which a product ion is generated by the elimination of a single H atom from

$[UO_2OPr(2\text{-}PrOH)]^+$. We note, however, that a fragmentation reaction that causes deprotonation (i.e. eliminate H^+) of the intact 2-propanol molecule would presumably lead to the net reduction of the complex charge state and production of a neutral gas-phase species (thus precluding its scan-out from the mass spectrometer and detection as an ion). As a result, we can tentatively conclude that the initial elimination of the two H atoms occurs as an elimination of H_2 from the 2-propanol molecule.

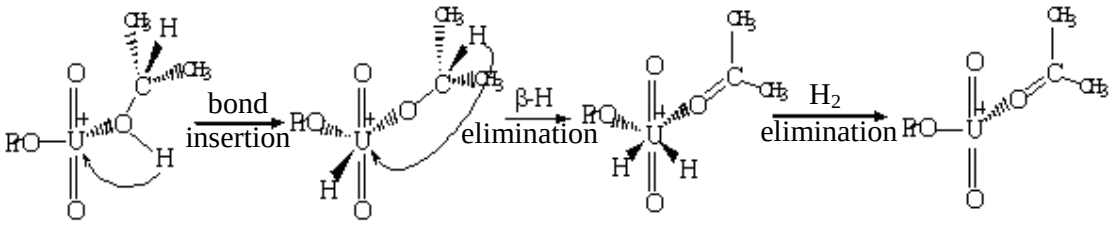

Figure 6.5. Scheme for elimination of H_2 from *bis*-ligated uranyl occurring by bond insertion followed by β-H transfer to the metal.

One way that this might occur would be by bond insertion involving the undercoordinated uranium metal center in the $[UO_2OPr(2PrOH)]^+$ complex. This would produce a $[UO_2(H)(OPr)_2]^+$ intermediate that would undergo H transfer (Figure 6.5), forming a *bis*-hydrido complex. This type of intermediate is well known to be an immediate precursor to H_2 elimination from complexes of organic molecules with early transition metal cations [128-131]. What are required for the reaction are empty *d* orbitals, which may in be available in the *bis*-ligated uranyl system. The lowest

unoccupied molecular orbitals in the uranyl system are two virtual 5*f*, which presumably would be acceptors for the two attached ligands OPr and PrOH [132]. Above these are two virtual 6*d* orbitals, that may be reactive for bond insertion; thus the uranyl system may be converted to transition metal-like reactivity by occupancy of the first two equatorial coordination sites.

A similar rationale may account for the subsequent loss of the methyl radical. Early transition metal cations are also known to participate in C-C bond insertion, which would produce an $[UO_2(CH_3)(acetaldehyde)(acetone)]^+$ intermediate. β-H transfer does not occur from this intermediate because it would have to involve the aldehydic hydrogen, loss of which would produce an undercoordinated C center. Therefore CID of this complex merely results in loss of the methyl radical, effectively reducing the uranyl core in the process.

A number of metal ions can be used to carry out the catalytic conversion of 2-propanol to acetone in condensed phases, and this prompted examination of other metal + 2-propanol systems. We were unable to generate cationic complexes composed of chromium (III) or chromium (VI) and 2-propanol with stoichiometries analogous to those containing the uranyl ion by ESI. ESI could be used to generate complex ions of similar general composition from solutions of Ca, Ni, Co, Zn or Pb nitrate, each with the metal in formal +2 oxidation state. However, the conversion of

2-propanol to acetone was not observed for any of these systems. This is somewhat surprising given the demonstrated tendency for supported Ni particles to selectively convert alcohols to ketones and aldehydes [128]. We did find that the conversion of 2-propanol to acetone occurred during the CID of a complex with formula $[Fe(NO_3)_2(2\text{-}PrOH)_2]^+$.

CONCLUSIONS

The experiments described in this chapter represent the first investigation of the gas-phase fragmentation reactions of complex ions containing the uranyl ion coordinated by 2-propanol. ESI generated complex ions with general composition $[UO_2A(2\text{-}PrOH)]^+$ where A = OH^-, NO_3^- or $2\text{-}PrO^-$. Regardless of the coordinating anion, multiple stage CID resulted in the formation of a species with composition $[UO_2OPr(2\text{-}PrOH)]^+$. For the precursor ions with composition $[UO_2OH(2\text{-}PrOH)]^+$ and $[UO_2NO_3(2\text{-}PrOH)]^+$, deuterium labeling of the alcohol –OH position suggests that $[UO_2OPr(2\text{-}PrOH)]^+$ is formed by proton transfer from the alcohol to hydroxide or nitrate during the elimination reaction.

Through the use of extensive deuterium labeling of 2-propanol, one can conclude that collisional activation in a multiple-stage CID experiment will cause the conversion of 2-propanol and 2-propoxide to acetone and acetaldehyde when both are ligands

within a gas-phase, mono-positive uranyl cation. The chemistry in the gas phase produces the same net reaction products as photochemical activation of uranyl exchanged into zeolites as previously reported. The same reactions were not observed when 2-propanol was replaced by 1-propanol, or when the uranyl moiety was replaced by divalent Ca, Ni, Co, Zn or Pb. A possible explanation for the dehydrogenation and the CH_3 radical elimination might be the occurrence of bond insertion by the metal center in the *bis*-ligated uranyl complex, which would be expected to have a LUMO consisting of unoccupied 6*d* orbitals that would confer transition metal-like behavior on the complex.

CHAPTER 7

PRODUCTION AND COLLISION-INDUCED DISSOCIATION OF GAS –PHASE WATER- AND ALCOHOL-COORDINATED URANYL COMPLEXES CONTAINING HALIDE OR PERCHLORATE ANIONS

INTRODUCTION

To improve the understanding of intrinsic uranium chemistry, and in particular the chemistry of species in higher oxidation states (i.e. +5, +6), our group [26,101,134,135] and others [136] have been exploring the use of electrospray ionization (ESI) to generate mono-positive uranyl-ligand cations for subsequent gasphase studies. As noted in chapter 3 and 4, ESI and multiple-stage CID have also been used to generate bare uranyl hydroxide, nitrate and acetate cations for subsequent investigations of intrinsic hydration tendencies [101]. The relative rates for the formation of the monohydrates $[UO_2A(H_2O)]^+$, with respect to A (where A = OH, NO_3 or CH_3COO), followed the trend: $CH_3COO>NO_3>>OH$. The trend was rationalized in terms of the donation of electron density by the strongly basic OH to the uranyl metal center and the reduction of Lewis acidity of U, and the presence of increased degrees of freedom to accommodate excess energy from the hydration reaction in the case of CH_3COO and NO_3. The monohydrates also reacted with water, forming dihydrates and then trihydrates. The rates for formation of the nitrate and acetate dihydrates, $[(UO_2A)(H_2O)_2]^+$, were very similar to the rates for formation of the

monohydrates; the presence of the first H_2O ligand had no influence on the addition of the second. In contrast, formation of $[(UO_2OH)(H_2O)_2]^+$ was nearly three times faster than the formation of the monohydrate.

The observed differences in reactivity for mono-positive cations containing hydroxide, nitrate and acetate motivated further attempts to generate gas-phase complexes containing other monovalent anions. In this chapter, experiments are described that involve the formation of gas-phase complexes with the general formulae $[UO_2A(H_2O)_n]^+$ and $[UO_2A(ROH)_3]^+$, where A = Cl, Br, I or ClO_4 and ROH = CH_3OH or CH_3CH_2OH, by ESI. The original goal was to use CID to reduce the complex coordination number for subsequent ligand-addition reaction studies of the $[UO_2A]^+$ cations. However, such species were only observed during the multiple-stage CID of the complexes containing Br and ClO_4. Multiple-stage CID of the complexes containing Cl or I instead resulted in the formation of the uranyl-hydroxide cation, $[UO_2OH]^+$, by a fragmentation reaction that involved the elimination of HA. A similar pathway was observed to a lesser extent for the complexes containing Br and ClO_4. In several cases, the elimination of the HA appeared to involve intra-complex proton transfer, which was confirmed by the multiple-stage CID of analogous complexes containing coordinated alcohol ligands in natural and deuterium (–OD) labeled form. Formation of $[UO_2OH]^+$ was also observed

following CID of the bare $[UO_2Br]^+$ and $[UO_2ClO_4]^+$ cations. In this case, the formation mechanism likely involved reactive collisions with H_2O in the ion trap to form an activated intermediate, which, in turn, dissociated via the elimination of neutral acid and retention of hydroxide by the product ion.

EXPERIMENTAL

The uranyl oxide (UO_3) used to prepare the various uranyl– anion solids examined in this study was a gift from J. David Van Horn at the University of Missouri-Kansas City. Solids assumed to be uranyl chloride, $UO_2(Cl)_2.(H_2O)_x$; bromide, $UO_2(Br)_2.(H_2O)_x$; iodide, $UO_2(I)_2.(H_2O)_x$; and perchlorate, $UO_2(ClO_4)_2.(H_2O)_x$ were prepared by first dissolving solid UO_3 in the respective mineral acids, followed by evaporation over gentle heat to dryness. The goal was not the rigorous synthesis of uranyl-halide compounds, but precursor materials for production of gas-phase uranyl-halide complexes by ESI. Preparation of a fluoride version was not attempted. As discussed below, the solutions prepared from each solid generated mass spectra that were analogous to those derived from solutions of uranyl nitrate in water in our earlier studies, 1, 2 and were composed primarily of the singly charged uranyl–anion complex coordinated by up to three solvent molecules. Therefore, the true composition of the solids prepared here was not determined. For ESI, stock solutions

(ca. 10^{-3} M based on measured amount of solid and assumed composition) of each uranyl solid were prepared by dissolving the appropriate amount of material in deionized H_2O.

ESI mass spectra were collected using the Finnigan LCQDeca^{TM} ion-trap mass spectrometer. The uranyl–anion stock solution and water/alcohol (1:1) solutions were infused into the ESI-MS instrument using the incorporated syringe pump at a flow rate of 5 mL/min.

CID experiments were performed at the same He pressure by setting the isolation width between 5 and 12 mass units (depending on the species), the activation Q (as labeled by instrument manufacturer, used to adjust the qz value for the resonant excitation of the precursor ion during the CID portion of the experiment) at 0.3 and the activation amplitude at 10–20% (of 5 V). In all cases, activation times for CID were 30 ms.

RESULTS AND DISCUSSION

Mass spectra and multiple-stage CID of hydrated complexes

The ESI mass spectra generated using the solutions prepared by dissolving the uranyl perchlorate and uranyl bromide solids in deionized H_2O are shown in Figs. 7.1(a) and 7.1(b), respectively. In general, the spectra (i.e. types of species and

relative abundances) in Fig. 7.1 are representative of those observed when the solutions derived from the chloride and iodide solids were used, and are also similar to the spectrum obtained by ESI of a uranyl nitrate solution [26]. Each solution generated abundant singly charged complexes with the general formula $[UO_2A(H_2O)_n]^+$, where A corresponded to the respective anions (including hydroxide) and n=1–3. The characteristic and expected isotopic peaks were observed for complexes containing chlorine and bromine atoms. The isotopic patterns were particularly important for the uranylchloride complexes, for which several of the ^{35}Cl-containing species have the same nominal m/z value as hydrated uranyl-hydroxide species. The relevant complex ions observed for the chloride, bromide, iodide and perchlorate solutions are summarized in Table 7.1.

The composition assignments shown in Table 7.1 were made with the assumption of direct anion coordination to the uranyl center. As discussed below, CID at various stages caused the elimination of, e.g., HCl or HBr, suggesting the possibility that the composition assignments might instead follow the formula $[UO_2OH(H_2O)_n(HCl)]$ or $[UO_2OH(H_2O)_n(HBr)]$. A significant ion population coordinating acid ligands might be expected to eliminate HA (where A represents any of the respective anions) at any CID stage because of a weaker interaction between

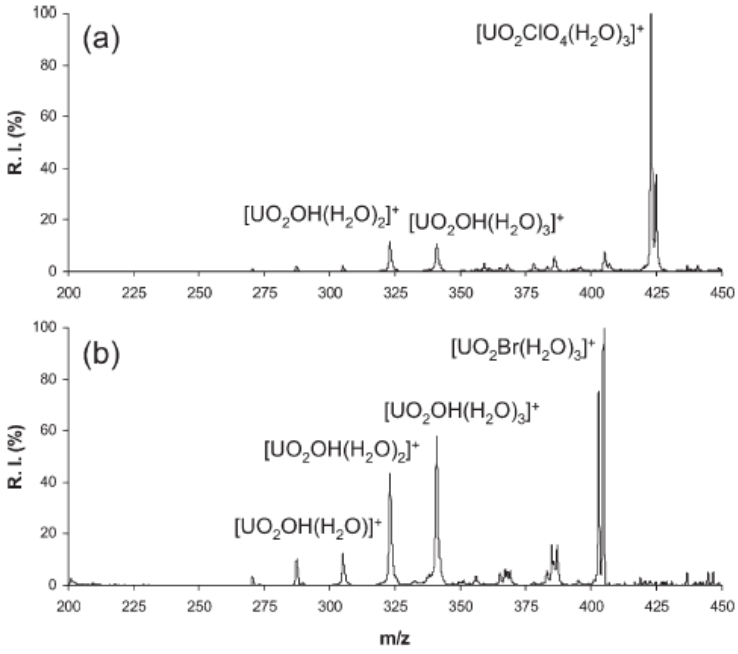

Figure 7.1. ESI mass spectra generated from aqueous solutions containing uranyl (a) perchlorate and (b) bromide solids. For the complete list of relevant species observed for all uranyl–anion compounds, refer to Table 7.1.

	m/*z* value	Composition
Uranyl hydroxide	287	$[UO_2OH]^+$
	305	$[UO_2OH(H_2O)]^+$
	323	$[UO_2OH(H_2O)_2]^+$
	341	$[UO_2OH(H_2O)_3]^+$
Uranyl chloride	323, 325	$[UO_2Cl(H_2O)]^+$
	341, 343	$[UO_2Cl(H_2O)_2]^+$
	359, 361	$[UO_2Cl(H_2O)_3]^+$
Uranyl bromide	367, 369	$[UO_2Br(H_2O)]^+$
	385, 387	$[UO_2Br(H_2O)_2]^+$
	403, 405	$[UO_2Br(H_2O)_3]^+$
Uranyl iodide	415	$[UO_2I(H_2O)]^+$
	433	$[UO_2I(H_2O)_2]^+$
	451	$[UO_2I(H_2O)_3]^+$
Uranyl perchlorate	387	$[UO_2ClO_4(H_2O)]^+$
	405	$[UO_2ClO_4(H_2O)_2]^+$
	423	$[UO_2ClO_4(H_2O)_3]^+$

Table 7.1. Relevant complex ions generated by ESI of uranyl-halide solids

HA and UO_2^{2+} compared to A^- and UO_2^{2+}. For example, calculated U–ligand bond distances within bis-uranyl complexes are 2.81 and 2.54 Å for coordinated HCl and Cl^-, respectively, [137] suggesting stronger coordination by the chloride anion. As described below, with H_2O-coordinating ligands, the loss of neutral acid (i.e. HA) was not observed in the first CID stage and, for the bromide, iodide and perchlorate versions of the complexes, was not observed until very high CID stages (MS^4 and higher). Our conclusion, therefore, is that the complex ions are best described using the formulae provided in Table 7.1.

The multiple-stage CID of $[UO_2OH(H_2O)_3]^+$ was investigated in an earlier study. Briefly, the first three stages (MS/ MS through MS^4) caused the sequential elimination of H_2O ligands to furnish $[UO_2OH]^+$. Subsequent CID of $[UO_2OH]^+$ caused the elimination of 17 mass units (u), or the reductive elimination of OH, to leave UO_2^+ at m/z 270. Figure 7.2 shows product ion spectra obtained from the multiple-stage CID of $[UO_2Cl(H_2O)_3]^+$ at m/z 359 and 361. Unlike several of the lower m/z uranyl-chloride complexes, the $[UO_2Cl(H_2O)_3]^+$ species was free from interference from an isobaric uranylhyroxide species. CID of $[UO_2Cl(H_2O)_3]^+$ (MS/MS stage, Fig. 7.2(a)) caused the elimination of a single H_2O ligand to generate $[UO_2Cl(H_2O)_2]^+$ at m/z 341 and 343. Two apparent product ions were observed following CID (MS/MS/MS or MS^3 stage,

Fig. 7.2(b)) of $[UO_2Cl(H_2O)_2]^+$. The first corresponded to the elimination of a second H_2O ligand to furnish $[UO_2Cl(H_2O)]^+$ at m/z 323 and 325. The second product ion appeared as a single isotope peak at m/z 305, a mass consistent with the formation of hydrated uranyl-hydroxide, $[UO_2OH(H_2O)]^+$. The neutral loss of 36 and 38 u to generate $[UO_2OH(H_2O)]^+$ is consistent with the elimination of $H^{35}Cl$ and $H^{37}Cl$, respectively. Subsequent CID of the species at m/z 305 (MS^4, spectrum not shown) generated $[UO_2OH]^+$ at m/z 287, which, in turn, lost 17 u at the MS^5 stage (spectrum not shown) to furnish UO_2^+.

The product ions generated by CID of $[UO_2Cl(H_2O)]^+$ (MS^4 stage, Fig. 7.2 (c)) included $[UO_2OH]^+$ via the elimination of HCl, and the hydrated version of the ion, $[UO_2OH(H_2O)]^+$. The $[UO_2Cl(H_2O)]^+$ precursor proved to be particularly labile. Figure 7.2 (d) shows the spectrum obtained when the species was isolated in the ion trap, without imposed collisional activation (i.e. activation amplitude set to 0%) for 30ms—the same activation time used for CID to generate the product ion spectrum shown in Fig. 7.2 (c). The spectrum in Fig. 7.2 (d) is similar to the one shown in Fig. 7.2 (b) and contains the $[UO_2OH(H_2O)]^+$ and $[UO_2Cl(H_2O)_2]^+$ product ions. The latter is formed by a ligand-addition reaction involving indigenous H_2O in the ion trap, which was confirmed by an increase in intensity for the species with increased isolation time. Generation of the former product, $[UO_2OH(H_2O)]^+$, presumably involves interactions

with H_2O during the isolation step. In this case, low-energy collisions between $[UO_2Cl(H_2O)]^+$ and gas-phase H_2O may cause the formation of an activated version of $[UO_2Cl(H_2O)_2]^+$*, which subsequently decomposes to form $[UO_2OH(H_2O)]^+$ by the elimination of HCl and retention of OH. The involvement of reactive collisions with indigenous H_2O during the isolation step is plausible because of earlier accounts that have demonstrated the participation of small neutral molecules such as N_2 and H_2O during CID in ion-trap instruments when present as contaminants within the He buffer/bath gas [120,121]. In addition, the involvement of reactive collisions with gas-phase H_2O/D_2O was demonstrated in an earlier study to account for the generation of $[UO_2OH]^+$ from the CID of the uranyl-2-propoxide cation, $[UO_2OCH(CH_3)_2]^+$ [135].

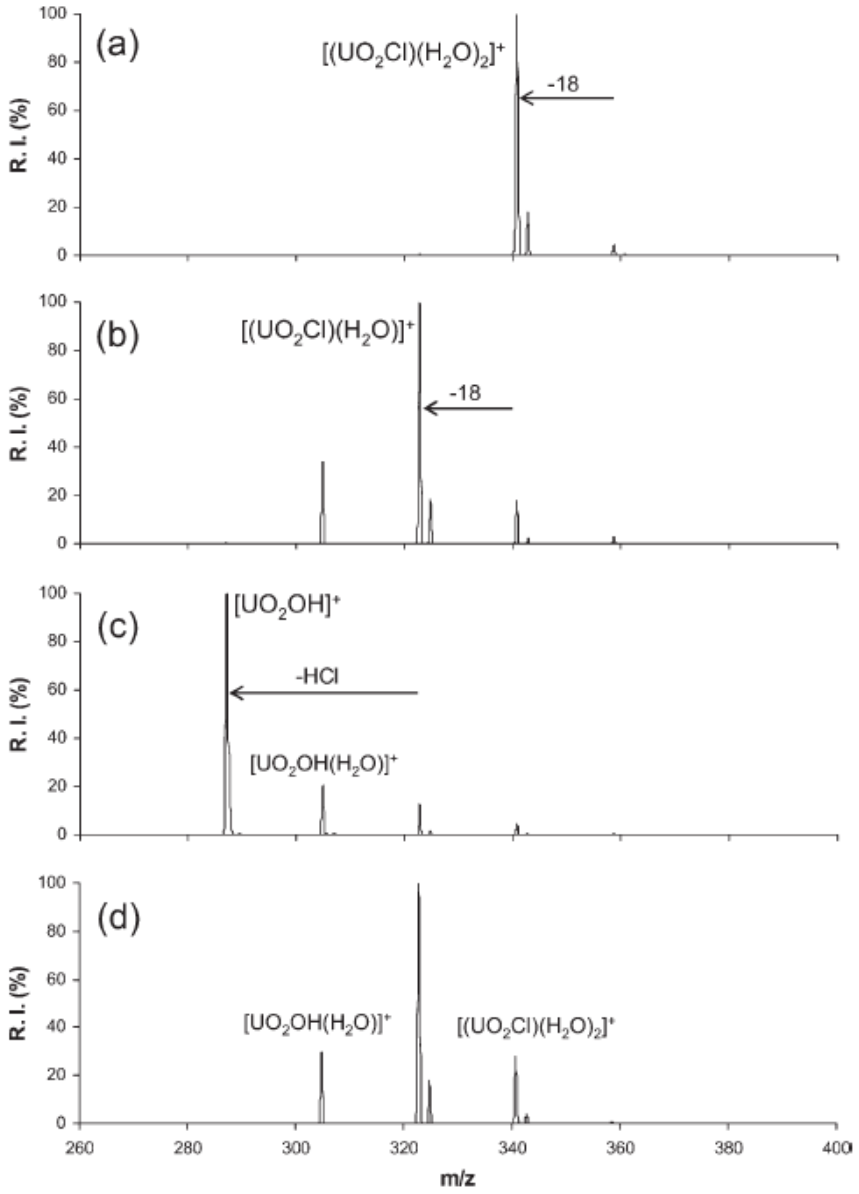

Figure 7.2. CID spectra for $[UO_2Cl(H_2O)_3]^+$ precursor complex: (a) MS/MS stage, dissociation of $[UO_2Cl(H_2O)_3]^+$; (b) MS^3 stage, dissociation of $[UO_2Cl(H_2O)_2]^+$; (c) MS^4 stage, dissociation of $[UO_2Cl(H_2O)]^+$; and (d) MS^4 stage, involving the isolation of $UO_2Cl(H_2O)]^+$ without imposed collisional excitation. The isotopic ratios for the fragment ions at m/z 341/343 and 323/325 are biased in favor of the ^{35}Cl-bearing ions because the isolation window for the MS/MS stage was centered at the most abundant isotopic ion (m/z 359, ^{35}Cl bearing), which tends to bias the ratio of the H_2O elimination ions in favor of the ^{35}Cl-bearing fragment ions.

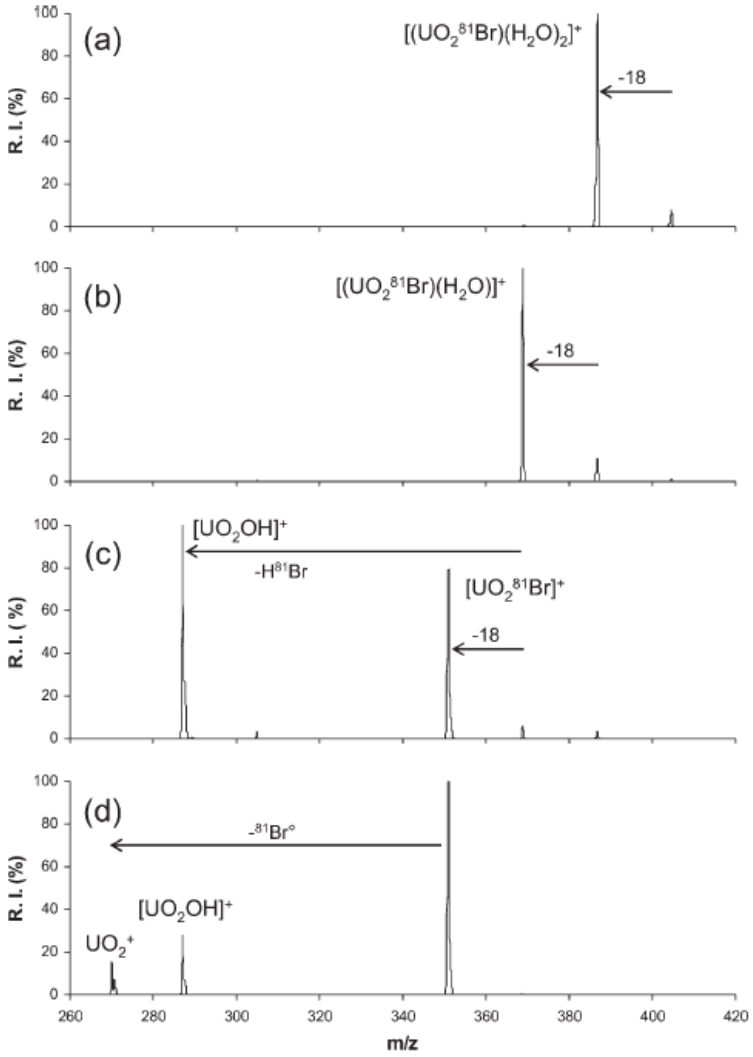

Figure 7.3. CID spectra for $[UO_2{}^{81}Br(H_2O)_3]^+$ precursor complex: (a) MS/MS stage, dissociation of $[UO_2{}^{81}Br(H_2O)_3]^+$; (b) MS^3 stage, dissociation of $[UO_2{}^{81}Br(H_2O)_2]^+$; (c) MS^4 stage, dissociation of $UO_2{}^{81}Br(H_2O)]^+$; and (d) MS^5 stage, CID of $[UO_2{}^{81}Br]^+$.

To simplify the display of MS^n results, product ion spectra shown in Fig. 7.3 for the CID of $[UO_2Br(H_2O)_3]^+$ are the result of the isolation and dissociation of only the ^{81}Br isotopic peak. The retention of Br in a product ion, or elimination of the same in a neutral species, was confirmed in all cases by experiments in which both the ^{79}Br and

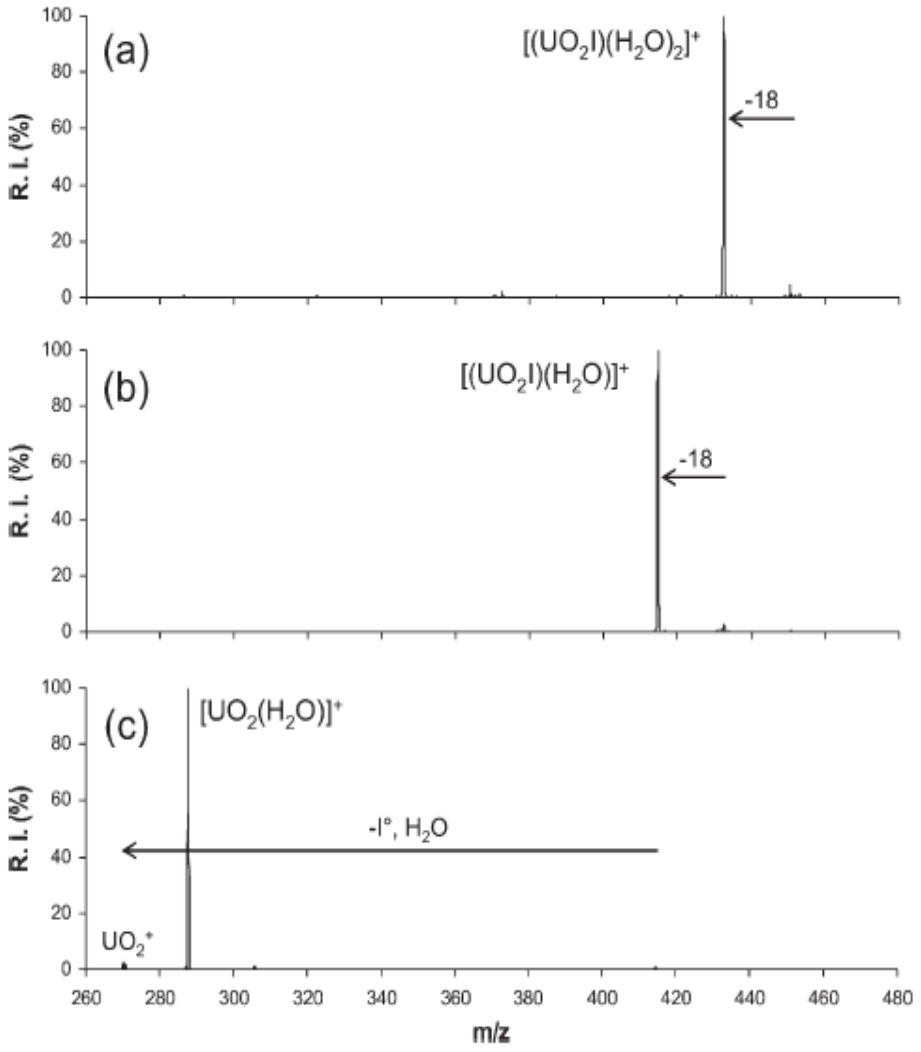

Figure 7.4. CID spectra for $[UO_2I(H_2O)_3]^+$ precursor complex: (a) MS/MS stage, dissociation of $[UO_2I(H_2O)_3]^+$; (b) MS^3 stage, dissociation of $[UO_2I(H_2O)_2]^+$; and (c) MS^4 stage, dissociation of $[UO_2I(H_2O)]^+$.

^{81}Br isotopic peaks were isolated for CID. As observed with the complex containing chloride, the CID of $[UO_2{}^{81}Br(H_2O)_3]^+$ (MS/MS stage, Fig. 7.3(a)) caused the elimination of a single H_2O ligand to generate $[UO_2{}^{81}Br(H_2O)_2]^+$ at m/z 387, and subsequent CID of this species (MS^3 stage, Fig. 7.3(b)) caused the loss of a second

H_2O ligand. At the MS^4 stage (Fig. 7.3(c)), dissociation of $[UO_2{}^{81}Br(H_2O)]^+$ led to two product ions: $[UO_2Br]^+$ at m/z 351 by elimination of the third H_2O ligand and $[UO_2OH]^+$ by elimination of $H^{81}Br$. The $[UO_2Br]^+$ species proved to be particularly stable to further dissociation, and only at relatively high activation amplitudes (ca. 30–40%) did CID (MS4, Fig. 7.3(d)) eventually generate two product ions. The first was $[UO_2OH]^+$, presumably generated via an activated complex with formula $[UO_2Br(H_2O)]^{+}*$, with subsequent dissociation to produce $[UO_2OH]^+$ and neutral $H^{81}Br$. The second product ion was $UO_2{}^+$ generated by reductive elimination of Br. Elimination of neutral Br was reminiscent of the loss of NO_3 in an earlier study of the CID of H_2O and alcohol-coordinated $[UO_2NO_3]^+$ [26].

Figure 7.4 shows product ion spectra obtained from the multiple-stage CID of $[UO_2I(H_2O)_3]^+$. The first and second CID stages (MS/MS and MS^3, Figs. 7.4(a) and 7.4(b), respectively) caused the elimination of single H_2O ligands. However, at the MS^4 stage, the product ions generated were a low-abundance $UO_2{}^+$ at m/z 270 and a dominant $[UO_2(H_2O)]^+$ at m/z 288. This surprising observation suggests reductive elimination of an iodine atom, forming a U(V) dioxo cation with one ligated H_2O spectating. Other explanations can be suggested: e.g., in an earlier CID study of $[UO_2NO_3]^+$, it was proposed that an activated complex with composition $[UO_2NO_3(H_2O)]^{+}*$ was formed by collisions with H_2O in the ion trap, followed by

reductive elimination of NO_3 to leave hydrated UO_2^+ [26]. In the present study it may be that the decomposition of a similar activated complex with composition $[UO_2I(H_2O)_2]^+$*, via the elimination of neutral I and H_2O, leads to the abundant $[UO_2(H_2O)]^+$ ion at m/z 288; however, we note that CID of stabilized $[UO_2I(H_2O)_2]^+$ does not produce $[UO_2(H_2O)]^+$ at m/z 288. A two-reaction process involving the initial formation of UO_2^+ with subsequent hydration in the ion trap was ruled out in that study because the high relative abundance of the hydrated peak could not be reconciled with the slow reaction rate for H_2O addition to UO_2^+ measured in an earlier, independent study [35]. This possibility cannot be unequivocally excluded here.

Results for the multiple-stage CID of $[UO_2ClO_4(H_2O)_3]^+$ were similar to those observed for the other complexes. The elimination of single H_2O ligands was observed at the MS/ MS, MS^3 and MS^4 stages (spectra not shown). At the MS^5 stage (spectrum not shown), CID of $[UO_2ClO_4]^+$ generated UO_2^+ and $[UO_2OH]^+$. The latter ion was presumably formed via a hydrated intermediate complex similar to one proposed for the dissociation of the chloride and bromide species.

Only the bromide and perchlorate complexes showed a tendency to generate the bare $[UO_2A]^+$ species (i.e. $[UO_2Br]^+$ or $[UO_2ClO_4]^+$) following CID of the H_2O-coordinated complexes. As noted above, the chloride and iodide versions tended to eliminate HA to generate $[UO_2OH]^+$. In general, the observed trend with

respect to the formation of the uranyl–anion complex does not correlate with calculations of UO_2–A bond distances or coordination energies within biscomplexes [137]. For example, the calculated bond distances are 2.54, 2.68 and 2.92Å for Cl, Br and I, respectively. The trend in calculated coordination energy is 2089, 2042 and 1939 kJ/mol for Cl, Br and I, respectively. Both trends suggest that the interaction between the anion and UO_2 is strongest for Cl and weakest for I and that the formation of $[UO_2Cl]^+$ was favored in the CID experiment over $[UO_2Br]^+$. No values for ClO_4 were available for comparison. The tendency to form $[UO_2OH]^+$ from the H_2O-coordinated uranyl–anion complexes does follow calculated proton affinities (without thermodynamic corrections) which are 1370, 1262 and 1303 kJ/mol for UO_2Cl_2, UO_2Br_2 and UO_2I_2 complexes, respectively [137]. Though somewhat circumstantial, the differences in proton affinities could presumably effect the activation of bound H_2O ligands within the complex, and, coupled with the relative tendencies of Cl^-, Br^- and I^- to accept H^+ to leave as HA, influence the relative intensities of the $[UO_2A]^+$ and $[UO_2OH]^+$ product ions observed in the CID spectra.

Multiple-stage CID of uranyl–halide complexes coordinated by alcohols

The loss of HCl and HBr from the $[UO_2Cl(H_2O)]^+$ and $[UO_2Br(H_2O)]^+$ ions, respectively, to form $[UO_2OH]^+$ suggested the possibility of an intra-complex proton

transfer from bound H_2O to Cl or Br. Such a proton-transfer process is not without precedent, and has been observed during the CID of gas-phase alcohol complexes incorporating Pb^{2+} [138]. The loss of HNO_3 was also observed during the CID of methanol- coordinated uranyl nitrate in our earlier study [26]. The apparent elimination of HA, rather than H_2O, in the present experiments is somewhat counterintuitive given the relative strengths of $HClO_4$, HCl, HBr and H_2O as acids. For example, the gas-phase acidities (DacidG298) reported by Ervin and DeTuri are 1372.395, 1331.68 and 1293.81 kJ/mol for HCl, HBr and HI, respectively, while the acidity for H_2O is 1605.3 kJ/mol [139]. The prominent elimination of the acid instead may reflect, at least in part, a stronger affinity of UO_2 for oxygen donors such as OH. For example, calculated U–ligand bond distances within bis-uranyl complexes, which reflect decreasing coordination energies, are 2.54, 2.68, and 2.92 Å for Cl^-, Br^- and I^-, respectively, compared to 2.12 Å for OH^- [137].

To explore further the possible influence of relative acidity and strength of donation by O-containing ligands on the tendency to eliminate HA from the gas-phase complexes, we generated uranyl–halide complexes coordinated by methanol or ethanol from solutions of the uranyl-halide compounds dissolved in 50:50 mixtures of H_2O and respective alcohols. Because the gas-phase acidities (DacidG298) are 1571.1 and 1557.7 kJ/mol for CH_3OH and CH_3CH_2OH (again compared to 1605.3

kJ/mol for H_2O [139]), we reasoned that the tendency for intra-complex proton transfer would increase for ions containing coordinating alcohol ligands. In addition, an inductive effect due to the alkyl substituents might increase the strength of the interaction between UO_2 and the alkoxide species generated after proton transfer and thus be a driving force for the elimination of the neutral acid during CID. The preference for formation of alkoxide species would be consistent with previously reported tendencies for lanthanide and actinide species to form alkoxide complexes [117-119], and calculations suggest that replacing O–H bonds with $O–CH_3$ within a uranyl complex increases the binding energy to the uranyl ion [137]. Our hypothesis was that the composite influence of increased acidity and electron donation by the alkoxides would manifest itself in an increased tendency to eliminate HCl, HBr, HI or $HClO_4$ at early CID stages (MS/MS and MS^3) particularly when compared to CID of the complexes containing H_2O ligands. To illustrate the influence of coordinating alcohol ligands on the tendency to eliminate the neutral acid species during CID, Figs. 7.5 and 7.6 show the multiple-stage dissociation of $[UO_2Cl(CH_3OH)_3]^+$ and $[UO_2Br(CH_3OH)_3]^+$ (the spectra for these two complexes are consistent with those for the complexes containing iodide and perchlorate). As apparent in Fig. 7.5 (a), CID of $[UO_2Cl(CH_3OH)_3]^+$ caused not only the elimination of a neutral CH_3OH ligand, but also the elimination of HCl. The elimination of HA was also observed as a

low-abundance ion at m/z 365 in the MS/MS spectrum of $[UO_2Br(CH_3OH)_3]^+$ (Fig. 7.6 (a)), although to a lesser extent, and in the CID (MS/MS) of $[UO_2I(CH_3OH)_3]^+$ (spectrum not shown). As described above, the elimination of HA was not observed at the MS/MS stage during the dissociation of the analogous $[UO_2A(H_2O)_3]^+$ complexes. The elimination of HCl and HBr occurred to a greater extent during the CID of $[UO_2Cl(CH_3OH)_2]^+$ and $[UO_2Br(CH_3OH)_2]^+$ (Figs. 7.5 (b) and 7.6 (b), respectively) and for the CID of $[UO_2I(CH_3OH)_2]^+$ and $[UO_2ClO_4(CH_3OH)]^+$ (spectra not shown). The

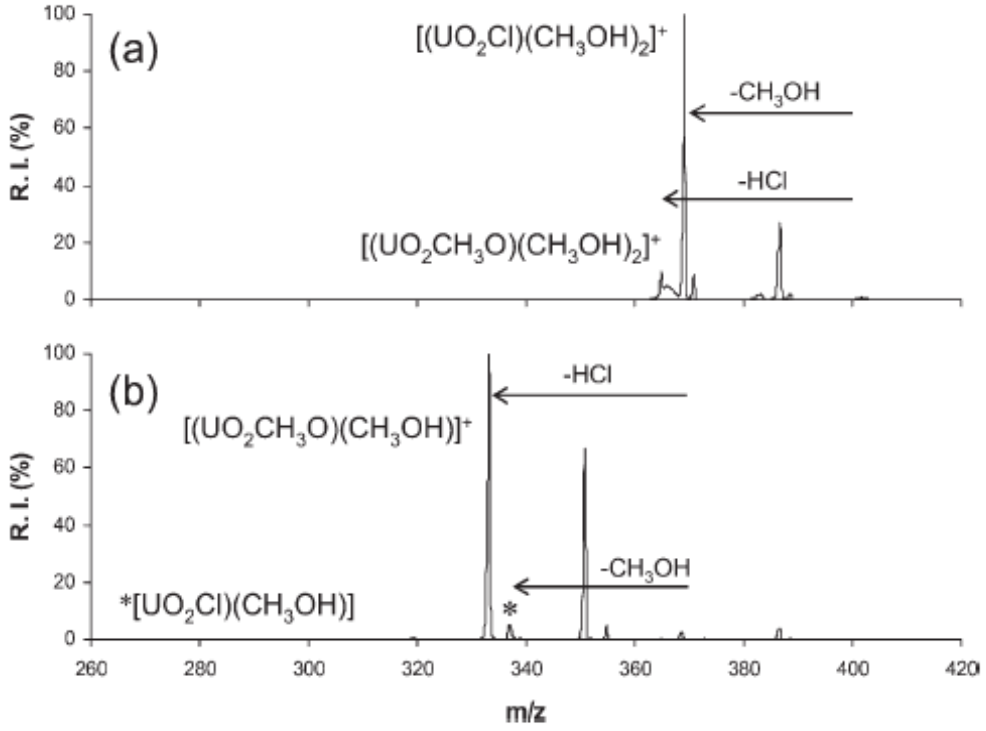

Figure 7.5. CID spectra for $[UO_2Cl(CH_3OH)_3]^+$ precursor complex: (a) MS/MS stage, dissociation of $[UO_2Cl(CH_3OH)_3]^+$ and (b) MS^3 stage, dissociation of $[UO_2Cl(CH_3OH)_2]^+$.

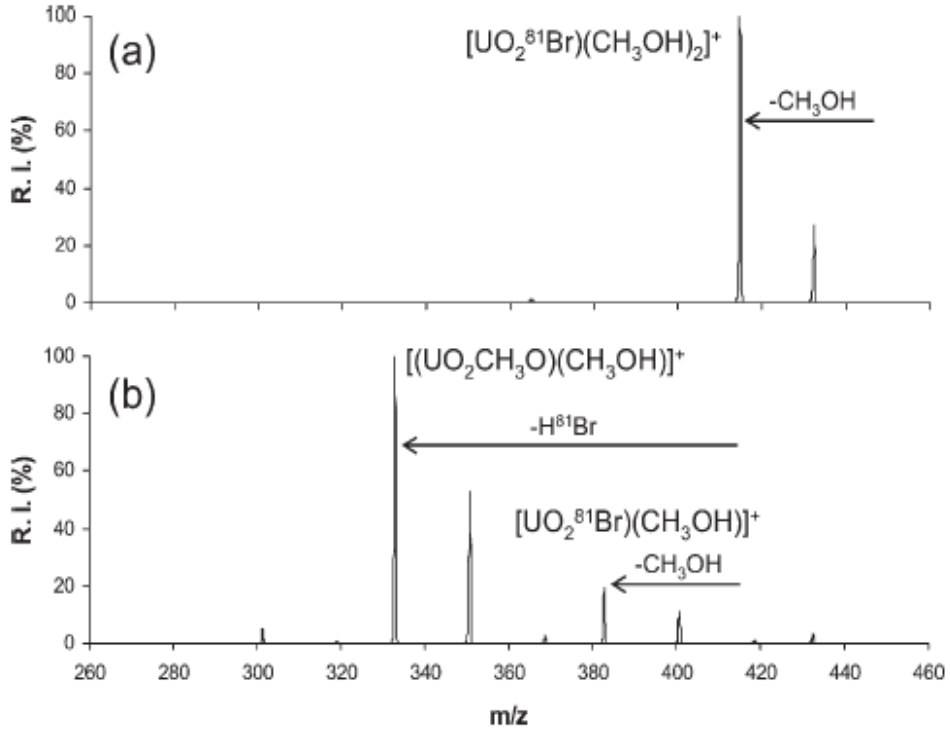

Figure 7.6. CID spectra for $[UO_2Br(CH_3OH)_3]^+$ precursor complex: (a) MS/MS stage, dissociation of $[UO_2Br(CH_3OH)_3]^+$ and (b) MS^3 stage, dissociation of $[UO_2Br(CH_3OH)_2]^+$.

general trend for the elimination of neutral acid relative to alcohol increased as $H_2O<CH_3OH<CH_3CH_2OH$. This observation supports the hypothesis that the strength of the coordinating ligand as a proton donor may, in part, drive the tendency to eliminate the coordinating halide as part of a neutral acid molecule. It is also likely that the free energy change for the reaction is guided by the UO_2–anion and UO_2–alkoxide bond energies.

To confirm the alcohol ligands as the origin of the proton transferred during the

elimination of neutral acid from the alcohol-ligated uranyl cations, a solution of uranyl chloride was prepared in a 50:50 mixture of CH_3OD and D_2O. ESI of the resulting solution produced as the main peak $[UO_2Cl(CH_3OD)_3]^+$ (spectrum not shown). Figure7.7 shows the product ion spectra resulting from the CID of $[UO_2Cl(CH_3OD)_3]^+$ (MS/MS, Fig. 7.7 (a)) and $[UO_2Cl(CH_3OD)_2]^+$ (MS^3, Fig. 7.7 (b)). In general, the fully coordinated uranyl cations show pronounced chemical mass shifts and peak fronting/tailing [24,122,140,141]. Yost and coworkers demonstrated a relationship between ion instability and the magnitude of the ion isolation width necessary to isolate species for CID [24]. To generate the spectra in Fig. 7.7, isolation widths of 3–4 u were required, which prohibited the isolation of a single isotopic peak. Even so, the main product ions generated from the CID of $[UO_2Cl(CH_3OD)_3]^+$ (Fig. 7.7 (a)) were $[UO_2Cl(CH_3OD)_2]^+$ and $[UO_2OCH_3(CH_3OD)_2]^+$. Though the relative intensity of the latter product was only 8%, the intensity of a peak 1 u higher, which would signify the elimination of HCl instead of DCl, was less than 0.01%. For the production of $[UO_2OCH_3(CH_3OD)]^+$ from $[UO_2Cl(CH_3OD)_2]^+$ (Fig. 7.7 (b)), the neutral loss was overwhelmingly DCl, with a neutral loss of HCl generating a peak of only 0.02%. The deuterium-labeling study therefore supports the hypothesis that the elimination of neutral acid occurs by an intra-complex proton-transfer reaction, with the alcohol and/or H_2O ligands serving as the source of the proton.

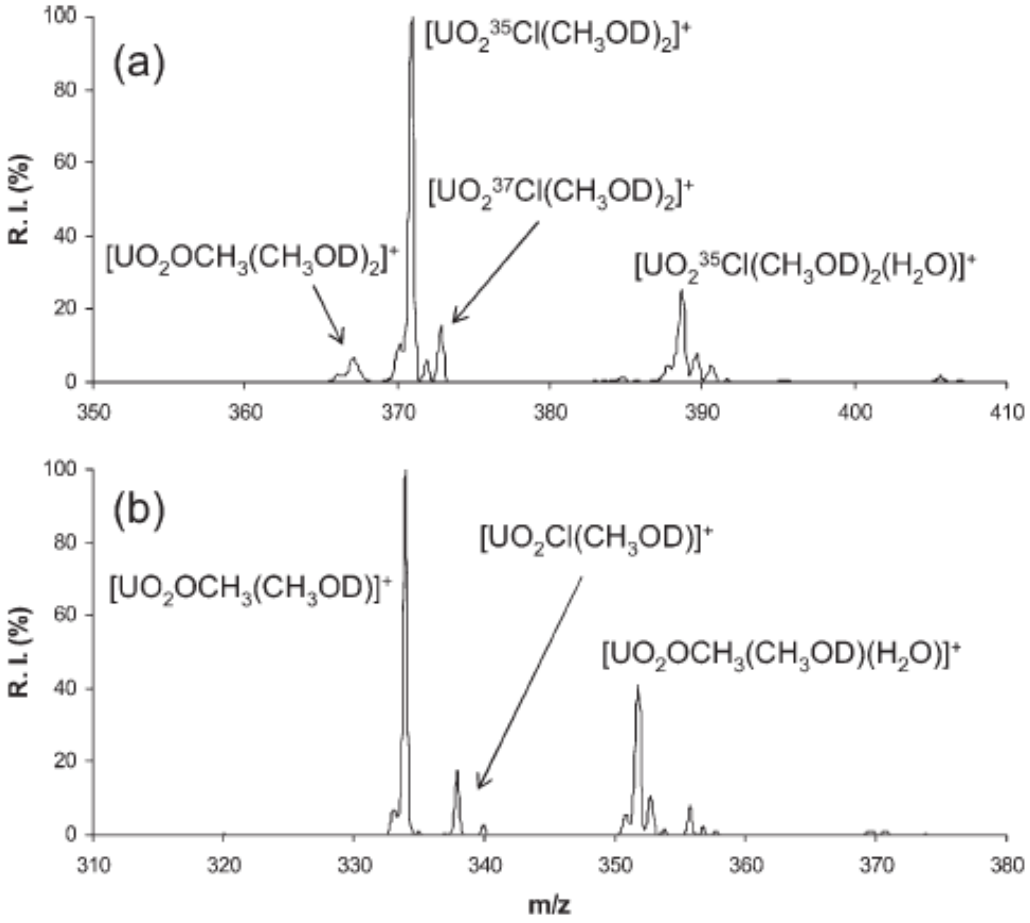

Figure 7.7. CID spectra for $[UO_2Cl(CH_3OD)_3]^+$ precursor complex: (a) MS/MS stage, dissociation of $[UO_2Cl(CH_3OD)_3]^+$ and (b) MS^3 stage, dissociation of $[UO_2Cl(CH_3OD)_2]^+$.

SUMMARY

The original goal of these experiments was to use ESI to generate gas-phase $[UO_2A]^+$ complexes (where A = Cl, Br, I or ClO_4^-) for subsequent ligand-addition studies, by way of the CID of precursor complexes with the general formula $[UO_2A(H_2O)_3]^+$. Multiple- stage CID of the complexes showed that the preferred dissociation pathways were the elimination of neutral H_2O ligands and the elimination

of HA. It was found, however, that $[UO_2A]^+$ was formed only from the bromide and perchlorate versions of the hydrated complexes. CID of thechloride and iodide versions instead led ultimately to formation of $[UO_2OH]^+$ and UO_2^+. The formation of $[UO_2OH]^+$ was also observed to a lesser extent following CID of the bromide and perchlorate complexes. In general, the tendency to generate $[UO_2OH]^+$ via the elimination of the HA complex does not correlate with calculations of UO_2–A bond distances or coordination energies within bis-complexes but instead follows the trend in calculated proton affinities for UO_2Cl_2, UO_2Br_2 and UO_2I_2 complexes, respectively. The correlation suggests that intra-complex proton transfer between ligands in the mixed $[UO_2A(H_2O)]^+$ species is a more important factor than the tenacity of the anion binding to the metal center.

The loss of acid became more pronounced when coordinating H_2O was replaced by MeOH or EtOH, consistent with a hypothesis that the reaction is influenced by a combination of the relative acidities of the ligands and the strength of uranyl–ligand bonds. The relative trends match those expected based on experimental values for the gas-phase acidity of H_2O and the alcohols, and calculated bond lengths and energies for bis-uranyl complexes. However, experimental values for intrinsic UO_2–O bond energies for complexes including H_2O or alcohol ligands are yet to be reported. Use of deuterated solvent allowed the preparation of complexes in which the alcohol

ligands contained –OD groups. CID of these species showed the preferred elimination of DA rather than HA, which supports the hypothesis for intra-complex proton transfer during the reaction to eliminate the neutral acid.

CHAPTER 8
GAS-PHASE COMPLEXES CONTAINING THE URANYL ION AND ACETONE

INTRODUCTION

Species containing U(IV) and U(VI) are commonly encountered in the environment, but have been less extensively studied by mass spectrometry because of a lack of practical means to generate complexes with U in these high oxidation states. Kemp *et al*. demonstrated that fast atom bombardment could be used to generate an extensive series of uranium oxo cations, including those with high apparent U oxidation states, from dioxouranium salts [142]. Gresham and coworkers later showed that sputtering of solid UO_3 by energetic ReO_4^- ions could be used to generate sufficient quantities of monopositive uranium oxo-cations for investigations of intrinsic hydration rates by ion-trap mass spectrometry (ITMS) [98]. More recently. ESI has proven to be an effective tool for generating ions containing U in the higher states, and has allowed the investigation of a wide range of uranium species by mass spectrometry and ion mobility-mass spectrometry [41,42,26,104,105,136].

Gas-phase doubly charged complexes containing the uranyl ion coordinated by neutral ligands have thus far remained elusive and the lack of effective methods for generating such species has impeded characterization of the intrinsic chemistry of the

di-cation and its compounds. In a landmark study, Schwarz and coworkers [22] were able to generate the “bare” uranyl di-cation by gas-phase oxidation and charge exchange reactions, which yielded a value for the second ionization potential for UO_2^{2+} that was consistent with vertical ionization energies that were generated using ab initio calculations. They noted that UO_2^{2+} was thermodynamically stable. In the experiments reported in this chapter, ESI was used to generate , from solutions of uranyl nitrate dissolved in mixtures of H_2O and acetone, gas-phase complexes containing UO_2^{2+} “solvated” by neutral ligands as well as more conventional monopositive cationic complexes in which, for example, uranyl-nitrate or hydroxide are coordinated by acetone ligands. CID and multiple stage tandem ion-trap mass spectrometry were used to elucidate the fragmentation pathways for the various complex ions. Several complex ions were also isolated and stored in the ion-trap for varying periods of time to investigate and compare intrinsic ligand (H_2O and acetone) addition reactions.

EXPERIMENTAL

ESI-MS, multiple-stage CID and ion-molecule reaction reactions were carried out using the procedures described in earlier chapters. Spray solutions for the ESI experiment were prepared by combining portions of a $UO_2(NO_3)_2 \bullet 6H_2O$ stock solution

with acetone such that the composition ranged from 2-75% acetone by volume.

ESI mass spectra were collected using the Finnigan LCQ-Deca ion-trap mass spectrometer. For stable gas-phase ions, peak shape profile and chemical mass shift data were collected using the ZoomScan function within the LCQ operating software. The ZoomScan function uses a slower scan-out rate to provide high resolution mass spectra over a 10 mass unit range, and a previous study by Yost and coworkers [122] demonstrated that general differences in ion stability can be determined using the peak shapes exhibited using this function on the LCQ platform. Chemical mass shifts in ITMS have been discussed in a number of previous reports [122,123,143-146]. The first observations of the shifts (measured ion masses significantly lower than calculated masses for the same species) were attributed to the geometry of the ion trap analyzer, and mass measurement inaccuracies due to geometry have been minimized in commercial ion traps by an increase of the axial dimension of the device [123,143]. Since that time, chemical effects such as polarizability and ion stability have been proposed to account for the persistence of chemical mass shifts in certain experiments [144-146]. Most relevant to the present study, Callahan and coworkers [140] and Yost and coworkers [141] suggested that the tendency for polyatomic species to dissociate during the scan out period during analytical scans will lead to significant peak fronting/tailing and chemical mass shifts. In our experiments, mass

shifts were calculated by subtracting the calculated ion mass (using exact isotope masses) from the measured ion mass.

CID was performed using isolation widths of 2-6 mass units (depending on the species), an activation Q (used to adjust the q_z value for the resonant excitation of the precursor ion during the CID experiment) value of .3, activation amplitudes of 10-20% (arbitrary to the LCQ system, represents a percentage of 5V peak to peak normalized for precursor ion mass) and activation times of 30 ms. For intrinsic ligand-addition reaction investigations, all charged species other than the uranyl complex of interest were resonantly ejected from the ion trap. The influence of the q_z setting on the reaction rates for two complex ions, one singly and one doubly charged uranyl-acetone ion, was tested. Through a series of q_z values ranging from .09 to .6, the difference in measured rates and rate constants was ~5-10%, and within the experimental error typical of the measurements in the ion-trap. This observation suggests that the q_z value within this range does not significantly influence the reaction rates for the species reported here and under the reaction conditions employed. This observation is consistent with simulations by Jackson *et al* which showed little difference in the root-mean-square kinetic energy of U^+ ions in He buffer gas for q_z values of .1 to .65 units [21].

In order to qualitatively compare the reactivity of the singly and doubly charged

species, the complex ions were isolated and stored within the ion trap for times ranging from 1 to 10,000 ms and reacted with neutral reagents (primarily adventitious H_2O along with acetone from the ESI spray solution) within the He bath gas. Following the isolation period, the precursor and product ions were scanned out of the trap and detected as part of the automated mass analysis operation. Reaction sequences and extent of reaction were evaluated by plotting fractional ion abundances versus reaction time. Because neutral concentrations in the electrospray ion trap experiment are subject to day-to-day variability, kinetic profiles of singly and doubly charged ions were acquired on the same day. The precision of individual ion abundances were on the order of 5-10% (relative standard deviation), and all trends were reproducible over several separate trials.

RESULTS AND DISCUSSION

ESI Mass Spectra

The ESI mass spectrum derived from $UO_2(NO_3)_2 \bullet 6H_2O$ dissolved in 40:60 H_2O/acetone, and using a capillary/desolvation temperature of 60°C, is shown in Figure 8.1 and the complex ions observed are summarized in Table 8.1. The influence of the capillary temperature on the ESI spectrum observed is discussed in a later section.

Species	Calculated Mass	Average Measured Mass	Standard Deviation (s)	(Measured mass - calculated mass)
$[UO_2]^+$	270.041	270.077	0.067	0.036
$[UO_2OH]^+$	287.043	287.093	0.006	0.050
$[UO_2NO_3]^+$	332.028	332.037	0.006	0.008
$[UO_2(acetone)_3(H_2O)]^{2+}$	231.088	230.893	0.023	-0.195
$[UO_2(acetone)_4]^{2+}$	251.104	251.020	0.000	-0.084
$[UO_2(acetone)_5]^{2+}$	280.125	279.940	0.010	-0.185
$[UO_2OH(acetone)_2]^+$	403.127	403.073	0.006	-0.053
$[UO_2OH(acetone)_3]^+$	461.168	460.993	0.006	-0.175
$[UO_2CH_2{=}COCH_3(acetone)_2]^+$	443.158	443.227	0.012	0.069
$[UO_2CH_2{=}COCH_3(acetone)_3]^+$	501.200	501.003	0.012	-0.196
$[UO_2NO_3(acetone)_2]^+$	448.112	448.010	0.000	-0.102
$[UO_2NO_3(acetone)_3]^+$	506.154	505.943	0.006	-0.210
$[Acetone+H]^+$	59.050	59.120	0.000	0.070
$[(Acetone)_2+H]^+$	117.091	117.000	0.000	-0.092

Table 8.1 . Mass to charge ratios, chemical composition and chemical mass shift values for uranyl containing complex ions observed following ESI of $UO_2(NO_3)_2{\bullet}(H_2O)_6$ (1mM concentration) dissolved in 50:50 H_2O/acetone.

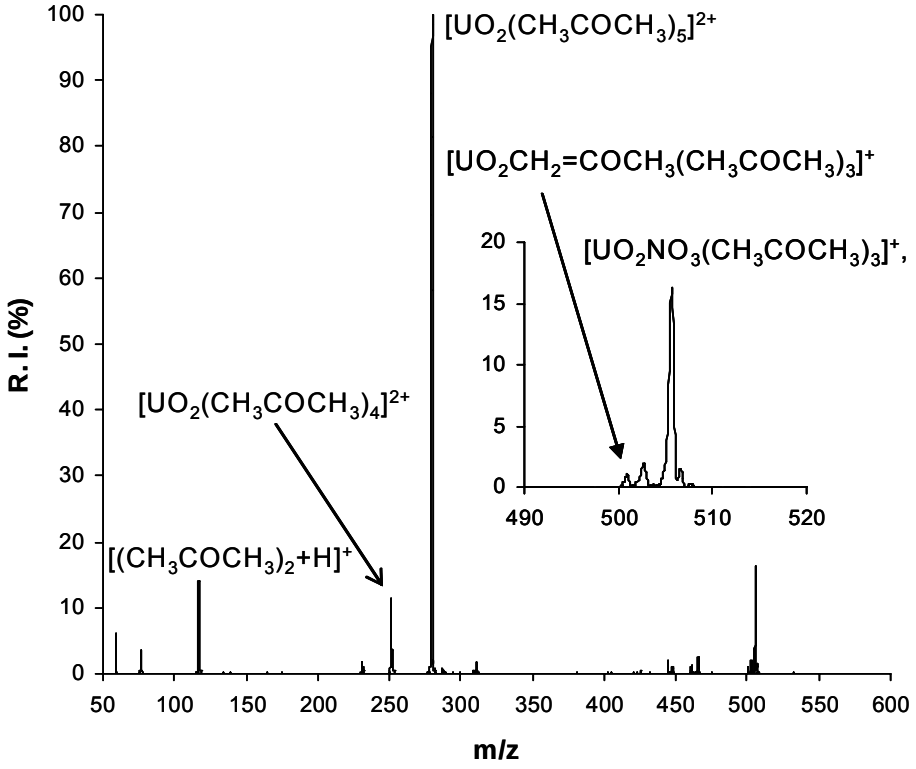

Figure 8.1. ESI mass spectrum of $UO_2(NO_3)_2 \bullet (H_2O)_6$ (1 mM concentration) dissolved in 50:50 H_2O/acetone. The heated capillary/desolvation temperature was 60°C. Complexes observed to contain the uranyl ion are listed in Table 8.1.

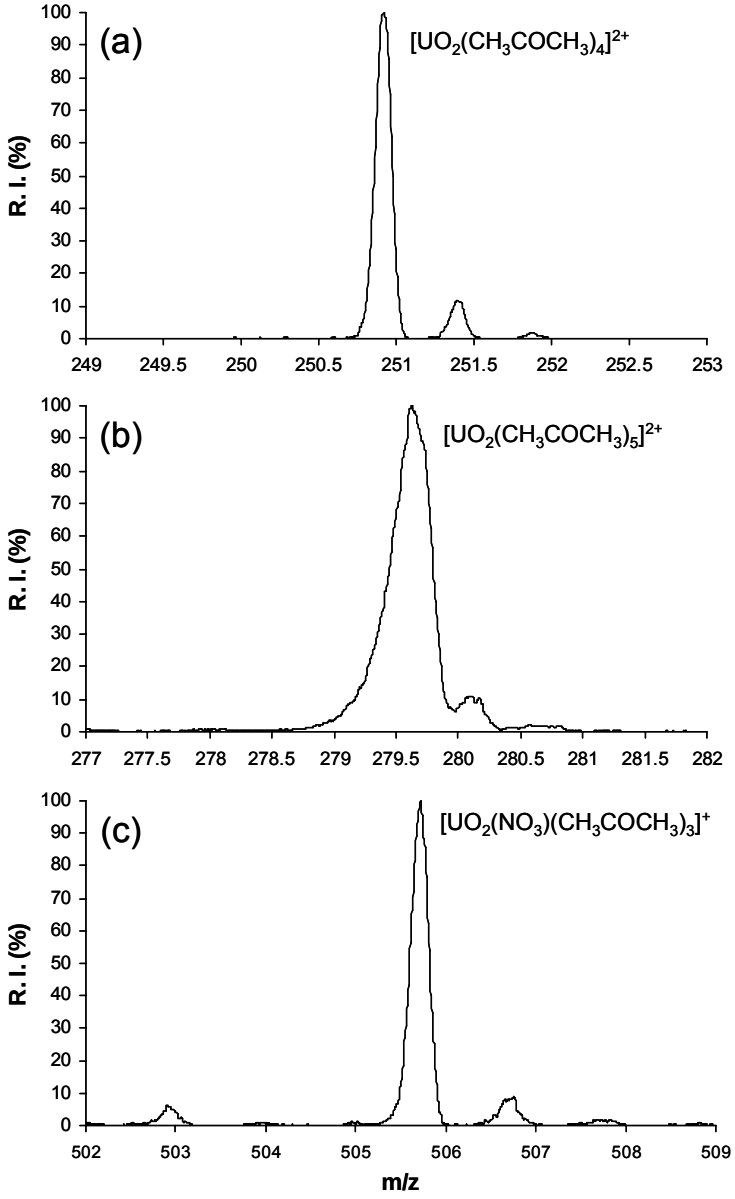

Figure 8.2. ZoomScan, high-resolution spectra of: (a) $[UO_2(acetone)_4]^{2+}$, (b) $[UO_2(acetone)_5]^{2+}$, and (c) $[UO_2NO_3(acetone)_3]^{+}$. Peaks are labeled with m/z value at centroid.

At 60°C, the principal species observed were $[UO_2(acetone)_4]^{2+}$, $[UO_2(acetone)_5]^{2+}$ and $[UO_2NO_3(acetone)_3]^{+}$ which appeared in the raw ESI spectrum at mass to charge

(m/z) ratios of ~ 251, 280 and 506 respectively. ZoomScan, high resolution mass spectra for these three species are provided in figure 8.2. In the high resolution mode the $[UO_2(acetone)_5]^{2+}$ ion (figure 8.2 (b)) appeared as a broad peak at m/z 279.6. The significant tail to the low mass side of the peak is consistent with ion dissociation during the analytical scan out of the ion trap prior to detection. An isotopic peak ~.5 mass units (u) higher at ca. m/z 280.1 (from ^{13}C within the acetone ligands) confirmed a charge state of +2 for the ion. The high resolution spectrum collected for the $[UO_2(acetone)_4]^{2+}$ ion (figure 8.2 (a)) contained peaks at ~250.9 and 251.43 u (separated by .5 u) which confirmed a charge state assignment of +2. In the high resolution spectrum the $[UO_2NO_3(acetone)_3]^{+}$ species appeared as base peak at m/z 505.7, with ^{13}C isotopic peak at m/z 506.7 (1 u higher). We had originally thought that the low abundance ion at m/z 503 (3 u lower) was due to the ^{235}U isotopic peak, but its abundance is too high for natural U; the ion is probably $[UO_2(CH_3CO_2)(acetone)_3]^{+}$ which arises from residual acetate that had previously been used in the instrument. The peak spacing for these species confirmed a charge state assignment of +1. Other species of particular interest generated by ESI were those with formula $[UO_2OH(acetone)_3]^{+}$ at m/z 461 and $[UO_2CH_2{=}COCH_3(acetone)_3]^{+}$ at m/z 501, the latter nominally composed of UO_2^{2+} coordinated by deprotonated acetone and neutral acetone ligands.

$[UO_2(acetone)_4]^{2+}$, $[UO_2(acetone)_5]^{2+}$ and $[UO_2NO_3(acetone)_3]^{+}$ remained the dominant species as the acetone concentration in the spray solution was decreased to 2% (v:v) (spectra not shown). However, at low acetone concentrations, formation of $[UO_2(acetone)_3(H_2O)]^{2+}$ (m/z 231) and $[UO_2(acetone)_4]^{2+}$ was favored over $[UO_2(acetone)_5]^{2+}$. The preference for acetone over water as a coordinating ligand in the gas phase constitutes a salient difference in gas-phase uranyl reactivity compared with that in solution, where water is preferred [147-149]. Acetone is a stronger gas-phase nucleophile than is water [150] which highlights the fact that conditions of aqueous solvation clearly weakens the electron-donating ability of acetone. The formation of doubly charged species is decreased at acetone concentrations greater than 60% (v:v), where the ESI spectrum became dominated by the singly charged species $[UO_2CH_2{=}COCH_3(acetone)_3]^{+}$ and $[UO_2NO_3(acetone)_3]^{+}$. The reason for preferential formation of the singly charged species at high acetone concentrations is not known.

Several of the uranyl-containing ions appeared in the ESI specta at m/z values lower than expected based on calculations from exact isotope masses, even after taking into consideration any uncertainty in measurement accuracy. As noted in the experimental section, the degree of peak fronting or tailing and the magnitude of this chemical mass shift are indicative of ion stability in ion-trap mass spectrometry

[122,140,141]. Chemical mass shift data are provided in Table 8.1 for those uranyl-acetone complex ions that were sufficiently stable to permit collection of ZoomScan high-resolution spectra, and peaks widths for the same ions are shown in Table 8.2. Peak width data were collected at the 10% peak intensity level (as reported by Yost and coworkers [122]) and at the full-width half maximum (FWHM). As shown in Table 8.1, the measured m/z ratios for protonated acetone (m/z 59) and $[UO_2OH]^+$ differed from expected, calculated masses by .07 and .05 u, respectively. Because the measured m/z values for these two ions were greater than the calculated values and thus not attributable to ion-dissociation process during the high-resolution scans that lead to chemical mass shifts, we chose $\pm$ .07 as a baseline for the mass measurement accuracy in these experiments. Mass differences *beyond* this value were then interpreted as chemical mass shifts due to ion instability.

The data in Table 8.1 demonstrate that the chemical mass shift increases as the number of coordinating ligands around the uranyl center increases. For example, the calculated chemical mass shifts for $[UO_2(acetone)_4]^{2+}$ and $[UO_2(acetone)_5]^{2+}$ are -.084 and -.185 u, respectively. The principal dissociation reaction for $[UO_2(acetone)_5]^{2+}$ involved the elimination of a single acetone ligand (vide infra), thus the origin of the large chemical shift for the $[UO_2(acetone)_5]^{2+}$ species was presumably dissociation to produce $[UO_2(acetone)_4]^{2+}$. The increase in shift was not

unique to the doubly charged complexes, as the chemical mass shifts for the singly charged, $[UO_2OH]^+$, $[UO_2CH_2{=}COCH_3]^+$ and $[UO_2NO_3]^+$ complexes containing 3 coordinating acetone ligands were more negative by .122, .127 and .108 u, respectively, when compared to analogous complexes containing only 2 neutral acetone ligands. As discussed below, the principal dissociation pathways for these species also included the elimination of single coordinating ligands.

Species	Average Width (10%)	Standard Deviation (s)	Average Width (50%)	Standard Deviation (s)
$[UO_2OH]^+$	0.10	0.00	0.08	0.00
$[UO_2(acetone)_4]^{2+}$	0.20	0.00	0.10	0.00
$[UO_2(acetone)_5]^{2+}$	0.58	0.00	0.28	0.01
$[UO_2OH(acetone)_2]^+$	0.22	0.01	0.11	0.00
$[UO_2OH(acetone)_3]^+$	0.50	0.01	0.26	0.01
$[UO_2CH_2{=}COCH_3(acetone)_2]^+$	0.19	0.01	0.10	0.01
$[UO_2CH_2{=}COCH_3(acetone)_3]^+$	0.43	0.01	0.23	0.01
$[UO_2NO_3(acetone)_2]^+$	0.21	0.01	0.11	0.01
$[UO_2NO_3(acetone)_3]^+$	0.53	0.01	0.27	0.01
$[Acetone+H]^+$	0.19	0.03	0.10	0.00
$[(Acetone)_2+H]^+$	0.34	0.00	0.17	0.00

Table 8.2. Peak width measurements for uranyl containing complexes obtained from ZoomScan spectra.

As shown in Table 8.2, trends similar to those for the chemical mass shifts were apparent in the measurements of the peak widths. The peak fronting/tailing was most apparent in the 10% peak width measurement. For example, the peak widths

increased from .20 u for $[UO_2(acetone)_4]^{2+}$ to .58 u for $[UO_2(acetone)_5]^{2+}$, and from .21 u for $[UO_2NO_3(acetone)_2]^{+}$ to .53 u for $[UO_2NO_3(acetone)_3]^{+}$. Regardless of the overall charge state, the chemical mass shift and the degree of peak fronting/tailing was greatest for uranyl complexes with the highest equatorial coordination number. Therefore, the data suggest that the species with high coordination number are the most susceptible to dissociation and least stable. This conclusion is in accord with extensive measurements of alkali-, and transition-metal-ligand bond dissociation energies, which in general decrease as the number of ligands increases [150].

Differences in chemical mass shift and peak width values among complexes of varying size were not unique to those with acetone ligands. For the sake of comparison, Table 8.3 contains data collected from ZoomScan spectra of uranyl complexes containing acetonitrile ligands. With acetonitrile as co-solvent in the ESI experiment, the major species observed included $[UO_2(acetonitrile)_4]^{2+}$, $[UO_2(acetonitrile)_4(H_2O)]^{2+}$, $[UO_2(acetonitrile)_5]^{2+}$, $[UO_2OH(acetonitrile)_3]^{+}$ and $[UO_2NO_3(acetonitrile)_3]^{+}$ (spectrum not shown). The chemical mass shift measured for $[UO_2(acetonitrile)_5]^{2+}$ complex was ca. -.187, while the shift for the $[UO_2(acetonitrile)_4]^{2+}$ species was +.147. The shape of the latter complex included a significant tail to the high-mass side, suggesting that the $[UO_2(acetonitrile)_4]^{2+}$ peak may be generated both directly by ESI and by the dissociation of larger complexes

such as $[UO_2(acetonitrile)_4(H_2O)]^{2+}$ and $[UO_2(acetonitrile)_5]^{2+}$. The latter process is in effect the opposite to the one that leads to the negative shift values observed for species such as $[UO_2(acetonitrile)_5]^{2+}$ and $[UO_2(acetone)_5]^{2+}$. A positive chemical shift value was also observed for the $[UO_2OH(acetonitrile)_2]^{+}$ while a large negative value was observed for the $[UO_2OH(acetonitrile)_3]^{+}$. For the uranyl-nitrate complexes, the $[UO_2OH(acetonitrile)_3]^{+}$ and $[UO_2OH(acetonitrile)_3]^{+}$ complexes showed chemical mass shifts of -.111 and -.258 u, respectively.

Thermal Dissociation of Complex Ions

Chemical mass shifts

Species	Calculated Mass	Average Measured Mass	Standard Deviation (s)	(Measured mass - calculated mass)
$[UO_2(ACN)_5]^{2+}$	237.587	237.4	0.021	-0.187
$[UO_2(ACN)_4]^{2+}$	217.073	217.220	0.001	0.147
$[UO_2OH(ACN)_2]^{+}$	369.096	369.120	0.005	0.024
$[UO_2OH(acetone)_3]^{+}$	410.123	409.910	0.007	-0.213
$[UO_2NO_3(acetone)_2]^{+}$	414.081	413.970	0.000	-0.111
$[UO_2NO_3(acetone)_3]^{+}$	455.108	454.850	0.005	-0.258

Peak widths

Species	Average Width (10%)	Standard Deviation (s)	Average Width (50%)	Standard Deviation (s)
$[UO_2(ACN)_5]^{2+}$	0.41	0.01	0.2	0.01
$[UO_2(ACN)_4]^{2+}$	0.47	0.01	0.16	0.01
$[UO_2OH(ACN)_2]^{+}$	0.79	0.01	0.32	0.01
$[UO_2OH(acetone)_3]^{+}$	0.49	0.01	0.17	0.01
$[UO_2NO_3(acetone)_2]^{+}$	0.23	0.01	0.13	0.01
$[UO_2NO_3(acetone)_3]^{+}$	0.47	0.01	0.24	0.01

Table 8.3. Chemical mass shifts and peak width measurements for

uranyl-acetonitrile (ACN) complex ions

The heated capillary of the atmospheric pressure ionization stack on the LCQ platform, used to desolvate ions following ESI and prior to injection into the ion trap, can significantly alter the relative intensity distribution of polyatomic ions observed in ESI mass spectra, and has been used as a “thermal reaction vessel” to investigate the thermal dissociation of ions generated by ESI [151,152]. To probe the stability of the uranyl complexes to thermal dissociation prior to injection into the ion trap, ion intensities were measured as a function of capillary temperature. Figure 8.3 shows a plot of the fraction of the total ion abundance for several singly and doubly charged ions plotted versus the temperature of the heated capillary. In the LCQ, the temperature is measured by a thermocouple attached to the capillary and may not accurately reflect the true temperature within the finite space traversed by the ionized species. The plot in figure 8.3 should therefore be considered a qualitative measure of the influence of increasing desolvation temperature on relative ion abundance.

At temperatures below 50°C (data not shown) the ESI spectrum was dominated by the protonated acetone monomer and dimer and protonated clusters of H_2O and acetone. For $[UO_2(acetone)_5]^{2+}$, the fraction of total ion abundance reached a maximum in the range 60-80°C and decreased as the temperature was raised from 80° to 120°C. The $[UO_2(acetone)_4]^{2+}$ species exhibited the highest fraction

abundance over the range 120 to 200°C.At 200°C the abundance of $[UO_2(acetone)_4]^{2+}$ was nearly matched by $[UO_2(acetone)_3(H_2O)]^{2+}$. For the singly charged uranyl-containing complexes, the abundance of $[UO_2NO_3(acetone)_3]^+$ reached a maximum at ca. 100°C, then decreased from 100-200°C as the abundance

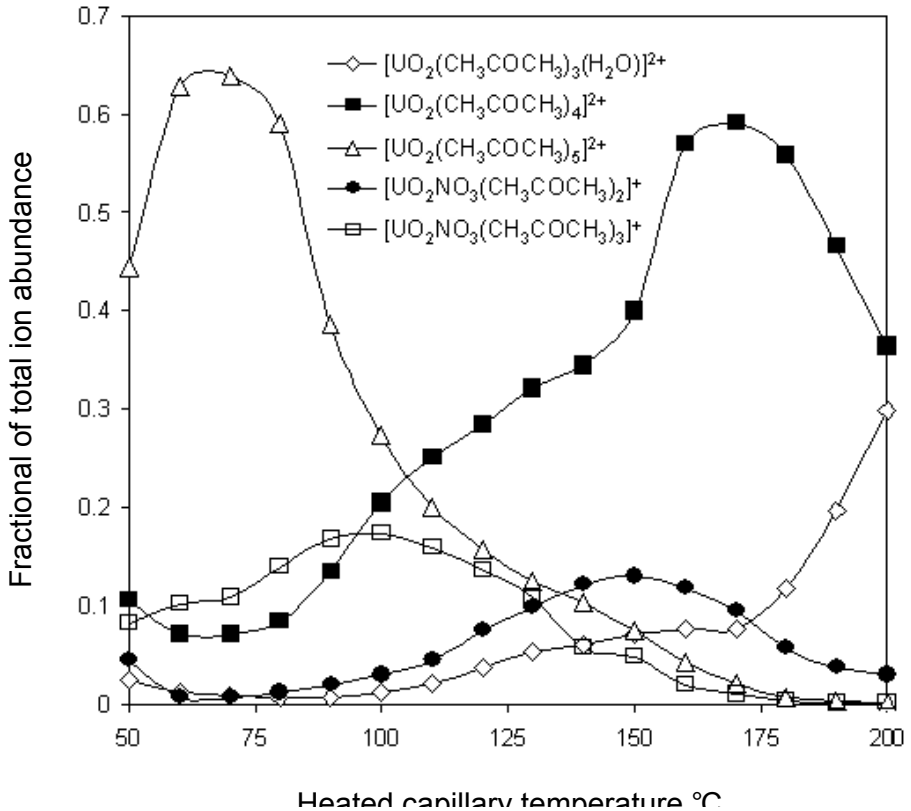

Figure 8.3. Plot of change in fraction of ion abundance versus heated capillary/desolvation temperature. Complex ions were derived from 1 mM $UO_2(NO_3)_2 \bullet (H_2O)_6$ in 50:50 H_2O/acetone.

of $[UO_2NO_3(acetone)_2]^+$ increased at higher temperatures. Similar profiles were observed for the $[UO_2OH(acetone)_3]^+$ and $[UO_2CH_2{=}COCH_3(acetone)_3]^+$ species,

which were omitted from figure 8.3 for the sake of clarity. Beyond 200°C the singly charged ions dominated the ESI spectra, and at ca. 250-300°C only the reduced uranyl ion, UO_2^+ and the uranyl hydroxide monopositive cation were observed in high abundance.

In general, similar thermal dissociation profiles were generated for complexes composed of uranyl ion and ligands such as acetophenone and acetonitrile. For the latter case, the complexes proved to be less stable to thermal dissociation than those containing acetone, suggesting stronger uranyl bonds to acetone as compared to acetonitrile. This is consistent with the oxophilic nature of the uranyl ion and preference for coordination by O atoms, and with calculations [46] that suggest that the bond distance between a uranyl center and formaldehyde ligands (2.31 Å within a bis-complex) is shorter than for acetonitrile (2.39 Å within an analogous complex).

Using Kohn-Sham Density Functional Theory calculations [46] to treat the hydration of UO_2^{2+}, Spencer *et al* determined that the most stable equatorial coordination number, n, for the $[UO_2(H_2O)_n]^{2+}$ complexes was 5. By calculating bond-dissociation energies for complexes with varying numbers of H_2O ligands (n), they found the trend to be $\Delta^{\triangle}E_{n=5} < {}^{\triangle}\Delta E_{n=6} < \Delta^{\triangle}E_{n=4}$. As apparent from Table 8.1, and as discussed below, a fully hydrated UO_2^{2+} complex ion (n=6) was not observed in the ESI experiment reported here. However for the uranyl-acetone system, the fact

that the n=5 complex decreased, and the n=4 increased with increasing desolvation temperature (figure 8.3) underscored the susceptibility of $[UO_2(acetone)_5]^{2+}$ to thermal dissociation, and clearly showed that in the gas-phase the complex containing 5 acetone ligands was less stable than one with 4. A recent experimental investigation of UO_2^{2+} in aqueous solution by Neuefeind *et al* [153] suggested that there exists in solution a dynamic equilibrium that favors coordination by five H_2O ligands around the equator over 4, but that tetracoordinate species are also present. NMR studies of uncomplexed UO_2^{2+} have been interpreted in terms of five H_2O ligands [149], although earlier experiments indicated only four [148]. In aggregate, the previously reported extent of complexation in condensed phase H_2O-UO_2^{2+} complexes was largely consistent with that observed in the present gas-phase uranyl-acetone system.

Accommodation of 5 acetone ligands around a uranyl center is likely sterically more demanding than the same number of H_2O ligands. A complete analysis of the influence of the number and orientation of acetone ligands on the stability and energies of gas-phase complexes will likely require detailed ab-initio calculations. To the best of our knowledge, such calculations have not been reported. The comparison of chemical shift and peak width data for complexes containing either acetone or acetonitrile ligands demonstrate that the incorporation of the latter, which

would be sterically less demanding for a complex with 5 ligands, does little to improve the stability of the complex (with the caveat that the bonding interactions between acetonitrile and acetone are likely significantly different). The mass shift and peak shape data, therefore, may point to general differences in gas-phase stability of uranyl-solvent complexes.

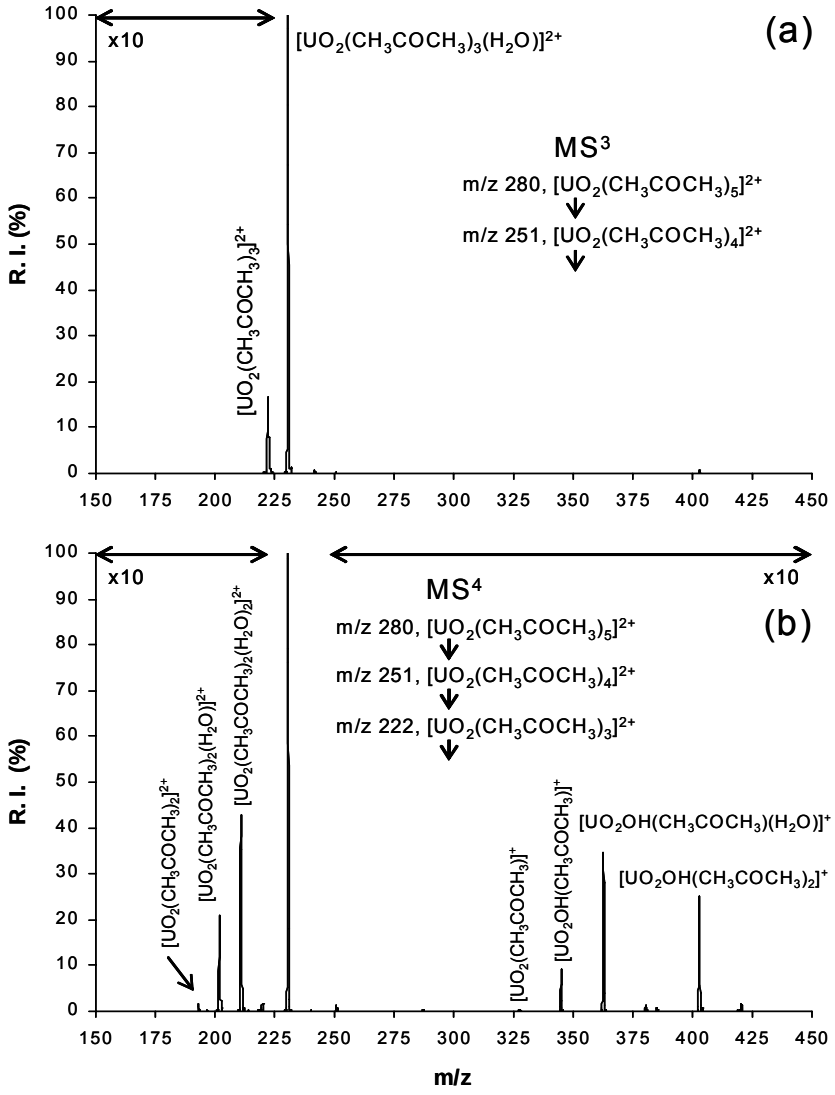

Figure 8.4. Product ion mass spectra for CID of: (a) $[UO_2(acetone)_4]^{2+}$ (MS^3 stage)

derived from dissociation of $[UO_2(acetone)_5]^{2+}$ and (b) $[UO_2(acetone)_3]^{2+}$ (MS^4 stage). Product ion compositions are provided in the text.

Multiple-stage Tandem Mass Spectrometry

The multiple-stage (MS^n) CID of the major, UO_2 specific complex ions was also investigated. For MS^n of $[UO_2(acetone)_5]^{2+}$, the initial CID stage (MS/MS or MS^2, spectrum not shown) caused the elimination of an acetone ligand to generate $[UO_2(acetone)_4]^{2+}$. The spectrum in Figure 8.4 (a) shows the result of CID of the $[UO_2(acetone)_4]^{2+}$ product ion (MS/MS/MS or MS^3 stage), which caused the formation of two apparent dissociation product ions: $[UO_2(acetone)_3]^{2+}$ as a minor peak at m/z 222 and $[UO_2(acetone)_3(H_2O)]^{2+}$ at m/z 231. Subsequent isolation of *only* $[UO_2(acetone)_3]^{2+}$, without imposed collisional excitation, generated $[UO_2(acetone)_3(H_2O)]^{2+}$ in abundance similar to that shown in figure 4a, indicating that the latter ion is likely generated by rapid hydration of $[UO_2(acetone)_3]^{2+}$ by ion-molecule reactions involving indigenous H_2O in the ion trap. CID of the species at m/z 222 in the next dissociation stage (MS^4 stage, figure 4b) generated $[UO_2(acetone)_2]^{2+}$ as a minor peak at m/z 193 and a series of intense hydrated versions of the complex at m/z 202 (one H_2O ligand added) and 211 (2 H_2O ligands added). The low abundance of the $[UO_2(acetone)_2]^{2+}$ at the MS^4 stage prohibited further isolation/CID stages. CID of the hydrated species at m/z 202 and 211 also failed to produce lower mass, doubly charged products. Rapid reactions with H_2O

instead re-generated the hydrates of $[UO_2(acetone)_2]^{2+}$.

Another dissociation pathway observed following the CID of $[UO_2(acetone)_3]^{2+}$ at the MS^4 stage involved formation of product ions with lower charge state (+1). For example, product ions at m/z 345, 363 and 403 (figure 4b) had m/z ratios consistent with the formation of $[UO_2OH(acetone)]^+$, $[UO_2OH(acetone)(H_2O)]^+$ and $[UO_2OH(acetone)_2]^+$, respectively. Subsequent CID of $[UO_2OH(acetone)]^+$ and $[UO_2OH(acetone)_2]^+$ (spectra not shown) ultimately led to the production of $[UO_2OH]^+$ at m/z 287 by the elimination of neutral acetone ligands. The formation of product ions containing OH, such as $[UO_2OH(acetone)]^+$ and $[UO_2OH(acetone)]^+$, from the doubly charged uranyl-acetone complex presumably involves reactive collisions with H_2O in the ion trap during CID, activation of the H_2O molecule and retention of hydroxide by the complex. The proposed involvement of H_2O as a collision partner is plausible based on recent work demonstrating that CID within ion trap instruments involves a significant number of activating collisions between precursor ions and small molecules such as N_2 and H_2O present as contaminants within the He bath gas [120,121]. The formation of a similar activated complex was invoked to explain the formation of a prominent hydrated UO_2^+ ion [26] following the CID of $[UO_2NO_3]^+$ and the generation of $[UO_2OH]^+$ from a uranyl-2-propoxide cation in earlier studies [13]. Assuming the formation of an activated complex including a bound H_2O molecule and

retention of OH by the complex (with associated charge reduction), dissociation of the $[UO_2(acetone)_3]^{2+}$ precursor to form $[UO_2OH(acetone)]^+$ and $[UO_2OH(acetone)_2]^+$ might also have produced protonated acetone dimer and monomer, respectively as complementary product ions. These latter product ions could not be observed during our experiments because of limitations to the low-mass cut-off imposed by the q_z value setting used during CID.

CID of the $[UO_2(acetone)_3]^{2+}$ species at the MS^4 stage also generated an ion at m/z 328, which is attributed to the formation of a complex containing the uranyl dioxo monocation (UO_2^+) and a single neutral acetone molecule. Subsequent CID of this species caused the elimination of neutral acetone to leave a peak at m/z 270. Formation of the reduced uranyl ion at m/z 270 was confirmed by a comparison of intrinsic hydration kinetics to previous measured rates for the species [98] (data not shown). At no point during the MS^n dissociation of the doubly charged complex was the bare uranyl ion, UO_2^{2+} observed. Instead, as described above, the observed tendency was either to generate doubly charged complexes containing a mixture of H_2O and acetone ligands and ultimately undergo charge reduction by charge transfer or acceptance of hydroxide. The reduction in charge state during CID is consistent with both the Lewis acidity of the uranyl ion and fact that the ionization energy of UO_2^+ (ca. 15 eV) [22] is greater than that of either acetone or water (9.7 and 12.6 eV,

respectively [154]).

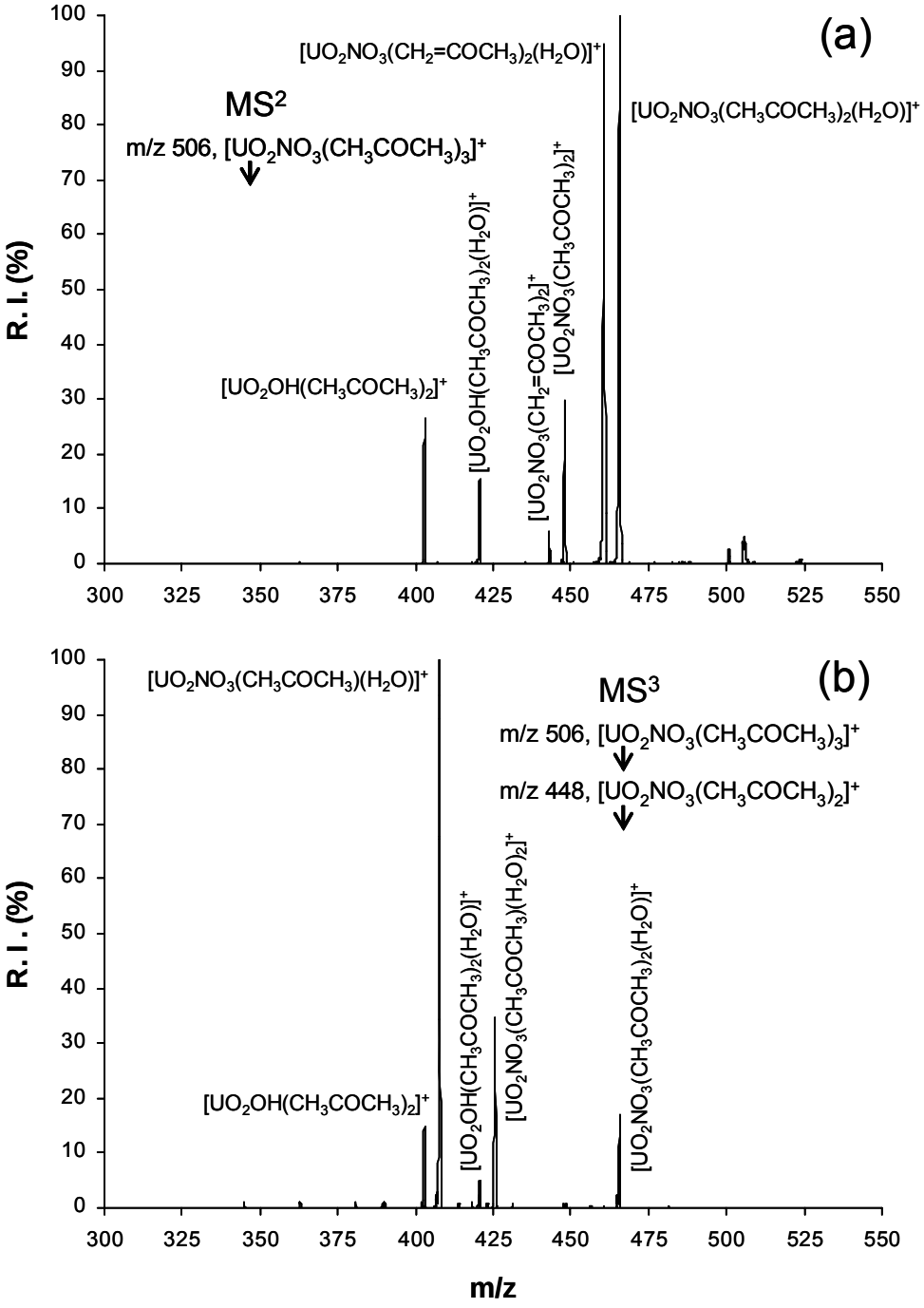

Figure 8.5. Product ion mass spectra for CID of: (a) $[UO_2NO_3(acetone)_3]^+$ (MS/MS or MS^2 stage) and (b) $[UO_2NO_3(acetone)_2]^+$ (MS^3 stage). Product ion compositions are provided in the text.

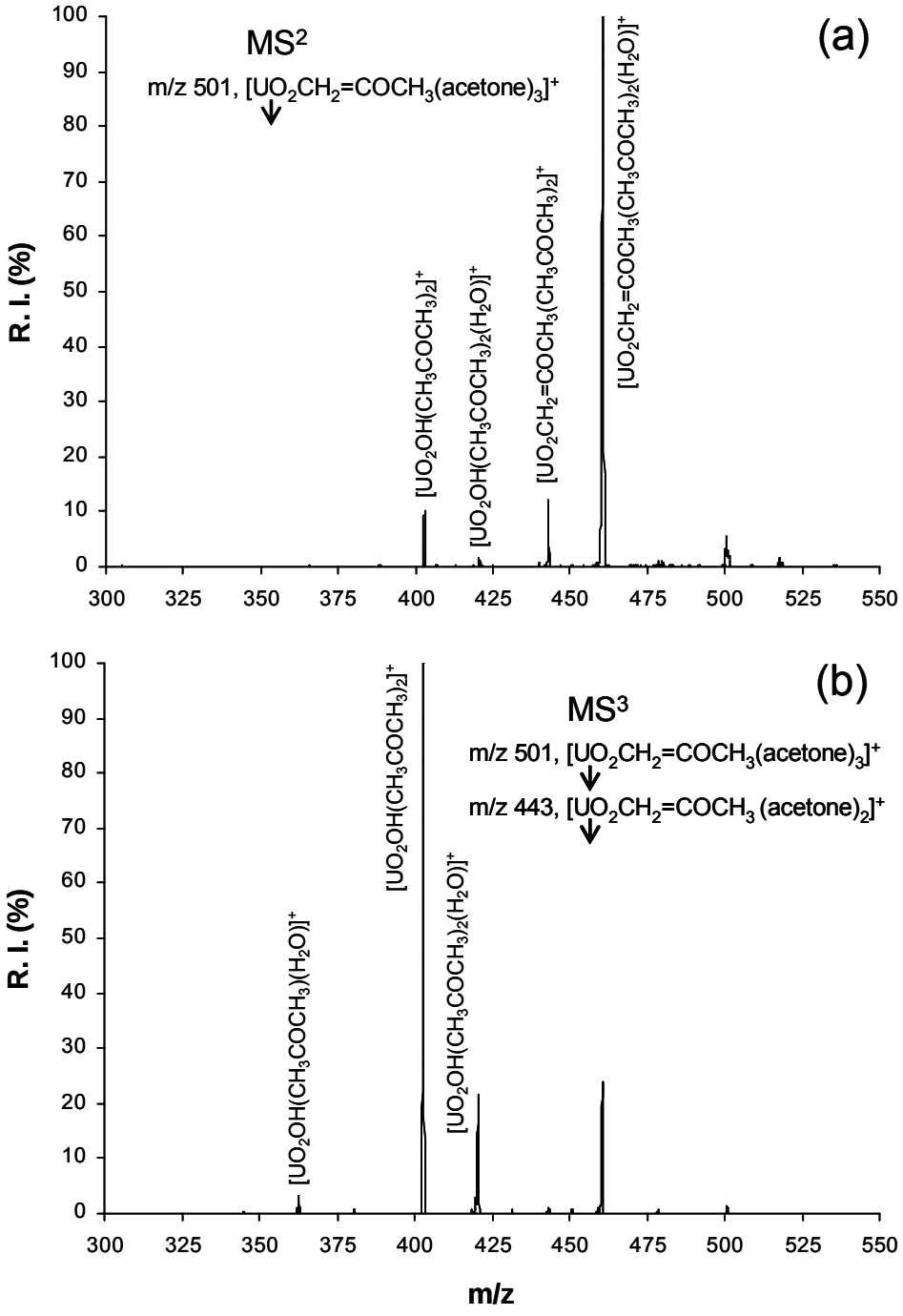

Figure 8.6. Product ion mass spectra for CID of: (a) $[UO_2CH_2{=}COCH_3(acetone)_3]^+$ (MS/MS or MS^2 stage) and (b) $[UO_2CH_2{=}COCH_3(acetone)_2]^+$ (MS^3 stage). Product ion compositions are provided in the text.

The strong tendency to accept or otherwise interact with H_2O ligands during CID experiments was also apparent during the MS^n dissociation of $[UO_2OH(acetone)_3]^+$, $[UO_2NO_3(acetone)_3]^+$ and $[UO_2CH_2{=}COCH_3(acetone)_3]^+$. For example, CID spectra for the dissociation of $[UO_2NO_3(acetone)_3]^+$ are shown in figure 8.5. At the MS/MS stage (figure 8.5 (a)), CID leads to three pathways that included (a) the elimination of an acetone ligand to form $[UO_2NO_3(acetone)_2]^+$ at m/z 448, (b) the elimination of HNO_3 (m/z 443, discussed below) and (c) the formation of $[UO_2OH(acetone)_2]^+$ at m/z 403: all three product ions appeared as minor peaks in the CID spectrum. The most abundant apparent products observed were instead hydrated (one additional H_2O ligand added) versions of the product ions at m/z 443 and 448. The $[UO_2OH(acetone)_2]^+$ ion was the principal dissociation product for the CID of $[UO_2OH(acetone)_3]^+$ (spectrum not shown), and the MS^n dissociation pathways were the same for both the nitrate and hydroxide precursor species. Subsequent CID of the $[UO_2NO_3(acetone)_2]^+$ species at m/z 448 (figure 8.5 (b)) caused the formation of $[UO_2OH(acetone)_2]^+$, $[UO_2NO_3(acetone)(H_2O)]^+$, $[UO_2OH(acetone)_2(H_2O)]^+$ and $[UO_2NO_3(acetone)(H_2O)_2]^+$ at m/z 403, 408, 421 and 426 respectively.

At the MS/MS stage, elimination of HNO_3 from $[UO_2NO_3(acetone)_3]^+$ generated a product ion at m/z 443, consistent with a species with formula

$[UO_2CH_2{=}COCH_3(acetone)_2]^+$. The same product was observed following the CID (MS/MS) of $[UO_2CH_2{=}COCH_3(acetone)_3]^+$ (Figure 8.6 (a)). The appearance of the species during the CID of $[UO_2NO_3(acetone)_3]^+$ suggests the proton transfer occurs, via keto-enol tautomerism, from an acetone ligand to NO_3, with subsequent elimination of neutral nitric acid. Deuterium labeled (d_6) acetone was used to generate $[UO_2NO_3(d_6acetone)_3]^+$. CID of this species (spectrum not shown) caused only the elimination of neutral deuterium labeled acetone ligand, with no observed loss of DNO_3 or HNO_3. However, the lack of a pathway involving the elimination of DNO_3 does not necessarily rule out a mechanism in which a proton was transferred from the protium form of acetone to nitrate: a kinetic isotope effect may alter the tendency for H/D transfer in the CID reaction and the probability for observing the reaction when using the deuterium labeled form of the complex, and we also note that the low abundance of m/z 443 may make observation of a low abundance fragmentation difficult. A mechanism for the elimination of HNO_3 that involves a reactive collision with gas-phase H_2O molecule can not explain the m/z value of the product ion, which clearly indicated the presence of a deprotonated acetone ligand.

As noted earlier, CID (MS/MS, figure 8.6 (a)) of $[UO_2CH_2{=}COCH_3(acetone)_3]^+$ generated $[UO_2CH_2{=}COCH_3(acetone)_2]^+$ at m/z 443, a hydrated form of the complex, $[UO_2CH_2{=}COCH_3(acetone)_2(H_2O)]^+$, at m/z 461 and a product ion at m/z 403. The

peak at m/z 403 was the major species formed following subsequent CID of $[UO_2CH_2{=}COCH_3(acetone)_2]^+$ (MS^3, figure 8.6 (b)), along with peaks at m/z 363 and 421, consistent with the formation of $[UO_2OH(acetone)_2]^+$, $[UO_2OH(acetone)(H_2O)]^+$ and $[UO_2OH(acetone)_2(H_2O)]^+$ respectively. The assignment of composition as acetone/H_2O ligated uranyl-hydroxide cation based on the observation that the subsequent CID of these species generated CID spectra that were very similar to those for product ions generated instead from the MS^n of $[UO_2OH(acetone)_3]^+$, i.e. directly from a uranyl-hydroxide based complex.

Gas-phase Ligand Addition Reactions

The general tendency for several uranium-acetone complexes to accept addition ligands via gas-phase association reaction was probed by selective isolation and storage of the species in the ion-trap without imposed collisional activation. Our previous investigation of the intrinsic tendency for monopositive uranyl-ligand cations (uranyl hydroxide, nitrate and acetate) demonstrated that the maximum number of H_2O molecules added, regardless of the species isolated, was 3 [98,26]. For the uranyl-hydroxide species in particular, the lack of a 4^{th} H_2O molecule suggested a preferred gas-phase equatorial coordination number of 4 (3 H_2O molecules and the OH ligand). Subsequent investigations of the intrinsic hydration of uranyl alkoxides

also showed the uptake of a maximum of 3 H_2O molecules. However, each of the species studied in the earlier investigations was a mono-positive cation and conclusive statements about the intrinsic tendency for true uranyl complexes to hydrate or otherwise participate in ion-molecule reactions requires a clear understanding of the influence of charge state on reaction rates and preferred coordination number. The species at m/z 501 generated by ESI, $[UO_2CH_2{=}COCH_3(acetone)_3]^+$, contains one less proton than the doubly charged ion at m/z 251, $[UO_2(acetone)_4]^{2+}$ but maintains an equal number of coordinating ligands around the UO_2 core. The lack of a proton causes the overall charge of the former complex to be lower than the latter. This fact allowed us to isolate and store in the ion trap species of nearly identical mass (and presumably conformation) but with different charge state to probe the influence of the latter parameter on the intrinsic tendency to accept ligands by gas-phase association reactions. Figure 8.7 shows the results of isolating the two species in the ion trap for periods ranging from 1 msec to 10 seconds. During the imposed isolation period, the species were exposed to H_2O and acetone contaminants within the He buffer gas. It was assumed in the experiments that coordination of the uranyl ion by the deprotonated acetone ligand occurs through the O atom, and that the overall coordination structure is similar for the two species. As noted in the experimental section, the reaction rates for both species did not

change significantly with changes in the q_z value during the isolation experiments.

In the present case, despite the high H_2O concentration in the ion trap, the doubly charged species showed a very low tendency to hydrate. Instead, the species reacted nearly to completion by adding a 5th acetone ligand. In contrast to this behavior, the singly charged species showed a greater tendency to hydrate, rapidly exchanging the H_2O ligand for acetone [98].

As shown in figure 8.7, both species showed a tendency to undergo ligand addition reactions. The results from a direct comparison of the doubly and singly charged UO_2-acetone complexes demonstrate significantly higher reaction tendencies for the former over the latter. Our previous experiments have established that the amount of adventitious H_2O in the ion trap is significantly (2-3 times) greater that neutral “reagent” admitted via its use as a component of the spray solvent [32]. It is interesting to note that the doubly charged species prefers to accept only the more basic acetone molecule, despite the high H_2O concentration in the ion trap, while the singly charged species shows a significant tendency to hydrate at short reaction times, rapidly exchanging the hydrated water for acetone. This appears to be the primary mode of acetone addition at short isolation times for this species. However, the singly charged species came to an apparent equilibrium with respect to acetone addition, which we interpret as reflecting a significant reverse reaction that is actually

the collisionally-assisted elimination of the 4th acetone ligand. Apparent reverse reactions have proven to be necessary in several earlier investigations of intrinsic hydration rates.

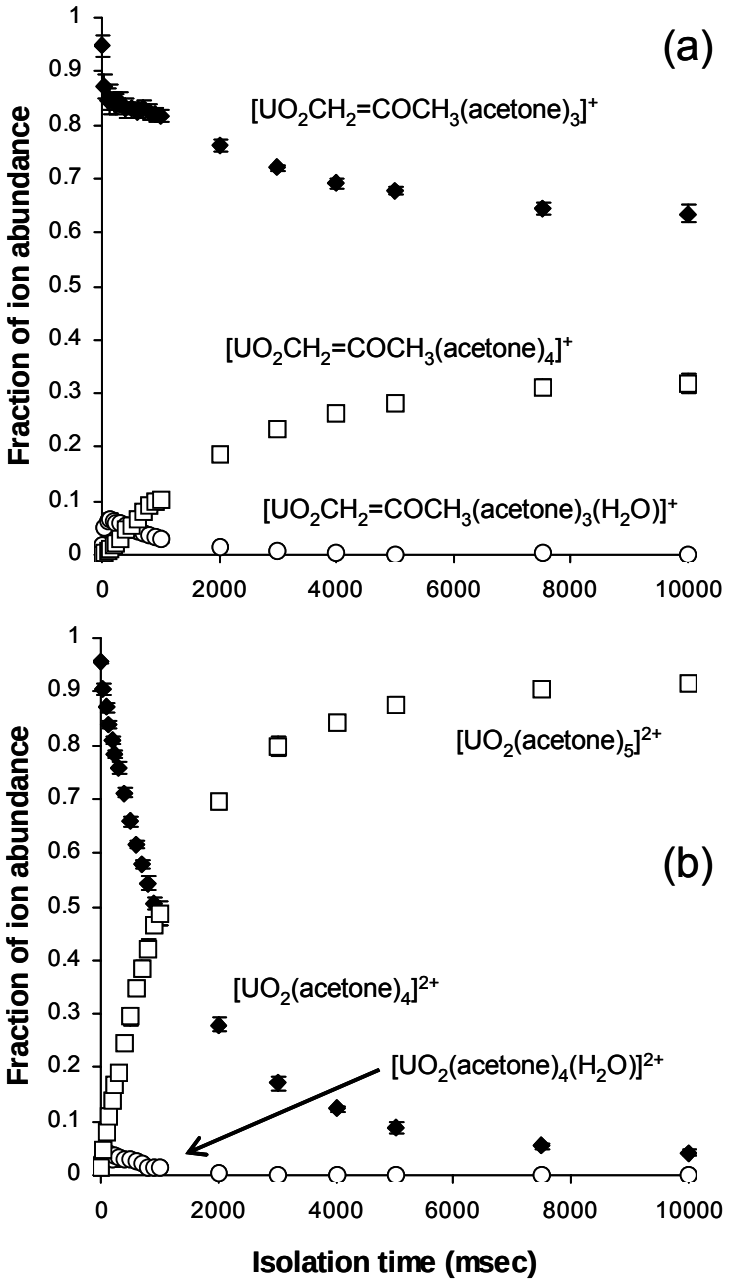

Figure 8.7. Plot of change in fraction of total ion abundance versus isolation time for storage of: (a) $[UO_2CH_2=COCH_3(acetone)_3]^+$ and (b) $[UO_2(acetone)_4]^{2+}$ in the ion trap,

without imposed collisional activation. Species were exposed to similar environments of H_2O and acetone in He.

Full kinetic modeling of the ligand addition reactions is currently underway and will be reported in detail in a future publication. Preliminary kinetic modeling suggests that the reactions for the doubly-charged complex include the (slow) direct addition of H_2O, exchange of H_2O for acetone, and direct addition of acetone. For the singly charged species, the modeling suggests that the reactions include the direct addition of H_2O and the exchange of bound H_2O for acetone. The modeling for this species also requires the inclusion of a significant back reaction involving the elimination of acetone. After long periods of isolation in the ion trap (> 1000 msec) modeling of kinetic profiles obtained from the experimental data suggest a significant decrease in the reactivity of the precursor species for $[UO_2(CH_2{=}CHOCH_3)(acetone)_3]^{+1}$ and, to a much lesser degree, for $[UO_2(NO_3)(acetone)_2]^+$ suggesting that ligand reorganization or rearrangement may be occurring. This apparent change in kinetic behavior was experimentally verified for $[UO_2(CH_2{=}COCH_3)(acetone)_3]^{+1}$, for which the fractional abundance of parent species remaining at isolation times greater than 4000 msec was great enough to allow re-isolation of the unreacted complex. Structural analyses of the most probable conformations for the singly-charged uranyl-acetone complex, $[UO_2CH_2{=}COCH_3(acetone)_3]^+$ and the doubly charged analog, are currently underway using density functional theory calculations.

Figure 8.8 shows the reaction kinetics profiles for $[UO_2OH(acetone)_2]^+$,

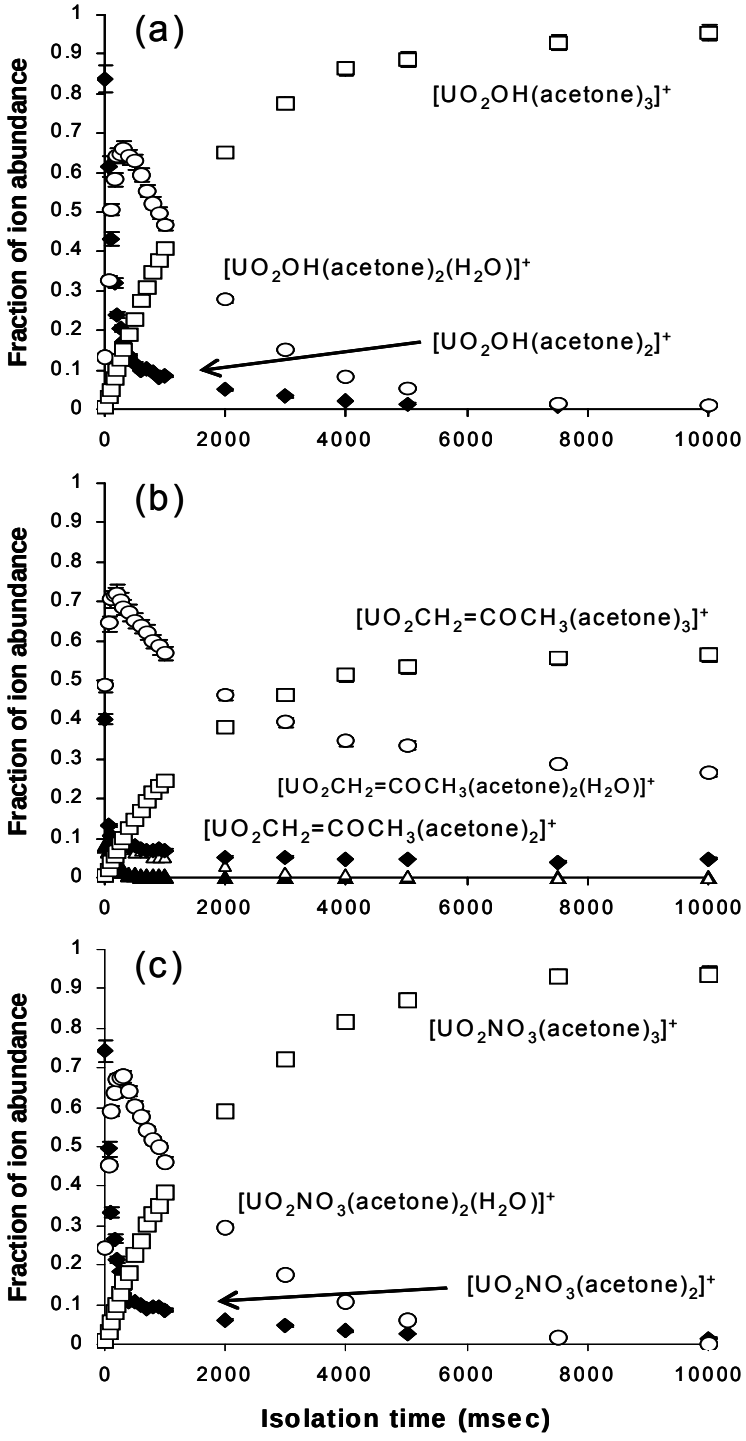

Figure 8.8. Plot of change in fraction of total ion abundance versus isolation time for storage of: (a) $[UO_2OH(acetone)_2]^+$, $[UO_2CH_2=COCH_3(acetone)_2]^+$ and (c)

$[UO_2NO_3(acetone)_2]^+$ in the ion trap, without imposed collisional activation. Species were exposed to similar environments of H_2O and acetone in He.

$[UO_2CH_2{=}COCH_3(acetone)_2]^+$ and $[UO_2NO_3(acetone)_2]^+$. Each species was isolated directly from the ESI spectrum, though each could also be generated using a single CID stage from fully-coordinated precursors. The "under-coordinated" complexes showed a greater tendency to accept H_2O ligands at earlier stages than the more coordinatively saturated $[UO_2CH_2{=}COCH_3(acetone)_3]^+$ and $[UO_2(acetone)_4]^+$ species.

SUMMARY

As discussed in this chapter, ESI was used to generate series of singly and, more importantly, doubly-charged complex ions containing UO_2 and acetone ligands. The most abundant ion generated by ESI under low energy desolvation conditions is the doubly charged $[UO_2(acetone)_5]^{2+}$, a species containing the preferred number of equatorial coordinating ligands as suggested by condensed phase and theoretical investigations. Chemical mass shifts and thermal dissociation data suggest that the elimination of one acetone ligand from the $[UO_2(acetone)_5]^{2+}$ species can be accomplished with only modest increases in energy, however the resulting $[UO_2(acetone)_4]^{2+}$ will readily add the ligand back, underscoring the stability of the pentacoordinated UO_2^{2+} complex. The influence of the +2 charge can be qualitatively

assessed by a comparison with the singly charged $[UO_2(CH_2{=}COCH_3)(acetone)_3]^+$: this ion will also add a fifth equatorial acetone ligand, but in the ion trap the reaction never proceeds to completion, and the apparent equilibrium favors the tetracoordinated, singly charged UO_2 complex.

Multiple stage CID demonstrated that the doubly charged species is reluctant to shed its full complement of coordinating ligands, preferring instead to generate hydrated product ions (H_2O replacing acetone ligands eliminated in the CID reactions), or undergo charge reduction reactions to cations such as $[UO_2OH]^+$ and UO_2^+ coordinated by acetone and/or H_2O. In contrast, elimination of all coordinating neutral ligands can be achieved in CID of singly charged complexes. Gas-phase ion molecule reactions involving $[UO_2CH_2{=}COCH_3(acetone)_3]^+$ and $[UO_2(acetone)_4]^+$ demonstrate that the singly charged species has a lower tendency to undergo ligand addition reactions compared with the doubly charged species.

The production of doubly-charged complexes is not limited to the use of acetone or acetonitrile co-solvent as demonstrated in this report. Preliminary studies indicate that true uranyl complexes can be created by ESI when 2 or 3-pentanone, acetophenone, tetrahydrofuran, dimethylsulfoxide or nitrobenzene are used in place of acetone. Efforts to generate doubly-charged, hydrated uranyl complexes have failed, even when using salts of the uranyl ion with weakly coordinating anions such

as perchlorate. As demonstrated in earlier studies, in aqueous solution devoid of a strongly coordinating ligand such as acetone, the ESI spectrum is dominated by $[UO_2A]^+$, where A is for example OH or NO_3, coordinated by solvent molecules.

CHAPTER 9

GAS-PHASE URANYL-NITRILE COMPLEX IONS

INTRODUCTION

As described in the previous chapters, gas-phase complexes containing the uranyl ion can also be generated by ESI [41,42,26,104-106,135,136,155,157], including doubly-charged complexes in which the uranyl ion is coordinated by acetone ligands [155]. One of our research goals is a comprehensive investigation of the influence of ligation on the intrinsic reactivity of gas-phase uranyl species. In multiple-stage (MS^n) collision-induced dissociation (CID) experiments described in the previous chapter, the doubly charged uranyl-acetone complexes did not shed their full complement of coordinating ligands, but instead generated hydrated product ions (where H_2O replaced acetone ligands eliminated in the CID reactions), or charge-reduction product ions containing $[UO_2OH]^+$ or UO_2^+ coordinated by acetone and/or H_2O. At no point in the MS^n experiments were gas-phase complex ions containing the uranyl ion and two or fewer acetone or H_2O ligands observed.

In the experiments reported in this chapter, ESI was used to generate gas-phase complex ions composed of the uranyl ion and nitrile (acetonitrile, propionitrile or benzonitrile) ligands. Unlike our earlier investigation of uranyl-acetone complex ions [155], the use of nitrile ligands in the present case allowed the

production of a series of gas-phase ions with general formula $[UO_2(RCN)_n]^{2+}$ with n=2-5. For acetonitrile, the bare uranyl ion and a complex composed of the uranyl ion and a single nitrile ligand (i.e. $[UO_2(acn)_1]^{2+}$) were also produced. Generation by ESI of this group of gas-phase species allowed a direct investigation of the influence of the number and type of coordinating ligands on the intrinsic reactions of ligated uranyl ion with H_2O in the gas-phase environment of an ion trap mass spectrometer.

EXPERIMENTAL

ESI-MS, multiple-stage CID and ion-molecule reactions were carried out using the procedures outlined in previous chapters. Spray solutions for the ESI experiment were prepared by combining portions of the $UO_2(NO_3)_2 \bullet 6H_2O$ stock solution and nitrile in a 1:100 relative molar ratio. For 1 mL total solution volume, the amount of nitrile added ranged from 5 μL for acn to 9.8 μL for bzn. These volumes of nitrile were sufficient to generate abundant doubly-charged uranyl-nitrile complexes, but low enough to avoid the introduction of significant partial pressures of neutral nitrile into the ion trap to participate in ion-molecule reactions. Ion charge states were confirmed by examining the isotopic peak spacing using the ZoomScan, high resolution function of the LCQ-Deca. Doubly charged species were identified by isotopic (primarily ^{12}C and ^{13}C from the nitrile ligands) peak spacing of .5 mass units.

To probe gas-phase ligand-addition and charge-exchange reactions, the doubly-charged uranyl-acn complex ions were isolated individually, stored within the ion trap and allowed to react with H_2O within the He bath gas. Isolation widths of .7 – 1.2 mass units were centered on the m/z value of the precursor ion. The isolation width for a given uranyl complex was chosen empirically to provide an optimal compromise between abundant ion signal and the isolation of single isotopic precursor ion peaks. For the isolation/reaction studies, the activation amplitude (arbitrary to the LCQ system, represents a percentage of 5V, normalized for precursor ion mass) was set at 0 V. The activation Q (used to adjust the q_z value for the resonant excitation of the precursor ion during the CID experiment) was set at .3. Following the isolation period, the precursor and product ions were scanned out of the trap and detected as part of the automated mass analysis operation. Direct comparisons of complex reactivity were carried out using 30 msec isolation times. The pressure within the vacuum system was ca. 1.2×10^{-5} torr during experimental trials. H_2O is present as an indigenous species in the vacuum system, and is admitted into the vacuum system directly because of its use as the spray solvent mixture. It is estimated that the partial pressure of H_2O was ca. 1×10^{-6} torr based on previous hydration studies using similar operating parameters [35,106]. Because ESI is an atmospheric pressure ionization method, N_2 and O_2 from the ambient environment

was likely present within the He bath gas. N_2 is also admitted into the ion trap because of its use as the ESI sheath gas. The ultimate goal of this study was to determine the influence of the number and type of nitrile ligands on the uranyl complex reactions with H_2O rather than a rigorous evaluation of gas-phase reaction rate constants. The latter would require accurate measurements of neutral reagent partial pressures, either by calibrated ion gauge measurements, or use of standard ion-molecule reactions that involve the reagents employed here.

For CID (MS/MS and MS^n), ion isolation parameters used were similar to those used for the ion storage/reactivity studies, except that collisional activation was carried out using activation amplitudes of 10-20%. Applied collision voltages of this magnitude were sufficient to reduce the precursor ion intensity to ~10% relative abundance.

m/z rato	Composition assignment
Acetonitrile	
135	UO_2^{2+}
155.5	$[UO_2(acn)_1]^{2+}$
176	$[UO_2(acn)_2]^{2+}$
185	$[UO_2(acn)_2(H_2O)_1]^{2+}$
194	$[UO_2(acn)_2(H_2O)_2]^{2+}$
196.5	$[UO_2(acn)_3]^{2+}$
203	$[UO_2(acn)_2(H_2O)_3]^{2+}$
205.5	$[UO_2(acn)_3(H_2O)_1]^{2+}$
214.5	$[UO_2(acn)_3(H_2O)_2]^{2+}$
217	$[UO_2(acn)_4]^{2+}$
226	$[UO_2(acn)_4(H_2O)_1]^{2+}$
237.5	$[UO_2(acn)_5]^{2+}$
Propionitrile	
190	$[UO_2(pn)_2]^{2+}$
199	$[UO_2(pn)_2(H_2O)_1]^{2+}$
208	$[UO_2(pn)_2(H_2O)_2]^{2+}$
217	$[UO_2(pn)_2(H_2O)_3]^{2+}$
217.5	$[UO_2(pn)_3]^{2+}$
226.5	$[UO_2(pn)_3(H_2O)_1]^{2+}$
235.5	$[UO_2(pn)_3(H_2O)_2]^{2+}$
245	$[UO_2(pn)_4]^{2+}$
254	$[UO_2(pn)_4(H_2O)_1]^{2+}$
272.5	$[UO_2(pn)_5]^{2+}$
Benzonitrile	
238	$[UO_2(bzn)_2]^{2+}$
289.5	$[UO_2(bzn)_3]^{2+}$
298.5	$[UO_2(bzn)_3(H_2O)_1]^{2+}$
341	$[UO_2(bzn)_4]^{2+}$
392.5	$[UO_2(bzn)_5]^{2+}$

Table 9.1. Uranyl complexes generated by ESI of $UO_2(NO_3)_2 \bullet (H_2O)_6$ in water/nitrile solution.

RESULTS AND DISCUSSION

ESI Mass Spectra

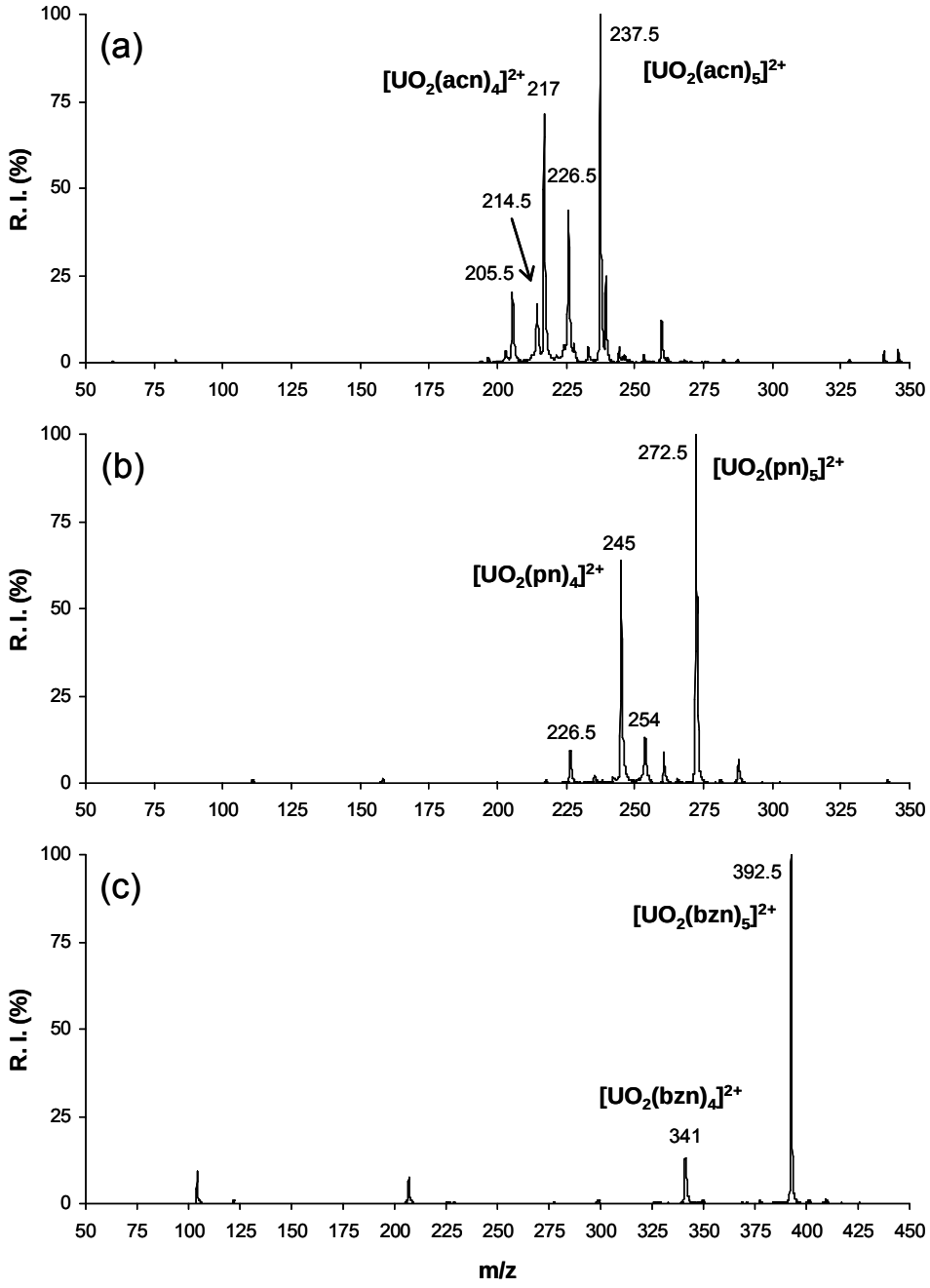

Figure 9.1 (a), (b), (c).

Figure 9.1 shows ESI mass spectra generated from spray solutions containing $[UO_2(NO_3)_2 \bullet (H_2O)_6]$ and acetonitrile (9.1 (a)), propionitrile (9.1 (b)) or benzonitrile (9.1 (c)) in a 1:100 relative molar ratio. A summary of the ion species (m/z ratios and proposed composition) observed in the three spectra is provided in table 9.1. Proposed compositions were confirmed using multiple-stage CID. As in our earlier study of doubly-charged complex ions generated from water-acetone mixtures [155], we found that the general distribution of ions in the ESI spectrum was influenced by the temperature of the heated capillary used in the LCQ-Deca to desolvate ions prior to their transmission to the ion trap mass spectrometer. The best compromise between high overall ion signal and maximum production of doubly charged species was found at desolvation capillary temperatures between 100° and 120°C. The spectra shown in figure 9.1 were collected at 120°C.

For each nitrile used in this study, the principal doubly-charged uranyl-nitrile complex ions generated were $[UO_2(RCN)_4]^{2+}$ and $[UO_2(RCN)_5]^{2+}$. Abundant doubly-charged complexes composed of uranyl ion with a mix of acn and H_2O ligands were also observed. As is apparent in figure 9.1, the intensities of analogous peaks were significantly lower when pn was used as the nitrile ligand, and were not discernable above background when bzn was used instead. The decrease in abundance of complexes containing H_2O ligands scaled with the increase in nitrile

basicity, and likely reflected changes in the competition between nitrile and H_2O ligands for equatorial binding sites of the uranyl ion in solution and during the ion-desolvation steps (on the LCQ platform, desolvation is affected both by an N_2 sheath gas and the heated capillary) prior to introduction of ions into the ion trap.

In general, weaker binding of H_2O ligands relative to nitrile ligands, particularly for the uranyl-acetonitrile system, was apparent in an examination of the peak shapes and m/z values measured for the mixed ligand complexes (data not shown). Those ions containing H_2O ligands featured pronounced tails to the low-mass side, and significant chemical mass shifts [123,155] (~.1 mass unit). Previous work has established that the peak tailing and mass shifts for gas-phase complex ions is due to ion instability and decomposition during analytical scans in the ion trap [122,141]. The previous work with uranyl-acetone complexes by our group demonstrated that the peak tails and chemical mass shifts increased with increasing coordination number, and reflected differences in complex ion stability [155].

Isolation of $[UO_2(acn)_n]^{2+}$, n=0-5

Mass spectra generated by the isolation of $[UO_2(acn)_n]^{2+}$, n=0-5, in the ion trap mass spectrometer (isolation/storage time of 30 msec) are shown in figure 9.2. It is important to note that in the isolation step, all ions except for the precursor ion of

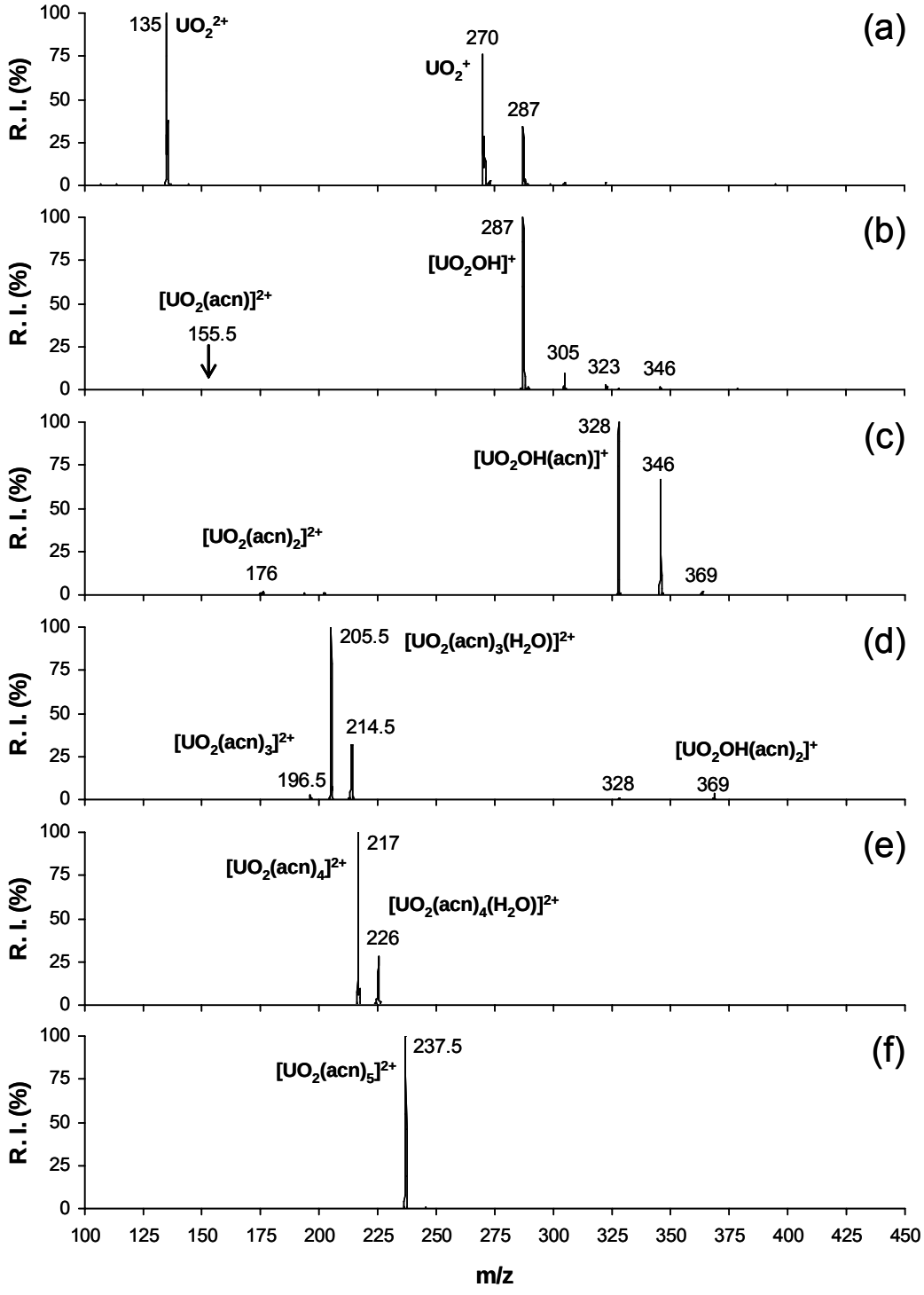

Figure 9.2. Product ion spectra generated by the isolation and storage of doubly-charged uranyl-acetonitrile complex ions in a quadrupole ion trap for 30 msec. (a) UO_2^{2+}, (b) $[UO_2(acn)_1]^{2+}$, (c) $[UO_2(acn)_2]^{2+}$, (d) $[UO_2(acn)_3]^{2+}$, (e) $[UO_2(acn)_4]^{2+}$, (f) $[UO_2(acn)_5]^{2+}$.

interest were resonantly ejected from the ion trap. Composition assignments for the precursor and product ion species shown in figure 9.2 and their relative intensities are listed in table 9.2. In general, two reaction pathways were observed: (a) the direct addition of one or more H_2O ligands to the doubly charged precursor ions and (b) charge reduction reactions that generated singly charged complex ions containing $[UO_2OH]^+$.

As shown in figure 9.2(a), isolation of UO_2^{2+} at m/z 135 resulted in the formation of UO_2^+ at m/z 270 and $[UO_2OH]^+$ at m/z 287. CID (formally MS^3) of the peak at m/z 287 produced UO_2^+ at m/z 270 via the elimination of 17 mass units (u), consistent with the proposed hydroxide composition. In addition, creation of the hydroxide was confirmed through a comparison of the intrinsic hydration rates of the species at m/z 287 to earlier investigation of the hydration of $[UO_2OH]^+$ derived from solutions of uranyl nitrate in pure water [106] (data not shown). The peak at m/z 135 was <1% relative abundance in the ESI mass spectrum and contributions of ^{18}O and ^{235}U to the isotopic distribution of the presumed UO_2^{2+} ion are minor. These two factors combined to make identification of the charge state for the species at m/z 135 by a high-resolution scan impossible. However, the appearance of product ions at m/z 270 and 287, and identification of the latter as $[UO_2OH]^+$, strongly supports the composition assignment for m/z 135 as UO_2^{2+}.

A decrease in the UO_2^{2+} peak intensity, and rise in UO_2^{+} and $[UO_2OH]^{+}$ peak intensities, were observed for isolation times extending to 1 second (data not shown). H_2O adducts to both UO_2^{+} and $[UO_2OH]^{+}$ were also observed at longer isolation/storage times. At no point, however, was direct H_2O ligand addition to UO_2^{2+} competitive with the charge reduction pathways (formation of UO_2^{+} and $[UO_2OH]^{+}$). Experimentally determined ionization energies in the range of 14-15 eV have been reported for monopositive dioxouranium cation, UO_2^{+} [22,156]. This range is significantly higher than the ionization energies of H_2O, acn or O_2 (ca. 12.6, 12.2 and 12.1 eV, respectively [159]), suggesting that electron transfer, when observed, could arise from collisions between any of these neutral molecular species and UO_2^{2+} in the gas-phase environment of the ion trap. The charge reduction process involving formation of uranyl-hydroxide species implicates collisions with gas-phase H_2O.

Isolation of $[UO_2(acn)_1]^{2+}$ at m/z 155.5 (figure 9.2 (b)) lead nearly exclusively to the charge-exchange product $[UO_2OH]^{+}$ at m/z 287. At extended isolation times (100-1000 msec, data not shown), peaks at m/z 305, 323 and 341, created by H_2O addition to $[UO_2OH]^{+}$, were also observed. The formation of the hydroxide would presumably proceed through reaction (9.1), which would involve a reactive collision with an H_2O molecule, transfer of a proton to the acetonitrile ligand, transfer of OH^{-} to the uranyl ion, and coulomb explosion to separate the charged products.

$$[UO_2(acn)_1]^{2+} + H_2O \rightarrow [UO_2(acn)_1(H_2O)]^{2+*} \leftrightarrow [UO_2OH(acnH)]^{2+*} \rightarrow [UO_2OH]^{+} + (acn)H^{+} \quad (9.1)$$

The default (normal range) scan waveform of the LCQ imposes a low-mass cut-off in the tandem mass spectrometry mode at m/z 50, prohibiting the observation of both charged products in reaction (9.1) within the product ion spectrum. Figure 9.3a shows the product ion spectrum generated when the m/z 155.5 precursor ion was isolated and stored in the ion trap using a low-mass waveform, which permits collection of mass spectra over the limited m/z range of 15-200. The only product ion observed in figure 9.3a appeared at m/z 42, the m/z ratio expected for protonated acn.

Precursor	Ligand addition products		Charge exchange products	
	m/z (rel. int. %)	composition	m/z (rel. int. %)	composition
UO_2^{2+}	N.O.		270 (76)	UO_2^+
			287 (43)	$[UO_2OH]^+$
			305 (2)	$[UO_2OH(H_2O)_1]^+$
			323 (2)	$[UO_2OH(H_2O)_2]^+$
$[UO_2(acn)_1]^{2+}$	N.O.		287 (100)	$[UO_2OH]^+$
			305 (10)	$[UO_2OH(H_2O)_1]^+$
			323 (2.5)	$[UO_2OH(H_2O)_2]^+$
			328 (1.5)	$[UO_2OH(acn)_1]^+$
			346 (1.2)	$[UO_2OH(acn)_1(H_2O)]^+$
$[UO_2(acn)_2]^{2+}$	185 (.1)	$[UO_2(acn)_2(H_2O)_1]^{2+}$	328 (100)	$[UO_2OH(acn)_1]^+$
	194 (.6)	$[UO_2(acn)_2(H_2O)_2]^{2+}$	346 (70)	$[UO_2OH(acn)_1(H_2O)]^+$
	203 (3)	$[UO_2(acn)_2(H_2O)_3]^{2+}$	369 (5)	$[UO_2OH(acn)_2]^+$
$[UO_2(acn)_3]^{2+}$	205.5 (100)	$[UO_2(acn)_3(H_2O)_1]^{2+}$	328 (.5)	$[UO_2OH(acn)_1]^+$
	214.5 (32)	$[UO_2(acn)_3(H_2O)_2]^{2+}$	369 (8)	$[UO_2OH(acn)_2]^+$
$[UO_2(acn)_4]^{2+}$	226 (30)	$[UO_2(acn)_4(H_2O)_1]^{2+}$	N.O.	
$[UO_2(acn)_5]^{2+}$	N.O.		N.O.	

Table 9.2. Product ion m/z values and composition assignments for isolation of $[UO_2(acn)_n]^{2+}$, n=0-5, and exposure to gas-phase H_2O.

Precursor	Ligand addition products		Charge exchange products	
	m/z (rel. int. %)	composition	m/z (rel. int. %)	composition
$[UO_2(pn)_2]^{2+}$	199 (2)	$[UO_2(pn)_2(H_2O)_1]^{2+}$	56 (33)	$(acn+H)^+$
	208 (32)	$[UO_2(pn)_2(H_2O)_2]^{2+}$	342 (30)	$[UO_2OH(pn)_1]^+$
	217 (37)	$[UO_2(pn)_2(H_2O)_3]^{2+}$	360 (100)	$[UO_2OH(pn)_1(H_2O)]^+$
			378 (3)	$[UO_2OH(pn)_1(H_2O)_2]^+$
$[UO_2(pn)_3]^{2+}$	226.5 (100)	$[UO_2(pn)_3(H_2O)_1]^{2+}$	56 (.5)	$(acn+H)^+$
	235.5 (32)	$[UO_2(pn)_3(H_2O)_2]^{2+}$	342 (.3)	$[UO_2OH(pn)_1]^+$
			397 (1)	$[UO_2OH(pn)_2]^+$
$[UO_2(pn)_4]^{2+}$	254 (21)	$[UO_2(pn)_4(H_2O)_1]^{2+}$	N.O.	
$[UO_2(pn)_5]^{2+}$	N.O.		N.O.	

Table 9.3. Product ion m/z values and composition assignments for isolation of $[UO_2(pn)_n]^{2+}$, n=2-5, and exposure to gas-phase H_2O.

Precursor	Ligand addition products		Charge exchange products	
	m/z (rel. int. %)	composition	m/z (rel. int. %)	composition
$[UO_2(bzn)_2]^{2+}$	247 (2)	$[UO_2(bzn)_2(H_2O)_1]^{2+}$	104 (1)	$(bzn+H)^+$
	256 (100)	$[UO_2(bzn)_2(H_2O)_2]^{2+}$	390 (2)	$[UO_2OH(bzn)_1]^+$
	265 (62)	$[UO_2(bzn)_2(H_2O)_3]^{2+}$	408 (7)	$[UO_2OH(bzn)_1(H_2O)]^+$
			426 (.3)	$[UO_2OH(bzn)_1(H_2O)_2]^+$
$[UO_2(bzn)_3]^{2+}$	298.5 (14)	$[UO_2(bzn)_3(H_2O)_1]^{2+}$	N.O.	
$[UO_2(bzn)_4]^{2+}$	350 (3)	$[UO_2(bzn)_4(H_2O)_1]^{2+}$	N.O.	
$[UO_2(bzn)_5]^{2+}$	N.O.		N.O.	

Table 9.4. Product ion m/z values and composition assignments for isolation of $[UO_2(bzn)_n]^{2+}$, n=2-5, and exposure to gas-phase H_2O.

Precursor	CID products	
	m/z (rel. int. %)	composition
$[UO_2(acn)_1]^{2+}$	287 (100)	$[UO_2OH]^+$
	305 (6)	$[UO_2OH(H_2O)_1]^+$
	323 (.6)	$[UO_2OH(H_2O)_2]^+$
	328 (3)	$[UO_2OH(acn)_1]^+$
	346 (1.2)	$[UO_2OH(acn)_1(H_2O)_1]^+$
$[UO_2(acn)_2]^{2+}$	287 (8.5)	$[UO_2OH]^+$
	328 (100)	$[UO_2OH(acn)_1]^+$
	346 (76)	$[UO_2OH(acn)_1(H_2O)]^+$
	364 (.6)	$[UO_2OH(H_2O)_2]^+$
$[UO_2(acn)_3]^{2+}$	176 (2)	$[UO_2(acn)_2]^{2+}$
	328 (50)	$[UO_2OH(acn)_1]^+$
	346 (26)	$[UO_2OH(acn)_1(H_2O)_1]^+$
	369 (5)	$UO_2OH(acn)_2]^+$
$[UO_2(acn)_4]^{2+}$	196.5 (4)	$[UO_2(acn)_3]^{2+}$
	205.5 (50)	$[UO_2(acn)_3(H_2O)]^{2+}$
	214.5 (17)	$[UO_2(acn)_3(H_2O)_2]^{2+}$
	287 (1)	$[UO_2OH]^+$
	369 (5)	$UO_2OH(acn)_2]^+$
$[UO_2(acn)_5]^{2+}$	217 (100)	$[UO_2(acn)_4]^{2+}$
	226 (26)	$[UO_2(acn)_4(H_2O)]^{2+}$

Table 9.5. Product ion m/z values and composition assignments for CID of $[UO_2(acn)_n]^{2+}$, n=1-5.

Figure 9.2 (c) shows the spectrum that resulted from the isolation of the $[UO_2(acn)_2]^{2+}$ complex ion at m/z 176. Adduct peaks corresponding to the direct addition of 1, 2 and 3 H_2O ligands to the doubly charged species were observed at m/z 185, 194 and 203 respectively. The charge-reduction pathway was dominant for $[UO_2(acn)_2]^{2+}$, leading to the formation of $[UO_2OH(acn)]^+$ at m/z 328, a hydrated version of the species at m/z 346 and a minor peak at m/z 369, $[UO_2OH(acn)_2]^+$. Figure 9.3 (b) shows the product ion spectrum generated when $[UO_2(acn)_2]^{2+}$ was isolated using the low-mass waveform, and the appearance of protonated acn at m/z 42 suggests that formation of the peak at m/z 328 occurs via a pathway similar the one proposed in reaction 9.1. CID of the peak at m/z 328 (formally MS^3) produced $[UO_2OH]^+$ at m/z 287 via elimination of 41 u, consistent with the presence of a single acn ligand within the precursor ion. Two pathways were observed for the CID of the peak at m/z 346 (formally MS^3): loss of 18 u (H_2O) to produce the species at m/z 328 and loss of 59 (H_2O and acn) to produce m/z 287.

The relative intensity of the species at 346 in figure 9.2 (c) was similar to the intensity for the same species in a separate experiment in which the m/z 328 product ion (generated by isolation and storage of the doubly charged species at m/z 176) was subsequently isolated and stored in the ion trap for 30 msec. This observation suggests that the species at m/z 346 observed in figure 9.2 (c) is the result of H_2O

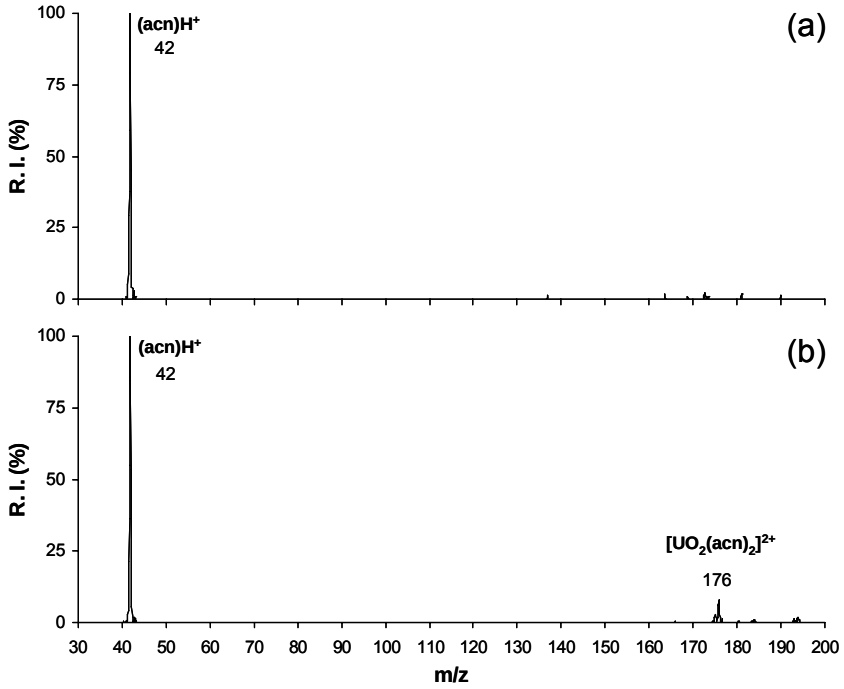

Figure 9.3. Product ion spectra generated by the isolation of doubly-charged uranyl-acetonitrile complex ions. (a) $[UO_2(acn)_1]^{2+}$, (b) $[UO_2(acn)_2]^{2+}$. Spectra were collected using the low mass waveform, which allows collection of spectra in the limited m/z range of 25 to 200.

addition to the m/z 328 product derived from the isolation of $[UO_2(acn)_2]^{2+}$. The minor product ion at m/z 369, however, was more abundant in the spectrum shown in figure 9.2 (c) than when the species at m/z 328 was independently isolated and stored, suggesting that the formation of this ion does not involve the addition of acn to $[UO_2OH(acn)]^+$ by an ion-molecule reaction (consistent with the low partial pressure of acn in the ion trap expected due to the small volume of the nitrile added to the spray solvent). The peak at m/z 369 may instead have been formed by direct hydroxide transfer to $[UO_2(acn)_2]^{2+}$ via the reaction:

$$[UO_2(acn)_2]^{2+} + 2\ H_2O \rightarrow [UO_2(acn)_2(H_2O)_2]^{2+*} \leftrightarrow [UO_2OH(acn)_2H_3O]^{2+*} \rightarrow [UO_2OH(acn)_2]^{+} + H_3O^{+}$$

(9.2)

With extended isolation times (100-1000 msec, data not shown), the $[UO_2OH(acn)(H_2O)]^+$ species at m/z 346 became the base peak, and a dihydrate species, $[UO_2OH(acn)(H_2O)_2]^+$, at m/z 364 also appeared.

For the isolation and storage of $[UO_2(acn)_3]^{2+}$and $[UO_2(acn)_4]^{2+}$ (figures 9.2 (d) and 9.2 (e), respectively), ligand addition reactions dominated the charge reduction processes. Isolation of $[UO_2(acn)_3]^{2+}$ at m/z 196.5 generated mono and dihyrdate versions, i.e. $[UO_2(acn)_3(H_2O)]^{2+}$ and $[UO_2(acn)_3(H_2O)_2]^{2+}$, of the complex at m/z 205.5 and 214.5, respectively. The charge reduction products observed for the isolation of $[UO_2(acn)_3]^{2+}$ included $[UO_2OH(acn)]^+$ and $[UO_2OH(acn)_2]^+$. Isolation of $[UO_2(acn)_4]^{2+}$ led to the addition of a single H_2O or acn ligand, and no charge reduction product ions were observed. With extended isolation times (data not shown), the $[UO_2(acn)_3]^{2+}$and $[UO_2(acn)_4]^{2+}$ complexes added 2 and 1 H_2O molecules, respectively, to furnish ions with 5 total equatorial ligands. As shown in figure 2f, isolation of $[UO_2(acn)_5]^{2+}$ produced no adduct species or charge reduction products. The absence of ligand addition reactions is generally consistent with a preferred equatorial coordination number of 5 for the uranyl ion in condensed-phase studies [147-149,153], theoretical calculations [46] and with previous studies of intrinsic ligand addition reactions for singly-charged gas-phase uranyl nitrate and acetate

complex ions [106] and doubly charged uranyl-acetone complexes [155].

Isolation of $[UO_2(pn)_n]^{2+}$, n=2-5

Mass spectra generated by the isolation of $[UO_2(pn)_n]^{2+}$, n=2-5, in the ion trap mass spectrometer are shown in figure 9.4. For pn, isolation of the bare uranyl ion or $[UO_2(pn)_1]^{2+}$ was not possible. We attribute this to a higher intrinsic hydration tendency for the pn complexes relative to the acn complexes, due to the increased number of vibrational degrees of freedom with the larger ligand. A larger number of oscillators may accommodate better reaction exothermicity and thus stabilize adducts as they are formed in association reactions. A similar effect was recently reported for the intrinsic hydration of Ag^+-alcohol complexes [32], and for uranyl-acetone complex cations [155]. A hydrated form of the complex, $[UO_2(pn)_1(H_2O)_1]^{2+}$, was produced by ESI. Attempts to dissociate this ion to generate the $[UO_2(pn)_1]^{2+}$ species were complicated by a rapid hydration reaction that re-formed $[UO_2(pn)_1(H_2O)_1]^{2+}$.

The formation of mono-, di- and tri-hydrates at m/z 199, 208 and 217, respectively, was observed following isolation of $[UO_2(pn)_2]^{2+}$ at m/z 190 (figure 9.3 (a)). The abundances of H_2O adducts to the pn complex were significantly higher those generated by isolation of the analogous acn complex for an equivalent period of time (figure 9.4 (c)), consistent with the positive influence of an increased number of vibrational degrees of freedom to accommodate reaction exothermicity.

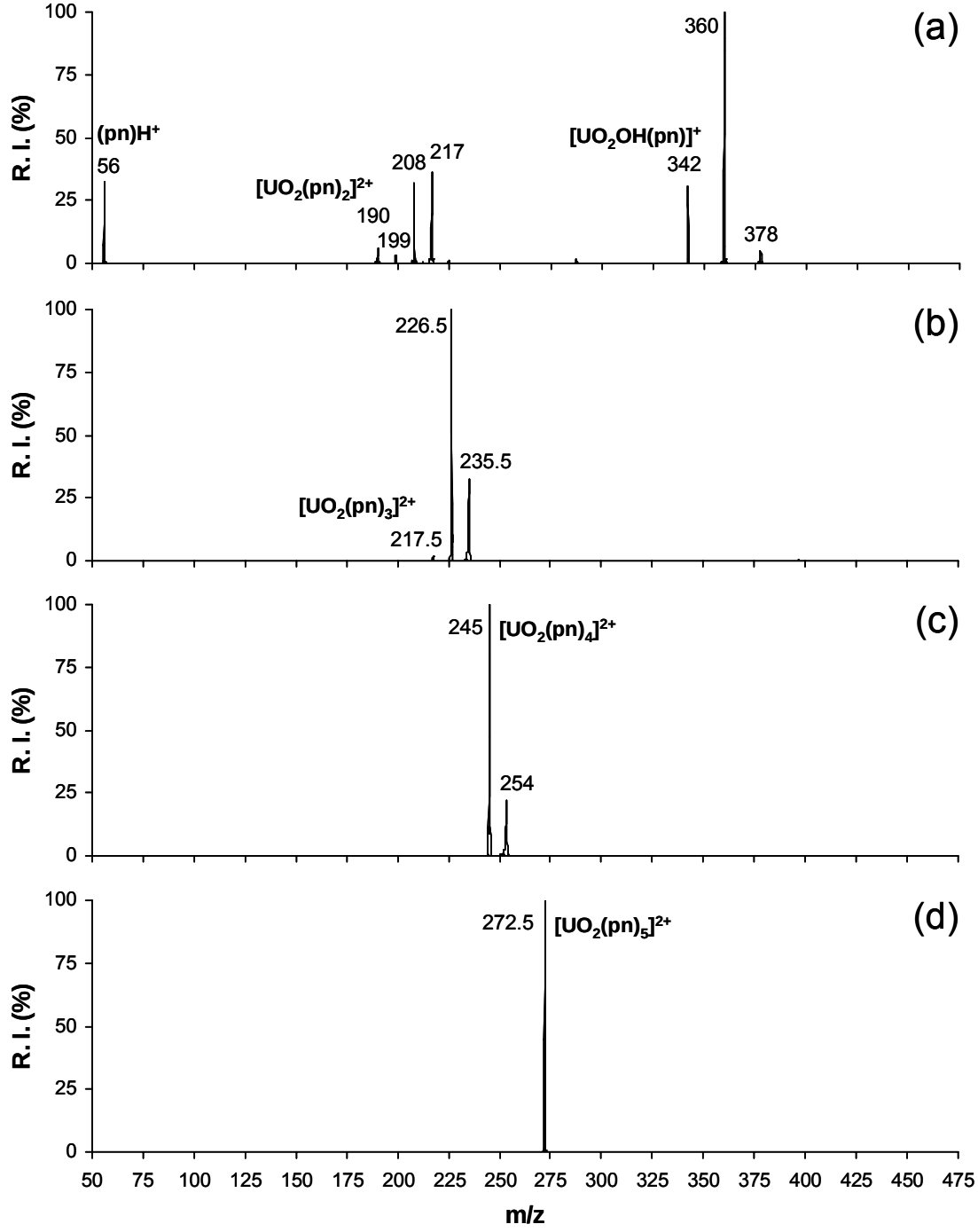

Figure 9.4. Product ion spectra generated by the isolation and storage of doubly-charged uranyl-propionitrile complex ions in a quadrupole ion trap for 30 msec. (a) $[UO_2(pn)_2]^{2+}$, (b) $[UO_2(pn)_3]^{2+}$, (c) $[UO_2(pn)_4]^{2+}$, (d) $[UO_2(pn)_5]^{2+}$.

As for the analogous acn complex, the dominant charge reduction reaction pathway observed for $[UO_2(pn)_2]^{2+}$ was formation of $[UO_2OH(pn)]^{+}$ at m/z 342 and a hydrated version of the species at m/z 360. The presence of pn and H_2O ligands was confirmed by loss of 55 u from the species at m/z 342 and of 18 and 73 u from the species at m/z 360 in subsequent CID steps (formal MS^3). The relative intensity of the species at 360 was similar to the intensity for the same species in a separate experiment in which the m/z 360 product ion (generated by isolation and storage of the doubly charged species at m/z 190) was subsequently isolated and stored in the ion trap for 30 msec, suggesting that the species at m/z 360 observed in figure 9.4 (a) is the result of H_2O addition to the m/z 342 product derived from the isolation of $[UO_2(pn)_2]^{2+}$. An important feature of the spectrum in figure 9.4 (a) is the appearance of a peak at m/z 56, consistent with the formation of protonated pn. The appearance of this peak further supports the formation of the uranyl-hydroxide product via a process that involved interactions with an H_2O collision partner, transfer of proton to a nitrile ligand, retention of the hydroxide ion and then fission of the activated complex as proposed in reaction (9.1).

Only direct ligand addition reactions were observed for the isolation and storage of $[UO_2(pn)_3]^{2+}$and $[UO_2(pn)_4]^{2+}$ (figures 9.4 (b) and 9.4 (c), respectively). The $[UO_2(pn)_3]^{2+}$ complex at m/z 217.5 generated mono and dihyrdate, $[UO_2(pn)_3(H_2O)]^{2+}$

and $[UO_2(pn)_3(H_2O)_2]^{2+}$, at m/z 226.5 and 235.5 respectively. The $[UO_2(pn)_4]^{2+}$ complex at m/z 245 added a single H_2O molecule to make the monohydrate at m/z 254. As with the acn version of the complex, no ligand addition was observed following the isolation of the $[UO_2(pn)_5]^{2+}$ complex at m/z 272.5. At extended isolation times (100-1000 msec, data not shown), the $[UO_2(pn)_3]^{2+}$and $[UO_2(pn)_4]^{2+}$ complexes added to 2 and 1 H_2O molecules, respectively, to furnish ions with 5 total equatorial ligands. A preliminary investigation of the hydration rates for the pn complexes suggest that the rates for H_2O addition are lower than for the acn complexes. A comprehensive investigation of ligand addition rates to the complexes, including kinetic modeling, is currently being conducted and will be reported at a later date.

Isolation of $[UO_2(bzn)_n]^{2+}$, n=2-5

Mass spectra generated by the isolation of $[UO_2(bzn)_n]^{2+}$, n=2-5, are shown in figure 9.5. As with pn, isolation of the bare uranyl ion or $[UO_2(bzn)_1]^{2+}$ was not possible. Unlike the results observed for the acn and pn complexes, the dominant products generated by isolation of $[UO_2(bzn)_2]^{2+}$ at m/z 238 (figure 9.4 (a)) were those formed by direction ligand addition (formation of mono-, di- and tri-hydrates at m/z 247, 256 and 265 respectively) rather than charge reduction. The intensities of these adducts were significantly higher that those generated from the isolation of the

analogous pn and acn complexes, which further supports the proposal that accommodation of reaction exothermicity by internal modes in the species with larger, more complex ligands enhances the potential for direct ligand addition. Though the charge-exchange products for the bzn complexes were of overall lower abundance, the species generated were analogous to those observed for the pn and acn complexes, namely $[UO_2OH(bzn)]^+$, $[UO_2OH(bzn)(H_2O)]^+$ and $[UO_2OH(bzn)(H_2O)_2]^+$ at m/z 390, 408 and 426, respectively. Composition assignments were confirmed through the observation of the elimination of bzn or bzn and H_2O in subsequent CID steps (formally MS^3).

For the isolation and storage of $[UO_2(bzn)_3]^{2+}$ (m/z 289.5) and $[UO_2(bzn)_4]^{2+}$ (m/z 341), shown in figures 9.5 (b) and 9.5 (c), only ligand addition reactions were observed, producing H_2O adducts at m/z 298.5 and 350 respectively. Isolation of $[UO_2(bzn)_4]^{2+}$ led to the addition of a single H_2O and $[UO_2(bzn)_5]^{2+}$ (figure 9.5 (d)) was unreactive. At extended isolation times, the intensity of the hydrate peaks increased more slowly than for the pn and acn versions of the complexes, and the addition of a second H_2O ligand to $[UO_2(bzn)_3]^{2+}$ was not favored. While further comment on the intrinsic hydration rates will be made at a later date, the decrease in apparent hydration tendency from acn to pn to bzn versions of $[UO_2(RCN)_3]^{2+}$ and $[UO_2(RCN)_4]^{2+}$ is likely attributable to a combination of increasing ligand basicity (bzn

> pn > acn), and thus greater donation of charge to the uranyl ion, and to potential steric effects about the equatorial coordination sites.

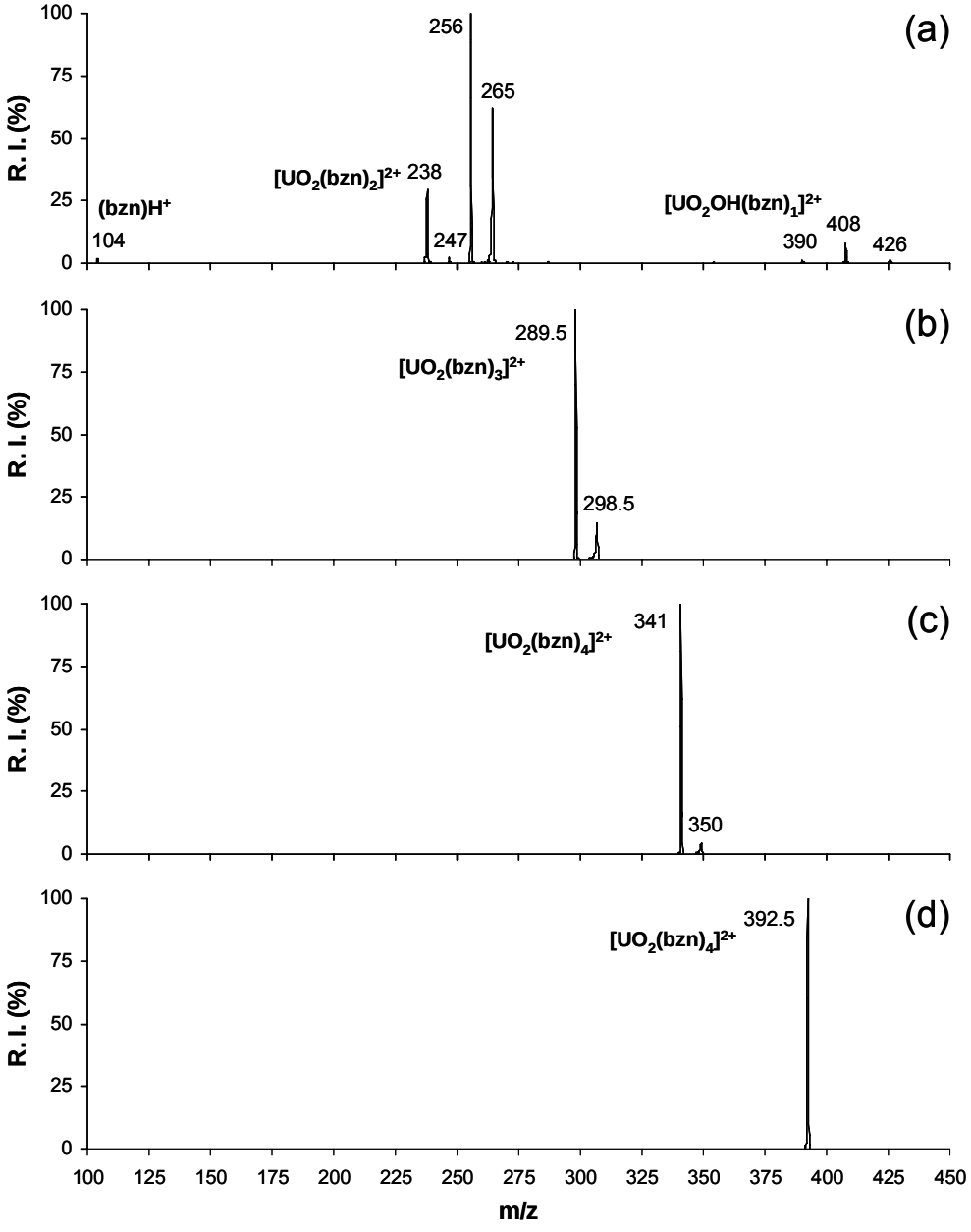

Figure 9.5. Product ion spectra generated by the isolation and storage of doubly-charged uranyl-benzonitrile complex ions in a quadrupole ion trap for 30 msec. (a) $[UO_2(bzn)_2]^{2+}$, (b) $[UO_2(acn)_3]^{2+}$, (c) $[UO_2(bzn)_4]^{2+}$, (d) $[UO_2(bzn)_5]^{2+}$.

Intrinsic reactivity with H_2O

In general, the tendency for direct H_2O ligand addition to the uranyl-nitrile complexes is influenced by the number of nitrile ligands in the precursor uranyl complex and their complexity. For example, H_2O addition was not observed for UO_2^{2+} and $[UO_2(acn)_1]^{2+}$, was observed to a small extent for $[UO_2(acn)_2]^{2+}$ and become dominant for $[UO_2(acn)_3]^{2+}$ and $[UO_2(acn)_4]^{2+}$. With respect to the nitrile ligand, the tendency for direct H_2O addition to precursor ions with 2 nitrile ligands increased with a trend acn < pn < bzn. For precursor ions with 3 nitrile ligands, the tendency for direct addition of H_2O instead followed the trend pn > acn > bzn. This suggests that the increase in number of degrees of freedom for pn over acn assists hydration, but that increasing basicity and/or steric hindrance for bzn over pn decreases the tendency for H_2O addition. The influence of increased nitrile ligand basicity, or more appropriately, donation of charge to the uranyl ion, is apparent in the decreased H_2O addition to the complexes with n=4 progressing from acn to pn to bzn.

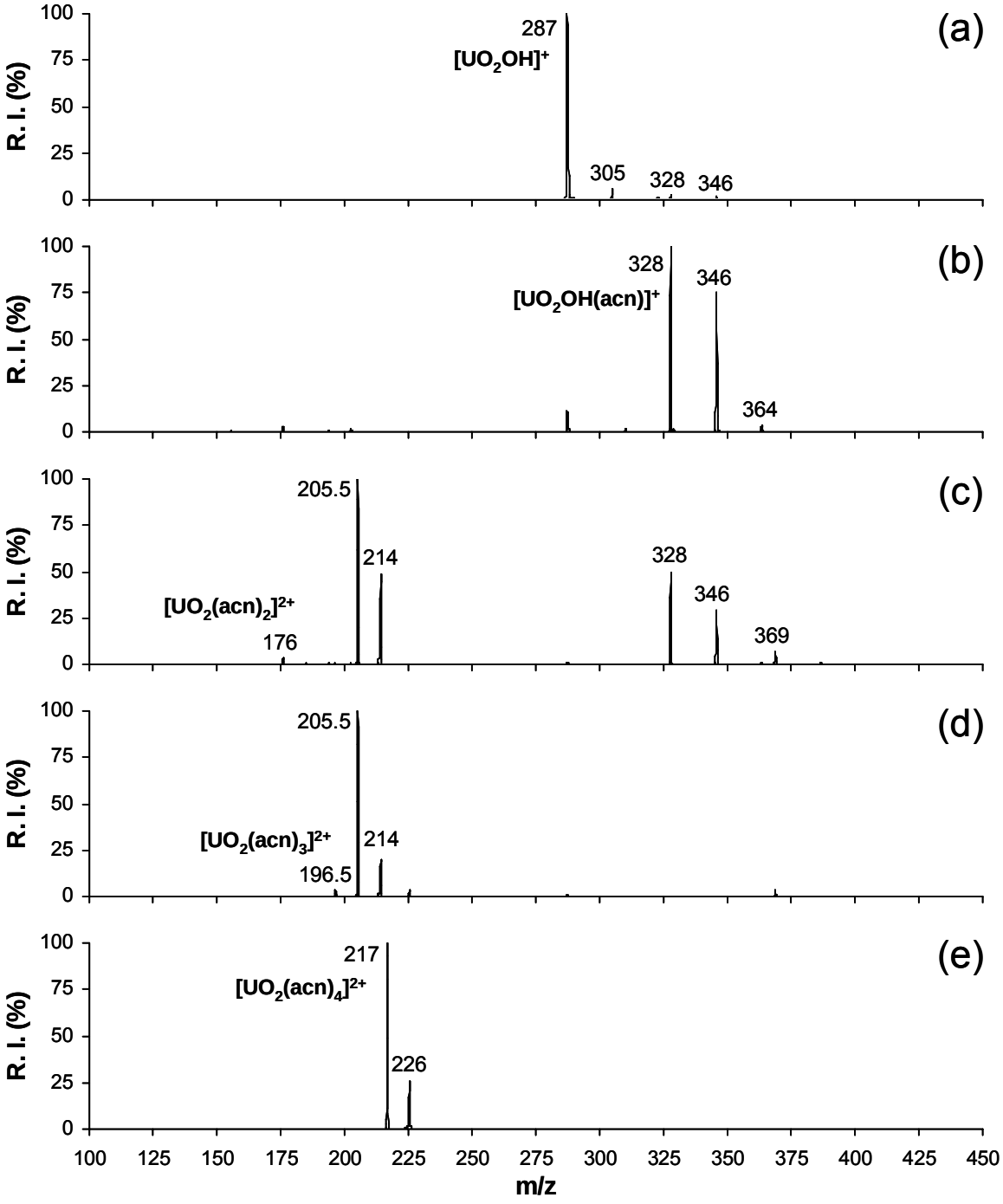

Figure 9.6. Product ion spectra generated by the isolation and collisional activation of doubly-charged uranyl-acetonitrile complex ions: (a) $[UO_2(acn)_1]^{2+}$, (b) $[UO_2(acn)_2]^{2+}$, (c) $[UO_2(acn)_3]^{2+}$, (d) $[UO_2(acn)_4]^{2+}$, and (e) $[UO_2(acn)_5]^{2+}$. Applied activation voltages were in the range of .35-.46 V, laboratory frame of reference.

The charge reduction reactions exhibited by the doubly-charged uranyl-nitrile complexes are consistent with those discussed previously for intra-complex transfer during the CID of H_2O complexes of divalent metal ions [160], the unimolecular dissociation of $[Cu(H_2O)_n]^{2+}$ [161], the CID of $[Mg(C_3H_7OH)_n]^{2+}$ [162] and $[Mg(CH_3OH)_n]^{2+}$ [163] and in reactions between H_2O and metal cluster cations [164]. For the propanol- and methanol-Mg^{2+} complexes in particular, the ultimate transfer of OH^- to the Mg ion involved bond-breaking within a methanol ligand. In the present case, formation of the hydroxide involves transfer of OH^- to the uranyl-nitrile complexes from a neutral, gas-phase H_2O molecule.

In general, the gas-phase reactions of doubly-charged metal ions and their complexes are dependent on the potential energy curve for ligand-addition, and the relative positions of avoided crossings associated with curves for reactions that lead to possible charge-exchange products. In the present study, the potential charge exchange reactions include: (a) electron transfer from a gas-phase molecule (in this case H_2O or acn) to the uranyl complex ion and (b) transfer of OH^- from gas-phase H_2O to the uranyl complex ion. Similar reaction pathways and the relative positions of avoided crossings of potential energy curves have been discussed by Stace [165] and by Schröder and Schwarz [166] for systems such as gas-phase, hydrated Cu^{2+} and UF^{n+} cations. The results obtained here for the uranyl complexes with 1-3 nitrile

ligands clearly show that a pathway involving electron transfer alone, through collisions with the neutral species present in the He bath gas, is not competitive with one that includes the formal transfer of OH^-. The decreased tendency for charge-transfer with increasing ligation within the precursor ion, as was observed for the uranyl complexes with 3-5 nitrile ligands, is consistent with earlier studies of mono- and hexa-hydrate metal ion complexes, in which the enthalpy change for hydrolysis (deprotonation of H_2O ligands) decreased as the degree of hydration within the complex ion increased [167, 168].

The intensity of the charge reduction products following isolation of UO_2^{2+} (generated when acn was used in the spray solvent) were relatively minor, which is surprising given the differences in magnitude between the ionization energy of UO_2^+ and H_2O, acn or O_2. As noted earlier, the m/z ratios of the product ions generated following isolation and storage of the precursor ion at m/z 135 strongly support a composition assignment of UO_2^{2+}. We can not completely eliminate the possibility of the presence of an isobaric contaminant ion. CID of the peak at m/z 135 produced the species at m/a 270 and 287, and no product ions at lower m/z ratios. This observation, combined with the argument presented above, supports the claim that the ion at m/z 135 is the uranyl ion.

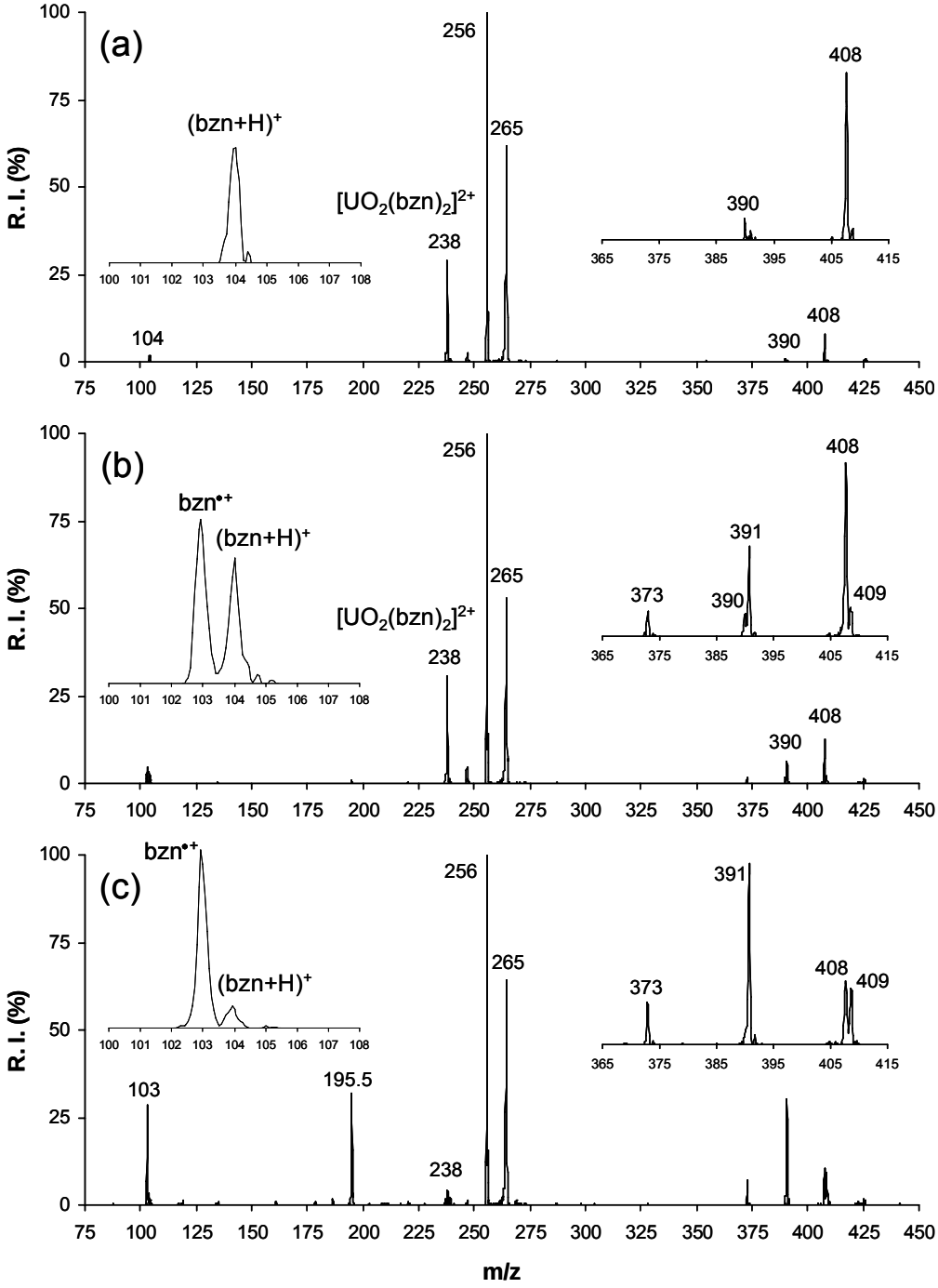

Figure 9.7. Product ion spectra generated by the isolation of $[UO_2(bzn)_2]^{2+}$: (a) 0 V applied activation voltage, (b) .5 V applied activation voltage and (c) .73 V applied activation voltage. Applied voltages are in the laboratory frame of reference.

The intensities of the charge reduction products at m/z 270 and 287, formed by the isolation of UO_2^{2+}, increased with extended isolation times (data not shown), which suggests that the rate for the reactions to product UO_2^+ and $[UO_2OH]^+$ are inherently slow. Comparison of the spectra shown in figures 9.2a and b demonstrates a significant difference in the apparent rates of the charge exchange reactions for UO_2^{2+} and $[UO_2(acn)]^{2+}$ when the two precursor ions are exposed to comparable gas-phase environments. As discussed earlier, formation of the uranyl-hydroxide product ions involves the elimination of protonated nitrile ligands as shown in reaction (1) and a reaction channel involving simple electron transfer from an H_2O molecule to generate nitrile-ligated UO_2^+ was not observed. Transfer of OH^- as in (1) would be favored thermodynamically by the formation of the stable hydroxide and protonated nitrile and assisted by the fission of an activated complex containing two weakly bound cationic species. The nitrile ligand "receptor" liberated during the formation of the hydroxide in (1) is absent in the case of UO_2^{2+}, which lowers the probability for the charge reduction reaction.

Collision-induced dissociation of $[UO_2(RCN)_n]^{2+}$

The tendency for the uranyl-nitrile complexes species to undergo charge reduction reactions to produce ligated $[UO_2OH]$ was also apparent during CID

experiments. As shown in figure 9.6 (a), CID of $[UO_2(acn)_1]^{2+}$ caused the formation of $[UO_2OH]^+$ and $[UO_2OH(acn)]^+$. The intensity of $[UO_2OH(acn)]^+$, when produced by CID of $[UO_2(acn)_1]^{2+}$, was greater than the intensity of the same ion when formed by the independent isolation and storage of $[UO_2OH]^+$. This observation supports the proposal that the ion at m/z 328 was formed as a direct CID product rather than as an acn adduct (formed by ion-molecule association reaction) to $[UO_2OH]^+$ after its formation from $[UO_2(acn)_1]^{2+}$. CID of $[UO_2(acn)_2]^{2+}$ at m/z 176 (9.6b) produced $[UO_2OH(acn)]^+$ and a hydrated adduct. Direct ligand elimination from $[UO_2(acn)_2]^{2+}$ to generate $[UO_2(acn)_1]^{2+}$ was not observed. CID of $[UO_2(acn)_3]^{2+}$ at m/z 196.5 (9.6c) generated three product ions: $[UO_2(acn)_2]^{2+}$ by the elimination of acn, and the formation of $[UO_2OH(acn)]^+$ and $[UO_2OH(acn)_2]^+$. CID of $[UO_2(acn)_4]^{2+}$ and $[UO_2(acn)_5]^{2+}$ (6d and e, respectively) demonstrated the elimination of a single acn ligand only.

In general, the CID of the pn versions of the complexes mirrored that of the acn complexes. Figure 9.7 shows three spectra collected for the $[UO_2(bzn)_2]^{2+}$ complex. In figure 9.7 (a), the spectrum was produced by the isolation, without imposed collisional activation, of the species for 30 msec. The spectra in 9.7(b) and 9.7(c) show the spectra that resulted from the CID of the same ion at activation amplitudes of 17 and 25%, respectively. As noted earlier, the charge reduction products observed

following isolation of $[UO_2(bzn)_2]^{2+}$, without CID, included protonated bnz at m/z 104, $[UO_2OH(bzn)]^+$ at m/z 390 and $[UO_2OH(bzn)(H_2O)]^+$ at m/z 408. As is apparent in figure 9.7(b), inducing collisional activation of $[UO_2(bzn)_2]^{2+}$ lead to the appearance of 4 new product ions: the bzn radical ion at m/z 103, and ions at m/z 373, 391 and 409. The ion at m/z 373 corresponds in mass to the formation of $[UO_2(bzn)]^+$, presumably in a process that involved oxidation of a bzn ligand and reduction of the uranyl ion. Subsequent CID of the ion at m/z 373 caused the formation of UO_2^+ at m/z 270 via the elimination of 103 u, consistent with the composition assignment. The species at m/z 391 and 409 have masses consistent with formation of $[UO_2(bzn)(H_2O)]^+$ $[UO_2(bzn)(H_2O)_2]^+$, respectively. Subsequent CID of the ions at m/z 391 and 409 (spectra not shown) showed the elimination of 18 u, consistent with the presence of H_2O ligands. At an activation amplitude of 25% (figure 7c), the charge exchange products resulting from electron transfer from bzn to the uranyl ion (i.e. m/z 103 and 373) and the hydrated forms of the products, and thus oxidation of a nitrile ligand, was higher than for reactions involving net hydroxide transfer from an H_2O collision partner. The appearance of the electron transfer products for the bzn complexes only, is consistent with the significantly lower ionization energy of bzn relative to pn and acn [159]. The proposal that the direct oxidation of ligands during CID is a high energy pathway is consistent with the dominant appearance of the charge reduction products

involving formation of ligated $[UO_2OH]^+$ following isolation of the range of doubly-charged uranyl-nitrile complexes and exposure to neutral H_2O in the ion trap. It is also evident that charge exchange reactions involving simple reduction of the doubly charged complexes by electron transfer (and oxidation of H_2O) is not a favored process for these precursor ions.

SUMMARY

In the experiments described in this chapter it was demonstrated that ESI can be used to generate gas-phase, doubly charged complex cations containing the uranyl ion, UO_2^{2+}, and several nitrile ligands. For acn, doubly charged ions with between 0 and 5 coordinating, neutral ligands, were generated. For pn and bzn, complex cations with between 2 and 5 nitrile ligands were generated. In general, for species with 0-3 nitrile ligands, two general reaction pathways were observed: (a) formation of adducts through the addition of one or more H_2O or acn ligand and (b) charge reduction reactions that led to formation of ligated $[UO_2OH]^+$. For the bare uranyl ion, UO_2^{2+}, only the charge-exchange products UO_2^+ and UO_2OH^+, and hydrated versions of these species, were observed. For $[UO_2(acn)_1]^{2+}$, reactions with H_2O produced almost exclusively $[UO_2OH]^+$. For $[UO_2(RCN)_2]^{2+}$ and $[UO_2(RCN)_3]^{2+}$ complexes containing acn, pn or bzn ligands, the principal charge reduction reaction observed

involved elimination of a single nitrile ligand as a protonated species and addition of hydroxide, through reactions that involved collisions with neutral H_2O. For precursor complexes with 3 or 4 nitrile ligands, the direct H_2O addition was favored over the charge reduction reactions. Precursor complexes with 5 nitrile ligands were unreactive when isolated under similar conditions.

With respect to the complexity/size of the nitrile ligand, the trend for direct H_2O addition to the complex with 2 nitrile ligands, i.e. $[UO_2(RCN)_2]^{2+}$, was bzn > pn > acn. However, for complexes with 3 nitrile ligands, the trend for direct addition of H_2O was pn > acn > bzn, suggesting that the increase in number of degrees of freedom for pn over acn assists hydration, but that increasing basicity and/or steric hindrance for bzn over pn decreases the tendency for H_2O addition. This proposal is supported by the low hydration tendency for the complex ion with 4 bzn ligands.

Comparison of the spectra generated by isolation and storage of the uranyl-benzonitrile complexes to spectra resulting from CID of the same species demonstrate that reaction pathways involving OH^- transfer are lower in energy than those involving direct oxidation of nitrile ligands, and pathways that involve reduction of precursor ion charge state via oxidation of neutral H_2O molecules.

CHAPTER 10

BINDING OF MOLECULAR O_2 TO DI- AND TRI-LIGATED $[UO_2]^+$

INTRODUCTION

The structure and reactivity of molecular uranium species have been topics of ongoing research because they dictate the behavior of the element at various junctures in the environment [169-171] and in the nuclear fuel cycle [62,172]. Positively charged, oxidized uranium species tend to act as Lewis acids, accepting electron density from donor ligands and participating in hydrolysis reactions at neutral pH. Uranium in the lower oxidation states is also highly oxophilic, as shown by several gas-phase studies that indicated oxidation by a number of neutral reagents. For example, gas-phase U^+ reacts with dioxygen to form UO^+, which reacts with a second O_2 to form the U(V) species UO_2^+ [103]. In similar fashion, U_2^+ is oxidized to UO_2^+ and UO_2^{2+} in serial reactions with O_2 and other oxidants [22,156] However, reactions of uranium cations with dioxygen to form complexes containing intact O_2 ligands have not been observed in the gas phase.

In the condensed phases, the uranyl dication forms complexes with dioxygen in an η^2-peroxo fashion, [174] including the uranyl peroxy minerals studtite $(UO_2)O_2(H_2O)_4$ and metastudtite $(UO_2)^-O_2(H_2O)_2$ [12]. There are several examples in

which two $[UO_2]^{2+}$ molecules are joined by peroxide in a μ-dioxo mode [176-181]. In these condensed-phase systems, a common theme is that binding of oxygen is very much dependent upon other ligands bound to the uranium center.

In contrast to peroxide binding, examples of superoxo dioxygen binding to actinide centers are scarce. Reversible attachment of dioxygen as superoxide to transition metal centers is well known [182-187], and attachment of O_2^{2-} is central to the functioning of hemoglobin [188], For actinide complexes, the autoxidation of $[UO_2]^{+}$ to form $[UO_2]^{2+}$ and peroxide [189] was speculated to proceed via a superoxo complex $[(UO_2)^{2+}(O_2)^{-}]$ in which uranium was formally oxidized to U(VI). With a single electron in its valence orbitals and an accessible higher metal oxidation state, $[UO_2]^{+}$ satisfies requirements for formation of a superoxo complex [19]. However, the chemistry of the U(V) dioxo cation is difficult to study in solution because of its tendency to undergo disproportionation [6, 85,190-192] reactions in which two U(V) species react to form U(IV) and U(VI) species, with $[UO_2]^{+}$ functioning as both an electron donor and an electron acceptor.

In this chapter, experiments are described that show that complexes containing the U(V) cation $[UO_2]^{+}$ will add molecular oxygen in the gas phase. In this study, the reactive motif of the U(V) species $[UO_2]^{+}$ is shown to be primarily that of a Lewis acid accepting electron density from donor ligands and forming noncovalent

complexes in the process. However, it is shown that some ligand complexes of $[UO_2]^+$ will also add molecular dioxygen, suggesting donation of electron density from the metal center.

EXPERIMENTAL SECTION

The gas-phase reactivity experiments were conducted using two different types of quadrupole ion trap mass spectrometers, one using particle desorption for ionization (secondary ion mass spectrometry) and one using electrospray. The two instrumental approaches provided corroborating information.

Ion Trap Secondary Ion Mass Spectrometry (IT-SIMS).

The ion trap secondary ion mass spectrometer (a Saturn 2000 ITMS from Varian (Walnut Creek, CA), modified using software written in-house) [194-196] is a unique instrument for examining the reactivity of metal oxide species. Briefly, it functions by bombarding solid metal oxide targets with a 7 keV ReO_4^- primary ion (obtained by applying a current of around 3 A to an amalgam of barium peroxide and rhenium powder), [197,199] which sputters ionic oxide species into the gas phase. In our experiments, the primary beam was gated to impact only the sample for the given ionization time. Ionization times were varied from 0.001 to 0.01 s to achieve high

signal-to-noise ratios and comparable abundance (2000-4000 counts s^{-1}) for each of the reactant ions examined. The sputtered ions were trapped in a He bath gas (1 x 10^{-4} Torr), and the ion of interest was isolated using selected ion storage [199] prior to reaction with gaseous neutrals. The secondary ions used in this experiment were all generated by bombardment of uranium (VI) oxide (Strem Chemicals, Newburyport, MA) [98]. The sample was mounted on the end of a 2.7 mm probe tip with double-sided tape (3M, St. Paul, MN). Isolated ions were then allowed to react with gaseous H_2O, acetone, and/or O_2 during a specified reaction time (0-3 s) that was systematically controlled. The ion trap was operated at a low mass cutoff of *m*/*z* 160 during the ionization and reaction time periods. After reaction, the product ions and remaining reactants were scanned out of the trap [199] and deflected onto a venetian blind dynode positioned in front of the multichannel plate detector, located off-axis between the end of the ion trap and the primary ion gun [194].

To determine the reaction pathways and kinetics, the time between ion isolation and detection was systematically increased. Spectra were recorded at logarithmically increasing time intervals (approximately two measurements per decade) in order to concentrate data collection early in the ligand addition cascades, where the chemistry was rapidly changing. At long reaction times, spectra were not collected at closely spaced time intervals because the chemistry was not changing

rapidly, and more importantly, the UO_3 target tended to develop surface charge under prolonged bombardment, which put a premium on data collection efficiency. At any given point in time, total ion abundance was normalized to 1000 ions, which was a convenient number for use in the kinetic modeling (vide infra).

As an alternative to condensation reactions, isolated complexes were subjected to collision-induced dissociation (CID) [199]. Ions stabilized in the quadrupole ion trap have a coherent oscillating ion motion in the ion trap and a random component derived from the thermal energy of the system. Dissociation results from hyperthermal collisions with the bath gas that are induced by application of a potential on the end caps at a frequency corresponding to the secular frequency of the motion of the ion. Dissociation of metal complexes containing two or more different ligands produces fragment ions corresponding to the elimination of the ligands, whose relative intensities can be correlated with metal cation affinities [200-202]. Interpretation of the results of these studies is tempered by uncertainty regarding the effective temperature of the dissociating ions, the possibility of reverse activation energy, and the fact that ΔS may not be negligible; [203] however, in instances where the mechanism for elimination of two ligands is similar, [204] the fragmentation kinetics as reflected by the relative abundances of the fragment ions can be suggestive of the relative binding energies of the eliminated ligands.

The atmosphere within the ion trap secondary ion mass spectrometer was modified by the addition of low partial pressures of acetone, H_2O, and O_2 to the He bath gas. Acetone (Optima grade, Fisher, Fairlawn, NJ) was first dried with molecular sieves, which were previously heated to ~175 °C and allowed to cool, to remove any dissolved water. The acetone was then subjected to several freeze-pump-thaw cycles with liquid nitrogen while connected to a roughing vacuum pump. The acetone was then admitted to the system as a vapor through a variable leak valve. Oxygen (UHP, Matheson, Newark, CA) and $^{18}O_2$ (99% enrichment, Isotec-Matheson, Miamisburg, OH) were admitted using a separate variable-leak valve. A third variable-leak valve was used to admit water (Optima grade, Fisher, Fairlawn, NJ), which was also subjected to three freeze-pump-thaw cycles with liquid nitrogen while under vacuum.

Calculation of reaction rate constants is critically dependent on accurate determination of the number density of the reactant neutrals. Pressure measurement was accomplished using a small electron ionization quadrupole mass spectrometer (Transpector 2 residual gas analyzer, Inficon, East Syracuse, NY) that was interfaced to the ion trap secondary ion mass spectrometer and was operated to continuously monitor ion channels corresponding to the components of the vacuum atmosphere, viz., He, H_2O, N_2, O_2, and acetone. The quadrupole mass spectrometer was carefully calibrated versus a Bayard Alpert ionization gauge. The ionization gauge was, in turn,

calibrated against a capacitance manometer for each gas except He, which was maintained at a pressure of 1 x 10^{-4} Torr as measured by the quadrupole mass spectrometer and checked with the ionization gauge.

Electrospray Ionization Mass Spectrometry (ESI-MS).

ESI mass spectra were collected using a Finnigan LCQ-Deca ion trap mass spectrometer (ThermoFinnigan Corp., San Jose, CA). The spray solutions used in these experiments consisted of the uranyl nitrate dissolved to a concentration of 1 mM in 10% (v:v) acetone/water. The solutions were infused into the ESI-MS instrument using the incorporated syringe pump at a flow rate of 3-5 μL/min. The atmospheric pressure ionization stack settings for the LCQinstrument (lens voltages, quadrupole, octapole voltage offsets, etc.) were optimized for maximum ion transmission to the ion trap mass analyzer by using the autotune routine within the LCQ Tune program. The heated capillary (desolvation) temperature was maintained at 250 °C. At this relatively high desolvation temperature, the ESI mass spectrum was dominated by singly charged species including bare and ligated $[UO_2(OH)]^+$, $[UO_2(NO_3)]^+$, and $[UO_2]^+$. The ion trap analyzer was operated at a pressure of ~1.5 x 10^{-5} Torr. Helium gas, admitted directly into the ion trap, was used as the bath/buffer gas to improve trapping efficiency and as the collision gas for CID experiments. To

investigate the tendency to add molecular O_2 via gas-phase reactions, a certified blend of He with 0.1 or 1.0% O_2 (Linweld, Wichita, KS) was used.

Ligand addition reactions (H_2O and/or O_2) were monitored by the isolation and storage of the UO_2^+ ion in the ion trap. The O_2 reagent was introduced with the He bath gas. The H_2O is a contaminant in the vacuum system and has been shown in past studies to be present at partial pressures sufficient to produce pseudo-first-order reaction conditions. In the present experiments, H_2O added to UO_2^+ in the electrospray ion trap. At the acetone concentration used in the spray solvent mixture, no appreciable acetone addition to UO_2^+ complexes was observed. The multiple-stage CID experiments [26] were performed by setting the isolation width between 5 and 12 mass units (depending on the species), the activation *Q* at 0.3 (as labeled by the instrument manufacturer, used to adjust the *qz* value for the resonant excitation of the precursor ion during the CID portion of the experiment), and the activation amplitude at 10-20% (of 5 V). In all cases, activation times for CID were 30 ms.

Kinetic Modeling.

Kinetic rates were extracted from the data by using the curve fit feature of Berkeley Madonna [205], which is a commercially available, general purpose

differential equation solver that utilizes a numerical Runge-Kutta integration algorithm. This program uses the downhill simplex method as documented in *Numerical Methods in C* for curve fitting [206], The model used for this fit was based on a pseudo-first-order approximation of the reactions with respect to the acetone, oxygen, and water concentrations. Rate constants were obtained by dividing the rates from Berkeley Madonna by the number density of the secondary reactant (e.g., acetone). The ability of the model to fit the data was assessed for each ion modeled by calculating the root-mean-square error (RMS) between the data and the model for each time at which a data point was collected and expressing the value as a percentage of the average ion abundance over the time course of the experiment. Good fits were indicated by %RMS values from 1% to ~30%, which was the case for the abundant ions in the forward ligand attachment cascades. Lower abundance ions could have values several times higher, but they still produced fits for models of simple ligand addition and elimination that were good qualitative fits of the data points.

Infrared Multiphoton Dissociation (IRMPD).

An IRMPD experiment on the $[UO_2(\text{dimethylformamide})n)_{n=2,3}(O_2)]^+$ complex was conducted using a free electron laser interfaced to a Fourier transform ion cyclotron

resonance mass spectrometer at the FOM Instituut voor Plasmafysica, Nieuwegein, The Netherlands. The experiment was described previously. [207,208] Complexes were formed using electrospray as described above, except using dimethylformamide instead of acetone. Complexes were isolated using the stored waveform inverse Fourier transform technique [209] and then dissociated by photoirradiation of the isolated complex ions.

Results and Discussion

Reactions of the U(V) Species $[UO_2]^+$.

The U(V) species $[UO_2]^+$ accounted for the most abundant ion in the SIMS spectrum of UO_3 at *m*/*z* 270. The major ions that emerged upon reaction of $[UO_2]^+$ in an atmosphere containing acetone (A), H_2O, and O_2 were as follows. After 0.06 s, a substantial fraction of $[UO_2]^+$ was converted to $[UO_2(A)]^+$ (Figure 10.1 (a)), and some of this had further reacted to form diligated $[UO_2(A)(H_2O)]^+$ and $[UO_2(A)_2]^+$ (Schemes 10.1 and 10.1S (Supporting Information)). After 0.3 s, abundant triligated complexes having compositions $[UO_2(A)_2(H_2O)]^+$ and $[UO_2(A)_3]^+$ formed, and some of thesewere converted to the tetraligated $[UO_2(A)_4]^+$ (Figure 10.1 b). The $[UO_2(A)_4]^+$ represented the end of the ligand addition cascade, involving only acetone and H_2O. In contrast to the behavior of ligated $[UO_2]^{2+}$ in the gas phase, [155] pentaligated $[UO_2]^+$ complexes

were not formed at the longest times experimentally accessible.

Scheme 10.1S. Main Reaction Pathways for the Addition of Acetone, H_2O, and/or O_2 to $[UO_2]^+$, Occurring in the Ion Trap Secondary Ion Mass Spectrometera[a]

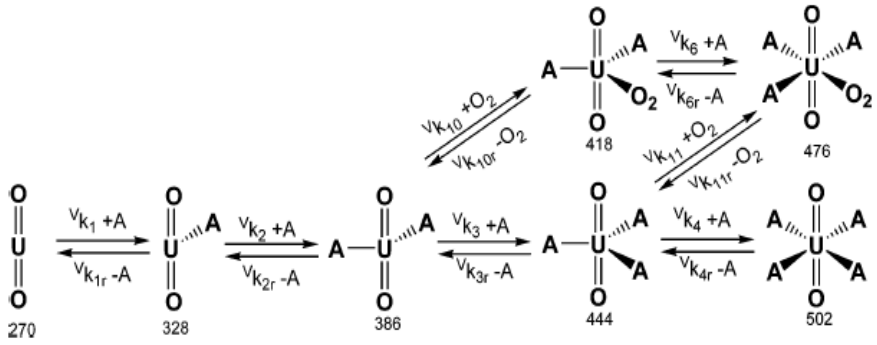

[a] The complete reaction scheme, which includes lower abundance ions, is found in the Supporting Information, Scheme 10.1S.

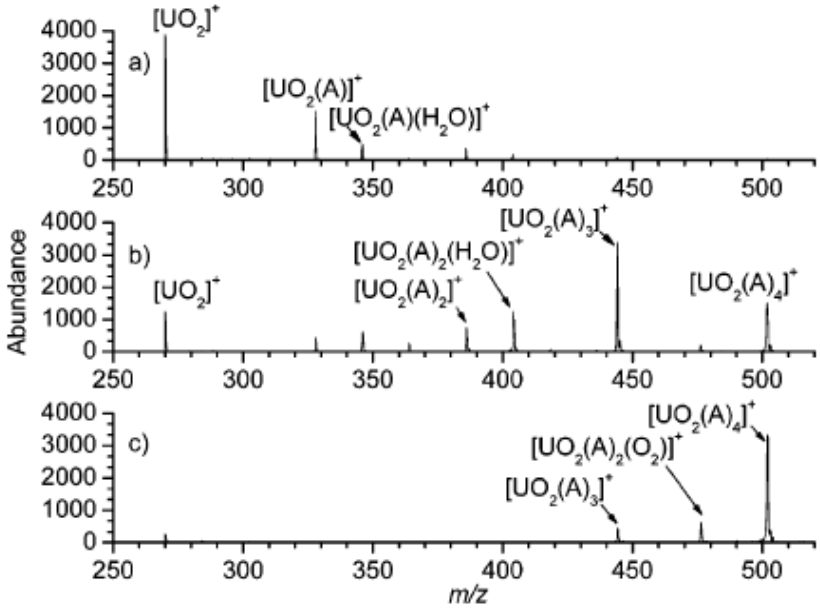

Figure 10.1. $[UO_2]^+$ formed and isolated in the vacuum atmosphere of the ion trap secondary ion mass spectrometer. Water and dioxygen were present at background concentrations (~5 x 10^{-7} Torr), and acetone was added to a pressure of ~1 x 10^{-6} Torr. The $[UO_2]^+$ reacted for (a) 0.06, (b) 0.3, and (c) 3 s.

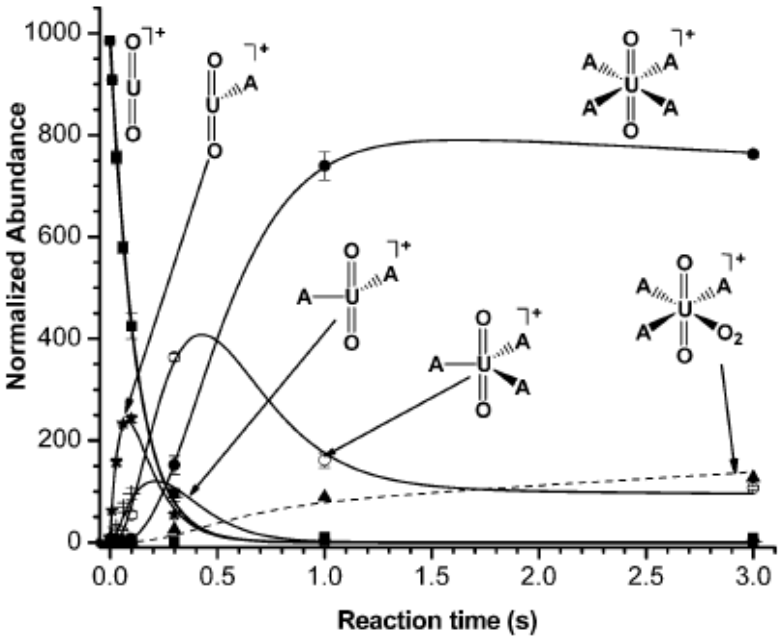

Figure 10.2. Kinetic profile for the major reactions formed from $[UO_2]^+$ in an atmosphere containing acetone, H_2O, and dioxygen. Data points represent the average of three runs. Lines represent the plot of the kinetic model for each of the ions.

Table 1. Forward Rate Constant Values for Addition of Acetone to $[UO_2]^+$ [a]

forward reaction	rate const, $^{V}k_n$	mean $^{V}k_n$ values	% efficiency (relative to k_{ADO})
$[UO_2]^+ + A \rightarrow [UO_2(A)]^+$	$^{V}k_1$	2×10^{-10}	10
$[UO_2(A)]^+ + A \rightarrow [UO_2(A)_2]^+$	$^{V}k_2$	2×10^{-10}	10
$[UO_2(A)_3]^+ + A \rightarrow [UO_2(A)_3]^+$	$^{V}k_3$	5×10^{-10}	20
$[UO_2(A)_3]^+ + A \rightarrow [UO_2(A)_4]^+$	$^{V}k_4$	9×10^{-11}	4
$[UO_2(A)_2]^+ + O_2 \rightarrow [UO_2(A)_2(O_2)]^+$	$^{V}k_{10}$	2×10^{-11}	3
$[UO_2(A)_3]^+ + O_2 \rightarrow [UO_2(A)_3(O_2)]^+$	$^{V}k_{11}$	1×10^{-11}	3

Table 10.1. The rate constant (*k*) values are in $cm^3\ s^{-1}$ $molecule^{-1}$. Table S10.1 in the Supporting Information contains rates calculated for all modeled addition reactions, and Table S10.2 contains rates for elimination reactions.

Most important to the present study, an ion was observed at *m*/*z* 476. This species corresponds to the addition of O_2 to the $[UO_2(A)_3]^+$ complex. At the longest

times of these experiments, all of the ion abundance was contained in $[UO_2(A)_4]^+$ and $[UO_2^-(A)_3(O_2)]^+$ (Figure 10.1 (c)). The temporal variations of the ions observed in this experiment enabled the reaction pathway in Schemes 10.1 and 10.1 S to be deduced, and thus allowed the development of a kinetic model that produced reaction profiles in good agreement with the measured data (Figure 10.2). The model was developed using ligand association and dissociation reactions that were assumed to be bimolecular and unimolecular, respectively. This is a simplified description of the actual physical system, in which the reactions are ternary [210,211] in the reactant ion, the neutral ligand, and the He bath gas; the latter reduces internal energy in the initially formed complexes, and hence the rate of dissociation reactions. Ligand exchange reactions between complexes were not considered because of low ion concentrations in the instrument.

In this experiment, the dominant reaction pathway was addition of acetone, reflected by the substantial reaction efficiencies (compared with average dipole orientation theory [49,212,213]) of reactions 1-3 (Tables 10.1 and S10.1). The efficiency for the addition of the fourth acetone was somewhat lower, which may be the effect of ligands shielding the reactive center for many approach trajectories. In addition, steric crowding of the $[UO_2^-(A)_4]^+$ appears to lead to greater complex instability, as reflected in the modeled rate constants for acetone elimination (Table

10.1 S2). The tetraligated complex had the largest rate constant for acetone elimination, and the observed trend was $[UO_2(A)_4]^+$ > $[UO_2(A)]^+$ > $[UO_2(A)_3]^+$ > $[UO_2(A)_2]^+$. Even with the elimination reactions, the overall addition of acetone in the gas phase was efficient, an observation that is consistent with the fact that the ligand is a strong *ó*-donor in the gas phase [131,150]. The efficiency observed contrasts with solution-phase behavior, in which acetone is a weakly binding ligand [148,149,190]. The preference of $[UO_2]^+$ cations for acetone observed in the present study was also consistent with a recent investigation of gas phase $[UO_2]^{2+}$ complexes [155] and with the high coordination energy of uranyl acetone complexes recently calculated by Marsden and co-workers. [137]

Side reactions with gaseous H_2O were also observed. The efficiency of H_2O addition was higher for the monoacetone ligated $[UO_2]^+$ species (reactions 10.7 and 10.9 in Scheme 10.1S) than for the diacetone complex (reaction 10.8). The temporal behavior of the lower abundance H_2O-containing complexes is provided in Figure 10.1 S1. For unligated $[UO_2]^+$, $[UO_2(A)_3]^+$, or $[UO_2(A)_4]^+$, addition of water did not occur to a measurable extent. The fact that H_2O did not add to $[UO_2]^+$ was somewhat surprising because this reaction occurs in the absence of acetone, [30] although relatively inefficient (ca. 3%) and with a fast back reaction. Addition of H_2O to the $[UO_2]^+$ di-, tri-, and tetraligated with acetone can be viewed similarly (i.e., occurring

with poor efficiency and/or fast reverse reactions). On the other hand, addition of H_2O to $[UO_2(A)]^+$ was remarkably efficient, which is reflected in the notable abundance of $[UO_2(A)(H_2O)]^+$ in Figure 10.1 (a). The $[UO_2(A)(H_2O)]^+$ species was not quickly stabilized, having a relatively large rate constant for elimination of H_2O. Also observed were the addition of a second H_2O or acetone ligand to form $[UO_2(A)(H_2O)_2]^+$ and $[UO_2(A)_2(H_2O)]^+$ at intermediate times. The fact that $[UO_2(A)(H_2O)]^+$ was formed in abundance likely reflects a fortuitous combination of a highly undercoordinated uranium cation with sufficient oscillators in the first acetone ligand enabling stabilization of the complex. Addition of H_2O to complexes containing more than one acetone may not occur because additional electron density contributed by the multiple acetone ligands lessens the ability of the weaker H_2O ligand to form stable bonds with uranium.

At the longest reaction times, no H_2O-containing complexes remained; the rate constant for elimination of H_2O from $[UO_2^-(A)_2(H_2O)]^+$ was about 50 times greater than that for the elimination of acetone (Table 10.1 S2), which is another indication of the much stronger binding of acetone in these systems. The net result of the more weakly bound H_2O-containing complexes with continued substitution by more strongly binding acetone is that eventually no H_2O complexes survive in the ion trap.

The most interesting observation, however, was the tendency of di- and

triligated $[UO_2]^+$ to add O_2 (Scheme 10.1, reactions 10.10 and 10.11). The addition was plainly observed at *m*/*z* 476, corresponding to $[UO_2(A)_3(O_2)]^+$ (Figure 10.1 (c)), and showed up at longer reaction times when most of the ion population had been converted to either tri- or tetraligated species. The $[UO_2^-(A)_3(O_2)]^+$ showed no tendency to add an additional ligand, suggesting that the coordination sites were fully occupied and that the precursor was $[UO_2(A)_3]^+$. The identification of the dioxygen adduct was confirmed in two ways: first, addition of O_2 to the ion trap secondary ion mass spectrometer resulted in production of a higher fraction of $[UO_2(A)_3(O_2)]^+$ compared with the other terminal product $[UO_2(A)_4]^+$, and second, addition of $^{18}O_2$ to the ion trap shifted the mass of the product to *m*/*z* 480, consistent with the proposed composition.

Subsequent experiments that utilized the electrospray ion trap (vide infra) indicated that diligated $[UO_2]^+$ also reacted with O_2 to form stable complexes, and this prompted a more thorough examination of the IT-SIMS results. A low-abundance ion formed at *m*/*z* 418 corresponded to $[UO_2(A)_2(O_2)]^+$ formed from $[UO_2(A)_2]^+$. Thus, both diacetone and triacetone $[UO_2]^+$ complexes reacted with O_2 to form stable adducts. In contrast, there was nothing in the mass spectra at any time frame to indicate addition of O_2 to tetra-, mono-, or unligated $[UO_2]^+$.

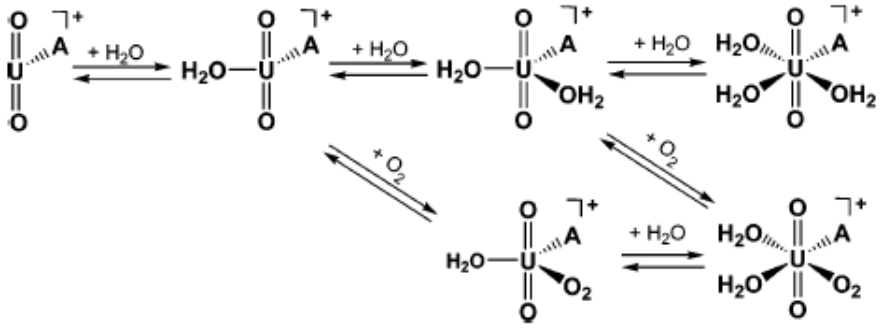

Scheme 10.2 S. Reaction Pathways for the Addition of H_2O and/or O_2 to $[UO_2A]^+$, Occurring in the ESI Ion Trap

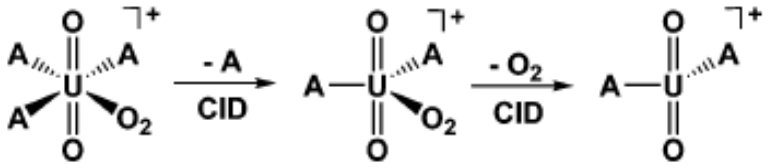

Scheme 10.3 S. Serial Collision-Induced Dissociation Reactions of theU(V) Species $[UO_2(A)_3(O_2)]^+$, Suggesting Alternating Ligand Binding Depending on the Extent of Ligation

These conclusions were substantiated by the reactions observed in the ESI ion trap experiments. The $[UO_2(A)]^+$ species was generated as a stable species by ESI using the relatively high capillary/desolvation temperature of 250 ℃. With the conditions employed in the ESI experiments, the predominant neutral reagents present in the ion trap were adventitious H_2O and O_2 that were admitted with the He bath gas. In this environment, $[UO_2(A)]^+$ added one H_2O to form $[UO_2(A)^-(H_2O)]^+$ (Scheme 10.2 S), but $[UO_2(A)]^+$ did not add O_2.

The diligated adduct then added O_2 to generate $[UO_2(A)^-(H_2O)(O_2)]^+$, and it also added a second H_2O to form $[UO_2^-(A)(H_2O)_2]^+$. At longer reaction times, $[UO_2(A)(H_2O)_2(O_2)]^+$ was also formed: an analysis of the kinetic evolution of the ion abundances showed that this ion was formed both from addition of O_2 to $[UO_2(A)(H_2O)_2]^+$ and from addition of H_2O to $[UO_2(A)(H_2O)(O_2)]^+$. The tetraligated $[UO_2(A)(H_2O)_3]^+$ was also formed in this experiment but showed no tendency to further react by adding O_2. Ligand binding was assessed by fragmenting the dioxygen complexes: [200-202] $[UO_2(A)_3(O_2)]^+$ was subjected to CID by applying an axial excitation frequency to the ions, which increased the average kinetic energy of the collisions of the complexes with the He bath gas [199]. This resulted in preferential elimination of acetone (Scheme 10.3), and subsequent CID of the $[UO_2(A)_2(O_2)]^+$ produced the opposite result, viz., O_2 was lost instead of acetone (i.e., no $[UO_2(A)(O_2)]^+$ was detected, indicating that it was at least 200 times less intense than the ion from O_2 loss). These results suggest that the binding energy of O_2 is intermediate between those of the second and third acetone ligands.

Conclusions on relative binding energy based on competitive fragmentation reactions must be considered with caution, because of uncertainty arising from the possibility of reverse activation energy, unequal reaction entropy changes, and variation in dissociation rates with variable kinetic energy. In the present case,

reverse activation energies are negligible, but variable entropy changes on elimination of acetone versus O_2 may alter conclusions on relative ligand binding strength in the $[UO_2(A)_2(O_2)]^+$ complex. If the entropy change for elimination of acetone is equivalent to that for elimination of O_2, then the fact that only O_2 elimination is observed would indicate that it is less tightly bound than acetone. However, the entropy increase on loss of acetone could conceivably be smaller, because C-O rotation may decrease upon elimination: if the C-O bond in the complex

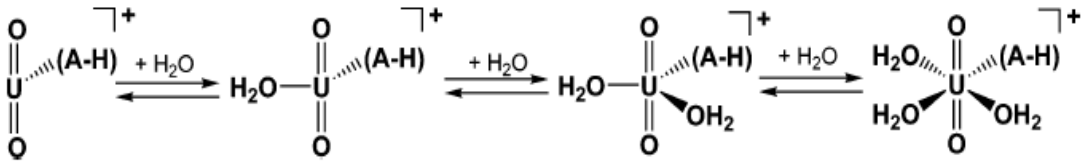

Scheme 10.4 S. Serial Addition of H_2O to the U(VI) Species $[UO_2((A\text{-}H)]^+$, Occurring in the ESI Ion Trap, Where (A-H) Is Deprotonated Acetone.

is predominantly a single bond, re-formation of the carbonyl double bond upon elimination would reduce rotation and cause a smaller increase in entropy for the overall process. A smaller entropy change for loss of acetone would add to the energetic requirements for elimination of acetone compared to loss of O_2, and in the extreme case, this could result in loss of O_2, even though the bond energy of acetone is less than that of O_2. However, recent infrared experiments have shown that the

double-bond character of the acetone carbonyl is not seriously compromised in triligated uranyl complexes (vide infra); [214] thus, it is unlikely that entropic considerations will change the order of ligand binding suggested by the CID experiments in this system. The conclusion is further substantiated by analogous CID behavior observed in the ESI ion trap for $[UO_2(A)(H_2O)_2(O_2)]^+$, which eliminated H_2O in the first fragmentation stage and then O_2 in the second; in this system, elimination of H_2O would lead to a lower net entropy change than would elimination of acetone.

Variable fragmentation with respect to kinetic energy is a second source of uncertainty. However, changes in the ratio of product ion abundances arising from competitive simple ligand cleavages were not observed over the energies available in the quadrupole ion trap. The order of ligand elimination was further evaluated by infrared multiphoton dissociation [207,208] of $[UO_2^-(ligand)_3(O_2)]^+$, where the ligand was the carbonyl species dimethylformamide. In the IRMPD experiment, the dominant reaction observed for $[UO_2(amide)_3(O_2)]^+$ was loss of a single amide. While loss of (amide + O_2) was also observed as a minor pathway, *no* loss of only O_2 was observed [214]. In contrast, the IRMPD behavior of $[UO_2(amide)_2(O_2)]^+$ showed elimination of only O_2, which indicated that, in the more undercoordinated complex, the O_2 ligand was less strongly bound than the amide ligands. The IRMPD experiments were consistent with the CID studies of the UO_2^+ complexes containing

acetone or H_2O and bound molecular O_2, suggesting that the strength of O_2 binding is intermediate between those of the second and third carbonyl ligands.

Taken together, the condensation and fragmentation experiments show that the ligand field plays a controlling role in dictating whether O_2 binding will occur, as does the presence of an unpaired electron in the valence orbital of the metal. The importance of the U(V) oxidation state in O_2 binding was highlighted by the reactivity of U(VI) and U(IV) dioxo cations, which did not bind dioxygen in a molecular fashion.

Reactions of the U(VI) Species $[UO_2OH]^+$ and $[UO_2(AH)]^+$.

Complexes containing uranium in the VI oxidation state nominally have no electrons in the valence orbitals to react with dioxygen, and they hence were not expected to form stable O_2^- containing complexes. Nevertheless, the experience with the U(V) system indicated the possibility of ligands altering the reactivity of the metal center, which prompted investigation of reactions of uranyl complexes in oxygen-containing atmospheres. Addition of O_2 to uranyl systems was not observed to occur, and this was most vividly illustrated by examining the reactions of the U(VI) complex $[UO_2(A\text{-}H)]^+$ (where (A-H) is deprotonated acetone), which was formed in the ESI ion trap experiment by CID.

Analysis of a uranyl/acetone/water solution showed a tetraligated complex

$[UO_2(A\text{-}H)(A)_3]^+$ at *m*/*z* 501 that was converted to $[UO_2(A\text{-}H)]^+$ by consecutive CID eliminations of three acetone ligands. The trapped product ion then reacted with three water ligands in serial fashion, forming $[UO_2(A\text{-}H)^-(H_2O)_{n=1\text{-}3}]^+$ (Scheme 10.4S). This result, and those for the hydroxyl uranyl species, underscores the importance of the unpaired electron in the U(V) species for fostering O_2 addition: in thepresent even-electron case, the ligand in $[UO_2(A\text{-}H)]^+$ is isoelectronic with the ligand in the U(V) species $[UO_2(A)]^+$ described above, the only difference being the presence of a proton in the latter. The consequence of the "missing" proton in the U(VI) complex is large, however, since it results in a negative charge on the ligand with no electron localized in the uranium valence orbitals: this eliminates the possibility of forming a stable complex with dioxygen.

The reactions of the analogous hydroxy uranyl cation reinforced this conclusion [106]. The production of $[UO_2OH]^+$ at *m*/*z* 287 (Figure 10.3 (a)) in the ion trap secondary ion mass spectrometer afforded the opportunity to examine the behavior of a second U(VI) species reacting competitively with acetone, water, and dioxygen. The principal conclusion from the experiment was that the hydroxyuranyl cation failed to add O_2 at any point, regardless of the nature or extent of ligation. At all reaction times, the chemistry was dominated by addition of acetone ligands, which occurred for $[UO_2OH]^+$ to the exclusion of H_2O; this was surprising since water was

shown to add, albeit at a slow rate, in a previous study [98]. At intermediate reaction times, $[UO_2OH]^+$ complexes containing two acetone ligands were formed (Figure 10.3 (b)), and at the longest times, $[UO_2OH(A)_3]^+$ was produced (Figure 10.3 (c)). The temporal profiles of the abundances of these ions (Figure 10.4) indicated the reaction pathway described in Scheme 10.5 S, reactions 10.1-10.3.

Reaction efficiencies for the acetone additions to the hydroxide complexes were 10-20% (Tables 10.2 and 10.4 S). Addition of a fourth acetone, generating an ion with five equatorial ligands, was not observed at any point. The rate constants calculated for elimination of acetone ligands from the complexes (Table 10.5) reveal a trend $[UO_2OH(A)_3]^+ \sim [UO_2OH(A)]^+ > [UO_2\text{-}OH(A)_2]^+$. With more than four equatorial ligands, the rate for acetone elimination is presumably even faster, as the hydroxyl complex with five equatorial ligands is not observed at all.

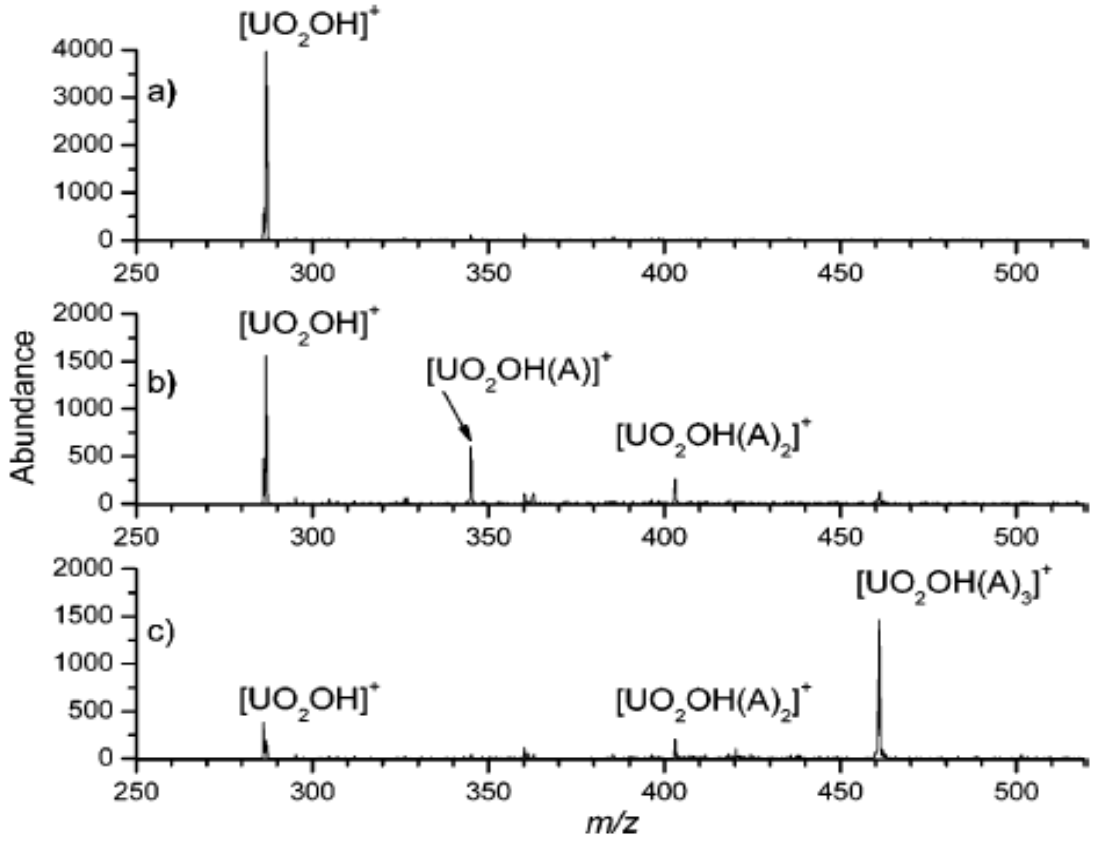

Figure 10.3. $[UO_2OH]^+$ formed and isolated in the vacuum atmosphere of the ion trap secondary ion mass spectrometer. Water and dioxygen were present at background concentrations (~5 x 10^{-7}Torr), and acetone was added to a pressure of ~1 x 10^{-6} Torr. $[UO_2]^+$ reacted for 0.01 (top), 0.3 (center), and 1 s (bottom).

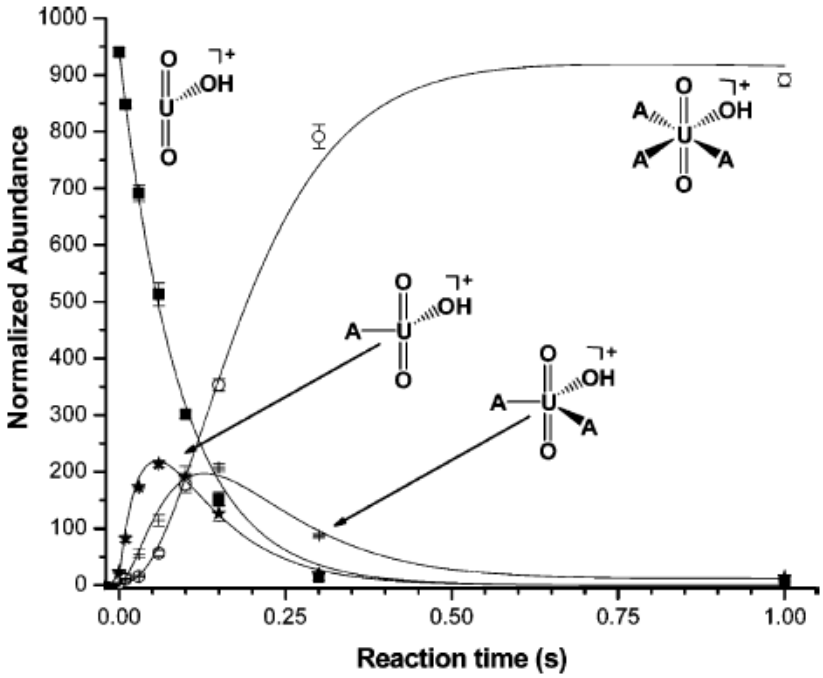

Figure 10.4. Kinetic profiles of the major ions formed from $[UO_2OH]^+$ in an atmosphere containing acetone, H_2O, and dioxygen. Abundances normalized to 1000 ions total (see Scheme 10.3S) are plotted versus time. Data points represent the average of three runs; error bars represent (1 standard deviation. Lines represent the plot of the kinetic model for each of the ions, generated using the mean data values. See Figure 10.2 for the kinetic profiles of the lower abundance ions.

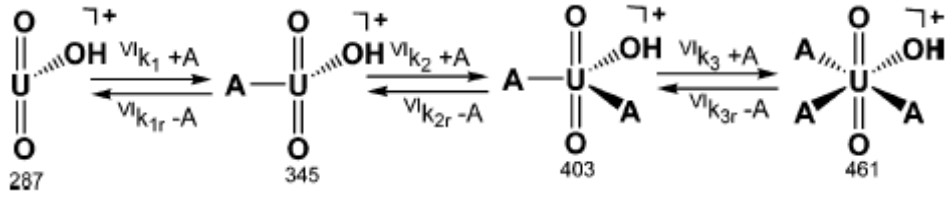

Scheme 10.5 S. Reaction Pathways for the Addition of Acetone and/or H_2O to $[UO_2OH]^+$, Occurring in the Ion Trap Secondary Ion Mass Spectrometer[a]

[a] The full scheme is found in the Supporting Information, Scheme 10.5 S.

During the course of the acetone addition reactions, side reactions (Scheme 10.5 S) produced low-abundance ions from the addition of H_2O to $[UO_2OH(A)]^+$ and $[UO_2OH(A)_2]^+$, but at no point did the abundance of these ions reach more than a few percent of the total ion population, and at the longest reaction times, they were not observed. The kinetic profile modeled for the low-abundance ions (Figure 10.2) produced good agreement with the data for all ions, except for low-abundance ion $[UO_2\text{-}OH(A)(H_2O)]^+$, which formed and disappeared at a rate that was faster than could be reasonably modeled: the addition of H_2O to $[UO_2OH(A)]^+$ was modeled at a rate faster than the maximum indicated by the collision constant, which suggested that there may be additional reactions forming $[UO_2OH(A)^-(H_2O)]^+$. At the longest reaction times, no H_2O-containing complexes were present in the spectra, suggesting that (as for the U(V) complexes described above) the water-containing complexes slowly eliminate H_2O, forming species that continued to react with acetone. This implies that the H_2O-containing complexes are less stable than those containing only acetone, and the rate constants produced by the kinetic model were 2 orders of magnitude higher for elimination of H_2O than for elimination of acetone for complexes having the same extent of ligation (elimination rate constants are provided in the Supporting Information, Table 10.5).

A second set of low-abundance ions were observed at *m*/*z* 327, 385, 443, and 501 (Scheme 10.5 S), corresponding to $[UO_2^-(A^-H)(A)_{n=0-3}]^+$. The (A-H) represents deprotonated acetone (the enolate), and a reasonable suggestion for its initial formation would be H transfer from an acetone to the hydroxy ligand, forming a complex containing (A-H) and water. This complex was observed in ESI-MS experiments (see above) and can eliminate H_2O. The resulting enolate ion then undergoes addition of up to three additional acetone molecules. Rate constants for sequential addition of the acetone ligands to the enolate complexes were somewhat imprecise (Table S4), which reflected uncertainty in measurement of the low abundances of the enolate-bearing ions rather than reactivity trends; this limitation notwithstanding, the reaction pathway involving addition of acetone ligands to the $[UO_2(A\text{-}H)]^+$ complex is reasonable and accounts for the appearance of these ions at various times during the course of the ligand addition cascade.

These cascading ligand addition reactions showed that the uranyl-anion pair complexes were highly reactive, functioning as Lewis acids toward electron-donating ligands, but at no point was molecular addition of dioxygen observed, which was similar to the behavior of complexes of yet another dioxo uranium ion, $[UOOH]^+$.

Reactions of the U(IV) Species $[UOOH]^+$.

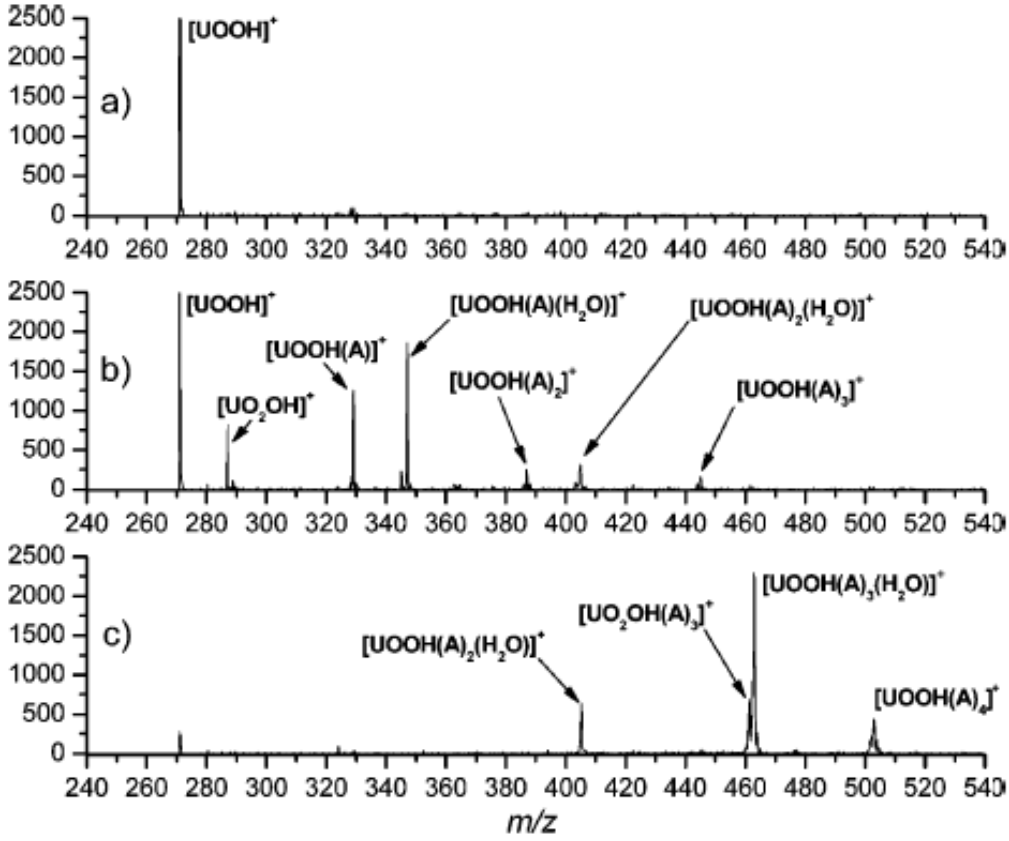

Figure 10.5. $[UOOH]^+$ formed and isolated in the vacuum atmosphere of the ion trap secondary ion mass spectrometer. Water and dioxygen were present at background concentrations (~5 x 10^{-7} Torr), and acetone was added to a pressure of ~1 x 10^{-6} Torr. $[UOOH]^+$ reacted for (a) 0. (b) 0.06, and (c) 1 s.

The reactions of $[UOOH]^+$ were studied by IT-SIMS, where the ion was made in sufficient abundance to enable reactivity investigations, but were not studied by ESI-MS because there was not a facile means for forming the U(IV) species using electrospray. The $[UOOH]^+$ is an intriguing cation because uranium is in the IV

oxidation state, with two electrons in the valence orbitals; thus, if occupation of these orbitals is solely responsible for reactivity with dioxygen, then there is a possibility that O_2 addition might also be observed in complexes of this ion.

The reactivity pattern for $[UOOH]^+$ (Figure 10.5) bore many similarities to that of $[UO_2]^+$, but with the following exceptions: (a) the $[UOOH]^+$ complexes did not add dioxygen, (b) complexes containing multiple H_2O ligands were not formed in abundance, and (c) a complex containing acetone and a H_2O ligand was the dominant product at the longest time scales accessible (the terminal addition product was primarily $[UOOH^-(A)_3(H_2O)]^+$, with lower abundance ions corresponding to $[UOOH(A)_4]^+$, $[UOOH(A)_2(H_2O)]^+$, and $[UO_2OH(A)_3]^+$ (Figure 10.5 (c)).

forward reaction	rate constant, ${}^{IV}k_n$	mean ${}^{IV}k_n$ value	% efficiency (relative to k_{ADO})
$[UOOH]^+ + A \rightarrow [UOOH(A)]^+$	${}^{IV}k_1$	5×10^{-10}	20
$[UOOH(A)]^+ + A \rightarrow [UOOH(A)_2]^+$	${}^{IV}k_2$	2×10^{-10}	10
$[UOOH(A)_2]^+ + A \rightarrow [UOOH(A)_3]^+$	${}^{IV}k_3$	6×10^{-10}	30
$[UOOH(A)_3]^+ + A \rightarrow [UOOH(A)_4]^+$	${}^{IV}k_4$	2×10^{-10}	10
$[UOOH(H_2O)]^+ + A \rightarrow [UOOH(A)(H_2O)]^+$	${}^{IV}k_5$	2×10^{-09}	100
$[UOOH(A)(H_2O)]^+ + A \rightarrow [UOOH(A)_2(H_2O)]^+$	${}^{IV}k_6$	3×10^{-10}	10
$[UOOH(A)_2(H_2O)]^+ + A \rightarrow [UOOH(A)_3(H_2O)]^+$	${}^{IV}k_7$	1×10^{-10}	5
$[UOOH]^+ + H_2O \rightarrow [UOOH(H_2O)]^+$	${}^{IV}k_8$	1×10^{-11}	30
$[UOOH(A)]^+ + H_2O \rightarrow [UOOH(A)(H_2O)]^+$	${}^{IV}k_9$	2×10^{-09}	100
$[UOOH(A)_2]^+ + H_2O \rightarrow [UOOH(A)_2(H_2O)]^+$	${}^{IV}k_{10}$	3×10^{-11}	1
$[UOOH(A)_3]^+ + H_2O \rightarrow [UOOH(A)_3(H_2O)]^+$	${}^{IV}k_{11}$	3×10^{-10}	10

Table 10.3 Forward Rate Constants and Efficiencies Modeled for the Reactions of $[UOOH]^+$ in a mixed acetone, water and dioxygen atmosphere

A careful examination of the temporal reaction profile showed initial production of the monoacetone complex $[UOOH(A)]^+$, $[UOOH(H_2O)]^+$ at lower abundance, and a minor amount of oxidation (vide infra). Once formed, $[UOOH(A)]^+$ displayed a dramatic preference for addition of H_2O (reaction 10.9, Scheme 10.6), this being preferred by a factor of 10 over addition of a second acetone ligand (reaction 2, and see reaction efficiencies in Tables 10.3 and 10.7S). Conversely, the H_2O adduct preferred to add acetone (reaction 5, Scheme 10.6), and there was no tendency to add a second H_2O. Both reactions 5 and 9 produce the mixedligand adduct $[UOOH(A)(H_2O)]^+$, which is the most abundant ion after about 0.1 s of reaction time. The very fast appearance of this ion and the relatively large RMS value (Table 10.9) for the temporal profile of the $[UOOH(H_2O)]^+$ suggest that there may be a third contributor to $[UOOH(A)(H_2O)]^+$. It is speculated that some fraction of the diacetone adduct $[UOOH(A)_2]^+$ may be converted to $[UOOH(A)(H_2O)]^+$ by hyperthermal collisions with H_2O, and in fact collision-induced substitution reactions have been evidenced by the products of CID of uranyl complexes [26]

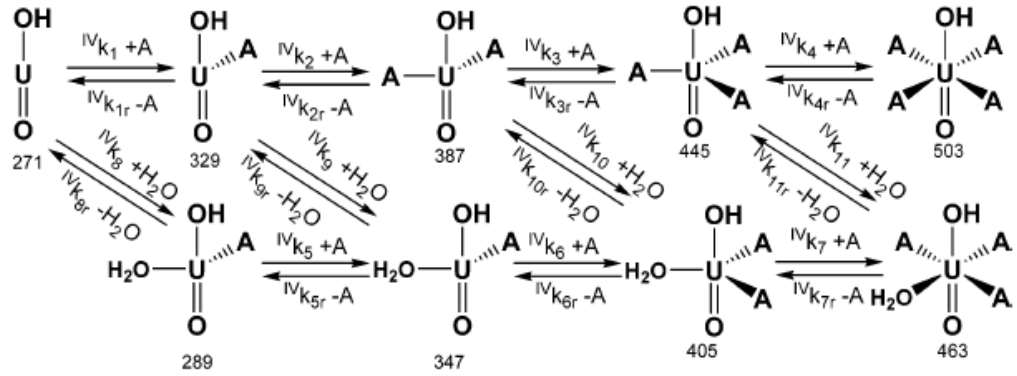

Scheme 10.6 S. Reaction Pathways for the Addition of Acetone and/or H_2O to $[UOOH]^{+a}$ [a]The full scheme, including low-abundance ions, is found in the Supporting Information, Scheme 10.6 S.

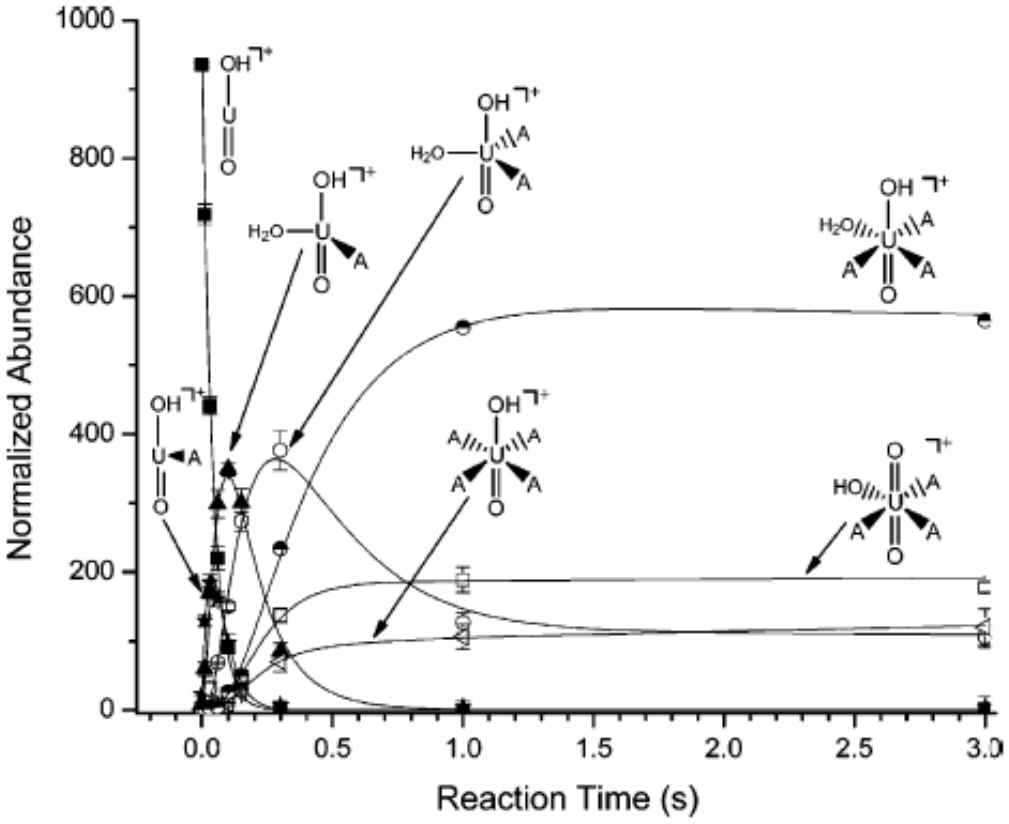

Figure 10.6. Kinetic profile for the major product ions produced from $[UOOH]^+$ in an atmosphere containing acetone, H_2O, and dioxygen. Data points represent the average of three runs. Lines represent the plot of the kinetic model for each of the ions. Low-abundance ion profiles are depicted in Figure 10.3.

Both $[UO(OH)(A)(H_2O)]^+$ and $[UOOH(A)_2]^+$ continue to add an additional ligand, as depicted in the kinetic profile (Figure 10.6) and by reactions 3, 6, and 10 (Scheme 10.6) and by reaction 12 (Scheme 10.6 S). An important observation is that, despite the rapid addition of the first H_2O ligand, additions of subsequent H_2O ligands are somewhat disfavored (reaction 10 is particularly inefficient), presumably because the presence of two valence electrons in the U(VI) system together with two donor ligands generates enough repulsive character at the U center that approach of a weak donor is discouraged. A second surprising observation is that, at the longest time frames investigated (to 3 s), a complex containing one H_2O ligand $[UOOH(A)_3(H_2O)]^+$ was still most abundant and did not appear to be converting to the all-acetone complex $[UOOH(A)_4]^+$. The rate constants for elimination of acetone and H_2O from $[UOOH(A)_3(H_2O)]^+$ are slow (Table 10.8), which suggests that this ion is relatively stable. However, it is not expected to be as stable as the all-acetone system, suggesting that, at very long ion lifetimes, the all-acetone complex should be formed from the complex containing a single H_2O.

The U(IV) species did not add molecular O_2 at any point during the ligand addition reactions, but it did undergo irreversible oxidation with O_2 to form $[UO_2OH]^+$, with an efficiency ($^{IV}k11$) that was in reasonable agreement with a previous measurement made using IT-SIMS [98]. The hydroxyuranyl cation proceeded to add

acetone as shown in Schemes 10.1 S and 10.3 S, with reactions occurring in parallel with the addition reactions of $[UOOH]^+$. An additional possibility for the appearance of the product $[UO_2OH(A)_n]^+$ cations is oxidation of acetone-ligated $[UOOH]^+$ precursors, as described by reactions 13-16 in Scheme 10.6 S. Additional electron density from the strongly donating acetone ligands may actually make these reactions more efficient. Modeling of the kinetic profiles of these ions did not support this hypothesis but did suggest that, while $[UOOH(A)_n]+$ oxidation was highly efficient for n) 0 and 2, complexes with one and three acetone ligands were largely unreactive. This result suggests that, as in the case of the dioxo U(V) complexes, the reactions of dioxo U(IV) complexes with dioxygen are very sensitive to alterations in the ligand field.

SUMMARY

The addition of O_2 to ligated $[UO_2]^+$ complexes is reminiscent of additions to transition metal complexes, [182,183,185,187] where the availability of an unpaired electron and a higher oxidation state fosters formation of metal-superoxide complexes. The fact that prior equatorial ligation is required points toward specific involvement of the unoccupied or partially occupied valence orbitals of the uranyl system, which are two δ_u and two Φ_u orbitals of 5f parentage [132,217] whose relative energy levels in ligated complexes are not known. Theoretical considerations would

suggest that addition of the first two σ-donor ligands would involve the two 5f Φu orbitals via an electrostatic interaction [132]. The resulting localization of the unpaired electron in a δ_u orbital may enable efficient overlap with the π^* orbital of dioxygen [182,185,218], enabling formation of a weak covalent bond. Evidence for electron transfer from the metal center to an acceptor ligand has been observed for U(III) complexes in situations where π-back-bonding is possible, [219-223] but it has not been previously observed for U(V) complexes. Transfer of one electron from the U(V) center to O_2 would result in an η^1 superoxo complex, in which O_2 is attached end-on to the metal. In transition metal and actinide chemistry, dioxygen binding resulting in η^2-bound peroxy complexes is also common, but this requires two unpaired electrons, which are not present in the ligated $[UO_2]^+$ molecule. The role of the two donor ligands may be two-fold, i.e., localizing the unpaired electron in an orbital conducive to electron transfer to the π^* orbitals of O_2, as mentioned above, and increasing the overall basicity of the metal center. This explanation for the reactivity of ligated $[UO_2]^+$ thus bears some similarity to that offered by Mehdoui et al. for U(III) complexes, where stronger σ-donating ligands fostered stronger π-back-bonding with π-acceptor ligands [224,225].

The candidate superoxo and peroxo structures would benefit from study using computational approaches, and in fact preliminary density functional theory

calculations in our laboratories have generated not only an η^1 superoxo structure but also an η^2 side-bound peroxo structure. The variable results highlight the fact that DFT calculations of actinide complexes are not simple on account of relativistic effects and spin-orbit coupling [226-228], and the present experimental measurements are in need of a determined computational investigation to provide a better understanding of the electronic configuration and reactivity of ligated forms of the $[UO_2]^+$ molecule and the structures of complexes resulting from their reactions.

CHAPTER 11

CONCLUSIONS AND FUTURE WORK

Uranium chemistry has been intensively studied in condensed phase in the past; however, due to the infinite variable presence in the solution phase the explicit investigation of the intrinsic behavior of uranium is confimed. Therefore, in order to improve the understanding of intrinsic uranium chemistry, particularly those exisit in the environment with higher oxidation states, we have been studying the species-dependent reactivity of a range of mono-positive uranyl-ligand cations using the combination of ESI and ITMS in the gas phase. Electrospray and ion-trap mass spectrometry allows isolation and storage of our uranyl-ligand ionized species with explicitly defined compositions, use a single or multiple collision-induced dissociation (CID) stages to determine chemical composition and structure, conduct energy-resolved CID experiments to assess relative ion stability and conduct time-resolved ion isolation experiments to probe gas-phase association reactions.

Our focus to date has been on the multiple-stage collision-induced dissociation (CID) of coordinated uranium dioxo cations, and on the intrinsic tendency to accept neutral ligands such as H_2O in the gas-phase. For example, multiple stage CID was used to characterize $[UO_2NO_3]^+$, $[UO_2OH]^+$ or $[UO_2OR]^+$ (R=-CH_3, -CH_2CH_3

and $-CH_2CH_2CH_3$) cations, coordinated by up to 3 coordinating solvent molecules, that were derived from solutions of uranyl nitrate dissolved in water or mixtures of water and alcohol. Highly coordinated species showed a tendency to eliminate intact coordinating water and alcohol ligands. In contrast, CID of $[UO_2(NO_3)(ROH)]^+$ eliminated nitric acid to furnish a ligated uranyl-alkoxide cation. For complexes with coordinating water molecules, the multiple-stage CID led to the generation of either $[UO_2OH]^+$ or $[UO_2NO_3]^+$.

ESI and multiple-stage CID have also been used to generate bare uranyl hydroxide, nitrate and acetate monocations for subsequent investigations of intrinsic hydration tendencies. The relative rates for the formation of the monohydrates $[(UO_2A)(H_2O)]^+$, with respect to A (where A=OH, NO_3 or CH_3COO), followed the trend: $CH_3COO > NO_3 >> OH$. The trend was rationalized in terms of the donation of electron density by the strongly basic OH to the uranyl metal center and the reduction of Lewis acidity of U, and the presence of increased degrees of freedom to accommodate excess energy from the hydration reaction in the case of CH_3COO and NO_3. The monohydrates also reacted with water, forming dihydrates and then trihydrates. The rates for formation of the nitrate and acetate dihydrates $[(UO_2A)(H_2O)_2]^+$ were very similar to the rates for formation of the monohydrates; the presence of the first H_2O ligand had no influence on the addition of the second. In

contrast, formation of the $[(UO_2OH)(H_2O)_2]^+$ was nearly three times faster than the formation of the monohydrate. In another study, we found that the uranyl-2-propoxide monocation, when coordinated by a singly 2-propanol molecule, mediated the conversion of the neutral alcohol to acetone, and the propoxide ligand to acetaldehyde during the multiple stage CID experiment.

Electrospray ionization and ion trap mass spectrometry was also used to investigate mono-positive gas-phase complexes of the general formula $[UO_2A(S)_n]^+$ where A=OH, Cl, Br. I or ClO_4, S=H_2O, CH_3OH or CH_3CH_2OH, and n=1-3. In this study we found for H2O-coordinated cations, the dissociation reactions observed included the elimination of H2O ligands and the loss of HA (where A = Cl, Br, and I). Only for the Br and ClO_4 versions did collision-induced dissociation of the hydrated species generate the bare, uranyl-anion complexes. CID of the chloride and iodide versions led instead to the production of the uranyl hydroxide and hyrated UO_2^+. Replacement of H_2O ligands by alcohol increased the tendency to eliminate HA, consistent with the higher intrinsic acidity of the alcohols compared to water and potentially stronger UO_2-O interactions within the alkoxide complexes compared to the hydroxide version.

In the study of gas-phase complexes containing uranyl ion and acetone we are able to investigate the singly and doubly charged species and its instrinic coordination

behavior. Another study with use of nitrile ligands allowed the production of a series of gas-phase ions with general formula $[UO_2(RCN)_n]^{2+}$ with n=2-5. For acetonitrile, the bare uranyl ion and a complex composed of the uranyl ion and a single nitrile ligand (i.e. $[UO_2(acn)_1]^{2+}$) were also produced. Generation by ESI of this group of gas-phase species allowed a direct investigation of the influence of the number and type of coordinating ligands on the intrinsic reactions of ligated uranyl ion with H_2O in the gas-phase environment of an ion trap mass spectrometer. Lastly we have look into the different reaction of uranium, which is the oxidation reaction. In this study we rise the amount of dioxygen entering the trap and separately investigate the instrinsic behavior of U(V) and U(VI) complexes. Through this study we found that with an unpaired electron in the U(V) complexes activate the system and draw dioxygen toward the cation, and their rates can be modeled. However there are still many factors such as bascity of various ligands which influence the rates of formation of these dioxygen adducts and it is a crucial factor that we have to study intensively in the future.

REFERENCES

LIST OF REFERENCES

1. Australian Uranium Association What is Uranium? How does it work? June 2006 www.uic.com.au/uran.htm

2. Evans, H. T. *Science* **1963**, *141*, 154.

3. Thompson, H. A.; Brown, G. E.; Parks, G. A. *Am. Mineral.* **1997**, *82*, 483-496.

4. Aberg, M.; Ferri, D.; Glaser, J.; Grenthe, I. *Inorg. Chem.* **1983**, *22*, 3986-3989.

5. Allen, P. G.; Bucher, J. J.; Shuh, D. K.; Edelstein, N. M.; Reich, T. *Inorg. Chem.* **1997**, *36*, 4676-4683.

6. Dent, A. J.; Ramsay, J. D. F.; Swanton, S. W. *J. Colloid Interface Sci.* **1992**, *150*, 45-60.

7. Nguyen-Trung, C.; Begun, G. M.; Palmer, D. A. *Inorg. Chem.* **1992**, *31*, 5280-5287.

8. Nguyen-Trung, C.; Palmer, D. A.; Begun, G. M.; Peiffert, C.; Mesmer, R. E. *J. Solution Chem.* **2000**, *29*, 101-129.

9. Perera, B. A.; Ince, M. P.; Talaty, E. R.; Van Stipdonk, M. J. *Rapid Commun. Mass Spectrom.* **2001**, *15*, 615-622.

10. Perera, B. A. G., A. L.; Barr, J. M.; Tekarli, S. M.; Anbalagan, V; Talaty, E. R.; Van Stipdonk, M. J. *J. Mass Spectrom.* **2002**, *37*, 401.

11. Talaty, E. R.; Perera, B. A.; Gallardo, A. L.; Barr, J. M.; Van Stipdonk, M. J. *J. Phys. Chem., A* **2001**, *105*, 8059-8068.

12. Van Stipdonk, M. J., Chien, W.; Anbalagan, V.; Gresham, G., Groenewold, G.; Oxidation of 2-propanol ligands during collision-induced dissociation of a gas-phase uranyl complex. I. J. Mass Spectrom.; 2004, 237, 175-183.

13 Downard K. *Mass Spectrometry a Foundaton Course* : The Royal Society of

Chemistry 2004.; P. 22

14. Hoffmann de Edmond, Vincent Stroobant. *Mass Spectrometry Principles and Applications*. : Wiley 2001.; 2nd, P. 33-36.

15. Karen R. Jonscher and John R. Yates, III; "The Whys and Wherefores of Quadrupole Ion Trap Mass Spectrometry" 21st September 1996. http://www.abrf.org/ABRFNews/1996/September1996/sep96iontrap.html

16. Hoffmann de Edmond, Vincent Stroobant. *Mass Spectrometry Principles and Applications*. : Wiley 2001.; 2nd, P. 72-82.

17. Gibson, J. K. *Int. J. Mass Spectrom. Ion Processes* **2002**, *213*, 1.

18. Gibson, J. K. *Organometallics* **1997**, *16*, 4214-4222.

19. Gibson, J. K. *J. Am. Chem. Soc.* **1998**, *120*, 2633-2640.

20. Gibson, J. K. *J. Mass Spectrom.* **1999**, *34*, 1166-1177.

21. Jackson, G. P.; King, F. L.; Goeringer, D. E.; Duckworth, D. C. *J. Phys. Chem., A* **2002**, *106*, 7788 - 7794.

22. Cornehl, H. H.; Heinemann, C.; Marcalo, J.; deMatos, A. P.; Schwarz, H. *Angew. Chem.-Int. Edit. Engl.* **1996**, *35*, 891-894.

23. Gibson, J. K. *J. Mass Spectrom.* **2001**, *36*, 284-293.

24. Peng, Y.; Plass, W. R.; Cooks, R. G. *J. Am. Soc. Mass Spectrom.* **2002**, *13*, 623 - 629.

25. Gresham, G. L.; Gianotto, A. K.; Harrington, P. B.; Cao, L.; Scott, J. R.; Olson, J. E.; Appelhans, A. D.; Van Stipdonk, M. J.; Groenewold, G. S. *J. Phys. Chem., A* **2003**, *submitted*.

26. Van Stipdonk M, Anbalagan V, ChienW, Gresham G, Groenewold G, Hanna D. Elucidation of the Collision Induced Dissociation pathways of Water and Alcohol Coordinated Complexes Containing the Uranyl Cation. *J. Am. Soc.*

Mass Spectrom. 2003; **14**: 1205-1214.

27. Brauman, J. I. Blair, L. K. *J. Am. Chem. Soc.* **1968**, *90*, 6561.

28. Brauman, J. I. Blair, L. K. *J. Am. Chem. Soc.* **1970**, *92*, 5986.

29. Perera, B.A.; Ince, M. P.; Talaty, E.R.; Van Stipdonk, M.J. Gas Phase Attachment of Water and Methanol to Ag(I) Complexes wtih α-Amino Acids in an Ion Trap Mass Spectrometer. Rapid Commun. Mass Spectrom. 2001, 15, 615-622.

30. Perera, B. A. ; Gallardo, A. L.; Barr, J. M.; Tekarli, S. M.; Anbalagan, V.; Talaty, E. R.; Vanstipdonk, M. J. Influence of a Ring Substituent on the Tendency to Form H_2O adducts to Ag^+ Complexes with Phenylalanine Analogues in an Ion Trap Mass Spectrometer. J. Mass Spectrom. 2002, 37, 401-413.

31. Talaty, E. R.; Perera, A. B. ; Gallardo, A. L. ; Barr , J. M.; Vanstipdonk, M. J. Elucidation of Fragmentation Pathways for the Collision Induced Dissociation of the Binary Ag(I) Comples with Phenylalanine. J. Phys. Chem. A 2001, 105, 8059-8068.

32. Hanna, D.; Silva, M.; Morrison, J.; Tekarli, S.; Anbalagan, V.; Vanstipdonk, M. J. Gas-Phase Hydration and Alcohol Addition Reactions of Complexes Composed of Ag^+ and a Single Alcohol Molecule. J. Phys. Chem. A 2003, 107, 5528-5537.

33. Vanstipdonk, M. J.; Gresham, G.; Groenewold, G.; Anbalagan, V.; Hanna, D.; Chien, W. Elucidation of the Collision Induced Dissociation Pathways of Water and Alcohol Coordinated Complexes Containing the Uranyl Cation. J. Am. Soc Mass Spectrom. 2003, 14, 1205-1214.

34. McLuckey, S. A.; Reid, G. E.; Wells, J. M. Ion Parking During Ion/Ion Reactions in Electrodynamic Ion Traps. Anal. Chem. 2002, 74, 336-346.

35. Gresham, G. L.; Gianotto, A. K.; Harrington, P. d. B. ; Cao, L.; Scott, J.R.; Olson, J.E.; Appelhans, A.D.; Van Stipdonk, M. J.; Groenewold, G. S. Gas-Phase Hydration of U(IV), U(V), and U(VI) Dioxo Monocations,. J. Phys. Chem. A 2003, 107, 8530-8538.

36. Gillespie, D.T. A General Method for Numerically Simulating the Stochastic Time Evolution of Coupled Chemical Reactions. J. Comput. Phys. 1976, 22, 403-434.

37. Gillespie, D.T. Exact Stochastic Simulation of Coupled Chemical Reactions. J. Phys. Chem. 1977, 81, 2340-2362.

38. Houlde, F. A. ; Hinsberg, W.D. Stochastic Simulations of Temperature Programmed Desorption Kinetics. Surf. Sci. 1995, 338, 329-346.

39. Hinsberg, W.D., Houle, F. A. Chemical Kinetics SimulatorVersion 1.01.

40. Weishaar, J.C. Bare Transition Metal Atoms in the Gas Phase: Reactions of M, M^+, and M^{2+} with Hydrocarbons. Acc. Chem. Res. 1993, 26, 213-219.

41. Moulin, C.; Charron, N.; Plancque, G.; Virelizier, H. *Appl. Spectrosc.* **2000**, *54*, 843-8.

42. Wu, Q. C., X.; Hofstadler, S. A.; Smith, R. D. *J. Mass Spectrom.* **1996**, *31*, 669-675.

43. Groenewold, G. S.; Hodges, B. D. M.; Scott, J.R.; Gianotto, A. K.; Appelhans, A. D.; Kessinger, G. F.; Wright, J. B. Oxygen-for-Sulfur Exchanged in the Gas Phase: Reactions of Al and Si Oxyanions with H_2S. J. Phys. Chem. A 2001, 105, 4059-4064.

44. Groenewold, G. S.; Scott, J. R.; Gianotto, A. K.; Hodges, B. D. M.; Kessinger, G. F.; Benson, M. T.; Wright, J. B. Gas-Phase Condensation Reactions of $Si_xO_yH_z^-$ Oxyanions with H_2O. J. Chem. Phys. A2001, 105,9681-9688.

45. Frisch, M. J.; Trucks, G. W.: Schlegel, H. B.; Scuseria, G. E.; Robb, M. A.; cheeseman, J. R.; Zarkrzewski, V. G.: Montgomery, J. A. J.; Stratmann, R. E.; Burant, J. C.; Dapprich, S.; MIllam, J. M.; Daniels, A. D.; Kudin, K. N.; Strain, M. C.;Farkas, O.; Tomasi, J.; Barone, V.; Cossi, M.; Cammi, R.; Mennucci, B.; Pomelli, C.; Adamo, C.; Clifford, S.; Ochterski, J.; Petersson, G.A.; Ayala, P.Y.; Cui, Q.; Morokuma, K.; Malick, D. K.; Rabuck, A. D.; Raghavachari, K.; Foresman, J. B.; Cioslowski, J.; Ortiz, J. V.; Stefanov, B.B.; Liu, G.; Liashenko, A.; Piskorz, P.; Komaromi, I.; Gomperts, R.; Martin, R.L.; Fox, D.J.; Keith, T.;

Al-Laham, M. A.; Peng, C.Y.; Nanayakkarra, A.; Gonzalez, C.; Challacombe, M.; Gill, P. M. W.; Johnson, B.; Chen, W.; Wong, M. W.; Andres, J. L.; Head-Gordon, M.; Replogle, E.S.; Pople, J. A. Gaussian 98, Revision A.5; Gaussian, Inc.; Pittsburgh, PA, 1998.

46. Spencer, S.; Gagliardi, L.; Handy, N. C.; Ioannou, A. G.; Skylaris, C.-K.; Willetts, A.; Simper, A. M. Hydration of UO_2^{2+} and PuO_2^{2+}. J. Phys. Chem. A1999, 103, 1831-1837.

47. Oda, Y.; Aoshima, A. Ab Initio Quantum Chemical Study on Charge Distribution and Molecular Structure of Uranyl (VI) Species with Raman Frequency. J. Nuc. Sci. Technol. 2002, 39, 647-654.

48. Jackson, G. P.; Gibson, J. K.; Duckworth, D. C. Gas-Phase Reactions of Bare and Oxo-Ligated Actinide and Lanthanide Cations with Pentamethylcyclopentadiene Studied in a Quadrupole AIon Trap Mass Spectrometer. Int. J. Mass Spectrom. 2002, 220, 419-441.

49. Su, T.; Chesnavich, W. J. Parametrization of the Ion-Polar Molecule Collision Rate Constant by Trajectory Calculations. J. Chem. Phys. 1982, 76, 5183-5185.

50. Su, T.; Chesnavich, Bowers, M. T. Parameterization of the Average Dipole Orientation Theory: Temperature Dependence. Int. J. Mass Spectrom. Ion Phys. 1975, 17, 211-212.

51. Su, T.; Chesnavich, Bowers, M. T.Ion-Polar Molecule Collisions. The Effect of Molecular Size on Ion-Polar Molecule Rate Constants. J. Am Chem. Soc. 1973, 95, 7609-7610.

52. Denning, R. G. Electronic Structure and Bonding in Actinyl Ions. Struct. Bond. 1992, 79, 215-276.

53. Vallet, V.; Wahlgren, U.; Schimmelpfennig, B.; Moll, H.; Szabo, Z.; Grenthe, I. Solvent Effects on Uranium(VI) Fluoride and Hydroxide Complexes Studied by EXAFS and Quantum Chemistry. Inorg. Chem. 2001, 40, 3516-3525.

54. Marinelli, P. J.; Squires, R. R. Sequential Solvation of Atomic Transistion-Metal Ions>195>the Second Solvent Molecule Can Bind More Strongly than the First. J. Am. Chem. Soc. 1989, 111; 4101-4103.

55. Magnera. T. F.; David, D. E.; Stulik, D.; Orth, R. G.; Jonkman, H. T.; Michl, J. Production of Hydrated Metal-Ions by Fast Ion or Atom Beam Sputtering-Collision-Induced Dissociation and Successive Hydration Energies of Gaseous Cu^+ with 1-4 Water-Molecules. J. Am. Chem. Soc. 1989, 111, 5036-5043.

56. Magnera. T. F.; David, D. E.; Michl, J. Gas-Phase Water and Hydroxyl Binding-Energies for Monopositive First Row Transition-Metal Ions. J. Am. Chem. Soc. 1989, 111, 4100-4101.

57. Langhoff, S. R.; Bauschlicher, C. W.; Partridge, H.; Sodupe, J. Theoretical Study of One and Two Ammonia Molecules Bound to the First Row Transition Metal Ions. J. Phys. Chem. 1991, 95, 10677-10681.

58. Bauschlicher, C. W.; Langhoff, S. R.; Partridge, H. The Binding-Energies of Cu^+-$(NH_3)_n$ (n = 1-4). J. Chem. Phys. 1991, 94, 2068-2072.

59. Walter, D.; Armentrout, P. B. Sequential Bond Dissociation Energies of M +(NH_3)(x) (x = 1-4) for M = Ti-Cu. J. Am. Chem. Soc. 1998, 120, 3176-3187.

60. Vachet, R. W.; Callahan, J. H. J. Mass Spectrom. 2000, 35, 311-320.

61. Weigel, F. Uranium. In *The Chemistry of the Actinide Elements*; J. J. Katz, L. R. Morss and G. T. Seaborg Eds.; Chapman and Hall: London, 1986; p. 169.

62. Greenwood, N. N.; Earnshaw, A. Chemistry of the Elements; Butterworth Heinemann: Oxford, Great Britain, 1997.

63. Murphy, W. M.; Shock, E. L. Environmental Aqueous Geochemistry of Actinides. In *Uranium: Mineralogy, Geochemistry and the Environment*; P. C. Burns and R. Finch Eds.; Mineralogical Society of America: Washington, D. C., 1999; p. 221.

64. Tsushima, S.; Reich, T. A Theoretical Study of Uranyl Hydroxide Monomeric and Dimeric Complexes. Chem. Phys. Lett. 2001, 347, 127-132.

65. Clark, D. L.; Conradson, S. D.; Donohoe, R. j.; Keogh, D.W.; Morris, D.E.; Palmer, P.D.; Rogers, R.D.; Tait, C. D. Chemical Speciation of the Uranyl Ion Under Highly Alkaline Conditions. Synthesis, Structures, and Oxo Ligand Exchanged Dynamics. Inorg. Chem. 1999, 38, 1456-1466.

66. Winkelmann G. Microbial siderophore-mediated transport. *Biochem. Soc. Trans.* 2002; **30**: 691.

67. Albrecht-Gary AM, Crumbliss AL. Coordination chemistry of siderophores: thermodynamics and kinetics of iron chelation and release. In *Metal Ions in Biological Systems*, vol 35. Marcel Dekker: New York, 1998; 239.

68. Drechsel H, Jung G. Peptide Siderophores. *J. Pept. Sci.* 1998; **4**:147.

69. Neubauer U, Furrer G, Schulin R. Heavy metal sorption on soil minerals affected by the siderophore desferrioxamine B: the role of Fe(III) (hydr)oxides and dissolved Fe(III). *Eur. J. Soil Sci.* 2002; **53**: 45.

70. John SG, Ruggiero CE, Hersman LE, Tung CS, Neu MP. Siderophore mediated plutonium accumulation by Microbacterium flavescens (JG-9). *Environ. Sci. Technol.* 2001; **35**: 2942.

71. John SG, Ruggiero CE, Hersman LE, Neu MP. Siderophoremediated plutonium uptake by the common soil aerobe Aureobacterium flavescens (JG-9). *Abstr. Pap. Am. Chem. Soc.*2000; **220**: U371.

72. Neu MP, Matonic JH, Ruggiero CE, Scott BL. Structural characterization of a plutonium(IV) siderophore complex:Single-crystal structure of Pu-desferrioxamine E. *Angew. Chem.,Int. Edit.* 2000; **39**: 1442.

73. Neubauer U, Furrer G. The use of voltammetry for sorption studies of heavy metals on mineral surfaces in presence of the siderophore desferrioxamine B. *Anal. Chim. Acta* 1999; **392**: 159.

74. Neubauer U, Nowack B, Furrer G, Schulin R. Heavy Metal Sorption on Clay

Minerals Affected by the Siderophore Desferrioxamine B. *Environ. Sci. Technol.* 2000; **34**: 2749.

75. Stradling GN. Recent Progress in Decorporation of Plutonium, Americium and Thorium. *Radiat. Prot. Dosim.* 1994; **53**: 297.

76. Stradling GN. Decorporation of actinides: a review of recent research. *J. Alloys Compd.* 1998; **271**: 72.

77. O'Boyle NC, Nicholson GP, Piper TJ, Taylor DM, Williams DR, Williams G. A Review of Plutonium(IV) Selective Ligands. *Appl. Radiat. Isot.* 1997; **48**: 183.

78. Neu M, Ruggiero C, John S, Matonic J, Reilly S. Interactions of plutonium with desferrioxamine siderophores utilized by soil microorganisms. In *Proceedings of the 2000 International Chemical Congress of Pacific Basin Societies (Pacifichem 2000)*, Honolulu, Hawaii, 2000; 563.

79. Evans LJ. Chemistry of metal retention by soils. *Environ. Sci. Technol.* 1989; **23**: 1046.

80. Hochella MFJ. Mineral Surfaces: Their Characterization and Their Chemical, Physical and Reactive Nature. *Min. Surf.* 1995; **5**: 17.

81. Brown GEJ, Henrich VE, Casey WH, Clark DL, Eggleston C, Felmy A, Goodman DW, Gratzel M, Maciel G, McCarthy MI, Nealson KH, Sverjensky DA, Toney MF, Zachara JM. Metal Oxide Surfaces and Their Interactions with Aqueous Solutions and Microbial Organisms. *Chem. Rev.* 1999; **99**: 77.

82. Francis AJ. Microbial dissolution and stabilization of toxic metals and radionuclides in mixed wastes. *Experientia* 1990; **46**: 840.

83. Brainard JR, Strietelmeier BA, Smith PH, Langston-Unkefer PJ, Barr ME, Ryan RR. Actinide Binding and Solubilization by Microbial Siderophores. *Radiochim. Acta* 1992; **58–9**: 357.

84. Bulman RA, Wedgwood AJ, Szabo G. Investigations into the Chemical Forms of Pu-239 in a West Cumbrian Salt-Marsh Soil Radiolabeled by an Environmental Process. *Sci. Total Environ.*1992; **114**: 215.

85. Choppin GR, Rizkalla EN. Solution chemistry of actinides and lanthanides. In *Handbook on the Physics and Chemistry of Rare Earths*, Gschneider JKA, Eyring L, Choppin GR, Lander GH (eds). North-Holland: Amsterdam, 1994; 559.

86. Francis AJ. Biotransformation of uranium and other actinides in radioactive wastes. Biotransformation of uranium and other actinides in radioactive wastes. J. *J. Alloys Compd.* 1998; **271–273**:78.

87. Gledhill M. Electrospray ionisation-mass spectrometry of hydroxamate siderophores. *Analyst* 2001; **126**: 1359.

88. McCormack P, Worsfold PJ, Gledhill M. Separation and Detection of Siderophores Produced byMarine Bacterioplankton Using High-Performance Liquid Chromatography with Electrospray Ionization Mass Spectrometry. *Anal. Chem.* 2003; **75**: 2647.

89. Kilz S, Lenz C, Fuchs R, Budzikiewicz H. A Fast Screening Method for the Identification of Siderophores from Fluorescent *Pseudomonas* spp. by Liquid Chromatography/Electrospray Mass Spectrometry. *J. Mass Spectrom.* 1999; **34**: 281.

90. Gatlin CL, Turecek F. Electrospray ionization of inorganic and organometallic complexes. In *Electrospray Ionization Mass Spectrometry*, Cole RB (ed). Wiley: New York, 1997; 527.

91. Stewart II. Electrospray mass spectrometry: a tool for elemental speciation. *Spectrochim. Acta, Part B* 1999; **54**: 1649.

92. Wang HJ, Agnes GR. Evaluation of electrospray mass spectrometry as a technique for quantitative analysis of kinetically labile solution species. *Anal. Chem.* 1999; **71**: 3785.

93. Ross ARS, Ikonomou MG, Orians KJ. Electrospray ionization of alkali and alkaline earth metal species. Electrochemical oxidation and pH effects. *J. Mass Spectrom.* 2000; **35**: 981.

94. Caudle MT, Stevens RD, Crumbliss AL. Electrospray Mass Spectrometry Study of 1:1 Ferric Dihydroxamates. *Inorg. Chem.* 1994; **33**: 843.

95. Boukhalfa H, Crumbliss AL. Multiple-Path Dissociation Mechanism for Mono- and Dinuclear Tris(hydroxamato)iron(III) Complexes with Dihydroxamic Acid Ligands in Aqueous Solution. *Inorg. Chem.* 2000; **39**: 4318.

96. Spasojevic I, Boukhalfa H, Stevens RD, Crumbliss AL. Aqueous Solution Speciation of Fe(III) Complexes with Dihydroxamate Siderophores Alcaligin and Rhodotorulic Acid and Synthetic Analogues Using Electrospray Ionization Mass Spectrometry. *Inorg. Chem.* 2001; **40**: 49.

97. Barbeau K, Rue EL, Bruland KW, Butler A. Photochemical Cycling of Iron in the Surface Ocean Mediated by Microbial Iron(III)-Binding Ligands. *Nature (London)* 2001; **413**: 409.

98. Gresham GL, Gianotto AK, Harrington PdB, Cao L, Scott JR, Olson JE, Appelhans AD, Van Stipdonk MJ, Groenewold GS. Gas-Phase Hydration of U(IV), U(V), and U(VI) Dioxo Monocations. *J. Phys. Chem. A* 2003; **107**: 8530-8538.

99. DeHoffmann E, Stroobant V. Fast-Atom-Bombardment Tandem Mass-Spectrometric Analysis of Hydroxamate Siderophores. *Biol. Mass Spectrom.* 1991; **20**: 142.

100. Kaltashov IA, Cotter RJ, FeinstoneWH, Ketner GW, Woods AS. Ferrichrome: Surprising stability of a cyclic peptide Fe-III complex revealed by mass spectrometry. *J. Am. Soc. Mass Spectrom.* 1997; **8**: 1070.

101. Heinemann, C.; Cornehl, H. H.; Schwarz, H. *J. Organomet. Chem*. **1995**, *501*, 201-209.

102. Gibson, J. K. *J. Vac. Sci. Technol. A-Vac. Surf. Films* **1997**, *15*, 2107-2118.

103. Armentrout, P. B.; Beauchamp, J. L. *Chem. Phys*. **1980**, **50**, 27-36.

104. Dion, H. M.; Ackerman, L. K.; Hill, H. H. *Talanta* **2002**, *57*, 1161-1171.

105. Dion, H. M. A., L. K.; Hill, H. H. *Int. J. Ion Mobil. Spectrom*. **2001**, *4*, 31-33.

106. Chien, W.; Anbalagan, V.; Zandler, M.; Van Stipdonk, M.; Hanna, D.; Gresham, G.; Groenewold, G. *J. Am. Soc. Mass Spectrom*. 15 **2004**, *777-783*.

107. Hartman, J. R.; Vachet, R. W.; Callahan, J. H. *Inorg. Chim. Acta* **2000**, *297*, 79-87.

108. Vachet, R. W.; Hartman, J. R.; Gertner, J. W.; Callahan, J. H. *Int. J. Mass Spectrom*. **2001**, *204*, 101-112.

109. Combariza, M. Y.; Vachet, R. W. *J. Am. Soc. Mass Spectrom*. **2002**, *13*, 813-825.

110. Wu, H. F.; Brodbelt, J. S. *Inorg. Chem*. **1995**, *34*, 615-621.

111. Scott, J. R.; Groenewold, G. S.; Gianotto, A. K.; Benson, M. T.; Wright, J. B. *J. Phys. Chem. A* **2000**, *104*, 7079-90.

112. Gianotto, A. K.; Hodges, B. D. M.; Benson, M. T.; Harrington, P. d. B.; Appelhans, A. D.; Olson, J. E.; Groenewold, G. S. *J. Phys. Chem. A* **2003**, *107*, 5948-5955.

113. Innorta, G.; Torroni, S.; Foffani, A.; Pontoni, L. *J. Mass Spectrom*. **1995**, *30*, 1633 - 1635.

114. Operti, L.; Splendore, M.; Vaglio, G. A.; Franklin, A. M.; Todd, J. F. J. *Int. J. Mass Spectrom. Ion Processes* **1994**, *136*, 25-33.

115. Suib, S. L.; Kostapapas, A.; Psaras, D. *J. Am. Chem. Soc*. **1984**, *106*, 1614-1620.

116. Suib, S. L.; Carrado, K. A. *Inorg. Chem*. **1975**, *24*, 863-867.

117. Berg, J. B. C., D. L.; Huffman, J. C.; Morris, D. E.; Sattelberger, A. P.; Streib, W. E.; Van der Sluys, W. G.; Watkin, J. G. *J. Am. Chem. Soc*. **1992**, *114*, 10811.

118. Van der Sluys, W. G. S., A. P. *Chem. Rev*. **1990**, *90*, 1027.

119. Avens, L. R. B., D. M.; Burns, C. J.; McKee, S. D.; Smith, W. H. *Inorg. Chem*. **1994**, *33*, 4245.

120. Catinella, S.; Pelizzi, N.; Barboso, S.; Favretto, D.; Seraglia, R.; Traldi, P. *Rapid Commun. Mass Spectrom.* **2002**, *16*, 1897-1902.

121. Goeringer, D. E.; Duckworth, D. C.; McLuckey, S. A. *J. Phys. Chem., A* **2001**, *105*, 1882-1889.

122. McClellan, J. E.; Murphy III, J. P.; Mulholland, J. J.; Yost, R. A. *Anal. Chem*. **2002**, 74, 402 - 412.

123. Wells, J. M.; Plass, W. R.; Patterson, G. E.; Zheng, O. Y.; Badman, E. R.; Cooks, R. G. *Anal. Chem*. **1999**, *71*, 3405-3415.

124. Burrows, H. D.; Kemp, T. J. *Chem. Soc. Rev*. **1974**, *3*, 139-165.

125. Azenha, M. E. D. G.; Burrows, H. D.; Formoshino, S. J.; Miguel, M. de G. *J. Chem. Soc. Faraday Trans*. **1989**, *85*, 2625-2634.

126. Wang, W.-D.; Bakac, A.; Espenson, J. H. *Inorg. Chem*. **1995**, *34*, 6034-6039.

127. Streitwieser, Jr. A.; Heathcock, C. H. *Introduction of Organic Chemistry*, 3rd ed. Macmillan Publishing Co., New York, pg. 210.

128. Armentrout, P. B. in *Gas Phase Inorganic Chemistry*, Russell, D. H., ed. Plenum Press, New York and London, 1989; pg. 1-40.

129. Armentrout, P. B., Beauchamp, J. L. *Acc. Chem. Res*. **1989**, *22*, 315-321.

130. Buckner, S. W., Freiser, B. S. in *Gas Phase Inorganic Chemistry*, Russell, D. H., ed. Plenum Press, New York and London, 1989; pg. 279-320.

131. Eller, K., Schwarz, H. *Chem. Rev*. **1991**, *91*, 1121-1177.

132. Pepper, M., Bursten, B. E. *Chem. Rev*. **1991**, *91*, 719-741.

133. Ali, A. H.; Zaera, F. *J. Mol. Catal. A* **2002**, *177*, 215-235.

134. Groenewold GS, Van Stipdonk MJ, Gresham GL, Hanna D, Chien W, Anbalagan V. J. Mass Spectrom. 2004; 39: 752.

135. Van Stipdonk MJ, Chien W, Anbalagan V, Gresham GL, Groenewold GS. Int. J. Mass Spectrom. 2004; 237: 175.

136. Pasilis SP, Pemberton JE. Inorg. Chem. 2003; 42: 6793-6800.

137. Clavaguera-Sarrio C, Hoyau S, Ismail N, Marsden CJ.J. Phys. Chem. A 2003; 107: 4515.

138. Akibo-Betts G, Barran PE, Puskar L, Duncombe B, Cox H, Stace AJ. J. Am. Chem. Soc. 2002; 124: 9257.

139. Ervin KM, DeTuri VF. J. Phys. Chem. A 2002; 106: 9947.

140. Vachet RW, Hartman JAR, Callahan JH. J. Mass Spectrom. 1998; 33: 1209-1225.

141. Murphy JP III, Yost RA. Rapid Commun. Mass Spectrom. 2000; 14: 270-273.

142. Kemp, T. J.; Jennings, K. R.; Read, P. A. *J. Chem. Soc. Dalton Trans*. 1995, 885-889.

143. Gill, L. A.; Wells, Amy, J. W.; Vaughn, W. E.; Cooks, R. G. *Int. J. Mass Spectrom*. **1999**, *188*, 87-93.

144. Bortolini, O.; Spalluto, G.; Traldi, P. *Org. Mass Spectrom*. **1994**, *29*, 269.

145. Traldi, P.; Favretto, D.; Catinella, S.; Bortolini, O. *Org. Mass Spectrom*. **1993**, *28*, 745.

146. Bortolini, O.; Catinella, S.; Traldi, P. *Org. Mass Spectrom*. **1992**, *27*, 927.

147. Burgess, J. “Metal Ions in Solution,” 1978, p. 169.

148. Fratiello, A.; Kubo, V.; Lee, R. E.; Schuster, R. E. *J. Phys. Chem.*, **1970**, *74*, 3726-3730.

149. Bardin, N.; Rubini, P.; Madic, C. *Radiochim. Acta*, **1998**, *83*, 189-194.

150. Rodgers, M. T.; Armentrout, P. B. *Mass Spectrom. Rev.*, **2000**, *19*, 215-247.

151. Busman, M. ; Rockwook, A. L.; Smith, R. D. *J. Phys. Chem*. **1992**, *96*, 2397.

152. Van Stipdonk, M. J. Ince, M. P. Perera, B. A. Martin, J. A. *Rapid Comm. Mass Spectrom*. **2002**, *16*, 355-363.

153. Neuefeind, J.; Soderholm, L.; Skanthakumar, S. *J. Phys. Chem. A* **2004**, *108*, 2733-2739.

154. Rosenstock, H. M.; Draxl, K.; Steiner, B. W.; Herron, J. T. *J. Phys. Chem. Ref. Data* **1977**, 6, Suppl. 1, 783.

155. Van Stipdonk, M. J.; Chien, W.; Anbalagan, V.; Bulleigh, K.; Hanna, D.; Groenewold, G. S. *J. Phys. Chem. A.* 2004, 108, 10448-10457.

156. Gibson, J. K.; Haire, R. G.; Santos, M.; Marçalo, J.; Pires de Matos, A. *J. Phys. Chem. A.* 2005, 109, 2768-2781.

157. Huan, H.; Chaudhary, S.; Van Horn, J. D. *Inorg. Chem*. 2005, 44, 813-815.

158. Li, H.; Plass, W. R.; Patterson, G. E.; Cooks, R. G. *J. Mass Spectrom*. 2002, 37, 1051-11058.

159. Lias, S.G.; Bartmess, J.E.; Liebman, J.F.; Holmes, J.L.; Levin, R.D.; Mallard, W.G. "Ion Energetics Data" in NIST Chemistry WebBook, NIST Standard Reference Database Number 69, Eds. P.J. Linstrom and W.G. Mallard, June 2005, National Institute of Standards and Technology, Gaithersburg MD, 20899 (http://webbook.nist.gov).

160. Blades, A. T.; Jayaweera, P.; Ikonomou, M. G.; Kebarle, P. *J. Chem. Phys*. 1990, 92, 5900-5906.

161. Stace, A. J.; Walker, N. R.; Firth, S. *J. Am. Chem. Soc*. 1997, 119, 10239-10240.

162. Woodward, C. A.; Dobson, M. P.; Stace, A. J. *J. Phys. Chem*. 1996, 100, 5605-5607.

163. Woodward, C. A.; Dobson, M. P.; Stace, A. J. *J. Phys. Chem. A*. 1997, 101, 2279-2287.

164. Mikhailov, V. A.; Barran, P. E.; Stace, A. J. *Phys. Chem. Chem. Phys*. 1999, 1, 3461-3465

165. Stace, A. J. *J. Phys. Chem. A*. 2002, 106, 7993-8005.

166. Schröder, D.; Schwarz, H. *J. Phys. Chem. A*. 1999, 103, 7385-7394.

167. Chang, C. M.; Wang, M. K. *Chem. Phys. Lett*. 1998, 286, 46-48.

168. George, P.; Glusker, J. P.; Trachtman, M.; Bock, C. W. *Chem. Phys. Lett*. 2002, 351, 454-456.

169. Morse, J. W.; Choppin, G. R. *Re*V*. Aquatic Sci.* **1991**, *4* (1), 1-22.

170. Silva, R. J.; Nitsche, H. *Radiochim. Acta* **1995**, *70/71*, 377-396.

171. Brookins, D. G. *Geochemical Aspects of Radioacti*V*e Waste Disposal*; Springer-Verlag: New York, 1984

172. Schulz, W. W.; Navratil, J. D. *Science and Technology of Tributyl Phosphate*; CRC Press: Boca Raton, FL, 1984.

173. Rizkalla, E. N.; Choppin, G. R. Lanthanides and Actinides Hydration andHydrolysis. In *Handbook on the Physics and Chemistry of Rare Earths*; Gschneider, K. A., Jr., Eyring, L., Choppin, G. R., Lander, G. H., Eds.; Vol. 18, Lanthanides/Actinides: Chemistry; North-Holland: Amsterdam, 1994; pp 529-558.

174. Alcock, N. W. *J. Chem. Soc. A* **1968**, 1588-1594.

175. Kubatko, K.-A. H.; Helean, K. B.; Navrotsky, A.; Burns, P. C. *Science* **2003**, *302*, 1191-1193.

176. Bhattacharjee, M.; Chaudhuri, M. K.; Purkayastha, R. N. D. *Inorg. Chem.* **1986**, *25*, 2354-2357.

177. Charpin, P. P.; Folcher, G.; Lance, M.; Vigner, N. E. D. *Acta Crystallogr.* **1985**, *C41*, 1302-1305.

178. Rose, D.; Chang, Y.-D.; Chen, Q.; Zubleta, J. *Inorg. Chem.* **1994**, *33*, 5167-5168.

179. Thuery, P.; Masci, B. *Supramol. Chem.* **2003**, *15*, 95-99.

180. Thuery, P.; Nierlich, M.; Baldwin, B. W.; Komatsuzaki, N.; Hirose, T. *J. Chem. Soc., Dalton Trans.* **1999**, 1047-1048.

181. Westland, A. D.; Tarafder, M. T. H. *Inorg. Chem.* **1981**, *20*, 3992-3995.

182. Momenteau, M.; Reed, C. A. *Chem. Re*V. **1994**, *94*, 659-698.

183. Dickman, M. H.; Pope, M. T. *Chem. Re*V. **1994**, *94*, 569-584.

184. Karlin, K. D.; Tolman, W. B.; Kaderli, S.; Zuberbuhler, A. D. *J. Mol. Catal. A* **1997**, *117* (1-3), 215-222.

185. Jones, R. D.; Summerville, D. A.; Basolo, F. *Chem. Re*V. **1979**, *79*, 139-179.

186. Vaska, L. *Acc. Chem. Res.* **1976**, *9*, 175-183.

187. Valentine, J. S. *Chem. Re*V. **1973**, *73*, 235-245.

188. Pauling, L.; Coryell, C. D. *Proc. Natl. Acad. Sci. U.S.A.* **1936**, *22*, 210-216.

189. Bakac, A.; Espenson, J. H. *Inorg. Chem.* **1995**, *34*, 1730-1735.

190. Burgess, J. *Metal Ions in Solution*; Ellis Horwood Ltd.: Chichester, UK, 1978; p 481.

191. Ekstrom, A. *Inorg. Chem.* **1974**, *13*, 2237-2241.

192. Morris, D. E. *Inorg. Chem.* **2002**, *41*, 3542-3547.

193. Anbalagan, V.; Chien, W.; Gresham, G. L.; Groenewold, G. S.; Van Stipdonk, M. J. *Rapid Commun. Mass Spectrom.* **2004**, *18*, 3028-3034.

194. Gresham, G. L.; Groenewold, G. S.; Olson, J. E. *J. Mass Spectrom.* **2000**, *35*, 1460-1469.

195. Groenewold, G. S.; Appelhans, A. D.; Ingram, J. C. *J. Am. Soc. Mass Spectrom.* **1998**, *9*, 35-41.

196. Groenewold, G. S.; Appelhans, A. D.; Ingram, J. C.; Gresham, G. L.; Gianotto, A. K. *Talanta* **1998**, *47*, 981-986.

197. Delmore, J. E.; Appelhans, A. D.; Peterson, E. S. *Int. J. Mass Spectrom. Ion Processes* **1995**, *146/147*, 15-20.

198. Johnson, K. B.; Delmore, J. E.; Appelhans, A. D. *Int. J. Mass Spectrom.* **2003**, *229*, 157-166.

199. Todd, J. F. J. *Practical Aspects of Ion Trap Mass Spectrometry*; CRC Press: New York, 1995; Vol. 1, p 4.

200. Brodbelt-Lustig, J. S.; Cooks, R. G. *Talanta* **1989**, *36* (1/2), 255-260.

201. Cooks, R. G.; Patrick, J. S.; Kotaiho, T.; McLuckey, S. A. *Mass Spectrom. Re*V. **1994**, *13*, 287-339.

202. Nourse, B. D.; Cooks, R. G. *Int. J. Mass Spectrom. Ion Processes* **1991**, *106*, 249-272.

203. Armentrout, P. B. *J. Mass Spectrom.* **1999**, *34*, 74-78.

204. Green-Church, K. B.; Limbach, P. A. *J. Am. Soc. Mass Spectrom.* **2000**, *11*, 24-32.

205. Zahnley, T.; Macey, R.; Oster, G. *Berkeley Madonna*, version 8.0.1; University

of California: Berkeley, CA, 2003.

206. Flowers, B. H. *Numerical Methods in C*++, 2nd ed.; Oxford University Press: New York, 2000.

207. Moore, D. T.; Oomens, J.; Eyler, J. R.; Meijer, G.; von Helden, G.; Ridge, D. P. *J. Am. Chem. Soc.* **2004**, *126*, 14726-14727.

208. Oomens, J.; Moore, D. T.; von Helden, G.; Meijer, G.; Dunbar, R. C. *J. Am. Chem. Soc.* **2004**, *126*, 724-725.

209. Marshall, A. G.; Wang, J. T.-C. L.; Ricca, T. L. *J. Am. Chem. Soc.* **1985**, *107*, 7893-7897.

210. Gilbert, R. G.; Smith, S. C. *Theory of Unimolecular and Recombination Reactions*, 1st ed.; Blackwell Scientific Publications: London, 1990.

211. Weishaar, J. C. *Acc. Chem. Res.* **1993**, *26*, 213-219.

212. Su, T.; Bowers, M. T. *J. Am. Chem. Soc.* **1973**, *95*, 7611-7613.

213. Su, T.; Bowers, M. T. *Int. J. Mass Spectrom. Ion Phys.* **1973**, *12*, 347-356.

214. Groenewold, G. S.; Van Stipdonk, M. J.; Oomens, J.; Polfer, N.; Gianotto, A. K., unpublished results.

215. Wallace, W. T.; Wyrwas, R. B.; Whetten, R. L.; Mitric, R.; Bonacic- Koutecky, V. *J. Am. Chem. Soc.* **2003**, *125*, 8408-8414.

216. Yoon, B.; Ha¨kkinen, H.; Landman, U. *J. Phys. Chem. A* **2003**, *107*, 4066-4071.

217. DeKock, R. I.; Baerends, E. J.; Boerrigter, P. M.; Snijders, J. G. *Chem. Phys. Lett.* **1984**, *105*, 308-316.

218. Cramer, C. J.; Tolman, W. B.; Theopold, K. H.; Rheingold, A. L. *Proc.Natl. Acad. Sci. U.S.A.* **2003**, *100*, 3635-3640.

219. Bursten, B. E.; Strittmatter, R. J. *J. Am. Chem. Soc.* **1987**, *109*, 6606-6608.

220. Bursten, B. E.; Rhodes, L. F.; Strittmatter, R. J. *J. Am. Chem. Soc.* **1989**, *111*, 2758-2766.

221. Brennan, J. G.; Stults, S. D.; Andersen, R. A.; Zalkin, A. *Organometallics* **1988**, *7*, 1329-1334.

222. Mazzanti, M.; Wietzke, R.; Pecaut, J.; Latour, J.-M.; Maldivi, P.; Remy, M. *Inorg. Chem.* **2002**, *41*, 2389-2399.

223. Kaltsoyannis, N.; Scott, P. *Chem. Commun.* **1998**, 1665-1666.

224. Mehdoui, T.; Berthet, J. C.; Thuery, P.; Ephritikhine, M. *Dalton Trans.* **2004**, 579-590.

225. Mehdoui, T.; Berthet, J. C.; Thuery, P.; Ephritikhine, M. *Dalton Trans.* **2005**, 1263-1272.

226. de Jong, W. A.; Visscher, L.; Nieuwpoort, W. C. *J. Mol. Struct.* **1999**, *458*, 41-52.

227. Hay, P. J.; Martin, R. L.; Schreckenbach, G. *J. Phys. Chem. A* **2000**, *104*, 6259-6270.

228. Schreckenbach, G.; Hay, P. J.; Martin, R. L. *J. Comput. Chem.* **1999**, *20*, 70-90.